NEW METHODS OF ASSEMBLING AND INHIBITING ASSEMBLY OF BIOLOGICAL IRON-SULFUR CLUSTERS

by

SAHEL MOHEBBI

(Under the Direction of Michael K. Johnson)

ABSTRACT

The objectives of this work were threefold. To synthesize and characterize thioferrate, a linear inorganic anionic polymer of iron and sulfide with a $(FeS_2)^{1-}$ repeating unit, and investigate thioferrate-mediated assembly of protein-bound Fe-S clusters. To determine the nature of the Fe^{2+} donor and the role of the Isc Fdx in bacterial Fe-S cluster assembly on the IscU scaffold protein. To investigate the ability of 5-, 6-, and 7-membered cyclic thiosulfinates to inhibit Fe^{2+} acquisition and $[2Fe\text{-}2S]^{2+}$ cluster assembly by IscU. The approach involved using a combination of spectroscopic techniques to characterize thioferrate and protein-bound Fe^{2+} and Fe-S centers. The results confirm that thioferrate can be used to reconstitute $[2Fe\text{-}2S]^{2+}$, linear $[3Fe\text{-}4S]^{1+}$ and $[4Fe\text{-}4S]^{2+}$ clusters in Fe-S proteins under anaerobic conditions. The presence of a protein-bound linear $[3Fe\text{-}4S]^{1+}$ clusters as major or minor components of all thioferrate reconstitutions suggests a mechanism involving transfer of a linear $[3Fe\text{-}4S]^{1+}$ fragment of thioferrate to the apo Fe-S protein, that can be used for *in situ* formation of $[2Fe\text{-}2S]^{2+}$ and $[4Fe\text{-}4S]^{2+}$ clusters. Spectroscopic and analytical studies demonstrated IscX binds one Fe^{2+} ion that is transferred rapidly to IscU, indicating IscX is the elusive Fe^{2+} donor for $[2Fe\text{-}2S]^{2+}$ cluster assembly on IscU. Parallel UV-visible absorption/EPR studies showed reduced Fdx is oxidized in the presence of IscS and L-Cys

and in a single turnover of IscS in the presence of stoichiometric IscU, Fe^{2+}-bound IscX, and L-Cys. However, no evidence for formation a cysteine persulfide radical anion intermediate on IscS, that would generate a trisulfide radical ion on IscU was observed. The results indicate IscS-mediated persulfide rather than $S^{\bullet-}$ transfer to IscU that is reduced by electrons from cysteinate-bound Fe^{2+} and reduced Fdx to yield a cysteinate-bound $[Fe\text{-}S]^{1+}$ intermediate. Finally, 5- to 7-membered cyclic thiosulfinate have been shown to be potent inhibitors of binding Fe^{2+} and $[2Fe\text{-}2S]^{2+}$ cluster assembly on IscU. The unique properties of this new class of thiol cross-linkers offers a new approach to investigate the mechanism of $[2Fe\text{-}2S]^{2+}$ cluster assembly on IscU and has the potential to function as a new type of anticancer therapy by inhibiting the growth of rapidly dividing cancer cells.

INDEX WORDS: Iron-sulfur cluster assembly, iron-sulfur proteins, thioferrate, scaffold protein, cyclic thiosulfinates, cross-linkers

NEW METHODS OF ASSEMBLING AND INHIBITING ASSEMBLY OF BIOLOGICAL IRON-SULFUR CLUSTERS

by

SAHEL MOHEBBI

B.S., Baha'i Institute for Higher Education, Iran, 2008

A Dissertation Submitted to the Graduate Faculty of The University of Georgia in Partial Fulfillment of the Requirements for the Degree

DOCTOR OF PHILOSOPHY

ATHENS, GEORGIA

2020

NEW METHODS OF ASSEMBLING AND INHIBITING ASSEMBLY OF BIOLOGICAL IRON-SULFUR CLUSTERS

by

SAHEL MOHEBBI

Major Professor:	Michael K. Johnson
Committee:	Michael W. W. Adams
	Todd C. Harrop

Electronic Version Approved:

Ron Walcott
Interim Dean of the Graduate School
The University of Georgia
August 2020

ACKNOWLEDGEMENTS

I would like to express my deepest and sincere gratitude to my advisor and mentor Dr. Michael Johnson for his continuous guidance, support, and encouragement throughout my graduate studies and beyond. It was a great honor and privilege to work and study under his guidance. I would also like to thank my advisory committee, Dr. Michael Adams and Dr. Todd Harrop, for thoughtful suggestions, insightful comments, and kind support throughout my graduate studies.

I wish to thank my colleagues and friends Ashley Holland, Soshawn Blair, and Tamanna Azam, for their constant help and support. I will cherish our friendship and the memorable time I have spent with you.

Words cannot express my gratitude for my family especially my beloved mother for her infinite and unconditional love, support, sacrifices, and prayers. I would like to wholeheartedly express my deepest gratitude to my loving, understanding, and caring husband, Badie Khaleghian, for his continuous support and encouragement throughout my graduate studies.

TABLE OF CONTENTS

Page

LIST OF TABLES

Page

LIST OF FIGURES

Page

CHAPTER ONE

INTRODUCTION AND LITERATURE REVIEW

Background

Iron-sulfur [Fe-S] clusters are one of the most ancient, ubiquitous and versatile types of biological metal containing cofactors (1,2). Proteins containing [Fe-S] clusters arose early in evolution likely by spontaneous formation of [Fe-S] clusters on polypeptides or by incorporation of preformed cubane [4Fe-4S] cluster into polypeptides, when the earth was anaerobic and rich in iron and sulfur (3). In general, the high level of iron and sulfur on Earth, their ability to readily assemble into clusters with tunable redox activity, and the pervasiveness of [Fe–S] clusters across all domains of life, support the hypothesis that [Fe–S] clusters were among the first protein bound-prosthetic groups (4). Certain metabolic pathways, e.g. glucose oxidation, of primitive archaebacteria and thermophiles that rely on [Fe-S] clusters provide evidence in support of evolutionary role of [Fe-S] clusters (1,5). [Fe-S] clusters are primarily integrated into proteins through coordination of the iron ions by cysteine residues, although alternative ligands such as histidine, aspartate, arginine, and serine are also known (2,6). Besides their primarily role of mediating biological electron transfer, [Fe-S] clusters can function in many diverse roles including structural, redox and non-redox catalysis, regulation of gene expression and enzymatic activity, iron or cluster storage, sulfur donor, disulfide reduction, radical generation, and DNA replication and repair (7-9). Moreover, major advances in understanding [Fe-S] cluster biogenesis have led to

the identification of numerous component proteins and provided insight into the molecular mechanisms of [Fe-S] cluster assembly (6).

Structures, redox, and electronic properties of biological [Fe-S] clusters

[Fe-S] clusters are structurally and functionally diverse cofactors that are found in all domains of life (10). The most common types of Fe-S centers are rubredoxins-type centers with Fe tetrahedrally ligated by four cysteinates, and clusters with cores composed of [2Fe-2S] rhombs, [4Fe-4S] cubes, and [3Fe-4S] cubes devoid of one Fe atom. Tetrahedral coordination about each cluster Fe is most commonly completed by cysteinate ligands (8), see Figure 1.1.

Rubredoxin centers, $Fe(SCys)_4$, lack inorganic sulfides therefore they are not strictly [Fe-S] clusters. However, they are included in Fe-S protein family in which non-heme Fe is coordinated by cysteinates and/or inorganic sulfides. Mononuclear Fe center with tetrahedral cysteine-S coordination share fundamental structural, electronic, and magnetic properties with [Fe-S] clusters therefore are often regarded as the simplest type of Fe-S centers, (see Figure 1.1.A). Rubredoxins are low molecular weight electron transfer proteins that undergo one- electron redox cycling between high-spin (S = 5/2) ferric and high-spin (S = 2) ferrous, with midpoint potentials ranging from +300 to − 87 mV (11,12). Flavorubredoxins are the most recently discovered members of this family. In *E. coli* they participate in nitric oxide reductase activity via electron transfer with midpoint redox potential of −240 mV (13,14).

Based on structural and electronic properties as well as the mechanisms of [Fe-S] cluster biogenesis, [2Fe-2S] clusters can be considered as the basic building block of all types of [Fe-S] clusters. The cubane [4Fe-4S] cluster can be visualized as two [2Fe-2S] clusters fused together and the [3Fe-4S] cluster as a cubane [4Fe-4S] cluster with loss of one Fe. Similarly, clusters with

higher nuclearity such as the [8Fe-7S] nitrogenase P-cluster can be visualized as two [4Fe-4S] clusters fused together and sharing a μ_6-S^{2-} (8), as shown in Figure 1.1.F.

[2Fe-2S] clusters are the simplest form of [Fe-S] clusters and are widely distributed throughout all kingdoms of life (15). Generally, [2Fe-2S] clusters have complete cysteinyl ligation in which each Fe atom is tetrahedrally coordinated by two μ_2-bridging sulfides and two cysteinate ligands (see Figure 1.1.B). [2Fe-2S] clusters function as electron carriers by cycling between $[2Fe\text{-}2S]^{2+,+}$ core oxidation states (12). The redox potential of all-cysteinyl-ligated $[2Fe\text{-}S]^{2+,+}$ couple ranges from +100 to −460 mV (16). The redox properties of [Fe-S] clusters depend on several factors such as protein environment, cluster ligation and solvent exposure, extent of hydrogen bonding interactions involving bridging sulfides and cysteinate S, and the extent of valence delocalization (17). Consequently, the redox properties of the [Fe-S] clusters are altered when Fe atoms are not all ligated by cysteine. For example, the Rieske-type [2Fe-2S] that are coordinated by two cysteinate ligands to one Fe and two histidyl ligands to the reducible Fe site have higher redox potential range from +380 to −150 mV due to the presence of more electropositive histidyl ligands (18). The redox potential of $[2Fe\text{-}2S]^{+,0}$ couple is ~ 1.0 V lower than the $[2Fe\text{-}2S]^{2+,+}$ couple (19) and hence not physiologically relevant. The spectroscopic and electronic properties of [Fe-S] clusters are dictated by intracluster magnetic interactions and the extent of valence delocalization. In the fully oxidized $[2Fe\text{-}2S]^{2+}$ and fully reduced $[2Fe\text{-}2S]^{0}$ clusters, two high spin ferric (S = 5/2) and two high spin ferrous (S = 2) ions are antiferromagnetically coupled, respectively, to yield EPR silent diamagnetic S = 0 ground states, see Figure 1.2. Upon one electron reduction, the resulting $[2Fe\text{-}2S]^{+}$ cluster can be valence-localized with S = 1/2 ground state due to antiferromagnetic coupling, or valence delocalized with S = 9/2 ground state due to ferromagnetic coupling between high-spin Fe^{2+} (S = 2) and high-spin Fe^{3+} (S = 5/2) (16,17), see Figure 1.2.

The majority of [3Fe-4S] clusters are cubane-type which are best visualized as a [4Fe-4S] cluster with loss of one Fe atom. In fact, many cubane-type [3Fe-4S] clusters are artifacts of oxidative degradation of [4Fe-4S] clusters (20). However, [3Fe-4S] clusters with a linear arrangement of irons have also been reported (21-25). All biological cubane [3Fe-4S] clusters are ligated exclusively by cysteine residues with tetrahedral coordination of each Fe atom. The redox potential of physiologically relevant cubane $[3Fe\text{-}4S]^{+,0}$ couple ranges between +90 and −460 mV. In oxidized cubane $[3Fe\text{-}4S]^{+}$ clusters, antiferromagnetic coupling of the three high-spin $S = 5/2$ ferric sites result in a $S = 1/2$ ground state, see Figure 1.2. The $S = 2$ ground state of one-electron-reduced cubane $[3Fe\text{-}4S]^{0}$ cluster arises from antiferromagnetic coupling between a $S = 9/2$ valence-delocalized $Fe^{2+}Fe^{3+}$ pair and a $S = 5/2$ valence-localized high spin ferric site (20), see Figure 1.2. The $[3Fe\text{-}4S]^{2-}$ cluster is accessible, but is unlikely to be physiologically relevant, as the midpoint potential of the $[3Fe\text{-}4S]^{0,2-}$ pair is ~ −700 mV at pH 7 and is strongly pH dependent, requiring the uptake of three protons (26,27). Linear [3Fe-4S] clusters have also been observed in both synthetic and biological studies, but have yet to shown to be physiologically relevant (24,25,28,29). Fe atoms in the linear [3Fe-4S] clusters reside in a tetrahedral environment of sulfur atoms with cysteinyl-S completing the coordination at the two terminal Fe sites (22,23). This cluster has only been identified in the $[3Fe\text{-}4S]^{+}$ oxidation state, which has a $S = 5/2$ ground state as a result of spin-coupling of the three $S = 5/2$ high-spin ferric sites, with the spin of the central Fe site being antiparallel to the spin of two terminal Fe sites (22,23). The coupling is highly asymmetric, with the central Fe having strong spin-coupling to both terminal Fe sites and weak exchange interaction between the two terminal Fe sites (22,23). Presence of this type of cluster in carrier proteins such as monothiol glutaredoxins (21), suggest a potential role for Grxs in

scavenging linear $[3Fe\text{-}4S]^{+}$ clusters released under oxidative stress conditions due to protein unfolding.

[4Fe-4S] clusters are the most common form of [Fe-S] clusters with a wide range of functions from electron transfer to enzyme catalysis and DNA repair (2,21,30-33). Most of biological [4Fe-4S] clusters have complete cysteinyl-S ligation. However, there are some examples of atypical [4Fe-4S] clusters with novel ligation. For instance, in some ferredoxins one of the Fe sites of the [4Fe-4S] cluster is ligated with an aspartate (34). In (de)hydratases and radical-SAM enzymes, substrate coordinates at a unique Fe site (35-39). [4Fe-4S] clusters exhibit a wide range of redox potential of +500 to −700 mV depending on the core oxidation state which can be 3+, 2+, 1+, or 0. The high-potential iron-sulfur protein (HiPIP)-type centers cycle between $[4Fe\text{-}4S]^{3+,2+}$ couple, with redox potentials ranging from +500 to +50 mV, since reduction involves an electron being added to a diferric pair to make a valence-delocalized mixed-valence pair (2,40). The redox potential of $[4Fe\text{-}4S]^{2+,+}$ couple is lower and ranges between +100 to −700 mV, as the electron is added to one of the two valence delocalized pairs to yield a diferrous pair. The extent of backbone NH---S hydrogen bonding and the extent of solvent exposure play key roles in determining the redox potential and which redox couple is used by specific [4Fe-4S] clusters (41). The [4Fe-4S] cluster in the nitrogenase Fe-protein can act as two-electron donor and is stable in three redox states 2+, 1+, and 0 (42-44). The ground state electronic and magnetic properties of [4Fe-4S] clusters have been interpreted in terms of antiferromagnetic couplings involving one or two valence-delocalized [2Fe-2S] building-block units with $S = 9/2$, see Figure 1.2. The $S = 1/2$ ground state for $[4Fe\text{-}4S]^{3+}$ clusters has been interpreted as a result of antiferromagnetic coupling between a $S = 5$ $Fe^{3+}Fe^{3+}$ pair and a $S = 9/2$ valence-delocalized $Fe^{3+}Fe^{2+}$ pair. $[4Fe\text{-}4S]^{3+}$ clusters generally exhibit axial EPR signals with $g_{ave} > 2.0$. $[4Fe\text{-}4S]^{2+}$ clusters have the $S = 0$ EPR-silent

ground states as a result of antiferromagnetic coupling between two S = 9/2 valence-delocalized $[2Fe\text{-}2S]^{+}$ fragments. Antiferromagnetic coupling of a S = 4 $Fe^{2+}Fe^{2+}$ pair and a S = 9/2 valence-delocalized $Fe^{3+}Fe^{2+}$ pair results in the S = 1/2 ground-state spin of $[4Fe\text{-}4S]^{+}$ cluster that usually exhibit a rhombic EPR signal with g_{ave} < 2.0. This EPR signal is fast relaxing and broadens significantly at temperatures above 30 K, which makes them distinguishable from similar EPR signal of S = 1/2 $[2Fe\text{-}2S]^{+}$ clusters (16). EPR and Mössbauer studies of the nitrogenase Fe protein revealed a S = 4 ground state for the $[4Fe\text{-}4S]^{0}$ cluster (43). The all-ferrous $[4Fe\text{-}4S]^{0}$ cluster has also been observed in a 2-hydroxylglutaryl-CoA dehydratase from *Acidaminococcis femrntans* (45-48). However, this redox state has rarely been observed in Nature. [4Fe-4S] clusters are not stable in the all-ferric 4+ oxidation state. Consequently, they are susceptible to intracellular oxidative degradation by O_2, O_2^{-}, and O_2^{2-} with concomitant loss of function (3,49,50).

Cluster conversions

Synthetic and protein-bound [Fe-S] clusters have a remarkable facility for undergoing cluster conversions in accord with their modular structures (51). In addition, they undergo ligand exchange and oxidative degradation reactions that are biologically significant (51). For instance, in regard to [Fe-S] cluster assembly, cluster interconversion can provide the means for generating the desired cluster type without resorting to *de novo* cluster synthesis. These frequent degradation and conversions into other structures are in response to changes in environment or intracellular conditions, such as exposure to O_2 or NO, chemical oxidants, reductants, denaturants, or changes in pH. As a response to external stimuli, the cluster conversions are often accompanied by changes in protein structures that can provide a means for regulating enzymatic activity or gene expression. The most common types of cluster transformations are interconversion between cubane [4Fe-4S] and [3Fe-4S] clusters, and between [4Fe-4S] and [2Fe-2S] clusters, see Figure 1.3. Cluster

interconversions can be illustrated by aconitase as it can accommodate a variety of different [Fe-S] clusters. Aconitase is a member of dehydratase family and catalyzes the reversible isomerization of citrate to isocitrate. In its active form, aconitase contains a $[4Fe\text{-}4S]^{2+,+}$ cluster with a non-cysteinyl ligation at a unique Fe site that is ligated by water or a hydroxyl group (52). Air exposure results in conversion of the active form of enzyme to inactive form by conversion of the $[4Fe\text{-}4S]^{2+,+}$ cluster to cuboidal $[3Fe\text{-}4S]^{+}$ cluster by oxidative removal of the unique Fe (53). The catalytically functional $[4Fe\text{-}4S]^{2+}$ cluster is readily reformed under reducing conditions because the $[3Fe\text{-}4S]^{0}$ cluster avidly incorporates ferrous ion, see Figure 1.3. Another remarkable cluster conversion involving swapping of ligated cysteinyl ligands occurs when the cuboidal $[3Fe\text{-}4S]^{+}$ form of inactive aconitase is treated with urea or is exposed to pH > 9. Under these conditions the cuboidal $[3Fe\text{-}4S]^{+}$ clusters are transformed to linear $[3Fe\text{-}4S]^{+}$ clusters, see Figure 1.3 (51). This process requires major rearrangement of the protein backbone whereby two of the original cysteine ligands of the cubane $[3Fe\text{-}4S]^{+}$ cluster are retained and two more remote cysteines are recruited in order to complete the ligation (23,51,54). By reducing the linear $[3Fe\text{-}4S]^{+}$ cluster in the presence of Fe^{2+} and lowering pH, the active $[4Fe\text{-}4S]^{2+,+}$ cluster can be reformed (23), see Figure 1.3.

Functions of biological [Fe-S] clusters

The chemical reactivity of Fe and S, together with variations in the composition, redox potential, oxidation state, physical accessibility of the cluster and effects of the local protein environments form the basis of [Fe-S] clusters various functions in biology (55). In spite of their inherent susceptibility to oxidation and degradation, [Fe-S] clusters have crucial functional roles because of their ability to accept or donate electrons, bind or interact with electron-rich substrates, and stabilize specific protein conformations (30). The most common function of [Fe-S] clusters is

electron transfer, due to the availability of multiple oxidation states and a wide range of redox potentials. Therefore, [Fe-S] clusters can serve as excellent donors and acceptors of electrons in a variety of biological reactions (6). Several large protein complexes and multiprotein electron relay systems take advantage of the redox properties of [Fe-S] clusters to conduct electron from one active site to another (56). Some examples include bacterial and mitochondrial respiratory complexes I-III, photosystem I, nitrogenase and hydrogenases (6).

The ability of [Fe-S] clusters to bind and activate substrates is central to their role in enzyme catalysis (6). Aconitase is a classic example of the ability of [Fe-S] clusters to catalyze non-redox reactions. A unique non-protein-coordinated Fe of a [4Fe-4S] cluster acts as a Lewis acid to promote sequential water abstraction and insertion reactions on a bound substrate to catalyze the conversion of citrate to isocitrate (32,52). A similar approach is also used to catalyze redox reactions in the large family of radical S-adenosylmethionine (SAM) enzymes that catalyze a diverse range of radical reactions involved in biosynthesis of numerous DNA precursors, vitamins, cofactors, and antibiotics (36,57). The redox-active [4Fe-4S] cluster in radical-SAM enzymes binds SAM at a unique Fe site in order to facilitate the reductive cleavage of SAM to yield highly reactive 5'-deoxyadenosyl radical that subsequently generates a substrate or protein radical by hydrogen abstraction to initiate radical reactions. A different approach to facilitating substrate binding by [Fe-S] clusters is by incorporating a heterometal site into [Fe-S] cluster at active site of the enzymes. One example is the Ni-requiring CO dehydrogenase. This enzyme catalyzes the reversible oxidation of CO to CO_2. The [Ni-4Fe-5S] active site can be visualized as a [3Fe-4S] cluster covalently attached to a μ_2-S-bridged NiFe fragment by the three μ_3-bridging S atoms with the square planar Ni site being the CO binding site (58). Another method that incorporates [Fe-S] clusters in enzyme active sites is attachment of a substrate-binding metal site

to a unique Fe site of [4Fe-4S] cluster via a bridging cysteinyl ligand. In this case, the [4Fe-4S] cluster provides a conduit for direct electron transfer to the active site. Examples include sulfite and nitrite reductase, which use a siroheme as the substrate binding site (59,60) and acetyl-CoA synthase that uses a dinickel center to facilitate CO insertion into a Ni-CH_3 bond to form an acetyl group (61-63).

The third general role of [Fe-S] clusters is sensing intracellular or environmental conditions to regulate gene expression (6). Some examples include the bacterial transcription factor FNR, IscR, and SoxR, that sense, O_2, [Fe-S] clusters and NO/superoxide, respectively. The O_2-induced $[4Fe\text{-}4S]^{2+}$ to $[2Fe\text{-}2S]^{2+}$ cluster conversion in FNR, presence of a $[2Fe\text{-}2S]^{2+}$ cluster in IscR, and the redox state of the $[2Fe\text{-}2S]^{2+,+}$ cluster in SoxR, control the switch between activating and repressed states of these regulatory proteins (6,64,65). The mammalian cytosolic iron regulatory protein 1 (IRP1) is a classic example of post-transcriptional regulation of gene expression by an [Fe-S] cluster. Under iron-replete conditions, IRP1 holds a [4Fe-4S] cluster and acts as an aconitase catalyzing the reversible isomerization of citrate into isocitrate. Under iron depleted conditions, the protein loses its labile cluster, which enables binding to iron responsive elements (IREs) in specific stem-loop structures of the messenger RNAs of proteins involved in iron uptake, storage, and distribution of iron in the cell (52,66-69). Binding of apo-IRP1 to 3'-located IREs protects mRNAs from nucleolytic degradation, leading to increased translation, whereas association with 5'-located IREs blocks translation by inhibiting ribosome scanning to the start AUG codon (6).

Disulfide reduction is another function of some $[4Fe\text{-}4S]^{2+}$ cluster-containing enzymes. Disulfide reduction is usually achieved by a family of flavoproteins using NADPH as two electron-donor (70). However, this reaction is performed by some $[4Fe\text{-}4S]^{2+}$ clusters-containing enzymes

via two sequential one-electron steps and novel site-specific cluster chemistry. For instance, ferredoxin-thioredoxin reductase (FTR) is a plant enzyme catalyzing the light-mediated reduction of the thioredoxin disulfide. The active site contains a $[4Fe\text{-}4S]^{2+}$ cluster and an adjacent asymmetrically disposed redox-active disulfide (71,72). One-electron reduction results in two-electron reduction of the FTR disulfide, coupled with one-electron oxidation of the $[4Fe\text{-}4S]^{2+}$ cluster, to yield a $[4Fe\text{-}4S]^{3+}$ cluster intermediate with a unique Fe site ligated by two cysteine residues and formation of mixed FTR/thioredoxin disulfide (71-73). A second one-electron reduction by ferredoxin reduces the $[4Fe\text{-}4S]^{3+}$ cluster, which results in restoration of the FTR disulfide and formation of reduced thioredoxin.

In many cases the precise role of [Fe-S] clusters is still unknown, and it is possible that some simply play structural roles (6). Such a function was originally proposed for [4Fe-4S] cluster-containing enzymes involved in DNA metabolism and repair. However, recent studies have demonstrated a redox role for the [4Fe-4S] clusters in locating DNA lesions that need to be repaired (30). Glycosylases are a diverse family of enzymes that recognize and remove damage bases in DNA (30). Several DNA glycosylases containing [4Fe-4S] clusters are involved in base excision repair such as adenine-DNA glycosylase (MutY), thymine-DNA, and endonuclease III. These enzymes have redox-active $[4Fe\text{-}4S]^{3+,2+}$ clusters only when bound to DNA (74-76). DNA-mediated cluster redox activity locates damaged DNA bases by mediating electron transfer through the π-stacked base pairs (76).

[Fe-S] cluster storage proteins are often encoded in operons of enzymes with large demand for [4Fe-4S] clusters such as hydrogenases and formylmethanofuran dehydroganse. For example, polyferredoxins in methanogenic archaea store up to 14 [4Fe-4S] clusters in 7 tandemly repeated 8Fe ferredoxin-like domains (8). Since [Fe-S] clusters are known to be assembled on scaffold

proteins prior to insertion into apo-proteins, it is likely that 8Fe Fds and polyferredoxins provide temporary storage site for [4Fe-4S] clusters to be used in protein maturation. In addition, a novel protein from hyperthermophilic anaerobic archaeon *Pyrococcus furiosus* has recently been discovered that stores Fe and S as an inorganic anionic linear polymer known as thioferrate, $(FeS_2^-)_n$, a structure previously unknown in biology (77). Iron sulfur storage protein A (IssA) forms nanoparticles reaching 300 nm in diameter. The purified nanoparticles appear to form from 20- nm diameter spheres, each containing ~ 6,400 Fe atoms, ~ 12,800 S atoms and ~ 170 IssA monomers (77). *In vitro*, the stored thioferrate core of IssA has been shown to provide the iron and sulfide for assembly of $[4Fe\text{-}4S]^{2+}$ cluster on apo-*Pf* Fd in the presence of DTT. *P. furiosus* almost exclusively contains [4Fe-4S] cluster-containing [Fe-S] proteins. Therefore, it appears that *P. furiosus* stores excess Fe and S, when they are highly abundant, in the form of thioferrate bound to IssA that can subsequently be mobilized for assembly of [4Fe-4S] clusters which are widely used in this organism (77). The mechanism by which the [Fe-S] cluster is assembled when using thioferrate as source of iron and sulfide is discussed in detail in Chapter 2.

Biogenesis of [Fe-S] clusters

In vitro [Fe-S] clusters can be assembled spontaneously from iron and sulfide ions under reducing and anaerobic condition. However, *in vivo* under partial oxidizing condition (78), this process is unlikely due to the cellular toxicity associated with free iron and sulfide ions in the concentrations needed for spontaneous Fe-S protein maturation (79-82). In addition, [Fe-S] clusters are often degraded rapidly by molecular oxygen and free iron ions produce reactive oxygen species via Fenton chemistry that can cause irreversible molecular damage, ultimately leading to cell death (79,80,83). Consequently, despite the relative structural and chemical simplicity of [Fe-S] clusters, their biosynthesis in living cells is a highly complex and coordinated process (6). As a

result, virtually all known forms of life have evolved complex and specialized machineries to orchestrate the safe, efficient, and specific biogenesis of [Fe-S] clusters and their delivery to proteins that are functionally dependent on these prosthetic groups (56). Three distinct systems for [Fe-S] cluster biosynthesis have been identified in prokaryotes: the nitrogen-fixation (NIF), the iron-sulfur cluster (ISC), and the sulfur-utilization factor (SUF) machineries. The ISC machinery produces the majority of [Fe–S] clusters needed for cellular activity, whereas the NIF and SUF systems play specialized roles in the maturation of proteins involved with nitrogen fixation and under oxidative stress conditions, respectively (8,84,85). In eukaryotes, the biosynthesis of [Fe-S] clusters are performed by two main multi-protein machineries, the ISC machinery which is localized in mitochondria and the cytosolic iron-sulfur cluster assembly (CIA) machinery which is localized in the cytosol (6). Plants also use the SUF machinery for [Fe-S] assembly in plastids. Despite the differences among the various biogenesis systems found in bacteria and eukaryotes, all the systems appear to have a general scheme for [Fe-S] cluster assembly comprising of two main steps. First, [Fe-S] clusters are assembled on a scaffold protein by a multiprotein complex containing a cysteine desulfurase. Second, the transfer of the assembled cluster to either a carrier protein or an apo acceptor protein. Each of these steps involve participation of several proteins and cofactors and coordinated reactions. The prokaryotic ISC system has served as a useful model for understanding [Fe-S] cluster assembly and delivery (86). Proteins associated with [Fe–S] cluster biogenesis play vital physiological roles, and the mechanisms of their biosynthesis have been investigated intensively (83). The proteins encoded by bacterial *isc* operon are IscR, IscS, IscU, IscA, HscB, HscA, Fdx, and IscX. IscR is a regulatory protein which in its cluster-bound form is responsible for blocking the transcription of all the downstream *isc* genes (65). The main two steps

of [Fe-S] cluster biogenesis by the bacterial ISC system are summarized below and shown in Figure 1.4

***De novo* [Fe-S] cluster assembly**

Scaffold proteins provide the platform for the biosynthesis of [Fe-S] clusters. IscU serves as the scaffold protein on which clusters are formed and transferred intact to various carriers or apo-[Fe-S] proteins (86,87). IscU has one of the most conserved sequence motifs in nature. It contains three highly conserved and physiologically essential cysteine residues that provide ligation to [Fe-S] clusters, a conserved histidine residue, and a conserved 'LPPVK' (Leu-Pro-Pro-Val-Lys) motif (8). Mass spectrometry studies have shown that any of the conserved cysteines on IscU can accept a sulfane sulfur implying that sulfur transfer from IscS to IscU does not involve a specific cysteine on IscU (88). However, this result may also be rationalized by more recent NMR studies, which show that apo-IscU is a metamorphic protein that can adopt two different conformational states in solution: a largely structured S-state conformation and a more dynamic and partially unfolded D-state conformation that interconvert on the order of 1 s^{-1} under physiological conditions (86,87)(89). This conformational flexibility enables IscU to be involved in a wide verity of interactions. Moreover, the conformational equilibrium is maintained with a subtle balance that can be altered by various conditions. For instance, binding of Zn^{2+}, Fe^{2+}, or a [2Fe-2S] cluster stabilizes the S-state (86,90,91). More interestingly, several proteins known to bind IscU prefer either the S- or D-state. The S-state is preferred by IscX and HscB, while the D-state is preferred by IscS and HscA (86,89,92,93). *In vitro* studies of the time-course of cysteine desulfurase-mediated cluster reconstitution on *Av* IscU have revealed sequential formation of homodimeric IscU containing one $[2Fe\text{-}2S]^{2+}$, two $[2Fe\text{-}2S]^{2+}$, and one $[4Fe\text{-}4S]^{2+}$ clusters via two-electron reductive coupling (94,95). The one $[2Fe\text{-}2S]^{2+}$ cluster-bound IscU is stable and resistant

to iron chelators. While one of the clusters in two $[2Fe\text{-}2S]^{2+}$ cluster-containing IscU is labile and can be selectively removed by EDTA. In addition, the resulting $[4Fe\text{-}4S]^{2+}$ cluster is oxygen sensitive and rapidly degrades to a single $[2Fe\text{-}2S]^{2+}$ cluster (95).

[Fe-S] cluster assembly critically depends on the function of a cysteine desulfurase as a sulfur donor (6). In bacteria, cysteine desulfurase IscS serves as a sulfur source for cluster assembly. The crystal structures of several desulfurases are known and show a dimeric two-domain protein. One domain harbors the pyridoxal-phosphate-binding site and the smaller domain contains the active-site cysteine (96,97). The homodimeric PLP-dependent IscS converts L-cysteine to L-alanine with formation of a cysteine persulfide on a flexible side chain, which can be transferred to a cysteine on IscU. IscS forms a heterotetrameric complex with IscU in which one IscU molecule is bound to each subunit of the IscS dimer (86,87). Mass spectrometry studies have provided evidence for multiple transfers of S^0 from IscS to form polysulfides on IscU (98).

Electrons are required for reduction of S^0 (present in cysteine) to sulfide (present in [Fe-S] cluster) (6). A reduced 2Fe ferredoxin (Fdx) and the Fe^{2+} substrate provide the electrons for reducing S^0 to S^{2-} in the initial $[2Fe\text{-}2S]^{2+}$ cluster assembly on IscU. Fdx may also be the reductant for the reductive coupling process in which two $[2Fe\text{-}2S]^{2+}$ clusters dimerize at the interface of the IscU to form a $[4Fe\text{-}4S]^{2+}$ cluster (95). Fdx has a $[2Fe\text{-}2S]^{2+,+}$ cluster ($E_m = -344$ mV *A. vinelandii* Isc Fdx) coordinated by four conserved cysteine residues and has an essential role in the maturation of Fe-S proteins as *ΔIscFdx* mutants are lethal (99). Studies in higher organisms have shown that depletion of the IscFdx homologue in yeast (Yah1p) has a dramatic decrease in mitochondrial Fe-S protein activities and results in accumulation of iron in the mitochondria (100). *In vitro* studies have shown that the $[2Fe\text{–}2S]^{2+}$ cluster assembled on IscU can be transferred to the apo-Fdx (101-103), implying that apo Fdx is one of the target proteins for maturation by [2Fe-

2S]-IscU. Interestingly, *in vivo* studies carried out in yeast revealed a mutual requirement of Isu1p and Yah1p for their conversion from apo to holo proteins that are essential for the function of the entire ISC system (104). Iscu1p depends on Yah1p as a source of electron for [Fe-S] cluster assembly, while Yah1p requires Iscu1p as a provider of its native [2Fe-2S] cluster (104). Therefore, Fdx in the ISC system is an unusual protein in that it is required for its own maturation.

Fe^{2+} rather than Fe^{3+} is required for $[2Fe\text{-}2S]^{2+}$ cluster assembly on IscU, but the identity of a specific Fe^{2+} donor has yet to be definitively established (6). The best candidates for a Fe^{2+} donor in bacteria are frataxin (CyaY) whose gene is external to the *isc* operon and IscX (83). IscX is a small acidic protein encoded by the last gene in the *isc* operon, which has been shown to bind Fe^{2+} with higher affinity than Fe^{3+}, interact with IscS, and participate in IscX-IscU-IscS ternary complex. The functional properties of IscX is currently unclear, but it has been suggested that IscX serves as both an iron donor to IscU and a regulator of IscS cysteine desulfurase activity, since it can suppress the IscS activity in the presence of IscU (92). The exact physiological role of the acidic bacterial frataxin (CyaY) is also not clear. CyaY/frataxin has weak Fe^{2+} ion binding, but can form a functional ternary complex with IscU/IscS in bacteria and Isu1/Nfs1in yeast (105-108) suggesting it may provide a negatively charged channel for Fe^{2+} ion entry into the IscU-IscS complex. In addition, CyaY/frataxin has been shown to be an allosteric regulator of cysteine desulfurase activity (83).

Transfer of the assembled [Fe-S] cluster

The second step of [Fe-S] cluster biogenesis comprises transfer of the cluster assembled on IscU to carrier proteins or to terminal acceptor proteins (6). The overall process of cluster transfer is specifically assisted by a dedicated molecular chaperone system involving HscA and co-chaperone HscB proteins that are both encoded within bacterial *isc* operon (109,110). Gene

knockout studies *in vivo* have demonstrated that both HscA and HscB and their eukaryotic yeast homologs (Ssq1 and Jac1) have crucial roles in the maturation of Fe-S proteins in both prokaryotic and eukaryotic organisms (111-115). HscA and HscB are closely related to the DnaJ and DnaK family of chaperone proteins, which are involved in general protein folding and unfolding. However, unlike DnaJ/K, HscA/B have only one substrate, IscU. HscA/Ssq1 can interact with both apo and holo form of IscU and binds to the highly conserved LPPVK motif (116-122), located adjacent to cluster binding site of IscU (90,123). This binding is facilitated by co-chaperon HscB/Jac1 which escorts IscU to HscA/Ssq1 (116). HscA and its eukaryotic homologs have low intrinsic ATPase activity that is stimulated by co-chaperone HscB. Binding of the [2Fe-2S]-IscU-HscB to HscA enhances the ATPase activity nearly 1000-fold (116). Consequently, in the presence of the acceptor protein, ATP hydrolysis supplies the energy to break the first CysS-Fe bond, initiating a series of bond-making/bond breaking events that, coupled with IscU conformational changes, results in transfer of the intact $[2Fe\text{-}2S]^{2+}$ cluster from IscU to the acceptor protein at a greatly accelerated rate (110).

The bacterial *isc* operon encodes an A-type carrier (ATC) protein, IscA, which like the IscU family has three conserved cysteines. The physiological role of IscA has been the subject of much debate since *in vitro* studies have shown that it is capable of binding $Fe^{2+/3+}$, $[2Fe\text{-}2S]^{2+}$ or $[4Fe\text{-}4S]^{2+}$ clusters in its dimeric form (124,125). However, gene knockout studies indicate that ATC proteins play a specific role in the maturation of [4Fe-4S] cluster-containing proteins in both prokaryotic and eukaryotic organisms (126,127). Moreover, *in vitro* studies have shown that ATC proteins can reversibly interconvert between $[2Fe\text{-}2S]^{2+}$ and $[4Fe\text{-}4S]^{2+}$ cluster-bound forms (128), suggesting a role in facilitating two-electron reductive coupling of two $[2Fe\text{-}2S]^{2+}$ clusters to form a $[4Fe\text{-}4S]^{2+}$ cluster that can be used for maturation of apo [4Fe-4S]-proteins.

Rapid, ATP-driven $[2Fe\text{-}2S]^{2+}$ cluster transfer from bacterial $[2Fe\text{-}2S]^{2+}$-IscU to apo-Grx5 in the presence of HscA and HscB (129), and evidence for complex formation between yeast analogs of HscA and monothiol glutaredoxins (130), suggest a physiological role for monothiol glutaredoxins (Grxs) as primary acceptors for the $[2Fe\text{-}2S]^{2+}$ clusters assembled on IscU (129,131). Grxs exist as apo monomeric forms and dimeric forms containing a subunit-bridging $[2Fe\text{-}2S]^{2+}$ cluster with each Fe coordinated at the subunit interface of a homodimer by the cysteinates of GSH and the rigorously conserved CGFS motif (132-134), see Figure 1. 5. The role of Grxs as $[2Fe\text{-}2S]^{2+}$ cluster carrier proteins is now well established. For example, monothiol Grxs are capable of delivering $[2Fe\text{-}2S]^{2+}$ clusters to terminal acceptor proteins such as apo ISC Fdx via intact cluster transfer at much faster rates than $[2Fe\text{-}2S]^{2+}$ cluster transfer from IscU in the presence of HscA/HscB co-chaperones and MgATP (129). Moreover, Grxs have been shown to be capable of rapid, unidirectional, intact, and quantitative $[2Fe\text{-}2S]^{2+}$ cluster transfer to A-type carrier (ATC) proteins, which mediate two-electron reductive coupling of two $[2Fe\text{-}2S]^{2+}$ clusters to form $[4Fe\text{-}4S]^{2+}$ clusters, that are transferred intact to apo Fe-S proteins or $[4Fe\text{-}4S]^{2+}$ cluster carrier proteins. Coupled with *in vivo* evidence for interactions between monothiol Grxs and ATC proteins, these results imply that these two classes of proteins are partners in cellular [Fe-S] cluster trafficking (131).

Human diseases associated with defects in [Fe-S] cluster biogenesis

The importance of [Fe-S] proteins for human health is documented by an increasing number of diseases associated with defects in [Fe-S] cluster biogenesis proteins (6). This is not surprising considering the essential roles played by [Fe-S] clusters in respiration and a wide range of metabolic processes (55). Minor defects in genes involved with [Fe-S] cluster assembly or in the Fe metabolism pathway can cause severe physiological disorders due to imbalances in cellular

Fe content. The most well-known disease linked with impaired [Fe-S] cluster biogenesis is Friedrich's ataxia (FRDA). FRDA is a neurodegenerative disease characterized by muscle weakness, dysarthria and heart diseases, loss of tendon reflexes, sensory loss and progressive damage to nervous system (135-138). The cause of FRDA is a mutation in frataxin gene that results in diminished frataxin activity, and accumulation of Fe in mitochondria, subsequently mitochondria Fe overload, oxidation damage and ultimately mitochondria failure (55). Another disease linked with defects of [Fe-S] cluster biogenesis is X-linked sideroblastic anemia with cerebellar ataxia (XLSA/A) that results in coordination difficulties and anemia (137-139) caused from mutations in gene encoding ABCB7, an ATP-binding cassette transporter in the inner mitochondria membrane, which exports a moiety required for extramitochondrial Fe-S protein biogenesis (55,56). Sideroblastic anemia is also associated with mutations in GLRX5, a mitochondrial protein required for [Fe-S] cluster biogenesis that acts as primary acceptor of [2Fe-2S] clusters assembled on ISCU (129,130). Deficiency of GLRX5 causes sideroblastic anemia by specifically impairing heme biosynthesis and depleting cytosolic Fe in human erythroblast (140). GLRX5 knockdown experiments in HeLa cells revealed that mitochondrial iron overload was associated with diminished mitochondrial aconitase activity indicative of a decrease in cytosolic iron levels (140).

Single point mutation in the gene encoding human ISCU (scaffold protein for mitochondria [Fe-S] cluster assembly) results in a hereditary myopathy with exercise acidosis intolerance caused by reduced activities of cluster-containing proteins in respiratory chain and cytosolic aconitase in muscle (141-147). In addition, deficiency in cysteine desulfurase causes phenotypes such as epilepsy, hypotonia, cardiomyopathy, multiple organ failure, and delay in development caused by reduced complex I, II, and III activity in liver and muscle (148). Mutation in *NFU1* gene encoding

mitochondria NFU1 protein that functions in the delivery and maturation of a specific subset of mitochondrial Fe-S proteins (149) results in a fatal infantile encephalopathy leading to death before age of 15 months with symptoms including failure to thrive, pulmonary hypertension, and neurological regression (150). In addition to diseases caused by mutations in genes encoding [Fe-S] proteins, degradation of [Fe-S] clusters by oxidative stress is also linked with several diseases. [Fe-S] cluster degradation is linked with loss of function as well as Fe accumulation in the cell that can lead to deleterious effects given that $OH^{\bullet}$ radicals, produced by reaction of $Fe^{3+,2+}$ with H_2O_2, can damage DNA (151,152). Diseases associated with oxidative stress include neurodegenerative diseases such as amyotrophic lateral sclerosis, Parkinson and Alzheimer, cardiovascular diseases, premature aging diseases, diabetes mellitus, and cancer (153,154).

Understanding both the physiological functions of Fe-S proteins and mechanism of [Fe-S] clusters assembly will undoubtedly enhance our ability to identify and treat disorders of associated with Fe overload and genetic defects associated with [Fe-S] cluster biogenesis proteins (56).

Summary of presented work

Chapter 2 reports spectroscopic characterization of synthesized thioferrate and reveals the mechanism of [Fe-S] cluster assembly using thioferrate as the source of Fe and S. The results show that synthesized thioferrate has similar structure to the protein bound thioferrate in IssA. Furthermore, reconstitutions of different apo Fe-S proteins mediated by thioferrate as the sole source of Fe and sulfide, have demonstrated the ability of thioferrate to reconstitute $[2Fe\text{-}2S]^{2+}$, linear $[3Fe\text{-}4S]^{1+}$ and $[4Fe\text{-}4S]^{2+}$ clusters. The results also suggest that both $[2Fe\text{-}2S]^{2+}$ and $[4Fe\text{-}4S]^{2+}$ clusters are formed by the apo Fe-S protein initially ligating a linear $[3Fe\text{-}4S]^{1+}$ cluster fragment of thioferrate, that subsequently loses one Fe^{3+} and two S^{2-} to form a bound $[2Fe\text{-}2S]^{2+}$ cluster or reductively adds one Fe^{2+} ion to form a bound $[4Fe\text{-}4S]^{2+}$ cluster.

Chapter 3 reports spectroscopic studies on the mechanism of bacterial $[2Fe\text{-}2S]^{2+}$ cluster assembly using the ISC system and *Azotobacter vinelandii* as a model organism. It identifies the Fe^{2+} donor, evaluates the possibility of formation a cysteine persulfide radical anion intermediate on IscS, and establishes the utility of cyclic thiosulfinates as potent inhibitors of IscU Fe^{2+} binding and $[2Fe\text{-}2S]^{2+}$ cluster assembly. UV-visible CD spectroscopy and ICP-MS results demonstrate stoichiometric Fe^{2+} binding to IscX, and provided direct evidence that IscX rapidly transfers a Fe^{2+} ion to IscU. Parallel UV-visible absorption and EPR studies of IscS in the presence of reduced Fdx and L-Cys, and single turnover of IscS in the presence of stoichiometric reduced Fdx, IscU, Fe^{2+}-bound IscX, and L-Cys have confirmed Fdx oxidation, but have failed to identify any sulfur-based radical species on IscS that would generate a trisulfide radical ion on IscU. Spectroscopic studies demonstrate 5-, 6-, and 7-membered cyclic thiosulfinate thiol cross-linkers as potent inhibitors of IscU Fe^{2+} binding as well as spontaneous and cysteine desulfurase-mediated $[2Fe\text{-}2S]^{2+}$ cluster assembly on IscU, that can serve as a mean to explore the mechanism of Fe binding and cluster formation on IscU.

Abbreviations

ATC protein, A-type carrier protein; *Av*, *Azotobater vinelandii*; DTT, dithiothreitol; *E. coli*, *Ec*, *Escherichia coli*; EDTA, ethylenediaminetetraacetic acid; EPR, Electron Paramagnetic Resonance; Fdx, ferredoxin; FNR, fumarate-nitrate reduction protein; FTR, ferredoxin–thioredoxin reductase; Grx, glutaredoxin; GSH, glutathione; HiPIP, High potential iron-sulfur protein; Hsc, heat shock cognate; NMR, nuclear magnetic resonance; *Pf*, *Pyrococcus furiosus*; PLP, pyridoxal phosphate; SAM, S-Adenosyl methionine; *S. cerevisiae*, *Sc*, *Saccharomyces cerevisiae*; Trx, thioredoxin

References

1. Beinert, H. (2000) Iron-sulfur proteins: ancient structures, still full of surprises. *J. Biol. Inorg. Chem.* **5**, 2-15

2. Johnson, M. K., and Smith, A. D. (2011) Iron–sulfur proteins. in *Encyclopedia of Inorganic Chemistry*, John Wiley & Sons, Ltd. pp 2589-2619

3. Imlay, J. A. (2006) Iron-sulphur clusters and the problem with oxygen. *Mol. Microbiol.* **59**, 1073-1082

4. Koonin, E. V., and Martin, W. (2005) On the origin of genomes and cells within inorganic compartments. *Trends Genet.* **21**, 647-654

5. Daniel, R. M., and Danson, M. J. (1995) Did primitive microorganisms use nonhem iron proteins in place of NAD/P? *J. Mol. Evol.* **40**, 559-563

6. Lill, R. (2009) Function and biogenesis of iron–sulphur proteins. *Nature* **460**, 831-838

7. Bandyopadhyay, S., Chandramouli, K., and Johnson, M. K. (2008) Iron–sulfur cluster biosynthesis. *Biochem. Soc. Trans.* **36**, 1112-1119

8. Johnson, D. C., Dean, D. R., Smith, A. D., and Johnson, M. K. (2005) Structure, function, and formation of biological iron-sulfur clusters. *Annu. Rev. Biochem.* **74**, 247-281

9. Beinert, H. (2000) A tribute to sulfur. *Eur. J. Biochem.* **267**, 5657-5664

10. Pandelia, M.-E., Lanz, N. D., Booker, S. J., and Krebs, C. (2015) Mössbauer spectroscopy of Fe/S proteins. *Biochim. Biophys. Acta* **1853**, 1395-1405

11. Ferreira, G. C., Moura, J. J. G., and Franco, R. (1999) Structural versatility of proteins containing rubredoxin-type centers. in *Iron Metabolism*. pp 341-358

12. Zanello, P. (2013) The competition between chemistry and biology in assembling iron–sulfur derivatives. Molecular structures and electrochemistry. Part I. {$Fe(S^{\gamma}Cys)_4$} proteins. *Coord. Chem. Rev.* **257**, 1777-1805

13. Vicente, J. B., and Teixeira, M. (2005) Redox and spectroscopic properties of the *Escherichia coli* nitric oxide-detoxifying system involving flavorubredoxin and its NADH-oxidizing redox partner. *J. Biol. Chem.* **280**, 34599-34608

14. Gomes, C. M., Vicente, J. B., Wasserfallen, A., and Teixeira, M. (2000) Spectroscopic studies and characterization of a novel electron-transfer chain from *Escherichia coli* involving a flavorubredoxin and its flavoprotein reductase partner. *Biochemistry* **39**, 16230-16237

15. Woese, C. R. (1994) There must be a prokaryote somewhere: microbiology's search for itself. *Microbiol. rev.* **58**, 1-9

16. Johnson, M. K., and Smith, A. D. (2005) Iron–sulfur proteins. in *Encyclopedia of Inorganic Chemistry*, 2 Ed., John Wiley & Sons, Ltd. pp 2589-2619

17. Subramanian, S., Duin, E. C., Fawcett, S. E. J., Armstrong, F. A., Meyer, J., and Johnson, M. K. (2015) Spectroscopic and redox studies of valence-delocalized $[Fe_2S_2]^{+}$ centers in thioredoxin-like ferredoxins. *J. Am. Chem. Soc.* **137**, 4567-4580

18. Link, T. A. (1999) The structures of Rieske and Rieske-type proteins. in *Adv. Inorg. Chem.*, 47. pp 83-157

19. Leggate, E. J., Bill, E., Essigke, T., Ullmann, G. M., and Hirst, J. (2004) Formation and characterization of an all-ferrous Rieske cluster and stabilization of the $[2Fe\text{-}2S]^{0}$ core by protonation. *Proc. Natl Acad. Sci. USA* **101**, 10913-10918

20. Fabrizi de Biani, F., and Zanello, P. (2017) The competition between chemistry and biology in assembling iron-sulfur derivatives. Molecular structures and electrochemistry. Part IV. {$[Fe_3S_4](S^{\gamma}Cys)_3$} proteins. *Inorg. Chim. Acta* **455**, 319-328

21. Zhang, B., Bandyopadhyay, S., Shakamuri, P., Naik, S. G., Huynh, B. H., Couturier, J., Rouhier, N., and Johnson, M. K. (2013) Monothiol Glutaredoxins Can Bind Linear $[Fe_3S_4]^{+}$ and $[Fe_4S_4]^{2+}$ Clusters in Addition to $[Fe_2S_2]^{2+}$ Clusters: Spectroscopic Characterization and Functional Implications. *J. Am. Chem. Soc.* **135**, 15153-15164

22. Hagen, K. S., Watson, A. D., and Holm, R. H. (1983) Synthetic routes to iron sulfide (Fe_2S_2, Fe_3S_4, Fe_4S_4, and Fe_6S_9), clusters from the common precursor $[Fe(SC_2H_5)_4]^{2-}$: structures and properties of $[Fe_3S_4(SR)_4]^{3-}$ and $[Fe_6S_9(SC_2H_5)_2]^{4-}$, examples of the newest types of Fe-S-SR clusters. *J. Am. Chem. Soc.* **105**, 3905-3913

23. Kennedy, M. C., Kent, T. A., Emptage, M., Merkle, H., Beinert, H., and Münck, E. (1984) Evidence for the formation of a linear [3Fe-4S] cluster in partially unfolded aconitase. *J. Biol. Chem.* **259**, 14463-14471

24. Richards, A. J. M., Thomson, A. J., Holm, R. H., and Hagen, K. S. (1990) The magnetic circular dichroism spectra of the linear trinuclear clusters $[Fe_3S_4(SR)_4]^{3-}$ in purple aconitase and in a synthetic model. *Spectrochim. Acta* **46**, 987-993

25. Girerd, J. J., Papaefthymiou, G. C., Watson, A. D., Gamp, E., Hagen, K. S., Edelstein, N., Frankel, R. B., and Holm, R. H. (1984) Electronic properties of the linear antiferromagnetically coupled clusters $[Fe_3S_4(SR)_4]^{3-}$, structural isomers of the $[Fe_3S_4]^{1+}$ unit in iron-sulfur proteins. *J. Am. Chem. Soc.* **106**, 5941-5947

26. Duff, J. L. C., Breton, J. L. J., Butt, J. N., Armstrong, F. A., and Thomson, A. J. (1996) Novel redox chemistry of [3Fe−4S] clusters: electrochemical characterization of the all-Fe(II) form of the [3Fe−4S] cluster generated reversibly in various proteins and its spectroscopic investigation in *Sulfolobus acidocaldarius* ferredoxin. *J. Am. Chem. Soc.* **118**, 8593-8603

27. Johnson, M. K., Duderstadt, R. E., and Duin, E. C. (1999) Biological and synthetic $[Fe_3S_4]$ clusters. in *Adv. Inorg. Chem.* pp 1-82

28. Paulsen, H., Ding, X. Q., Grodzicki, M., Butzlaff, C., Trautwein, A. X., Hartung, R., and Wieghardt, K. (1994) Spectroscopic and theoretical studies on a three-iron cluster with linear arrangement. *Chem. Phys.* **90**, 485-490

29. Duderstadt, R. E., Brereton, P. S., Adams, M. W. W., and Johnson, M. K. (1998) Spectroscopic evidence for a new type of $[Fe_3S_4]$ cluster in a mutant form of *Pyrococcus furiosus* ferredoxin. *J. Am. Chem. Soc.* **120**, 8525-8526

30. Fuss, J. O., Tsai, C.-L., Ishida, J. P., and Tainer, J. A. (2015) Emerging critical roles of Fe-S clusters in DNA replication and repair. *Biochim. Biophys. Acta* **1853**, 1253-1271

31. Fontecave, M. (2006) Iron-sulfur clusters: ever-expanding roles. *Nat. Chem. Biol.* **2**, 171-174

32. Flint, D. H., and Allen, R. M. (1996) Iron−sulfur proteins with nonredox functions. *Chem. Rev.* **96**, 2315-2334

33. Broderick, J. B. (2004) Iron-sulfur clusters in enzyme catalysis. *Comprehensive Coordination Chemistry II* **8**, 739-757

34. Gruner, I., Frädrich, C., Böttger, L. H., Trautwein, A. X., Jahn, D., and Härtig, E. (2011) Aspartate 141 is the fourth ligand of the oxygen-sensing $[4Fe\text{-}4S]^{2+}$ cluster of *Bacillus subtilis* transcriptional regulator Fnr. *J. Biol. chem.* **286**, 2017-2021

35. Calzolai, L., Gorst, C. M., Zhao, Z. H., Teng, Q., Adams, M. W., and La Mar, G. N. (1995) ^{1}H NMR investigation of the electronic and molecular structure of the four-iron cluster ferredoxin from the hyperthermophile *Pyrococcus furiosus*. Identification of Asp 14 as a cluster ligand in each of the four redox states. *Biochemistry* **34**, 11373-11384

36. Frey, P. A., Hegeman, A. D., and Ruzicka, F. J. (2008) The radical SAM superfamily. *Crit. Rev. Biochem. Mol. Biol.* **43**, 63-88

37. Nicolet, Y., Amara, P., Mouesca, J.-M., and Fontecilla-Camps, J. C. (2009) Unexpected electron transfer mechanism upon AdoMet cleavage in radical SAM proteins. *Proc. Natl. Acad. Sci.* **106**, 14867-14871

38. Jarrett, J. T. (2003) The generation of 5′-deoxyadenosyl radicals by adenosylmethionine-dependent radical enzymes. *Curr. Opin. Chem. Biol.* **7**, 174-182

39. Cheek, J., and Broderick, J. B. (2001) Adenosylmethionine-dependent iron-sulfur enzymes: versatile clusters in a radical new role. *J. Biol. Inorg. Chem.* **6**, 209-226

40. Zanello, P. (2017) The competition between chemistry and biology in assembling iron–sulfur derivatives. Molecular structures and electrochemistry. Part V. $\{[Fe_4S_4](SCys^{\gamma})_4\}$ proteins. *Coord. Chem. Rev.* **335**, 172-227

41. Torres, R. A., Lovell, T., Noodleman, L., and Case, D. A. (2003) Density functional and reduction potential calculations of Fe_4S_4 clusters. *J. Am. Chem. Soc.* **125**, 1923-1936

42. Watt, G. D., and Reddy, K. R. N. (1994) Formation of an all ferrous Fe_4S_4 cluster in the iron protein component of *Azotobacter vinelandii* nitrogenase. *J. Inorg. Biochem.* **53**, 281-294

43. Angove, H. C., Yoo, S. J., Burgess, B. K., and Münck, E. (1997) Mössbauer and EPR evidence for an all-ferrous Fe_4S_4 cluster with $S = 4$ in the Fe protein of nitrogenase. *J. Am. Chem. Soc.* **119**, 8730-8731

44. Strop, P., Takahara, P. M., Chiu, H.-J., Angove, H. C., Burgess, B. K., and Rees, D. C. (2001) Crystal structure of the all-ferrous $[4Fe\text{-}4S]^0$ form of the nitrogenase iron protein from *Azotobacter vinelandii*. *Biochemistry* **40**, 651-656

45. Chakrabarti, M., Münck, E., and Bominaar, E. L. (2011) Density functional theory study of an all ferrous 4Fe-4S cluster. *Inorg. Chem.* **50**, 4322-4326

46. Yoo, S. J., Angove, H. C., Burgess, B. K., Münck, E., and Peterson, J. (1998) Magnetic circular dichroism study of the all-ferrous [4Fe-4S] cluster of the Fe-protein of *Azotobacter vinelandii* nitrogenase. *J. Am. Chem. Soc.* **120**, 9704-9705

47. Hans, M., Buckel, W., and Bill, E. (2008) Spectroscopic evidence for an all-ferrous $[4Fe\text{-}4S]^0$ cluster in the superreduced activator of 2-hydroxyglutaryl-CoA dehydratase from *Acidaminococcus fermentans*. *J. Biol. Inorg. Chem.* **13**, 563-574

48. Outten, F. W. (2015) Recent advances in the Suf Fe-S cluster biogenesis pathway: beyond the *Proteobacteria*. *Biochim. Biophys. Acta* **1853**, 1464-1469

49. Jang, S., and Imlay, J. A. (2007) Micromolar intracellular hydrogen peroxide disrupts metabolism by damaging iron-sulfur enzymes. *J. Biol. Chem.* **282**, 929-937

50. Imlay, J. A. (2013) The molecular mechanisms and physiological consequences of oxidative stress: lessons from a model bacterium. *Nat. Rev. Microbiol.* **11**, 443-454

51. Beinert, H., Holm, R. H., and Münck, E. (1997) Iron-sulfur clusters: nature's modular, multipurpose structures. *Science* **277**, 653-659

52. Beinert, H., Kennedy, M. C., and Stout, C. D. (1996) Aconitase as iron−sulfur protein, enzyme, and iron-regulatory protein. *Chem. Rev.* **96**, 2335-2374

53. Kent, T. A., Dreyer, J. L., Kennedy, M. C., Huynh, B. H., Emptage, M. H., Beinert, H., and Münck, E. (1982) Mössbauer studies of beef heart aconitase: evidence for facile interconversions of iron-sulfur clusters. *Proc. Natl Acad. Sci. USA* **79**, 1096-1100

54. Plank, D. W., Kennedy, M. C., Beinert, H., and Howard, J. B. (1989) Cysteine labeling studies of beef heart aconitase containing a 4Fe, a cubane 3Fe, or a linear 3Fe cluster. *J. Biol. Chem.* **264**, 20385-20393

55. Rouault, T. A., and Tong, W. H. (2008) Iron-sulfur cluster biogenesis and human disease. *Trends Genet.* **24**, 398-407

56. Sheftel, A., Stehling, O., and Lill, R. (2010) Iron–sulfur proteins in health and disease. *Trends Endocrinol. Metab.* **21**, 302-314

57. Challand, M. R., Driesener, R. C., and Roach, P. L. (2011) Radical S-adenosylmethionine enzymes: mechanism, control and function. *Nat. Prod. Rep.* **28**, 1696-1721

58. Dobbek, H., Svetlitchnyi, V., Gremer, L., Huber, R., and Meyer, O. (2001) Crystal structure of a carbon monoxide dehydrogenase reveals a [Ni-4Fe-5S] cluster. *Science* **293**, 1281-1285

59. Crane, B. R., Siegel, L. M., and Getzoff, E. D. (1995) Sulfite reductase structure at 1.6 Å: evolution and catalysis for reduction of inorganic anions. *Science* **270**, 59-67

60. Crane, B. R., Siegel, L. M., and Getzoff, E. D. (1997) Structures of the siroheme- and Fe_4S_4-containing active center of sulfite reductase in different states of oxidation: heme activation via reduction-gated exogenous ligand exchange. *Biochemistry* **36**, 12101-12119

61. Doukov, T. I., Iverson, T. M., Seravalli, J., Ragsdale, S. W., and Drennan, C. L. (2002) A Ni-Fe-Cu center in a bifunctional carbon monoxide dehydrogenase/acetyl-CoA synthase. *Science* **298**, 567-572

62. Darnault, C., Volbeda, A., Kim, E. J., Legrand, P., Vernède, X., Lindahl, P. A., and Fontecilla-Camps, J. C. (2003) Ni-Zn-[Fe_4-S_4] and Ni-Ni-[Fe_4-S_4] clusters in closed and open α subunits of acetyl-CoA synthase/carbon monoxide dehydrogenase. *Nat. Struct. Mol. Biol.* **10**, 271-279

63. Svetlitchnyi, V., Dobbek, H., Meyer-Klaucke, W., Meins, T., Thiele, B., Römer, P., Huber, R., and Meyer, O. (2004) A functional Ni-Ni-[4Fe-4S] cluster in the monomeric acetyl-CoA synthase from *Carboxydothermus hydrogenoformans*. *Proc. Natl Acad. Sci. USA* **101**, 446-451

64. Zhang, B., Crack, J. C., Subramanian, S., Green, J., Thomson, A. J., Le Brun, N. E., and Johnson, M. K. (2012) Reversible cycling between cysteine persulfide-ligated [2Fe-2S] and cysteine-ligated [4Fe-4S] clusters in the FNR regulatory protein. *Proc. Natl. Acad. Sci. USA* **109**, 15734-15739

65. Schwartz, C. J., Giel, J. L., Patschkowski, T., Luther, C., Ruzicka, F. J., Beinert, H., and Kiley, P. J. (2001) IscR, an Fe-S cluster-containing transcription factor, represses expression of *Escherichia coli* genes encoding Fe-S cluster assembly proteins. *Proc. Natl Acad. Sci. USA* **98**, 14895-14900

66. Walden, W. E., Selezneva, A. I., Dupuy, J., Volbeda, A., Fontecilla-Camps, J. C., Theil, E. C., and Volz, K. (2006) Structure of dual function iron regulatory protein 1 complexed with ferritin IRE-RNA. *Science* **314**, 1903-1908

67. Rouault, T. A. (2006) The role of iron regulatory proteins in mammalian iron homeostasis and disease. *Nat. Chem. Biol.* **2**, 406-414

68. Wallander, M. L., Leibold, E. A., and Eisenstein, R. S. (2006) Molecular control of vertebrate iron homeostasis by iron regulatory proteins. *Biochim. Biophys. Acta* **1763**, 668-689

69. Volz, K. (2008) The functional duality of iron regulatory protein 1. *Curr. Opin. Struct. Biol.* **18**, 106-111

70. Argyrou, A., and Blanchard, J. (2004) Flavoprotein disulfide reductases: advances in chemistry and function. *Prog. Nucleic Acid Res. Mol. Biol.* **78**, 89-142

71. Dai, S., Schwendtmayer, C., Schurmann, P., Ramaswamy, S., and Eklund, H. (2000) Redox signaling in chloroplasts: cleavage of disulfides by an iron-sulfur cluster. *Science* **287**, 655-658

72. Walters, E. M., and Johnson, M. K. (2004) Ferredoxin:thioredoxin reductase: disulfide reduction catalyzed via novel site-specific [4Fe–4S] cluster chemistry. *Photosynth. Res.* **79**, 249-264

73. Walters, E., Garcia-Serres, R., Jameson, G., Glauser, D., Bourquin, F., Manieri, W., Schürmann, P., Johnson, M., and Huynh, B. (2005) Spectroscopic characterization of site-specific [Fe_4S_4] cluster chemistry in ferredoxin:thioredoxin reductase: implications for the catalytic mechanism. *J. Am. Chem. Soc.* **127**, 9612-9624

74. Hinks, J. A., Evans, M. C., De Miguel, Y., Sartori, A. A., Jiricny, J., and Pearl, L. H. (2002) An iron-sulfur cluster in the family 4 uracil-DNA glycosylases. *J. Biol. Chem.* **277**, 16936-16940

75. Boal, A. K., Yavin, E., Lukianova, O. A., O'Shea, V. L., David, S. S., and Barton, J. K. (2005) DNA-bound redox activity of DNA repair glycosylases containing [4Fe-4S] clusters. *Biochemistry* **44**, 8397-8407

76. Boal, A. K., Genereux, J. C., Sontz, P. A., Gralnick, J. A., Newman, D. K., and Barton, J. K. (2009) Redox signaling between DNA repair proteins for efficient lesion detection. *Proc. Natl Acad. Sci. USA* **106**, 15237-15242

77. Vaccaro, B. J., Clarkson, S. M., Holden, J. F., Lee, D.-W., Wu, C.-H., Poole Ii, F. L., Cotelesage, J. J. H., Hackett, M. J., Mohebbi, S., Sun, J., Li, H., Johnson, M. K., George, G. N., and Adams, M. W. W. (2017) Biological iron-sulfur storage in a thioferrate-protein nanoparticle. *Nat. Commun.* **8**, 16110

78. Malkin, R., and Rabinowitz, J. C. (1966) The reconstitution of clostridial ferredoxin. *Biochem. Biophys. Res. Commun.* **23**, 822-827

79. Fridovich, I. (1997) Superoxide anion radical ($O_2^{-\cdot}$), superoxide dismutases, and related matters. *J. Biol. Chem.* **272**, 18515-18517

80. Fridovich, I. (1998) Oxygen toxicity: a radical explanation. *J. Exp. Biol.* **201**, 1203-1209

81. Sawyer, D. T., and Valentine, J. S. (1981) How super is superoxide? *Acc. Chem. Res.* **14**, 393-400

82. Stohs, S. J., and Bagchi, D. (1995) Oxidative mechanisms in the toxicity of metal ions. *Free Radic. Biol. Med.* **18**, 321-336

83. Kim, J. H., Bothe, J. R., Alderson, T. R., and Markley, J. L. (2015) Tangled web of interactions among proteins involved in iron-sulfur cluster assembly as unraveled by NMR, SAXS, chemical crosslinking, and functional studies. *Biochim. Biophys. Acta* **1853**, 1416-1428

84. Albrecht, A. G., Netz, D. J. A., Miethke, M., Pierik, A. J., Burghaus, O., Peuckert, F., Lill, R., and Marahiel, M. A. (2010) SufU is an essential iron-sulfur cluster scaffold protein in Bacillus subtilis. *J. Bacteriol.* **192**, 1643-1651

85. Blanc, B., Gerez, C., and Ollagnier de Choudens, S. (2015) Assembly of Fe/S proteins in bacterial systems: Biochemistry of the bacterial ISC system. *Biochim. Biophys. Acta* **1853**, 1436-1447

86. Kim, J. H., Tonelli, M., and Markley, J. L. (2012) Disordered form of the scaffold protein IscU is the substrate for iron-sulfur cluster assembly on cysteine desulfurase. *Proc. Natl. Acad. Sci. USA* **109**, 454-459

87. Markley, J. L., Kim, J. H., Dai, Z., Bothe, J. R., Cai, K., Frederick, R. O., and Tonelli, M. (2013) Metamorphic protein IscU alternates conformations in the course of its role as the scaffold protein for iron–sulfur cluster biosynthesis and delivery. *FEBS Lett.* **587**, 1172-1179

88. Smith, A. D., Frazzon, J., Dean, D. R., and Johnson, M. K. (2005) Role of conserved cysteines in mediating sulfur transfer from IscS to IscU. *FEBS Lett.* **579**, 5236-5240

89. Kim, J. H., Füzéry, A. K., Tonelli, M., Ta, D. T., Westler, W. M., Vickery, L. E., and Markley, J. L. (2009) Structure and dynamics of the iron−sulfur cluster assembly scaffold protein IscU and its interaction with the cochaperone HscB. *Biochemistry* **48**, 6062-6071

90. Ramelot, T. A., Cort, J. R., Goldsmith-Fischman, S., Kornhaber, G. J., Xiao, R., Shastry, R., Acton, T. B., Honig, B., Montelione, G. T., and Kennedy, M. A. (2004) Solution NMR structure of the iron–sulfur cluster assembly protein U (IscU) with zinc bound at the active site. *J. Mol. Biol.* **344**, 567-583

91. Shimomura, Y., Wada, K., Fukuyama, K., and Takahashi, Y. (2008) The asymmetric trimeric architecture of [2Fe–2S] IscU: implications for its scaffolding during iron–sulfur cluster biosynthesis. *J. Mol. Biol.* **383**, 133-143

92. Kim, J. H., Bothe, J. R., Frederick, R. O., Holder, J. C., and Markley, J. L. (2014) Role of IscX in iron-sulfur cluster biogenesis in *Escherichia coli*. *J. Am. Chem. Soc.* **136**, 7933-7942

93. Kim, J. H., Tonelli, M., Frederick, R. O., Chow, D. C.-F., and Markley, J. L. (2012) Specialized Hsp70 chaperone (HscA) binds preferentially to the disordered form, whereas J-protein (HscB) binds preferentially to the structured form of the iron-sulfur cluster scaffold protein (IscU). *J. Biol. Chem.* **287**, 31406-31413

94. Agar, J. N., Krebs, C., Frazzon, J., Huynh, B. H., Dean, D. R., and Johnson, M. K. (2000) IscU as a scaffold for iron−sulfur cluster biosynthesis: sequential assembly of [2Fe-2S] and [4Fe-4S] clusters in IscU. *Biochemistry* **39**, 7856-7862

95. Chandramouli, K., Unciuleac, M.-C., Naik, S., Dean, D. R., Huynh, B. H., and Johnson, M. K. (2007) Formation and properties of [4Fe-4S] clusters on the IscU scaffold protein. *Biochemistry* **46**, 6804-6811

96. Kaiser, J. T., Clausen, T., Bourenkow, G. P., Bartunik, H.-D., Steinbacher, S., and Huber, R. (2000) Crystal structure of a NifS-like protein from *Thermotoga maritima*: implications for iron sulphur cluster assembly. *J. Mol. Biol.* **297**, 451-464

97. Cupp-Vickery, J. R., Urbina, H., and Vickery, L. E. (2003) Crystal structure of IscS, a cysteine desulfurase from *Escherichia coli*. *J. Mol. Biol.* **330**, 1049-1059

98. Smith, A. D., Agar, J. N., Johnson, K. A., Frazzon, J., Amster, I. J., Dean, D. R., and Johnson, M. K. (2001) Sulfur transfer from IscS to IscU: the first step in iron−sulfur cluster biosynthesis. *J. Am. Chem. Soc.* **123**, 11103-11104

99. Jung, Y.-S., Gao-Sheridan, H. S., Christiansen, J., Dean, D. R., and Burgess, B. K. (1999) Purification and biophysical characterization of a new [2Fe-2S] ferredoxin from *Azotobacter vinelandii*, a putative [Fe-S] cluster assembly/repair protein. *J. Biol. Chem.* **274**, 32402-32410

100. Lange, H., Kaut, A., Kispal, G., and Lill, R. (2000) A mitochondrial ferredoxin is essential for biogenesis of cellular iron-sulfur proteins. *Proc. Natl. Acad. Sci. USA* **97**, 1050-1055

101. Bonomi, F., Iametti, S., Ta, D., and Vickery, L. E. (2005) Multiple turnover transfer of [2Fe2S] clusters by the iron-sulfur cluster assembly scaffold proteins IscU and IscA. *J. Biol. Chem.* **280**, 29513-29518

102. Wu, S.-p., Wu, G., Surerus, K. K., and Cowan, J. A. (2002) Iron−sulfur cluster biosynthesis. kinetic analysis of [2Fe-2S] cluster transfer from holo ISU to apo Fd: role of redox chemistry and a conserved aspartate. *Biochemistry* **41**, 8876-8885

103. Mansy, S. S., Wu, G., Surerus, K. K., and Cowan, J. A. (2002) Iron-sulfur cluster biosynthesis. *Thermatoga maritima* IscU is a structured iron-sulfur cluster assembly protein. *J. Biol. Chem.* **277**, 21397-21404

104. Mühlenhoff, U., Gerber, J., Richhardt, N., and Lill, R. (2003) Components involved in assembly and dislocation of iron-sulfur clusters on the scaffold protein Isu1p. *EMBO J.* **22**, 4815-4825

105. Prischi, F., Konarev, P. V., Iannuzzi, C., Pastore, C., Adinolfi, S., Martin, S. R., Svergun, D. I., and Pastore, A. (2010) Structural bases for the interaction of frataxin with the central components of iron–sulphur cluster assembly. *Nat. Commun.* **1**, 95

106. Schmucker, S., Martelli, A., Colin, F., Page, A., Wattenhofer-Donzé, M., Reutenauer, L., and Puccio, H. (2011) Mammalian frataxin: an essential function for cellular viability through an interaction with a preformed ISCU/NFS1/ISD11 iron-sulfur assembly complex. *PloS one* **6**, e16199

107. Gerber, J., Mühlenhoff, U., and Lill, R. (2003) An interaction between frataxin and Isu1/Nfs1 that is crucial for Fe/S cluster synthesis on Isu1. *EMBO Rep.* **4**, 906-911

108. Cook, J. D., Kondapalli, K. C., Rawat, S., Childs, W. C., Murugesan, Y., Dancis, A., and Stemmler, T. L. (2010) Molecular details of the yeast frataxin− Isu1 interaction during mitochondrial Fe− S cluster assembly. *Biochemistry* **49**, 8756-8765

109. Silberg, J. J., Hoff, K. G., Tapley, T. L., and Vickery, L. E. (2001) The Fe/S assembly protein IscU behaves as a substrate for the molecular chaperone Hsc66 from *Escherichia coli*. *J. Biol. Chem.* **276**, 1696-1700

110. Chandramouli, K., and Johnson, M. K. (2006) HscA and HscB stimulate [2Fe-2S] cluster transfer from IscU to apoferredoxin in an ATP-dependent reaction. *Biochemistry* **45**, 11087-11095

111. Takahashi, Y., and Nakamura, M. (1999) Functional assignment of the ORF2-iscS-iscU-iscA-hscB-hscA-fdx-0RF3 gene cluster involved in the assembly of Fe-S clusters in *Escherichia coli1*. *J. Biochem.* **126**, 917-926

112. Tokumoto, U., and Takahashi, Y. (2001) Genetic analysis of the isc operon in *Escherichia coli* involved in the biogenesis of cellular iron-sulfur proteins. *J. Biochem.* **130**, 63-71

113. Voisine, C., Cheng, Y. C., Ohlson, M., Schilke, B., Hoff, K., Beinert, H., Marszalek, J., and Craig, E. A. (2001) Jac1, a mitochondrial J-type chaperone, is involved in the biogenesis of Fe/S clusters in *Saccharomyces cerevisiae*. *Proc. Natl Acad. Sci. USA* **98**, 1483-1488

114. Lutz, T., Westermann, B., Neupert, W., and Herrmann, J. (2001) The mitochondrial proteins Ssq1 and Jac1 are required for the assembly of iron sulfur clusters in mitochondria. *J. Mol. Biol.* **307**, 815-825

115. Kim, R., Saxena, S., Gordon, D. M., Pain, D., and Dancis, A. (2001) J-domain protein, Jac1p, of yeast mitochondria required for iron homeostasis and activity of Fe-S cluster proteins. *J. Biol. Chem.* **276**, 17524-17532

116. Hoff, K. G., Silberg, J. J., and Vickery, L. E. (2000) Interaction of the iron-sulfur cluster assembly protein IscU with the Hsc66/Hsc20 molecular chaperone system of *Escherichia coli*. *Proc. Natl Acad. Sci. USA* **97**, 7790-7795

117. Hoff, K. G., Ta, D. T., Tapley, T. L., Silberg, J. J., and Vickery, L. E. (2002) Hsc66 substrate specificity is directed toward a discrete region of the iron-sulfur cluster template protein IscU. *J. Biol. Chem.* **277**, 27353-27359

118. Silberg, J. J., Tapley, T. L., Hoff, K. G., and Vickery, L. E. (2004) Regulation of the HscA ATPase reaction cycle by the co-chaperone HscB and the iron-sulfur cluster assembly protein IscU. *J. Biol. Chem.* **279**, 53924-53931

119. Mayer, M. P., Brehmer, D., Gässler, C. S., and Bukau, B. (2001) Hsp70 chaperone machines. in *Adv. Protein Chem.* pp 1-44

120. Silberg, J. J., and Vickery, L. E. (2000) Kinetic characterization of the ATPase cycle of the molecular chaperone Hsc66 from *Escherichia coli*. *J. Biol. Chem.* **275**, 7779-7786

121. Cupp-Vickery, J. R., Peterson, J. C., Ta, D. T., and Vickery, L. E. (2004) Crystal structure of the molecular chaperone HscA substrate binding domain complexed with the IscU recognition peptide ELPPVKIHC. *J. Mol. Biol.* **342**, 1265-1278

122. Hoff, K. G., Cupp-Vickery, J. R., and Vickery, L. E. (2003) Contributions of the LPPVK motif of the iron-sulfur template protein IscU to interactions with the Hsc66-Hsc20 chaperone system. *J. Biol. Chem.* **278**, 37582-37589

123. Liu, J., Oganesyan, N., Shin, D. H., Jancarik, J., Yokota, H., Kim, R., and Kim, S. H. (2005) Structural characterization of an iron-sulfur cluster assembly protein IscU in a zinc-bound form. *Proteins* **59**, 875-881

124. Krebs, C., Agar, J. N., Smith, A. D., Frazzon, J., Dean, D. R., Huynh, B. H., and Johnson, M. K. (2001) IscA, an alternate scaffold for Fe−S cluster biosynthesis. *Biochemistry* **40**, 14069-14080

125. Mapolelo, D. T., Zhang, B., Naik, S. G., Huynh, B. H., and Johnson, M. K. (2012) Spectroscopic and functional characterization of iron–sulfur cluster-bound forms of *Azotobacter vinelandii* ^{Nif}IscA. *Biochemistry* **51**, 8071-8084

126. Tan, G., Lu, J., Bitoun, J. P., Huang, H., and Ding, H. (2009) IscA/SufA paralogues are required for the [4Fe-4S] cluster assembly in enzymes of multiple physiological pathways in *Escherichia coli* under aerobic growth conditions. *Biochem. J.* **420**, 463-472

127. Mühlenhoff, U., Richter, N., Pines, O., Pierik, A. J., and Lill, R. (2017) Specialized function of yeast Isa1 and Isa2 proteins in the maturation of mitochondrial [4Fe-4S] proteins. *J. Biol. Chem.* **292**, 17979

128. Brancaccio, D., Gallo, A., Mikolajczyk, M., Zovo, K., Palumaa, P., Novellino, E., Piccioli, M., Ciofi-Baffoni, S., and Banci, L. (2014) Formation of [4Fe-4S] clusters in the mitochondrial iron–sulfur cluster assembly machinery. *J. Am. Chem. Soc.* **136**, 16240-16250

129. Shakamuri, P., Zhang, B., and Johnson, M. K. (2012) Monothiol glutaredoxins function in storing and transporting [Fe_2S_2] clusters assembled on IscU scaffold proteins. *J. Am. Chem. Soc.* **134**, 15213-15216

130. Uzarska, M. A., Dutkiewicz, R., Freibert, S.-A., Lill, R., and Mühlenhoff, U. (2013) The mitochondrial Hsp70 chaperone Ssq1 facilitates Fe/S cluster transfer from Isu1 to Grx5 by complex formation. *Mol. Biol. Cell.* **24**, 1830-1841

131. Mapolelo, D. T., Zhang, B., Randeniya, S., Albetel, A.-N., Li, H., Couturier, J., Outten, C. E., Rouhier, N., and Johnson, M. K. (2013) Monothiol glutaredoxins and A-type proteins: partners in Fe-S cluster trafficking. *Dalton Trans* **42**, 3107-3115

132. Couturier, J., Przybyla-Toscano, J., Roret, T., Didierjean, C., and Rouhier, N. (2015) The roles of glutaredoxins ligating Fe–S clusters: sensing, transfer or repair functions? *Biochim. Biophys. Acta* **1853**, 1513-1527

133. Li, H., and Outten, C. E. (2012) Monothiol CGFS glutaredoxins and BolA-like proteins: [2Fe-2S] binding partners in iron homeostasis. *Biochemistry* **51**, 4377-4389

134. Iwema, T., Picciocchi, A., Traore, D. A. K., Ferrer, J.-L., Chauvat, F., and Jacquamet, L. (2009) Structural basis for delivery of the intact [Fe_2S_2] cluster by monothiol glutaredoxin. *Biochemistry* **48**, 6041-6043

135. Isnard, R., Kalotka, H., Dürr, A., Cossée, M., Schmitt, M., Pousset, F., Thomas, D., Brice, A., Koenig, M., and Komajda, M. (1997) Correlation between left ventricular hypertrophy and GAA trinucleotide repeat length in Friedreich's ataxia. *Circulation* **95**, 2247-2249

136. Campuzano, V., Montermini, L., Molto, M. D., Pianese, L., Cossee, M., Cavalcanti, F., Monros, E., Rodius, F., Duclos, F., Monticelli, A., Zara, F., Canizares, J., Koutnikova, H., Bidichandani, S. I., Gellera, C., Brice, A., Trouillas, P., De Michele, G., Filla, A., De Frutos, R., Palau, F., Patel, P. I., Di Donato, S., Mandel, J. L., Cocozza, S., Koenig, M., and Pandolfo, M. (1996) Friedreich's ataxia: autosomal recessive disease caused by an intronic GAA triplet repeat expansion. *Science* **271**, 1423-1427

137. Karthikeyan, G., Santos, J. H., Graziewicz, M. A., Copeland, W. C., Isaya, G., Houten, B. V., and Resnick, M. A. (2003) Reduction in frataxin causes progressive accumulation of mitochondrial damage. *Hum. Mol. Genet.* **12**, 3331-3342

138. Mandavilli, B. S., Santos, J. H., and Van Houten, B. (2002) Mitochondrial DNA repair and aging. *Mutat Res.* **509**, 127-151

139. Bottomley, S. S. (2006) Congenital sideroblastic anemias. *Curr. Hematol. Rep.* **5**, 41-49

140. Ye, H., Jeong, S. Y., Ghosh, M. C., Kovtunovych, G., Silvestri, L., Ortillo, D., Uchida, N., Tisdale, J., Camaschella, C., and Rouault, T. A. (2010) Glutaredoxin 5 deficiency causes sideroblastic anemia by specifically impairing heme biosynthesis and depleting cytosolic iron in human erythroblasts. *J. Clin. Invest.* **120**, 1749-1761

141. Larsson, L. E., Linderholm, H., Mueller, R., Ringqvist, T., and Soernaes, R. (1964) Hereditary metabolic myopathy with paroxysmal myoglobinuria due to abnormal glycolysis. *J. Neurol. Neurosurg. Psychiatry* **27**, 361-380

142. Haller, R. G., Henriksson, K. G., Jorfeldt, L., Hultman, E., Wibom, R., Sahlin, K., Areskog, N. H., Gunder, M., Ayyad, K., and Blomqvist, C. G. (1991) Deficiency of skeletal muscle succinate dehydrogenase and aconitase. Pathophysiology of exercise in a novel human muscle oxidative defect. *J. Clin. Invest.* **88**, 1197-1206

143. Mochel, F., Knight, M. A., Tong, W.-H., Hernandez, D., Ayyad, K., Taivassalo, T., Andersen, P. M., Singleton, A., Rouault, T. A., Fischbeck, K. H., and Haller, R. G. (2008)

Splice mutation in the iron-sulfur cluster scaffold protein ISCU causes myopathy with exercise intolerance. *Am. J. Hum. Genet.* **82**, 652-660

144. Olsson, A., Lind, L., Thornell, L. E., and Holmberg, M. (2008) Myopathy with lactic acidosis is linked to chromosome and caused by an intron mutation in the ISCU gene resulting in a splicing defect. *Hum. Mol. Genet.* **17**, 1666-1672

145. Sanaker, P. S., Toompuu, M., Hogan, V. E., He, L., Tzoulis, C., Chrzanowska-Lightowlers, Z. M., Taylor, R. W., and Bindoff, L. A. (2010) Differences in RNA processing underlie the tissue specific phenotype of ISCU myopathy. *Biochim. Biophys. Acta* **1802**, 539-544

146. Legati, A., Reyes, A., Ceccatelli Berti, C., Stehling, O., Marchet, S., Lamperti, C., Ferrari, A., Robinson, A. J., Muhlenhoff, U., Lill, R., Zeviani, M., Goffrini, P., and Ghezzi, D. (2017) A novel de novo dominant mutation in ISCU associated with mitochondrial myopathy. *J. Med. Genet.* **54**, 815-824

147. Kollberg, G., Tulinius, M., Melberg, A., Darin, N., Andersen, O., Holmgren, D., Oldfors, A., and Holme, E. (2009) Clinical manifestation and a new ISCU mutation in iron–sulphur cluster deficiency myopathy. *Brain* **132**, 2170-2179

148. Farhan, S. M. K., Wang, J., Robinson, J. F., Lahiry, P., Siu, V. M., Prasad, C., Kronick, J. B., Ramsay, D. A., Rupar, C. A., and Hegele, R. A. (2014) Exome sequencing identifies NFS1 deficiency in a novel Fe-S cluster disease, infantile mitochondrial complex II/III deficiency. *Mol. Genet. Genomic Med.* **2**, 73-80

149. Bandyopadhyay, S., Naik, S. G., O'Carroll, I. P., Huynh, B.-H., Dean, D. R., Johnson, M. K., and Dos Santos, P. C. (2008) A proposed role for the *Azotobacter vinelandii* NfuA protein as an intermediate iron-sulfur cluster carrier. *J. Biol. chem.* **283**, 14092-14099

150. Navarro-Sastre, A., Tort, F., Stehling, O., Uzarska, M. A., Arranz, J. A., Del Toro, M., Labayru, M. T., Landa, J., Font, A., Garcia-Villoria, J., Merinero, B., Ugarte, M., Gutierrez-Solana, L. G., Campistol, J., Garcia-Cazorla, A., Vaquerizo, J., Riudor, E., Briones, P., Elpeleg, O., Ribes, A., and Lill, R. (2011) A fatal mitochondrial disease is associated with defective NFU1 function in the maturation of a subset of mitochondrial Fe-S proteins. *Am. J. Hum. Genet.* **89**, 656-667

151. Liochev, S. I., and Fridovich, I. (1994) The role of $O^{2.-}$ in the production of $HO^{\cdot}$: *in vitro* and *in vivo*. *Free Radic. Biol. Med.* **16**, 29-33

152. Keyer, K., and Imlay, J. A. (1996) Superoxide accelerates DNA damage by elevating free-iron levels. *Proc. Natl Acad. Sci. USA* **93**, 13635-13640

153. Uttara, B., Singh, A. V., Zamboni, P., and Mahajan, R. T. (2009) Oxidative stress and neurodegenerative diseases: a review of upstream and downstream antioxidant therapeutic options. *Curr. neuropharmacol.* **7**, 65-74

154. Hybertson, B. M., Gao, B., Bose, S. K., and McCord, J. M. (2011) Oxidative stress in health and disease: the therapeutic potential of Nrf2 activation. *Mol. Aspects Med.* **32**, 234-246

155. Crouse, B. R., Meyer, J., and Johnson, M. K. (1995) Spectroscopic evidence for a reduced Fe_2S_2 cluster with a $S = 9/2$ ground state in mutant forms of *Clostridium pasteurianum* 2Fe ferredoxin. *J. Am. Chem. Soc.* **117**, 9612-9613

156. Achim, C., Golinelli, M.-P., Bominaar, E. L., Meyer, J., and Münck, E. (1996) Mössbauer study of Cys56Ser mutant 2Fe ferredoxin from *Clostridium pasteurianum*: evidence for double exchange in an $[Fe_2S_2]^+$ cluster. *J. Am. Chem. Soc.* **118**, 8168-8169

157. Johnson, M. K., Duin, E. C., Crouse, B. R., Golinelli, M. P., and Meyer, J. (1998) Valence-delocalized $[Fe_2S_2]^+$ clusters. in *Spectroscopic Methods in Bioinorganic Chemistry*, American Chemical Society. pp 286-301

158. Surerus, K. K., Münck, E., Moura, I., Moura, J. J. G., and LeGall, J. (1987) Evidence for the formation of a $ZnFe_3S_4$ cluster in *Desulfovibrio gigas* ferredoxin II. *J. Am. Chem. Soc.* **109**, 3805-3807

159. Breton, J. L., Duff, J. L. C., Butt, J. N., Armstrong, F. A., George, S. J., Pétillot, Y., Forest, E., Schäfer, G., and Thomson, A. J. (1995) Identification of the iron-sulfur clusters in a ferredoxin from the archaeon *Sulfolobus acidocaldarius*. *Eur. J. Biochem.* **233**, 937-946

160. Venkateswara Rao, P., and Holm, R. H. (2004) Synthetic analogues of the active sites of iron−sulfur proteins. *Chem. Rev.* **104**, 527-560

Figure 1.1. Schematic representation of most common structures of Fe-S centers as determined by X-ray crystallography. Structures are taken from the coordinates deposited in the Protein Data Bank: (A) Fe^{3+} center in rubredoxin from *Desulfovibrio vulgaris*, PDB ID# 8RXN; (B) $[2Fe\text{-}2S]^{2+}$ cluster in *Anabaena pcc* 7120 Fd, PDB ID# 1FRD; (C) $[2Fe\text{-}2S]_R^{2+}$ Rieske-type cluster in *Sulfolobus acidocaldarius* Rieske protein, PDB ID# 1JM1; (D) $[3Fe\text{-}4S]^{+}$ cluster in *Azotobacter vinelandii* 7Fe FdI, PDB ID# 6FDR; (E) $[4Fe\text{-}4S]^{2+}$ cluster in *Azotobacter vinelandii* 7Fe FdI, PDB ID# 6FDR; (F) $[8Fe\text{-}7S]^{N}$ P-cluster in dithionite-reduced *Azotobacter vinelandii* nitrogenase MoFe protein, PDB ID# 1M1N. Color code: magenta, Fe; yellow, S; green, C; blue, N. Unlabeled S atoms correspond to bridging sulfides. Adapted from reference (16).

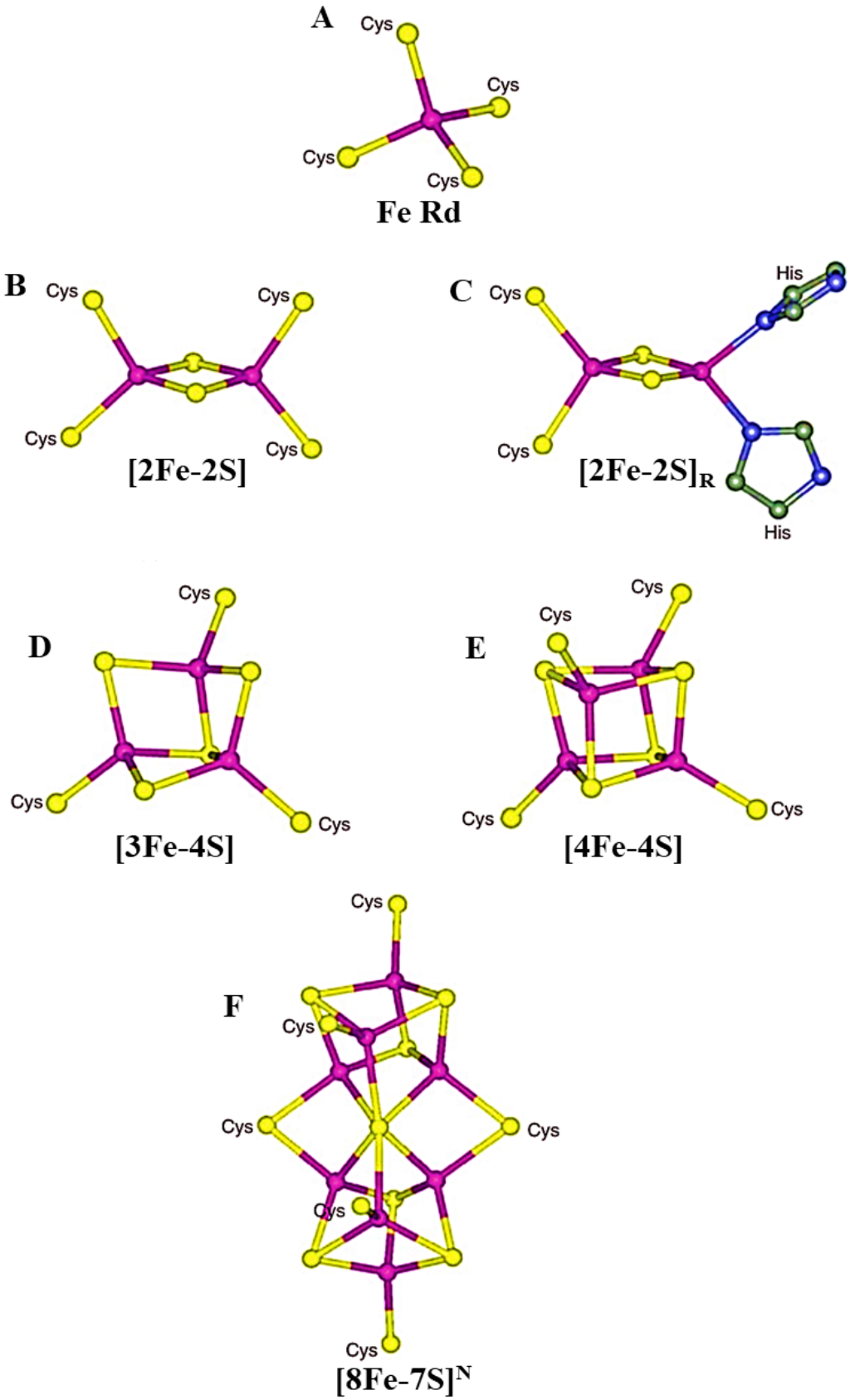
A
Cys
Cys
Cys
Cys
Fe Rd
B
Cys
Cys
Cys
Cys
[2Fe-2S]
C
Cys
His
Cys
[2Fe-2S]R
His
D
Cys
Cys
Cys
[3Fe-4S]
E
Cys
Cys
Cys
Cys
[4Fe-4S]
F
Cys
Cys
Cys
Cys
Cys
Cys
[8Fe-7S]N

Figure 1.2. Ground state spin (*S*) and valence localization/delocalization schemes for fundamental types of Fe−S centers. Valence-delocalized $[2Fe\text{-}2S]^{+}$ clusters with $S = 9/2$ ground states have only been observed in Cys-to-Ser variants of thioredoxin-like 2Fe ferredoxins (155-157), but valence-delocalized $[2Fe\text{-}2S]^{+}$ fragments are an integral part of many higher nuclearity clusters. The $[3Fe\text{-}4S]^{-}$ clusters are shown in parenthesis since they have not been observed in proteins, and only have been identified as a fragment in heterometallic cuboidal clusters (158). Three electron reduction of the $[3Fe\text{-}4S]^{+}$ cluster to yield the $[3Fe\text{-}4S]^{2-}$ cluster occurs with the concomitant addition of three protons (159). Color code: red, Fe^{3+}; blue, Fe^{2+}; green, $Fe^{2.5+}$; yellow, S; grey, O. Adapted from reference (16).

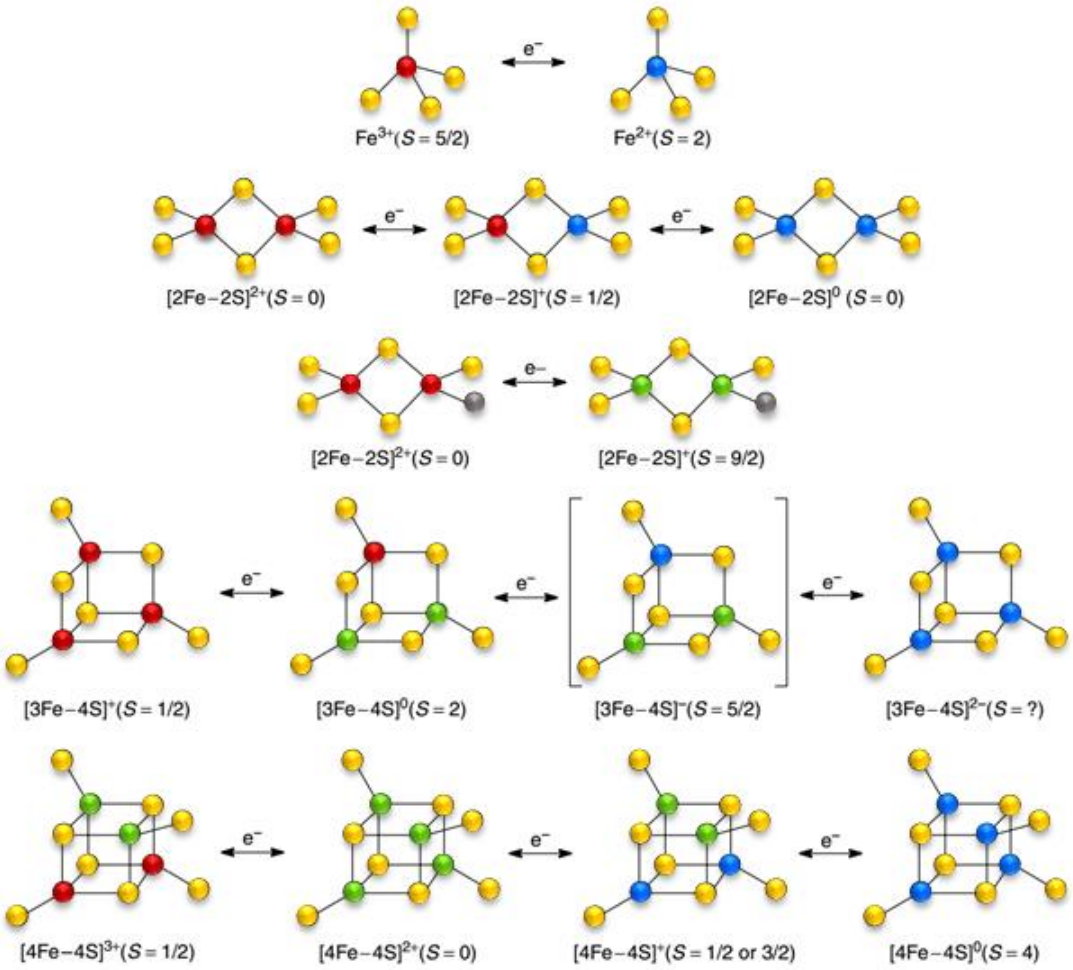
e⁻
Fe3+(S = 5/2)
Fe2+(S = 2)
[2Fe−2S]2+(S = 0)
[2Fe−2S]+(S = 1/2)
[2Fe−2S]0 (S = 0)
e–
[2Fe−2S]2+(S = 0)
[2Fe−2S]+(S = 9/2)
[3Fe−4S]+(S = 1/2)
[3Fe−4S]0(S = 2)
[3Fe−4S]−(S = 5/2)
[3Fe−4S]2−(S = ?)
[4Fe−4S]3+(S = 1/2)
[4Fe−4S]2+(S = 0)
[4Fe−4S]+(S = 1/2 or 3/2)
[4Fe−4S]0(S = 4)

Figure 1.3. Schematic representation of the types of cluster conversions observed in Fe-S proteins. M^{+} : Cu^{+} and Tl^{+} ; M^{2+} : Cr^{2+} , Mn^{2+} ,Co^{2+} ,Ni^{2+} ,Zn^{2+} ,Cd^{2+}. Adapted from reference (16,160).

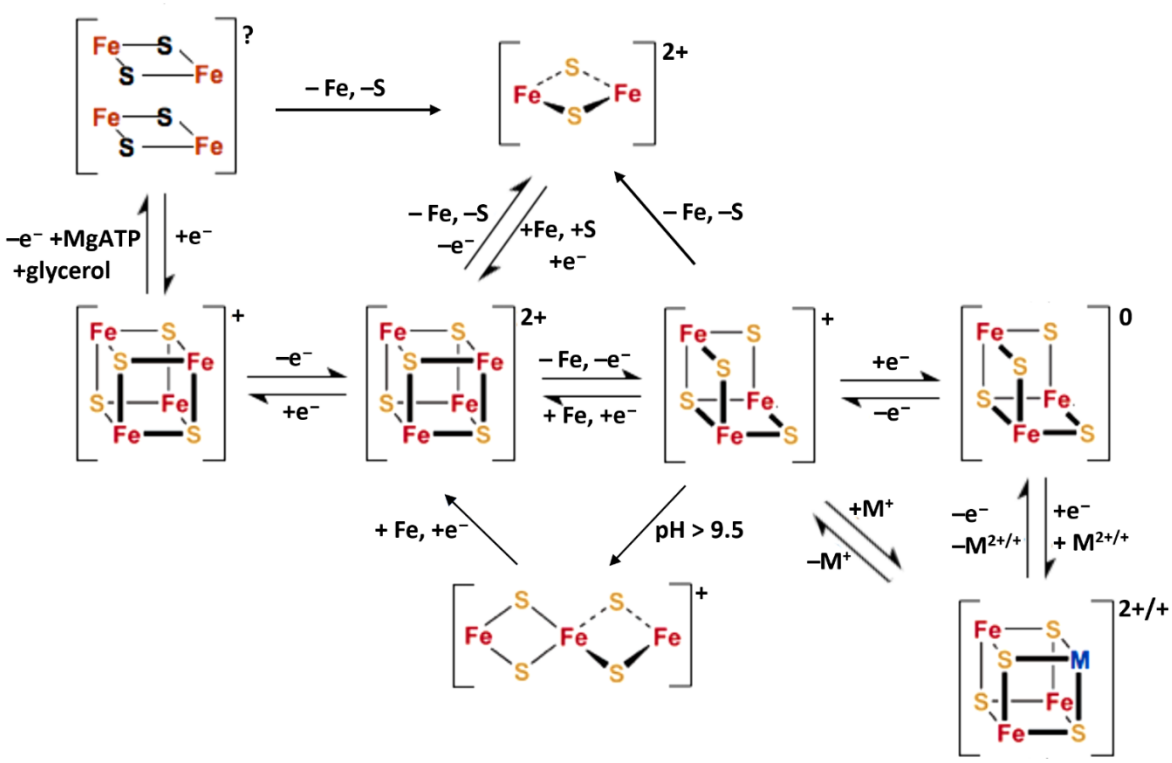
?
– Fe, –S
2+
–e⁻ +MgATP
+glycerol
+e⁻
– Fe, –S
–e⁻
+Fe, +S
+e⁻
– Fe, –S
+
–e⁻
+e⁻
2+
– Fe, –e⁻
+ Fe, +e⁻
+
+e⁻
–e⁻
0
+ Fe, +e⁻
pH > 9.5
+M⁺
–M⁺
–e⁻
–M²⁺/⁺
+e⁻
+ M²⁺/⁺
+
2+/+

Figure 1.4. Schematic model for [Fe-S] cluster biogenesis. The overall mechanism involves cysteine desulfurase-mediated assembly of a transient $[2Fe\text{-}2S]^{2+}$ cluster on the IscU scaffold protein, and subsequent transfer of $[2Fe\text{-}2S]^{2+}$ cluster to apo Fe-S proteins. Sulfur generated by cysteine-desulfurase as IscS-bound persulfide (-SSH) and iron are shown in yellow and orange circles, respectively. Both Fe^{2+} substrate and $[2Fe\text{-}2S]^{1+}$-Fdx serve as electron donors to reduce the S^0 present in cysteine persulfide to the sulfide present in $[2Fe\text{-}2S]^{2+}$clusters. The intact transfer of the $[2Fe\text{-}2S]^{2+}$ cluster on IscU to a dedicated Grx primary acceptor protein is facilitated by a dedicated co-chaperone system, HscA/HscB/MgATP. Grxs then transfer $[2Fe\text{-}2S]^{2+}$ clusters to apo Fe-S proteins and ATC proteins, which mediate two-electron reductive coupling of two $[2Fe\text{-}2S]^{2+}$ clusters to form $[4Fe\text{-}4S]^{2+}$ clusters, that are transferred intact to apo Fe-S proteins or $[4Fe\text{-}4S]^{2+}$ cluster carrier proteins.

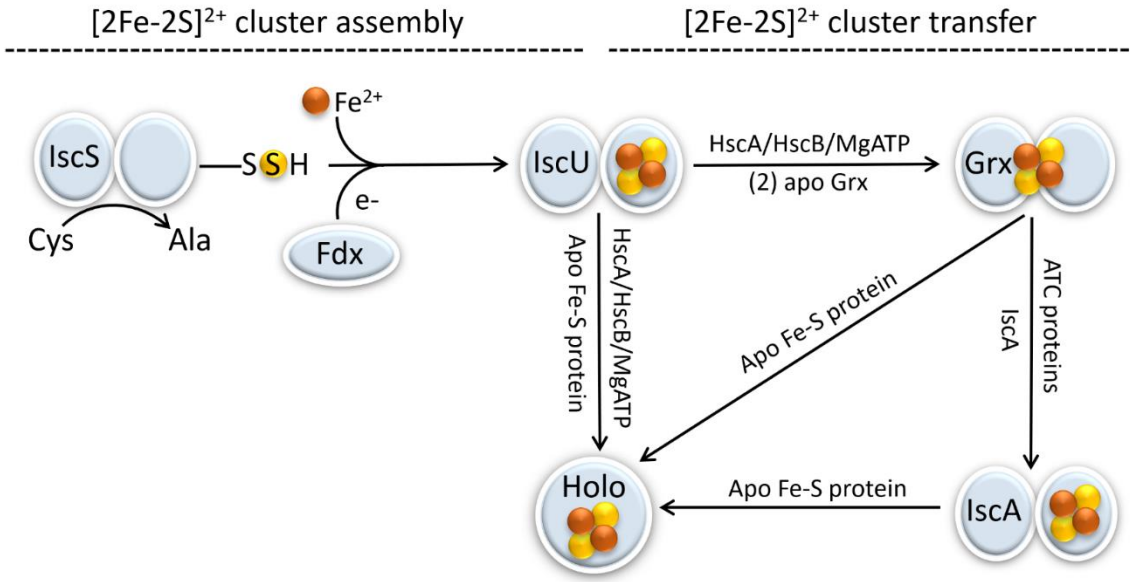
[2Fe-2S]2+ cluster assembly
[2Fe-2S]2+ cluster transfer
IscS
Cys
Ala
S S H
Fe2+
e-
Fdx
IscU
HscA/HscB/MgATP
(2) apo Grx
Grx
Apo Fe-S protein
HscA/HscB/MgATP
Apo Fe-S protein
IscA
ATC proteins
Holo
Apo Fe-S protein
IscA

Figure 1.5. X-ray crystal structure of *E. coli* Grx4 (PDB 2WCI) with close-up view of $[2Fe\text{-}2S]^{2+}$ cluster ligation by GSH. The crystal structure of a $[2Fe\text{-}2S]^{2+}$-bridged CGFS Grx homodimer demonstrate that each Fe is coordinated by cysteinates of the rigorously conserved CGFS motif and GSH. The two GSH molecules are covalently bound to the $[2Fe\text{-}2S]^{2+}$ cluster but held in place by non-covalent interactions with each Grx4 monomer. Adapted from reference (133).

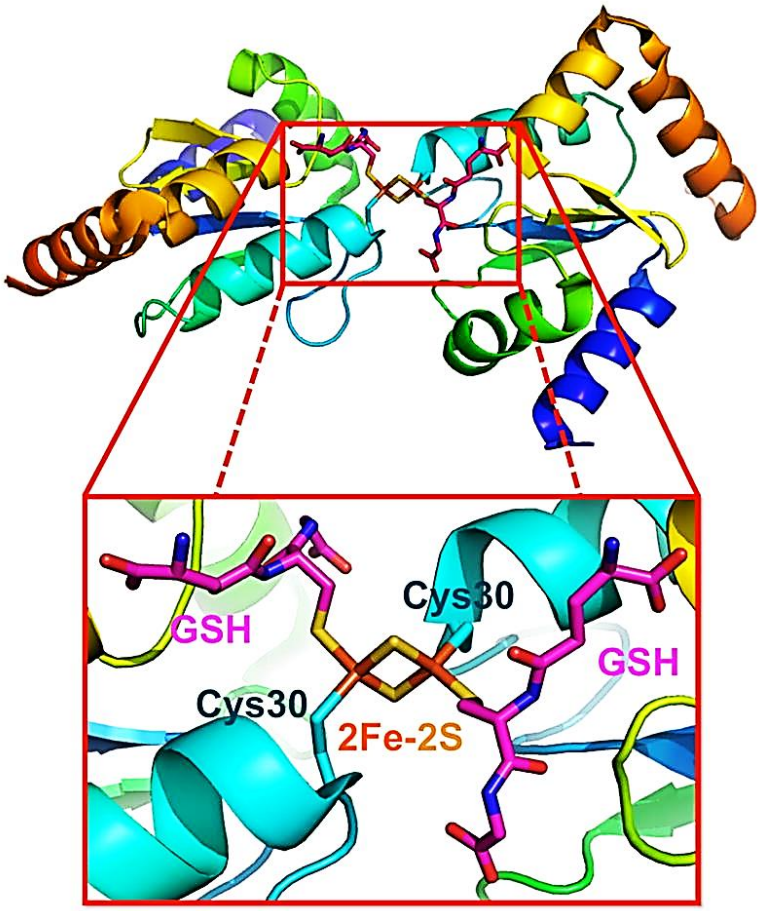
GSH
Cys30
Cys30
GSH
2Fe-2S

CHAPTER TWO

THIOFERRATE AS A SOURCE OF IRON AND SULFUR FOR IRON-SULFUR CLUSTER ASSEMBLY

Sahel Mohebbi[1], Julien J. H. Cotelesage,[2] Graham N. George[2], Michael W. W. Adams[3], and Michael K. Johnson[1]

To be submitted to J. Biol. Chem.

[1]Department of Chemistry Center for Metalloenzyme Studies, University of Georgia, Athens, Georgia 30602, USA. [2]Department of Geological Sciences and Chemistry, University of Saskatchewan, Saskatoon, Saskatchewan S7N 5C5, Canada. [3]Department of Biochemistry and Molecular Biology, University of Georgia, Athens, Georgia 30602, USA.

Abbreviations

Av, *Azotobacter vinelandii*; CD, circular dichroism; DT, dithionite; DTT, dithiothreitol; *Ec*, *Escherichia coli* ; EDTA, ethylenediaminetetraacetic acid; EPR, electron paramagnetic resonance; EXAFS, extended X-ray absorption fine structure; FAC, ferric ammonium citrate; FAS, ferrous ammonium sulfate; Fdx, ferredoxin; Grx, glutaredoxin; GSH, glutathione; IPTG, isopropyl β-D-thiogalactoside, IssA, iron-sulfur storage protein A; LB, Lysogeny broth; *P. furiosus*, *Pf*, *Pyrococcus furiosus*; PMSF, phenylmethylsulphonyl fluoride; *Sc*, *Saccharomyces cerevisiae*; TCA, tricarboxylic acid; TCEP, tris(2-carboxyethyl)phosphine.

Abstract

The iron-sulfur storage protein IssA is the most highly upregulated protein when the hyperthermophilic anaerobic archaeon *Pyrococcus furiosus* is grown using elemental sulfur as the terminal electron acceptor and in the presence of excess iron. IssA stores excess Fe and S as thioferrate, a linear inorganic anionic polymer with a $(FeS_2)^{1-}$ repeating unit, that was previously unknown in biology. IssA forms nanoparticles reaching 300 nm in diameter that are composed of spherical 20-nm diameter units, each containing ~6,400 Fe atoms and ~ 170 IssA monomer. *In vitro* studies have shown that the thioferrate core of IssA can provide iron and sulfide for assembly of $[4Fe\text{-}4S]^{2+}$ cluster on apo *P. furiosus* ferredoxin in the presence of dithioltreitol suggesting that *in vivo* a hitherto unidentified thiol reagent disassembles the thioferrate core into smaller pieces by binding Fe^{3+}, $[2Fe\text{-}2S]^{2+}$, or linear $[3Fe\text{-}4S]^{1+}$ fragments, which can assemble into $[4Fe\text{-}4S]^{2+}$ clusters on acceptor proteins. In this study we have synthesized and characterized thioferrate using UV-visible absorption and X-ray absorption spectroscopy. The results confirm the presence of thioferrate nanoparticles associated with IssA. In addition, thioferrate is shown to be competent for *in vitro* maturation of $[2Fe\text{-}2S]^{2+}$ clusters in monothiol glutaredoxins and ferredoxins and $[4Fe\text{-}4S]^{2+}$ clusters in ferredoxins. The presence of linear $[3Fe\text{-}4S]^{1+}$ clusters as major or minor Fe-S cluster components in all the thioferrate-mediated reconstitutions investigated, strongly suggests a reconstitution mechanism involving transfer of a linear $[3Fe\text{-}4S]^{1+}$ fragment to apo Fe-S proteins that can be used for *in situ* formation of $[2Fe\text{-}2S]^{2+}$ and $[4Fe\text{-}4S]^{2+}$ clusters.

Introduction

Iron-sulfur [Fe-S] clusters are one of the most ancient and versatile types of protein cofactors (1). The most common types of [Fe-S] clusters comprise $[2Fe\text{-}2S]^{2+,1+}$, cubane-type $[3Fe\text{-}4S]^{1+,0}$, and $[4Fe\text{-}4S]^{3+,2+,1+}$ cores, which are ligated to proteins primarily or exclusively through cysteine residues, with histidine, aspartate, serine, and arginine residues also known to be cluster ligands (1).They are found in all three kingdoms of life and the unique structural, chemical, and redox properties of [Fe-S] clusters facilitate diverse roles in biology including electron transfer, coupled electron-proton transfer, substrate binding and activation, iron or cluster storage, regulation of gene expression and enzyme activity, disulfide reduction, and sulfur donation (1). *In vitro* [Fe-S] clusters can often be assembled in apo proteins via spontaneous self-assembly using iron and sulfide ions under reducing and/or anaerobic conditions (2). However, *in vivo* under partial oxidizing condition, this process is unlikely due to cellular toxicity associated with free iron and sulfide in concentrations needed for spontaneous Fe-S protein maturation (3-6). Moreover, [Fe-S] clusters, particularly [4Fe-4S] clusters, are degraded rapidly by molecular oxygen. The resulting Fe^{3+} and Fe^{2+} ions produce reactive oxygen species (e.g. peroxide, superoxide, and hydroxyl radicals) via Fenton chemistry that can cause irreversible molecular damage, ultimately leading to cell death (4,5,7). Consequently, despite the relative structural and chemical simplicity of [Fe-S] clusters, their biosynthesis in living cells is a highly complex and coordinated process (8). Cells maintain tightly regulated machineries for [Fe-S] cluster biosynthesis (9).

Three distinct systems for [Fe-S] cluster biosynthesis have been identified in prokaryotes: the nitrogen-fixation (NIF), the iron-sulfur cluster (ISC), and the sulfur-utilization factor (SUF) machineries (1,10,11). In eukaryotes, the biosynthesis of [Fe-S] clusters are performed by two main multi-protein machineries, the ISC machinery localized in mitochondria and the cytosolic

iron-sulfur cluster assembly (CIA) machinery localized in the cytosol (8). The biogenesis of iron-sulfur proteins comprises two main steps, first the transient assembly of [Fe-S] clusters on a scaffold protein using Fe^{2+} ions and sulfur provided by a cysteine desulfurase. Second the transfer of the assembled [2Fe-2S] cluster to recipient proteins, either cluster carrier proteins or apo acceptor proteins.

Recently, an alternative method for assembling [Fe-S] clusters was proposed in the anaerobic hyperthermophilic archaeon *Pyrococcus furiosus* (*Pf*), which is replete with Fe-S proteins and almost exclusively contains [4Fe-4S] clusters. *P. furiosus,* which grows optimally near 100 °C in hydrothermal vents and can use elemental sulfur as a terminal electron acceptor, was shown to store Fe^{3+} and S^{2-} ions as a thioferrate mineral using the IssA iron-sulfur storage protein (12). Thioferrate occurs naturally as the mineral erdite and can be synthesized from ferric and sulfide. However, thioferrate has never previously been reported in a living system (13-15). Thioferrates contain Fe^{3+} and S^{2-} ions in linear inorganic anionic polymer chains with repeating FeS_2^- units. Each iron is coordinated tetrahedrally by sulfur atoms (13,16) and the infinite linear edge sharing FeS_4 polymeric chains are separated by charge balancing cations (13,17). The ability of thioferrate-loaded IssA to reconstitute a $[4Fe\text{-}4S]^{2+}$ cluster in apo *Pf* Fdx, an abundant electron carrier in this organism, provided *in vitro* evidence that the stored thioferrate in IssA can be mobilized and used for assembly of $[4Fe\text{-}4S]^{2+}$ clusters (12). The detailed mechanism of this process has yet to be determined. However, since this reconstitution occurred in the presence of the dithiol reagent, dithiothreitol (DTT), but not in the presence of alternative reductants dithionite or TCEP, it was postulated that transferable fragments of Fe^{3+}, $[2Fe\text{-}2S]^{2+}$ or linear $[3Fe\text{-}4S]^{1+}$ are chelated and disassembled from the thioferrate polymer by DTT (*in vitro*) or a cellular thiol (*in vivo*). These fragments could subsequently be assembled into $[4Fe\text{-}4S]^{2+}$ clusters by spontaneous

self-assembly under reducing conditions from released Fe^{3+} and S^{2-} ions, or via two-electron reductive coupling of two $[2Fe\text{-}2S]^{2+}$ clusters, or by addition of Fe^{2+} and one electron to a linear $[3Fe\text{-}4S]^{+}$ cluster, as reported in biological systems and synthetic models, see Figure 2.1 (12,18,19).

To investigate the mechanism of [Fe-S] cluster assembly using thioferrate as the sole source of iron and sulfide, we report herein spectroscopic characterization of synthesized thioferrate using UV-visible absorption/CD and X-ray absorption spectroscopy (XAS) and thioferrate-mediated reconstitution of apo Fe-S proteins from different families that contain $[2Fe\text{-}2S]^{2+}$, linear $[3Fe\text{-}4S]^{1+}$, and $[4Fe\text{-}4S]^{2+}$ clusters in their holo form. The results confirm that thioferrate is associated with IssA and demonstrate the ability of apo iron-sulfur proteins to obtain fragments of thioferrate via ligand exchange and to use these fragments to generate the native [Fe-S] clusters under anaerobic conditions. The *in vitro* results obtained in this study strongly suggest that formation of $[4Fe\text{-}4S]^{2+}$ and $[2Fe\text{-}2S]^{2+}$ clusters involves the initial transfer of a linear $[3Fe\text{-}4S]^{1+}$ cluster fragment of thioferrate to the apo protein.

Experimental procedures

Protein expression and purification. *Pf* Fdx was purified as previously described (20). *Av* Grx5 and *Sc* Grx5 were overexpressed and purified as previously described (21,22). *Av* Fdx plasmid was amplified and verified by amino acid sequencing. Amplified plasmid was transformed into the *Ec* expression strain BL21(DE3) and incubated on LB-agar plates with 100 mg/L ampicillin at 37 °C. Colonies containing Fdx plasmid were grown at 37 °C and 250 rpm in LB media supplemented with 100 mg/L ampicillin and 50mg/L FAC. The bacterial culture was induced by adding 100 mg/L Isopropyl β-D-1-thiogalactopyranoside (IPTG) supplemented with 50 mg/L FAC at exponential phase and further cultivated at 34 °C and 225 rpm for 4 hours. Cells

were harvested by centrifugation at 5,000 g for 10 minutes at 4 °C. The cell pellets were stored at –80 °C until further use.

For aerobic purification of *Av* Fdx, cells expressing recombinant *Av* Fdx were thawed and resuspended in 100 mM Tris-HCl buffer, pH 7.8, lysed on ice by sonication intermittently then centrifuged to remove cell debris from the suspension at 12,000 rpm, 4 °C for 1 hour. Brown fractions containing $[2Fe\text{-}2S]^{2+}$ cluster-bound *Av* Fdx were eluted from a Q-sepharose column (GE healthcare) using a linear gradient of 0-1 M NaCl. These fractions were further purified using a phenol-sepharose column using decreasing ammonium sulfate concentration. The purity and integrity of the purified protein were assessed by SDS-PAGE analysis and mass spectrometry.

Preparation of apo form of *Sc* Grx5, *Av* Grx5, *Pf* Fdx, and *Av* Fdx. Apo forms of *Sc* Grx5 and *Av* Grx5 were prepared by incubating protein samples with 20-fold excess of potassium ferricyanide and 50-fold excess of EDTA on ice for 1 hour under anaerobic conditions. The protein samples were then run through a 20 mL HiTrap™ Desalting column (GE Healthcare) using rigorously degassed buffer (100 mM Tris-HCl, pH 7.5) in order to separate and remove EDTA and potassium ferricyanide. The resulting apo proteins were concentrated separately by Amicon ultrafiltration using a YM5 membrane.

Apo-*Pf* Fdx was prepared using the method of Moulis and Meyer (23), except that a 2-h incubation with 8% (w/v) TCA at room temperature was required to fully bleach and precipitate the protein. After centrifugation, the apo protein pellet was dissolved in degassed 100 mM Tris-HCl buffer, pH 7.5, under anaerobic conditions. The protein was buffer exchanged 3 times under anaerobic conditions by Amicon ultrafiltration using a YM3 membrane to remove any remaining released iron.

Apo *Av* Fdx was prepared using the method of Moulis and Meyer (23) except a 5-minute incubation with 8% (w/v) TCA was required. After centrifugation, the protein pellet was dissolved in 100 mM Tris-HCl buffer, pH 7.5. The apo protein was then treated with DTT to the final concentration of 1mM and 50-fold excess of EDTA for 1 hour on ice under anaerobic conditions. The protein sample was then run through a 20 mL HiTrap^{TM} Desalting column (GE Healthcare) to remove EDTA and reducing agent. Apo protein sample was concentrated by Amicon ultrafiltration using a YM3 membrane.

Thioferrate synthesis. For aerobic preparation of thioferrate under alkaline conditions, 45.8 mM FAC and 133.2 mM sodium sulfide were prepared in 100 mM CAPS buffer, pH 10, supplemented with 150 mM NaCl. FAC was added to sodium sulfide until the reaction mixture turned into a green colored solution with absorption features corresponding to those established previously for thioferrate (13). For synthesis of thioferrate at a lower pH values, 50 mM Tris-HCl buffer, pH 8, supplemented with 150 mM NaCl was used to prepare FAC and sodium sulfide solutions. The same procedure was used for anaerobic thioferrate synthesis, except that both FAC and sodium sulfide were exposed to Ar in the glovebox for 10 minutes prior to addition of degassed buffer.

Samples for EXAFS studies were prepared using FAC (45.8 mM) and sodium sulfide (133.2 mM) stock solutions made under strictly anaerobic conditions with 50 mM Tris-HCl buffer, pH 8, supplemented with 150 mM NaCl and 20% glycerol. Freshly prepared thioferrate samples were made with a 16-fold excess of sodium sulfide over FAC, delivered into EXAFS cuvette via Hamilton syringe, and immediately frozen in liquid nitrogen under anaerobic conditions. A portion of this sample was kept tightly sealed under anaerobic conditions (O_2 < 2 ppm) for 44 hours before loading into EXAFS cuvettes and freezing in liquid nitrogen. Samples for EPR studies were made

from freshly made thioferrate prepared with the same procedure described for EXAFS sample except no glycerol glassing agent was added. Thioferrate samples were transferred to a calibrated EPR tube and sealed under anaerobic conditions and immediately frozen in liquid nitrogen. In addition, a control EPR sample with the same FAC concentration (with no sodium sulfide) was prepared.

Thioferrate-mediated reconstitution of [Fe-S] clusters in *Sc* Grx5, *Av* Grx5, *Pf* Fdx, and *Av* Fdx. For all the experiments, thioferrate samples were made with 16-fold excess of sodium sulfide using 50 mM Tris-HCl buffer, at pH 8, supplemented with 150 mM NaCl under anaerobic conditions. Prior to reconstitution, apo *Sc* Grx5 was incubated with 40 mM TCEP for 1 hour under anaerobic conditions to cleave disulfide bonds. TCEP was removed by buffer exchange using Amicon ultra centrifugal filtration with a YM3 membrane. TCEP-pretreated apo *Sc* Grx5 was reconstituted anaerobically using a 5-fold excess of bound Fe and a 10-fold excess of bound sulfide in the form of thioferrate in the presence of 3 mM GSH and incubated at room temperature overnight. The reconstituted sample was then loaded onto a Hi-Trap Q-Sepharose column (GE healthcare) previously equilibrated with anaerobic buffer (100 mM Tris-HCl, pH 7.5, with 3 mM GSH) and purified with a 0-1 M NaCl gradient. The eluted colored fractions were pooled and concentrated via Amicon ultra centrifugal filtration with a YM3 membrane.

Prior to reconstitution, apo-*Av* Grx5 was incubated with 3 mM GSH for 1 hour under anaerobic conditions. Reconstitution involved incubation of GSH-pretreated apo-*Av* Grx5 with thioferrate with 4-fold excess of bound Fe and 8-fold excess of bound sulfide under anaerobic conditions at room temperature overnight. Excess reagents were removed by passing the reconstitution mixture through a previously equilibrated Hi-Trap Q-Sepharose column (GE healthcare) with anaerobic buffer (100 mM Tris-HCl, pH 7.5, with 3 mM GSH,) and purified with

an increasing linear gradient of 0-1 M NaCl. The eluted colored fractions were pooled and concentrated using Amicon ultra centrifugal filtration with a YM3 membrane.

Reconstitution of *Pf* Fdx involved mixing DTT-pretreated apo-Fdx with a 12-fold excess of bound Fe and a 24-fold excess of bound sulfide in form of thioferrate in the presence of 10 mM DTT, and incubating overnight at room temperature. The sample was then loaded onto a Hi-Trap Q-Sepharose column (GE healthcare) previously equilibrated with anaerobic buffer (100 mM Tris-HCl, pH 7.5) and purified with an increasing linear gradient of 0-1 M NaCl. The colored fractions eluted were combined and concentrated by Amicon ultra centrifugal filtration with a YM3 membrane.

Reconstitution of *Av* Fdx involved mixing DTT-pretreated apo *Av* Fdx with thioferrate containing 8-fold excess of bound Fe and 16-fold excess of bound sulfide under anaerobic conditions at room temperature. The reconstitution process was monitored for 6 hours via UV-visible absorption and CD spectroscopy until completion. Sample was then purified using a pre-equilibrated Hi-Trap Q-Sepharose column (GE healthcare) with anaerobic buffer (100 mM Tris-HCl, pH 7.5) with a 0-1 M NaCl gradient. The eluted colored fractions were pooled and concentrated using Amicon ultra centrifugal filtration with a YM3 membrane. This reconstitution was repeated as described above except the colored fractions were kept separately and their content and integrity were compared with holo-$[2Fe\text{-}2S]^{2+}$ Fdx using UV-visible absorption and CD spectra.

Analytical and Spectroscopic characterization methods. Mass spectrometry experiments were carried out by University of Georgia Proteomic and Mass Spectrometry Facility. Concentrations of proteins were determined using the *DC*™ Protein Assay (Bio-Rad) with bovine serum albumin as the standard. Concentrations of iron were determined colorimetrically using

bathophenanthroline under reducing conditions after digestion of proteins in 0.8% potassium permanganate and 0.2 M HCl (24). Anaerobic samples for spectroscopic studies were prepared in a Vacuum Atmosphere glove box under argon atmosphere (O_2 < 2 ppm). UV-visible absorption and CD spectra were recorded in septa-sealed 0.1 or 1 cm quartz cuvettes at room temperature using a Shimadzu UV-3101 PC scanning spectrophotometer and a Jasco J-715 spectropolarimeter, respectively. X-band (~9.35 GHz) EPR spectra were recorded using an EMXplus spectrometer (Bruker, Billerica, MA) equipped with an EMXplus standard cavity and an ESR 900 (4112HV) helium flow cryostat (Oxford Instruments, Concord, MA) fitted to a cryogen-free Stinger F70L unit. XAS data acquisition and analysis were carried out by Dr. Graham George (University of Saskatchewan) at SSRL, CA.

Results

Characterization of thioferrate. Colloidal suspensions of sodium thioferrate made from FAC and Na_2S under aerobic conditions at pH 10 exhibit four pronounced UV-visible absorption bands at 330 nm, 435 nm, 533 nm, and 637 nm, similar to what has been observed for $NaFeS_2$ alkaline thioferrate prepared from $Fe(NO_3)_3$ and NaSH in the presence of $NaNO_3$ at pH 11 (13). As expected, the CD spectrum of thioferrate is very weak and featureless. Addition of FAC to Na_2S up to the optimum ratio of S^{2-}/Fe^{3+} of 16 causes simultaneous increase in the intensity of the absorption bands, as shown Figure 2.2. Further addition of FAC results in broadening, decreased intensity, and blue shifts of these absorption bands. However, addition of sodium sulfide to restore the optimum ratio of S^{2-}/Fe^{3+} of 16 reverses these changes in the absorption bands. As a function of time, the visible absorption spectrum of thioferrate under aerobic conditions initially undergoes a rapid increase in intensity, followed by more gradual decrease in intensity of the absorption bands as a result of flocculation of the colloidal suspension of thioferrate, as shown in Figure 2.3.

Eventually the dark green thioferrate particles separate from the solution. Under aerobic conditions the dark green color of thioferrate particles convert into orange solids indicative of ferric oxide/hydroxide formation within few days. This process does not occur under anaerobic conditions and is suppressed in the presence of larger excesses of sulfide (i.e. 48-fold excess), which stabilize thioferrate under aerobic conditions, as judged by the persistence of dark green thioferrate particles for months. Thioferrate samples prepared at pH 8 in the presence of 150 mM NaCl have similar absorption features to those observed at pH 10 and behave similarly over time under aerobic conditions except instead of formation of ferric oxide/hydroxide, thioferrate particles decompose and turn into an orange solution. No significant difference in the absorption spectra of thioferrate samples at pH 8 was observed between reactions performed under anerobic and aerobic conditions. However, thioferrate particles kept their green color under anaerobic conditions even at low concentrations of sulfide for months.

In accord with antiferromagnetic coupling of high spin Fe^{3+} ions in a linear chain, no EPR signals were observed at 10 K for freshly made thioferrate samples under anaerobic conditions. Moreover, the absence of an isotropic g = 4.3 resonance, demonstrates the absence of free Fe^{3+} ions in the solution (data not shown). In addition, a g = 4.3 resonance was not observed in the EPR spectrum of the supernatant collected from thioferrate after sedimentation, suggesting no Fe^{3+} ions were released from thioferrate polymer chains over the time. As a control, a sharp and intense derivative signal at g = 4.3 was observed in the EPR spectrum of a sample of FAC with the same Fe^{3+} ion concentration as in thioferrate sample under the same experimental conditions.

X-ray absorption spectroscopy at Fe K-edge was used to characterize the structure of freshly prepared anaerobic thioferrate and the changes in the structure for samples aged for 44 hours under anaerobic conditions. The UV-visible absorption spectra of these samples are shown

in Figure 2.4 and the Fe K-edge EXAFS oscillations with the corresponding EXAFS Fourier transforms and best fit simulations are shown in Figure 2.5. Notably, the UV-visible absorption spectrum of aged thioferrate under anaerobic conditions is very similar to that of IssA. The Fe EXAFS data of freshly made and aged thioferrate samples are dominated by intense backscattering from four Fe-S interactions at 2.244 Å and 2.255 Å, respectively, and from two Fe…Fe interactions at 2.745 Å and 2.716 Å, respectively. In addition, freshly made and aged thioferrate also show a less-intense outer-shell Fourier transform peak at 5.495 Å and 5.431 Å, respectively, twice that of the shorter Fe…Fe interaction, that can only result from the long range Fe…Fe…Fe multiple scattering in a linear polymer. The Fe EXAFS of both samples are very similar. Aged thioferrate has a slightly longer Fe-S distances, but slightly shorter Fe…Fe distances, with a better-defined long-range peak. Consequently, the Fe EXAFS data indicates long-range Fe….Fe interaction corresponding to linear arrangement of Fe atoms similar to Fe K-edge EXAFS of the thioferrate-bound IssA and aconitase at high pH, which contains a linear $[3Fe\text{-}4S]^{1+}$ cluster (12,25). A comparison of the EXAFS-determined Fe-S and short and long range Fe….Fe distances in freshly prepared and aged thioferrate with those previously reported for the thioferrate-bound IssA is shown in Table 2.1.

***In vitro* thioferrate-mediated reconstitution of linear $[3Fe\text{-}4S]^{1+}$ clusters in *Sc* Grx5.** Monothiol Grxs are well established as [Fe-S] cluster trafficking proteins that bind $[2Fe\text{-}2S]^{2+}$ clusters at the subunit interface of a homodimer by the cysteinates of two exogenous GSHs and the rigorously conserved CGFS of each monomer (26-28). This binding arrangement allows for flexibility in cluster binding and monothiol Grxs are also known to bind linear $[3Fe\text{-}4S]^{1+}$ clusters with the same ligands as for $[2Fe\text{-}2S]^{2+}$ clusters and $[4Fe\text{-}4S]^{2+}$ clusters (21). The latter are formed by anaerobic reconstitution in the absence of GSH in a subset of monothiol Grxs that contain a

second conserved cysteine and cysteine mutagenesis studies indicate that the $[4Fe\text{-}4S]^{2+}$ clusters are ligated at the subunit interface by the two conserved cysteines in each monomer (21). *Sc* Grx was chosen for thioferrate-mediated reconstitution experiments because of its preference to bind linear $[3Fe\text{-}4S]^{1+}$ rather than $[2Fe\text{-}2S]^{2+}$ clusters in cysteine desulfurase-mediated reconstitution reactions in the presence of excess GSH (21). Thioferrate-mediated reconstitution of TCEP-pretreated *Sc* Grx5 under anaerobic conditions was carried out at room temperature in the presence of excess GSH, followed by repurification using ion-exchange chromatography. The resulting absorption spectrum comprises several pronounced features in the visible and near UV region at 330, 403, 515, and 570 nm, see Figure 2.6, and shares close similarity to published spectra for linear $[3Fe\text{-}4S]^{1+}$ clusters assembled by cysteine desulfurase-mediated reconstitution of *Sc* Grx5, synthetic complexes, and alkaline (purple) aconitase (21,29,30). The UV-visible CD spectra depend on the chirality of the cluster environment. Consequently, UV-visible CD spectra are more variable for linear $[3Fe\text{-}4S]^{1+}$ clusters in different proteins. However, based on the close similarity in the form and intensity of the UV-visible absorption and CD spectra, the cluster composition of thioferrate- and cysteine desulfurase-mediated reconstitutions of *Sc* Grx under analogous conditions are identical, within experimental error, see Figure 2.6. The cluster composition of the cysteine desulfurase-mediated reconstitution of *Sc* Grx used in Figure 2.6 was established by Mössbauer spectroscopy based on total Fe content to be 72% linear $[3Fe\text{-}4S]^{1+}$, 11% $[2Fe\text{-}2S]^{2+}$, 6% $[4Fe\text{-}4S]^{2+}$, and 11% adventitiously bound Fe^{2+} (21). Hence, a very similar cluster composition is inferred for thioferrate-mediated reconstitution of *Sc* Grx. These results demonstrate that thioferrate is very effective in reconstituting linear $[3Fe\text{-}4S]^{1+}$ clusters in proteins that can accommodate this type of cluster.

***In vitro* thioferrate-mediated reconstitution of $[2Fe\text{-}2S]^{2+}$ clusters in *Av* Grx5.** In contrast to *Sc* Grx5, anaerobically purified *Av* Grx5 and cysteine desulfurase-mediated reconstituted *Av* Grx5 exclusively contain $[2Fe\text{-}2S]^{2+}$ clusters, as judged by UV-visible absorption/CD (see Figure 2.7) and resonance Raman spectroscopy, along with protein and Fe analytical studies (22,31). Consequently, *Av* Grx5 provides an appropriate test of the ability of thioferrate-mediated reconstitution to assemble $[2Fe\text{-}2S]^{2+}$ clusters. Incubation of apo-*Av* Grx5 with thioferrate at room temperature under anaerobic conditions in the presence of GSH, followed by repurification, resulted in formation of cluster-loaded *Av* Grx5 as shown by the UV-visible absorption and CD spectra shown in Figure 2.7. The absorption features of the cluster-bound *Av* Grx5 in the visible and near-UV range are very similar to those previously reported for the subunit-bridging $[2Fe\text{-}2S]^{2+}$ clusters in *Av* Grx5 and monothiol Grxs in general, with dominant peaks at 322 and 403 nm and a broad shoulder centered near 515 nm (26,31-33). In addition to $[2Fe\text{-}2S]^{2+}$ clusters, the presence of linear $[3Fe\text{-}4S]^{1+}$ clusters is also apparent in the thioferrate reconstituted sample, based on the weak, but characteristic absorption bands centered at 566 and 513 nm (21,29,30). This is supported by comparison of the CD spectra of cysteine desulfurase- and thioferrate-reconstituted *Av* Grx5, see Figure 2.7. Thioferrate-reconstituted *Av* Grx5 exhibits weaker CD with subtle changes in the form of $[2Fe\text{-}2S]^{2+}$ cluster CD spectrum. Subtraction of 60% of the pure $[2Fe\text{-}2S]^{2+}$ cluster CD from the thioferrate-reconstituted CD results in a CD spectrum that closely resembles the CD spectrum of linear $[3Fe\text{-}4S]^{1+}$ cluster-bound monothiol Grxs shown in Figure 2.6, with broad positive bands centered at 560 and 470 nm and a broad negative band centered at 350 nm. The intensity of the CD spectrum corresponding to linear $[3Fe\text{-}4S]^{1+}$ clusters in thioferrate-reconstituted *Av* Grx5 compared to that of the rigorously quantified CD spectrum of linear $[3Fe\text{-}4S]^{1+}$ clusters in *Sc* Grx5 indicates that thioferrate-reconstituted *Av* Grx5 contains

~20% linear $[3Fe\text{-}4S]^{1+}$ clusters and ~80% $[2Fe\text{-}2S]^{2+}$ clusters. Overall, these results show that thioferrate is capable of reconstituting $[2Fe\text{-}2S]^{2+}$ clusters in monothiol Grxs and raise the possibility that the mechanism of reconstitution involves transfer of a linear $[3Fe\text{-}4S]^{1+}$ fragment, which subsequently decays by losing one Fe^{3+} and two S^{2-} to form a $[2Fe\text{-}2S]^{2+}$ cluster.

***In vitro* thioferrate-mediated reconstitution of $[4Fe\text{-}4S]^{2+}$ clusters in *Pf* Fdx.** In order to assess the ability of synthesized thioferrate to provide iron and sulfide for $[4Fe\text{-}4S]^{2+}$ clusters assembly, and to compare the results with those observed for IssA-mediated reconstitution (12), thioferrate-mediated reconstitution of apo-*Pf* Fdx under anaerobic conditions was conducted. Since a $[4Fe\text{-}4S]^{2+}$ cluster is more reduced than the all-ferric thioferrate, reconstitution was carried out in the presence of a reducing agent, DTT. No sedimentation was observed after centrifugation of the reaction mixture following overnight reconstitution. After chromatographic removal of excess thioferrate reagents, a cluster-loaded form of *Pf* Fdx was obtained as shown by UV-visible absorption and CD spectra, see Figure 2.8. The type and quantitation of the thioferrate-reconstituted clusters were assessed based on comparison with the UV-visible absorption and CD spectra of native holo-*Pf* Fdx, see Figure 2.8. The absorption spectrum of thioferrate-reconstituted *Pf* Fdx exhibits a broad band centered at 400 nm, that is characteristic of a $[4Fe\text{-}4S]^{2+}$ cluster, albeit with 50% occupancy as ε_{400} is 50% of that observed for native holo *Pf* Fdx. Interestingly, very similar results were observed for room-temperature IssA-mediated reconstitution of apo-*Pf* Fdx (12). The corresponding UV-visible CD spectrum is also indicative of a $[4Fe\text{-}4S]^{2+}$ center and is very similar to that of native holo-*Pf* Fdx. However, there are small shifts and changes in CD intensity that suggest the presence of another type of cluster. Indeed, subtraction of 50% of the holo *Pf* Fdx CD spectrum from the thioferrate-reconstituted CD results in a CD spectrum that resembles the CD spectrum of linear $[3Fe\text{-}4S]^{1+}$ cluster-bound monothiol Grxs shown in Figure

2.6, except for a positive rather than a negative band at ~350 nm. Hence, the CD data suggests a minor contribution from a linear $[3Fe\text{-}4S]^{1+}$ cluster. Overall, these results show that thioferrate is capable of reconstituting $[4Fe\text{-}4S]^{2+}$ clusters in *Pf* Fdx and support the possibility that the mechanism of reconstitution involves transfer of a linear $[3Fe\text{-}4S]^{1+}$ fragment, which undergoes addition of a Fe^{2+} ion under reducing conditions to form a $[4Fe\text{-}4S]^{2+}$ cluster.

***In vitro* thioferrate-mediated reconstitution of $[2Fe\text{-}2S]^{2+}$ clusters in *Av* Fdx.** As purified holo *Av* Fdx contains one $[2Fe\text{-}2S]^{2+}$ cluster per monomer, which exhibits a UV-visible absorption spectrum with partially resolved bands at 337and 322 nm, well-resolved bands at 458 and 414 nm and broad tail centered at ~550 nm, and an intense CD spectrum comprising at least eight distinct $CysS^{-}$-to-Fe^{3+} or S^{2-}-to-Fe^{3+} charge transfer bands, see Figure 2.9 (34). Identical UV-visible absorption and CD spectra were obtained for samples of apo *Av* Fdx reconstituted using a cysteine desulfurase-mediated reaction. In contrast, thioferrate-mediated reconstitution of apo *Av* Fdx involving overnight incubation of apo-Fdx with thioferrate under anaerobic conditions, followed by purification by ion-exchange chromatography, yielded a different cluster content based on the marked differences in the UV-visible absorption and CD spectra, see Figure 2.9. The UV-visible absorption spectrum of thioferrate-mediated reconstituted *Av* Fdx lacks the band at 337 nm and has additional prominent bands at 525 and 580 nm, which are characteristic of a linear $[3Fe\text{-}4S]^{1+}$ cluster. The UV-visible CD spectrum is characteristic of the native $[2Fe\text{-}2S]^{2+}$ center, albeit at ~18% occupancy based on the CD intensity and the lack of any additional CD bands indicates weak CD intensity for the linear $[3Fe\text{-}4S]^{1+}$ center.

Purification of thioferrate-reconstituted *Av* Fdx with a more gradual NaCl gradient facilitated isolation of *Av* Fdx fractions containing only $[2Fe\text{-}2S]^{2+}$ or linear $[3Fe\text{-}4S]^{1+}$ clusters, see Figure 2.10. This enables detailed spectroscopic characterization of both types of cluster

assembled in thioferrate-reconstituted *Av* Fdx. The UV-visible absorption and CD spectra of the $[2Fe\text{-}2S]^{2+}$ center are identical to that of the holo Fdx, albeit with intensities corresponding to ~20% cluster occupancy. The linear $[3Fe\text{-}4S]^{1+}$ center has characteristic absorption bands centered at 320, 415, 525, and 580 nm and a weak CD spectrum that is very similar to those observed for the linear $[3Fe\text{-}4S]^{1+}$ centers found in monothiol Grxs and *Pf* Fdx except for opposite signs for CD bands at 480 and 560 nm that result from differences in the chirality of the cluster environment in different proteins. Overall the results demonstrate that thioferrate is capable of reconstituting linear $[3Fe\text{-}4S]^{1+}$ clusters in an Isc Fdx that customarily only accommodates $[2Fe\text{-}2S]^{2+}$ clusters and suggest that $[2Fe\text{-}2S]^{2+}$ assemble occurs by degradation of bound linear $[3Fe\text{-}4S]^{1+}$ clusters.

Discussion

In this work, we have investigated the nature and properties of thioferrate as well as the mechanism of [Fe-S] cluster assembly on apo Fe-S proteins using thioferrate as the source of iron and sulfide. Using a combination of spectroscopic techniques, we demonstrate that a green colloidal suspension of thioferrate can be formed rapidly from FAC and sodium sulfide under aerobic or anaerobic conditions in the pH range 8-10. The UV-visible absorption spectrum of thioferrate comprises several intense S^{2-}-to-Fe^{3+} charge transfer transitions and is in excellent agreement with previously published spectra of $NaFeS_2$ thioferrate (13). The uniform development of the thioferrate absorption spectrum over time at high concentrations of sodium sulfide (S^{2-}/Fe^{3+} > 16) on addition of FAC implies that all spectral peaks arise from the same species (13). It also indicates the increase in thioferrate concentration as a result of increasing length of the polymer chains. As the reaction proceeds further the uniform decrease in the intensity of the absorption bands with no obvious shifts in the spectrum is consistent with flocculation process observed for colloidal suspensions rather than precipitation by depression of solubility or ion effects (13). The

dark green color of the flocculated thioferrate coupled with the close resemblance of its absorption spectrum to fresh thioferrate, although broadened and less well-defined, all indicate that no major structural changes occur throughout the process of flocculation. This was confirmed by EXAFS analysis which revealed that freshly made thioferrate and flocculated suspension that formed after 44 hours both comprised a linear arrangement of iron atoms in form of linear $(FeS_2^-)_n$ polymer with two sulfides bridging each pair of ferric ions. It appears that as a function of time during charge neutralizing flocculation, sodium cations arrange their positions between the anionic polymer chains. In *Pf* IssA, charge neutralization is most likely achieved by the unstructured, proline-rich, C-terminal tail, which comprises predominantly of cationic, aromatic, and glycine residues and is proposed to wrap around the negatively charged thioferrate (12).

In this study we have observed that further flocculation results in sedimentation and isolation of an intense green-colored solid in both aerobically and anaerobically synthesized thioferrates. Under aerobic conditions, the green solid thioferrate persists for a few days at pH 8, before gradually hydrolysis to yield an orange solution. At pH 10 the green thioferrate solid is converted to an orange solid of ferric oxide/hydroxide. In contrast, the green thioferrate particles persist with no change for months under anaerobic conditions. Based on these observations and previous studies, it would appear that $(FeS_2^-)_n$ is susceptible to nucleophilic attack (13). However, this reaction is suppressed by S^{2-} as no color change in the thioferrate solid particles was observed in S^{2-}-rich conditions, i.e. 48-fold excess, at pH 10 under aerobic conditions. Moreover, thioferrates are unstable at low pH values ($pH \leq 6.8$) indicating they are also susceptible to electrophilic attacks on sulfide bridges, which would also result in fragmentation of the polymer (13).

This work shows that thioferrate can rapidly form from S^{2-} and Fe^{3+} ions at physiologically relevant pH values. Consequently, although not generally recognized, thioferrate is a common impurity in reconstituted and oxidatively denatured Fe-S proteins, as judged by the characteristic absorption spectrum. This has led to widespread misinterpretation of thioferrate as a protein-bound [Fe-S] cluster. In particular, colloidal thioferrate has often been incorrectly assigned as protein-bound linear $[3Fe\text{-}4S]^{1+}$ clusters, which as a thioferrate fragment, has a somewhat similar absorption spectrum. This led to the erroneous interpretation that protein-bound linear $[3Fe\text{-}4S]^{1+}$ clusters were degradation products of denatured $[2Fe\text{-}2S]^{2+}$, cubane $[3Fe\text{-}4S]^{1+}$, and $[4Fe\text{-}4S]^{2+}$ clusters in ferredoxins (35-39). This was corrected when the authors of these papers found that "iron sulfides" formed in the absence of protein can have the same spectrum, but the "iron sulfides" were not identified as thioferrate (40). As shown in this work, such erroneous interpretations are easily avoided because of the differences in the properties and spectroscopic signatures of colloidal thioferrate and protein-bound linear $[3Fe\text{-}4S]^{1+}$ clusters. For example, colloidal thioferrate can easily be removed by centrifugation. Moreover, the UV-visible absorption bands of thioferrate (330 nm, 435 nm, 533 nm, and 637 nm) are all significantly red-shifted compared to synthetic and protein-bound linear $[3Fe\text{-}4S]^{1+}$ clusters (320, 415, 525, and 580 nm) and only protein-bound linear $[3Fe\text{-}4S]^{1+}$ clusters exhibit a UV-visible CD spectrum. In addition, thioferrate exhibits a weak and very broad EPR signal centered near $g = 2$ that is only observed above ~60 K due to antiferromagnetic coupling of the high-spin ferric ions (12), whereas linear $[3Fe\text{-}4S]^{1+}$ clusters have a $S = 5/2$ ground state with a characteristic EPR spectrum (21,29,30,41).

The EXAFS results for thioferrate obtained in this work provide definitive confirmation that IssA binds thioferrate. This result, coupled with the demonstrated ability of thioferrate-associated *Pf* IssA to reconstitute a $[4Fe\text{-}4S]^{2+}$ cluster in apo *Pf* Fdx (12), provided the impetus to

investigate the effectiveness of thioferrate in reconstituting [Fe-S] clusters in $[2Fe\text{-}2S]^{2+}$ and $[4Fe\text{-}4S]^{2+}$ Fdxs and monothiol Grxs proteins. The results provide significant impact on understanding IssA role in [Fe-S] cluster biogenesis and show that thioferrate is capable of reconstituting $[2Fe\text{-}2S]^{2+}$, linear $[3Fe\text{-}4S]^{1+}$, and $[4Fe\text{-}4S]^{2+}$ clusters, with the latter requiring reducing equivalents in the form of DTT. In all cases, the reconstitution products were shown to contain linear $[3Fe\text{-}4S]^{1+}$ clusters as a major or minor component, even though two of proteins investigated, *Pf* Fdx and *Av* Fdx are known to have exclusive preference for binding and reconstituting $[4Fe\text{-}4S]^{2+}$ and $[2Fe\text{-}2S]^{2+}$ clusters, respectively (20,34). Moreover, the only protein that was reconstituted fully was *Sc* Grx5, which is known to have a preference for binding linear $[3Fe\text{-}4S]^{1+}$ clusters (21). These results suggest that the mechanism of thioferrate [Fe-S] cluster reconstitution involves thioferrate binding to two cysteine residues on the apo protein, followed by cleavage of the polymer chain to form a bound linear $[3Fe\text{-}4S]^{1+}$ cluster. $[4Fe\text{-}4S]^{2+}$ cluster formation would then be accomplished by addition of one Fe^{2+} ion and one electron under reducing conditions and $[2Fe\text{-}2S]^{2+}$ clusters formation would involve lose of one Fe^{3+} and two S^{2-}. Both cluster transformations would likely required major protein conformational changes and hence would be the rate-determining steps.

Acknowledgment

We thank Dr. Dennis Dean and co-workers for providing the plasmid for the recombinant expression of *Av* Grx5 and *Av* Fdx.

References

1. Johnson, D. C., Dean, D. R., Smith, A. D., and Johnson, M. K. (2005) Structure, function, and formation of biological iron-sulfur clusters. *Annu. Rev. Biochem.* **74**, 247-281

2. Malkin, R., and Rabinowitz, J. C. (1966) The reconstitution of *clostridial* ferredoxin. *Biochem. Biophys. Res. Commun.* **23**, 822-827

3. Sawyer, D. T., and Valentine, J. S. (1981) How super is superoxide? *Acc. Chem. Res.* **14**, 393-400

4. Fridovich, I. (1998) Oxygen toxicity: a radical explanation. *J. Exp. Biol.* **201**, 1203-1209

5. Fridovich, I. (1997) Superoxide anion radical ($O_2^{-\cdot}$), superoxide dismutases, and related matters. *J. Biol. Chem.* **272**, 18515-18517

6. Stohs, S. J., and Bagchi, D. (1995) Oxidative mechanisms in the toxicity of metal ions. *Free Radic. Biol. Med.* **18**, 321-336

7. Kim, J. H., Bothe, J. R., Alderson, T. R., and Markley, J. L. (2015) Tangled web of interactions among proteins involved in iron-sulfur cluster assembly as unraveled by NMR, SAXS, chemical crosslinking, and functional studies. *Biochim. Biophys. Acta* **1853**, 1416-1428

8. Lill, R. (2009) Function and biogenesis of iron–sulphur proteins. *Nature* **460**, 831-838

9. Py, B., and Barras, F. (2010) Building Fe–S proteins: bacterial strategies. *Nat. Rev. Microbiol.* **8**, 436-446

10. Albrecht, A. G., Netz, D. J. A., Miethke, M., Pierik, A. J., Burghaus, O., Peuckert, F., Lill, R., and Marahiel, M. A. (2010) SufU is an essential iron-sulfur cluster scaffold protein in *Bacillus subtilis*. *J. Bacteriol.* **192**, 1643-1651

11. Blanc, B., Gerez, C., and Ollagnier de Choudens, S. (2015) Assembly of Fe/S proteins in bacterial systems: biochemistry of the bacterial ISC system. *Biochim. Biophys. Acta* **1853**, 1436-1447

12. Vaccaro, B. J., Clarkson, S. M., Holden, J. F., Lee, D.-W., Wu, C.-H., Poole Ii, F. L., Cotelesage, J. J. H., Hackett, M. J., Mohebbi, S., Sun, J., Li, H., Johnson, M. K., George, G. N., and Adams, M. W. W. (2017) Biological iron-sulfur storage in a thioferrate-protein nanoparticle. *Nat. Commun.* **8**, 16110

13. Taylor, P., and Shoesmith, D. W. (1978) The nature of green alkaline iron sulfide solutions and the preparation of sodium iron(III) sulfide, $NaFeS_2$. *Can. J. Chem.* **56**, 2797-2802

14. Al-Ahmad, S. A., Kampf, J. W., Dunham, R. W., and Coucouvanis, D. (1991) Oxidation by elemental sulfur and coupling of iron/sulfur complexes. Synthesis and structural characterization of $(Et_4N)_4[Fe_4S_6(SEt)_4]$, a new Fe/S cluster with a linear Fe_4 backbone. *Inorg. Chem.* **30**, 1163-1164

15. Konnert, J. A., and Evans, H. T. (1980) The crystal structure of erdite, $NaFeS_2 \cdot 2H_2O$. *Am. Mineral.* **65**, 516-521

16. Sweeney, W. V., and Coffman, R. E. (1972) Magnetic properties of potassium dithioferrate: A linear chain antiferromagnet and model compound for the exchange interactions in two-iron ferredoxins. *Biochim. Biophys. Acta* **286**, 26-35

17. Seidov, Z., Krug von Nidda, H.-A., Hemberger, J., Loidl, A., Sultanov, G., Kerimova, E., and Panfilov, A. (2002) Magnetic susceptibility and ESR study of the covalent-chain antiferromagnets $TlFeS_2$ and $TlFeSe_2$. *Phys. Rev. B* **65**, 014433

18. Beinert, H., Holm, R. H., and Münck, E. (1997) Iron-sulfur clusters: nature's modular, multipurpose structures. *Science* **277**, 653-659

19. Chandramouli, K., Unciuleac, M.-C., Naik, S., Dean, D. R., Huynh, B. H., and Johnson, M. K. (2007) Formation and properties of [4Fe-4S] clusters on the IscU scaffold protein. *Biochemistry* **46**, 6804-6811

20. Aono, S., Bryant, F. O., and Adams, M. W. (1989) A novel and remarkably thermostable ferredoxin from the hyperthermophilic archaebacterium *Pyrococcus furiosus*. *J. Bacteriol.* **171**, 3433-3439

21. Zhang, B., Bandyopadhyay, S., Shakamuri, P., Naik, S. G., Huynh, B. H., Couturier, J., Rouhier, N., and Johnson, M. K. (2013) Monothiol glutaredoxins can bind linear $[Fe_3S_4]^+$ and $[Fe_4S_4]^{2+}$ clusters in addition to $[Fe_2S_2]^{2+}$ clusters: spectroscopic characterization and functional implications. *J. Am. Chem. Soc.* **135**, 15153-15164

22. Shakamuri, P., Zhang, B., and Johnson, M. K. (2012) Monothiol glutaredoxins function in storing and transporting $[Fe_2S_2]$ clusters assembled on IscU scaffold proteins. *J. Am. Chem. Soc.* **134**, 15213-15216

23. Moulis, J. M., and Meyer, J. (1982) Characterization of the selenium-substituted 2[4Fe-4Se] ferredoxin from *Clostridium pasteurianum*. *Biochemistry* **21**, 4762-4771

24. Fish, W. W. (1988) Rapid colorimetric micromethod for the quantitation of complexed iron in biological samples. *Methods Enzymol.* **158**, 357-364

25. Gailer, J., George, G. N., Pickering, I. J., Prince, R. C., Kohlhepp, P., Zhang, D., Walker, F. A., and Winzerling, J. J. (2001) Human cytosolic iron regulatory protein 1 contains a linear iron−sulfur cluster. *J. Am. Chem. Soc.* **123**, 10121-10122

26. Bandyopadhyay, S., Gama, F., Molina-Navarro, M. M., Gualberto, J. M., Claxton, R., Naik, S. G., Huynh, B. H., Herrero, E., Jacquot, J. P., Johnson, M. K., and Rouhier, N. (2008) Chloroplast monothiol glutaredoxins as scaffold proteins for the assembly and delivery of [2Fe–2S] clusters. *EMBO J. 27*, 1122-1133

27. Iwema, T., Picciocchi, A., Traore, D. A., Ferrer, J. L., Chauvat, F., and Jacquamet, L. (2009) Structural basis for delivery of the intact $[Fe_2S_2]$ cluster by monothiol glutaredoxin. *Biochemistry* **48**, 6041-6043

28. Johansson, C., Roos, Annette K., Montano, Sergio J., Sengupta, R., Filippakopoulos, P., Guo, K., von Delft, F., Holmgren, A., Oppermann, U., and Kavanagh, Kathryn L. (2010) The crystal structure of human GLRX5: iron–sulfur cluster co-ordination, tetrameric assembly and monomer activity. *Biochem. J.* **433**, 303-311

29. Hagen, K. S., Watson, A. D., and Holm, R. H. (1983) Synthetic routes to iron sulfide (Fe_2S_2, Fe_3S_4, Fe_4S_4, and Fe_6S_9), clusters from the common precursor $[Fe(SC_2H_5)_4]^{2-}$: structures and properties of $[Fe_3S_4(SR)_4]^{3-}$ and $[Fe_6S_9(SC_2H_5)_2]^{4-}$, examples of the newest types of Fe-S-SR clusters. *J. Am. Chem. Soc.* **105**, 3905-3913

30. Kennedy, M. C., Kent, T. A., Emptage, M., Merkle, H., Beinert, H., and Münck, E. (1984) Evidence for the formation of a linear [3Fe-4S] cluster in partially unfolded aconitase. *J. Biol. Chem.* **259**, 14463-14471

31. Zhang, B. (2013) *Spectroscopic and functional characterization of monothiol glutaredoxins and the fumarate nitrate reduction regulatory protein.* Ph.D. Thesis, University of Georgia

32. Li, H., Mapolelo, D. T., Dingra, N. N., Naik, S. G., Lees, N. S., Hoffman, B. M., Riggs-Gelasco, P. J., Huynh, B. H., Johnson, M. K., and Outten, C. E. (2009) The yeast iron regulatory proteins Grx3/4 and Fra2 form heterodimeric complexes containing a [2Fe-2S] cluster with cysteinyl and histidyl ligation. *Biochemistry* **48**, 9569-9581

33. Li, H., Mapolelo, D. T., Randeniya, S., Johnson, M. K., and Outten, C. E. (2012) Human glutaredoxin 3 forms [2Fe-2S]-bridged complexes with human BolA2. *Biochemistry* **51**, 1687-1696

34. Jung, Y. S., Gao-Sheridan, H. S., Christiansen, J., Dean, D. R., and Burgess, B. K. (1999) Purification and biophysical characterization of a new [2Fe-2S] ferredoxin from *Azotobacter vinelandii*, a putative [Fe-S] cluster assembly/repair protein. *J. Biol. Chem.* **274**, 32402-32410

35. Moczygemba, C., Guidry, J., Jones, K. L., Gomes, C. M., Teixeira, M., and Wittung-Stafshede, P. (2001) High stability of a ferredoxin from the hyperthermophilic archaeon *A. ambivalens*: involvement of electrostatic interactions and cofactors. *Protein Sci.* **10**, 1539-1548

36. Jones, K., Gomes, C. M., Huber, H., Teixeira, M., and Wittung-Stafshede, P. (2002) Formation of a linear [3Fe-4S] cluster in a seven-iron ferredoxin triggered by polypeptide unfolding. *J. Biol. Inorg. Chem.* **7**, 357-362

37. Higgins, C. L., and Wittung-Stafshede, P. (2004) Formation of linear three-iron clusters in *Aquifex aeolicus* two-iron ferredoxins: effect of protein-unfolding speed. *Arch. Biochem. Biophys.* **427**, 154-163

38. Griffin, S., Higgins, C. L., Soulimane, T., and Wittung-Stafshede, P. (2003) High thermal and chemical stability of *Thermus thermophilus* seven-iron ferredoxin. *Eur. J. Biochem.* **270**, 4736-4743

39. Wittung-Stafshede, P., Gomes, C. M., and Teixeira, M. (2000) Stability and folding of the ferredoxin from the hyperthermophilic archaeon *Acidianus ambivalens*. *J. Inorg. Biochem.* **78**, 35-41

40. Leal, S. S., Teixeira, M., and Gomes, C. M. (2004) Studies on the degradation pathway of iron-sulfur centers during unfolding of a hyperstable ferredoxin: cluster dissociation, iron release and protein stability. *J. Biol. Inorg. Chem.* **9**, 987-996

41. Richards, A. J. M., Thomson, A. J., Holm, R. H., and Hagen, K. S. (1990) The magnetic circular dichroism spectra of the linear trinuclear clusters $[Fe_3S_4(SR)_4]^{3-}$ in purple aconitase and in a synthetic model. *Spectrochim. Acta.* **46**, 987-993

Table 2.1. Comparison of the EXAFS-determined Fe-S and Fe…Fe distances in freshly prepared and aged thioferrate with those previously reported for the thioferrate-bound IssA. N: number of scattering atoms, R: bond length, σ^2: Debye-Waller factor.

		N	***R* (Å)**	**σ^2 (Å^2)**
Freshly prepared thioferrate	Fe–S	4	2.244(1)	0.0028(1)
	Fe⋯Fe	2	2.745(1)	0.0037(1)
	Fe⋯Fe⋯Fe	2	5.495(2)	0.0089(2)
Thioferrate after 44 hours	Fe–S	4	2.255(1)	0.0035(1)
	Fe⋯Fe	2	2.716(1)	0.0033(1)
	Fe⋯Fe⋯Fe	2	5.431(2)	0.0069(2)
IssA	Fe–S	4	2.243(1)	0.0044(1)
	Fe⋯Fe	2	2.704(1)	0.0032(1)
	Fe⋯Fe⋯Fe	2	5.408	0.0064

Figure 2.1. Proposed reaction for $[2Fe\text{-}2S]^{2+}$ and linear $[3Fe\text{-}4S]^{1+}$ fragments of thioferrate to form a $[4Fe\text{-}4S]^{2+}$ cluster. Ferric is shown in normal typeface. Valence-delocalized $Fe^{2.5+}$ is shown in bold and is circled. RS^- represents an organic sulfur ligand, i.e. alkyl thiolates in synthetic clusters and cysteinate residues in proteins.

[2Fe-2S]$^{2+}$ cluster

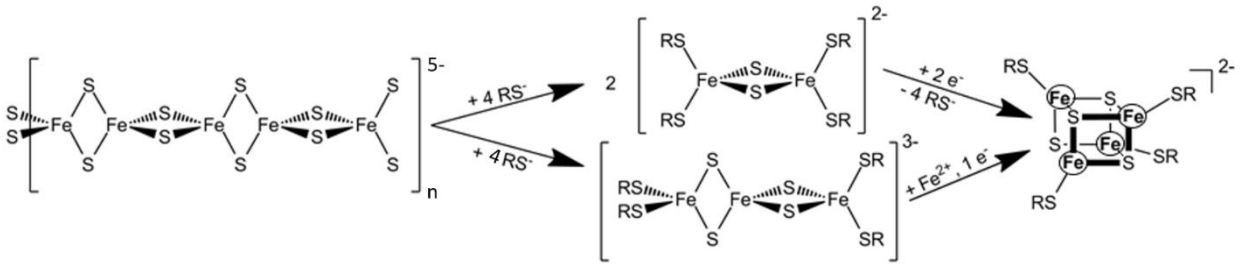

Thioferrate Linear [3Fe-4S]$^{1+}$ cluster [4Fe-4S]$^{2+}$ cluster

Figure 2.2. UV-visible absorption spectra of sodium thioferrate as a function of S^{2-} to Fe^{3+} ion ratios under aerobic conditions. Spectra were recorded in 0.1 cm cuvettes in 100 mM CAPS buffer, pH 10, supplemented with 150 mM NaCl. Inset shows the green colloidal suspension of sodium thioferrate obtained with a 16-fold excess of sodium sulfide.

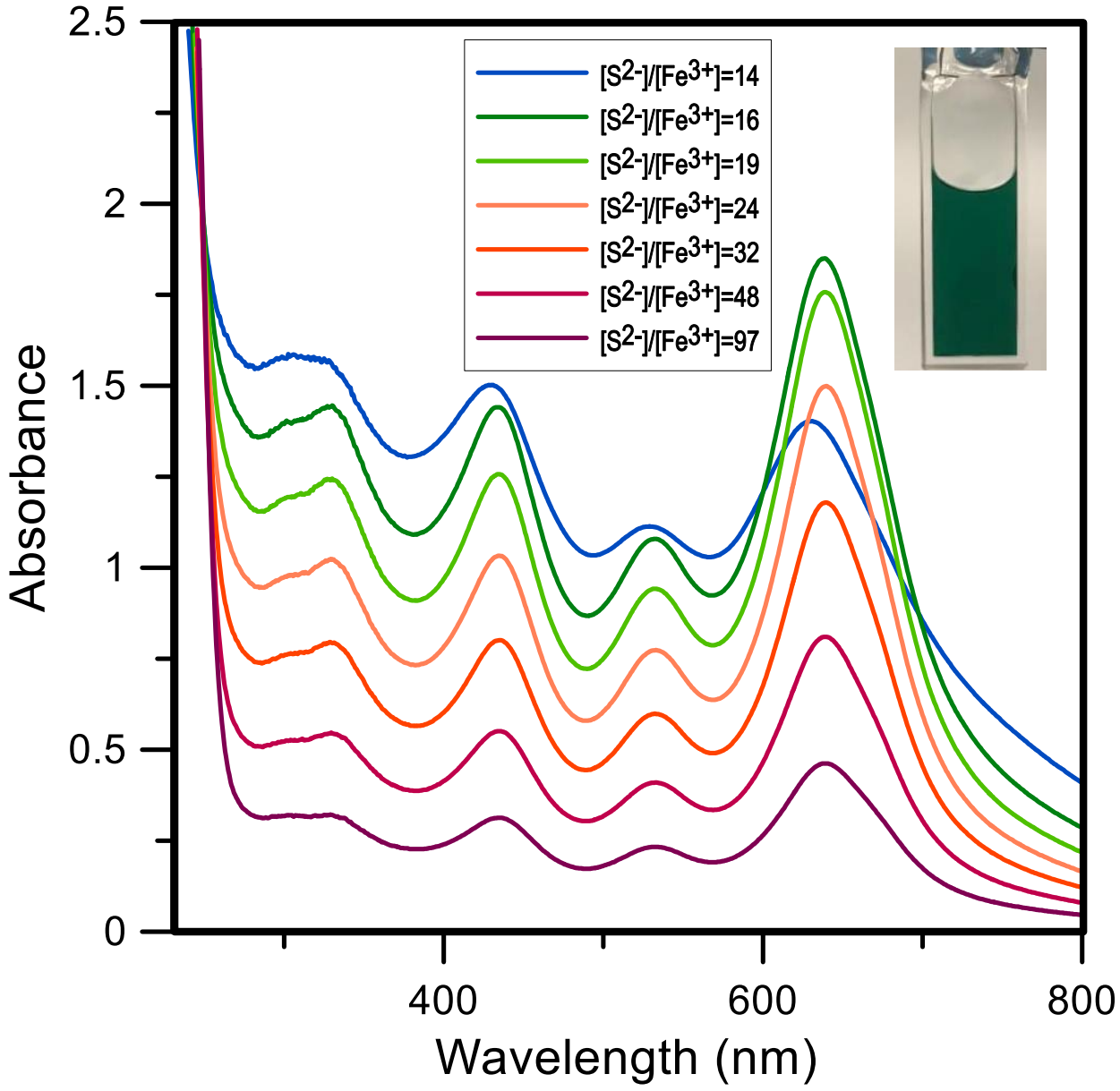
[S2-]/[Fe3+]=14
[S2-]/[Fe3+]=16
[S2-]/[Fe3+]=19
[S2-]/[Fe3+]=24
[S2-]/[Fe3+]=32
[S2-]/[Fe3+]=48
[S2-]/[Fe3+]=97
Absorbance
Wavelength (nm)
0
0.5
1
1.5
2
2.5
400
600
800

Figure 2.3. UV-visible absorption spectra of thioferrate under aerobic conditions as a function time at pH 10. (A) Development of UV-visible absorption spectrum of thioferrate. The first scan was started 30 seconds after mixing ferric ammonium citrate with a 19-fold excess sodium sulfide (black line). Subsequent scans were taken at 1-minute intervals (gray lines), until features reach the maximum intensity (red line). (B) Flocculation process of colloidal suspensions thioferrate. The first spectrum corresponds to the last scan in (A) and is shown as a red line. Subsequent scans were taken at 10-minute intervals (gray lines) and the absorption spectrum of thioferrate after 4 hours is shown as a blue line. Spectra were recorded under aerobic conditions in 0.1 cm cuvette in 100 mM CAPS buffer, pH 10, supplemented with 150 mM NaCl. Inset shows the orange ferric oxide/hydroxide formed from thioferrate particles with 16-fold excess sodium sulfide under aerobic conditions, and dark green thioferrate particles with no color change after 2 months in the presence of 48-fold excess sodium sulfide.

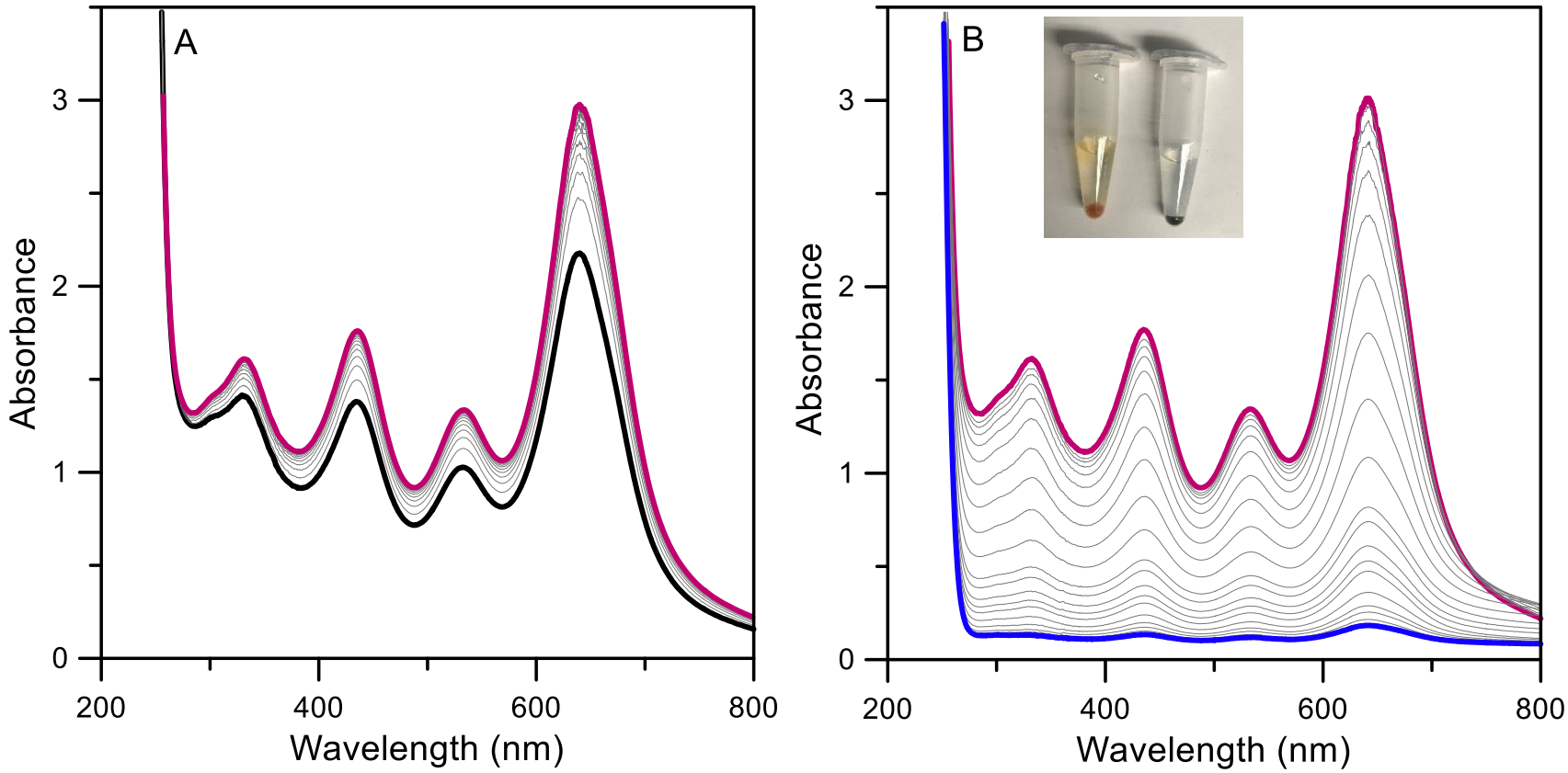
A
B
Absorbance
Wavelength (nm)
0
1
2
3
200
400
600
800

Figure 2.4. UV-visible absorption spectra of anaerobically prepared thioferrate samples used for XAS analysis. The sample was prepared under anaerobic conditions with 3.8 mM Fe^{3+} and 61 mM Na_2S prepared in 50 mM Tris-HCl buffer, pH 8, supplemented with 150 mM NaCl, and 20% (v/v) glycerol. The spectrum of the as prepared sample is shown as a black line and the spectrum of the sample aged for 44 hours at room temperature under anaerobic conditions is shown as a red line. Spectra were recorded in a 0.1 cm cuvette.

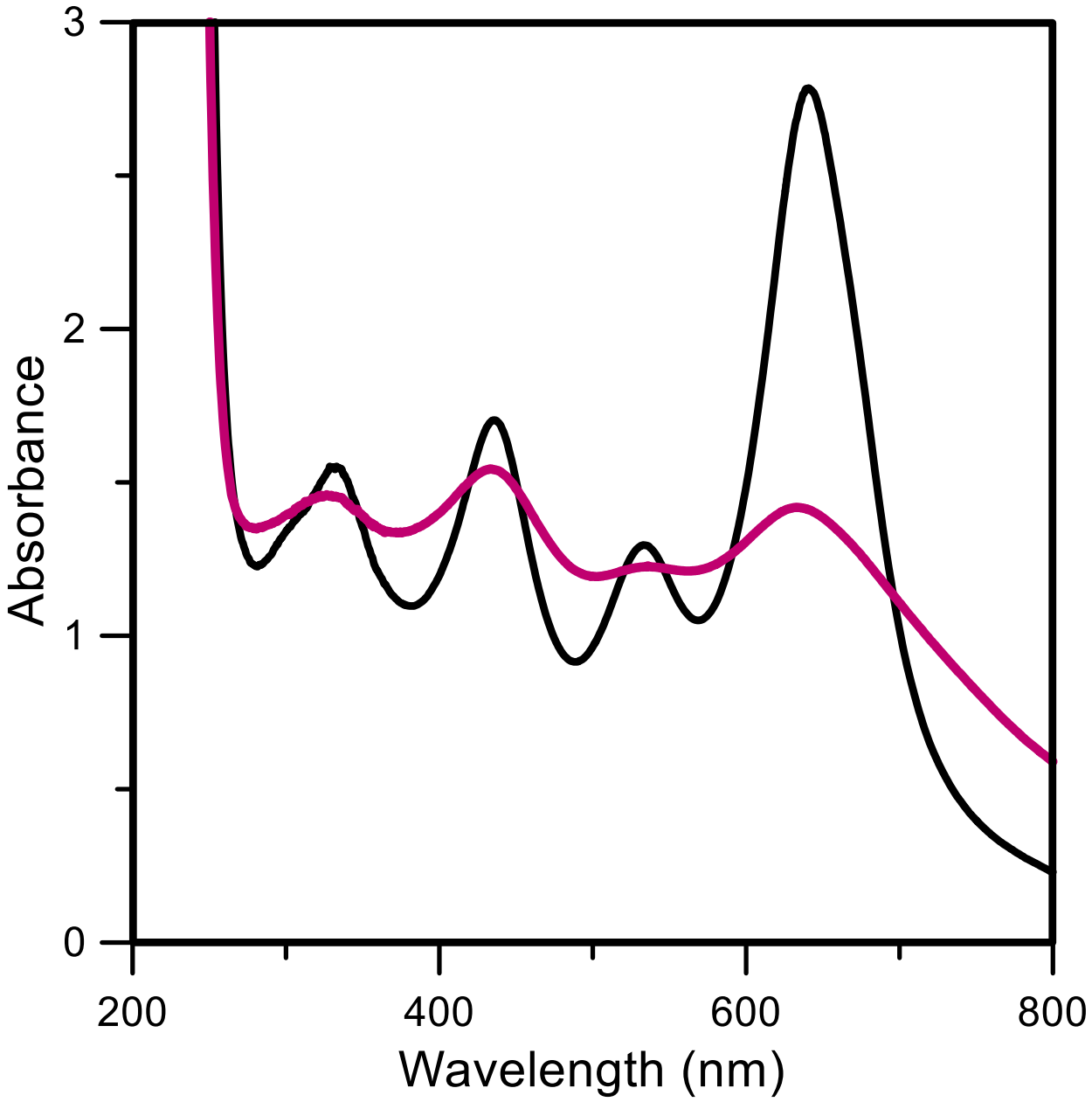
3
2
1
0
Absorbance
200
400
600
800
Wavelength (nm)

Figure 2.5. Sodium thioferrate Fe K-edge EXAFS spectra (top panel) and Fourier transforms (bottom panel). Samples were prepared with 3.8 mM Fe^{3+} and 61 mM Na_2S in 50 mM Tris-HCl buffer, pH 8, supplemented with 150 mM NaCl, and 20% glycerol under anaerobic conditions and kept sealed under strict anaerobic conditions. Each panel compares data for as prepared thioferrate (top spectrum and Fourier transform) and aged thioferrate that has been kept for 44 hours at room temperature under anaerobic conditions (bottom spectrum and Fourier transform). Experimental data are shown as blue lines and best fits are shown as red lines. The best fits indicate that aged thioferrate has a longer Fe-S, with a larger Debye-Waller factor ((2.255(1) Å, σ^2: 0.0035(1) $Å^2$ vs 2.244(1) Å, σ^2: 0.0028(1) $Å^2$), but a shorter Fe⋯Fe with a smaller Debye-Waller factor ((2.716(1) Å , σ^2: 0.0033(1) $Å^2$ vs 2.745(1) Å, σ^2: 0.0037(1) $Å^2$) than in the freshly prepared thioferrate. Similarly, the long-range Fe⋯Fe⋯Fe multiple scattering peak in the aged thioferrate sample is shorter with a smaller Debye-Waller factor ((5.431(2) Å, σ^2: 0.0069(1) $Å^2$ vs 5.495(2) Å, σ^2: 0.0089(2) $Å^2$) and is better defined than in the freshly prepared thioferrate.

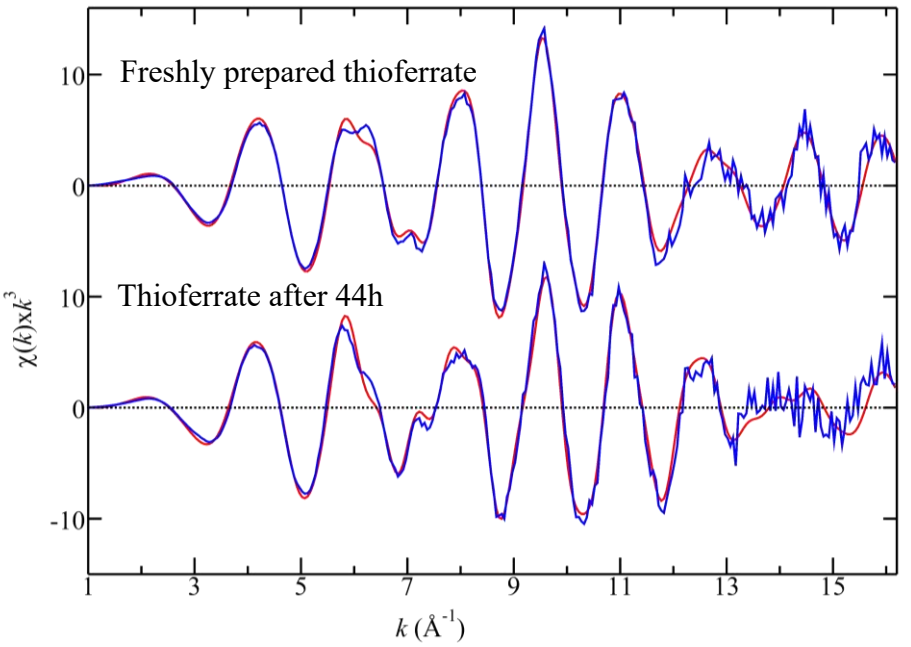
Freshly prepared thioferrate
Thioferrate after 44h
χ(k)xk3
k (Å-1)

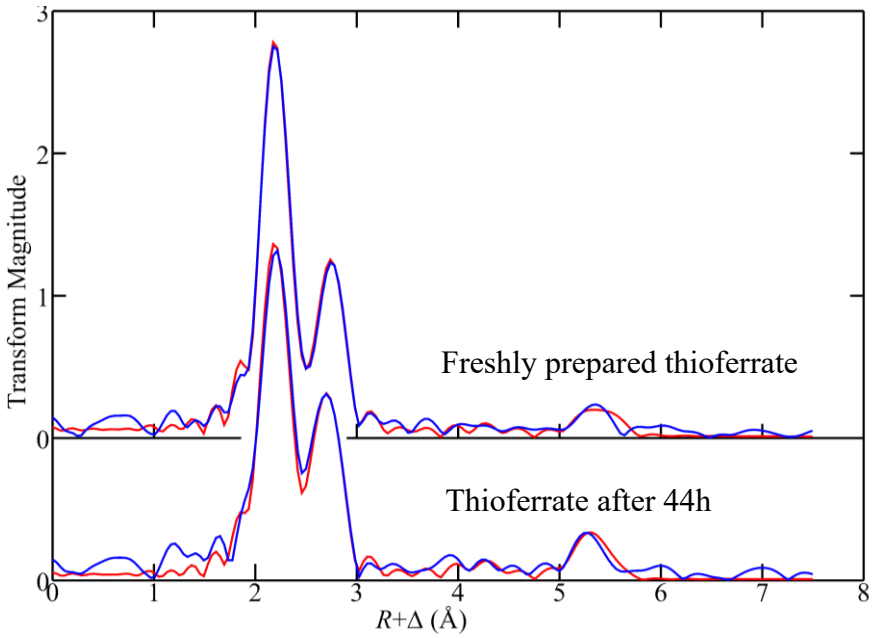
Transform Magnitude
Freshly prepared thioferrate
Thioferrate after 44h
R+Δ (Å)

Figure 2.6. Comparison of the UV-visible absorption and CD spectra of repurified products of cysteine desulfurase-mediated (red lines) and thioferrate-mediated (black lines) reconstitutions of *Sc* Grx5. Samples were in 100 mM Tris-HCl buffer, pH 7.5, with 250 mM NaCl and 1 mM GSH. Spectra were recorded under anaerobic conditions in sealed 1 cm cuvettes. ε and Δε values are based on protein monomer concentration.

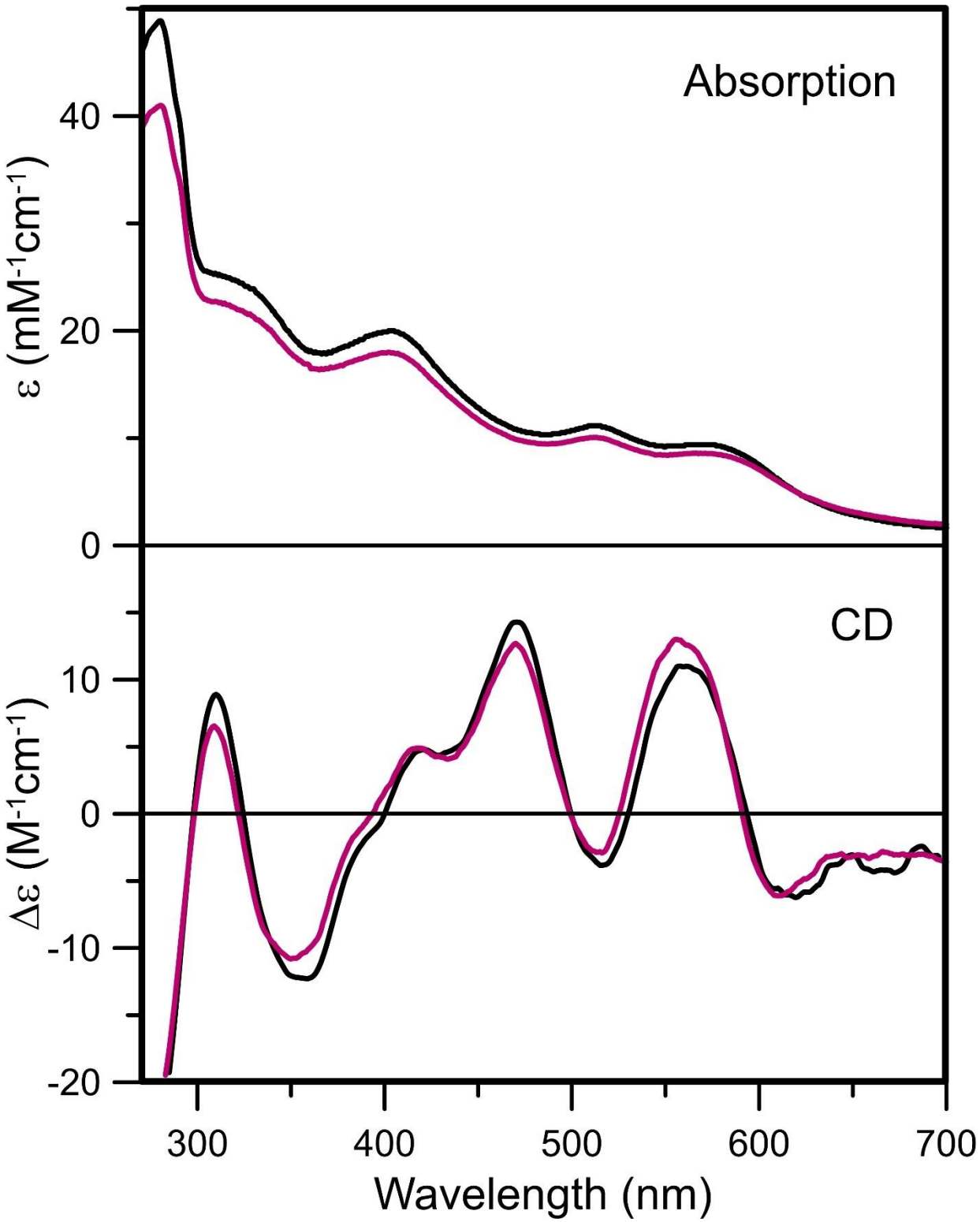
Absorption
CD
ε (mM-1cm-1)
Δε (M-1cm-1)
40
20
0
10
0
-10
-20
300
400
500
600
700
Wavelength (nm)

Figure 2.7. Comparison of the UV-visible absorption and CD spectra of holo $[2Fe\text{-}2S]^{2+}$ cluster-bound *Av* Grx5 (red lines) and repurified thioferrate-reconstituted apo *Av* Grx5 (black lines). Subtraction of 60% of the CD spectrum of holo $[2Fe\text{-}2S]^{2+}$ cluster-bound *Av* Grx5 from that of thioferrate-reconstituted apo *Av* Grx5, reveals the contribution of linear $[3Fe\text{-}4S]^{1+}$ clusters to the CD spectrum of thioferrate-reconstituted *Av* Grx5 (blue line). Samples were in 100 mM Tris-HCl buffer, pH 7.5, with 250 mM NaCl and 1 mM GSH. Spectra were recorded under anaerobic conditions in sealed 1 cm cuvettes. ε and $\Delta\varepsilon$ values are based on protein dimer concentration.

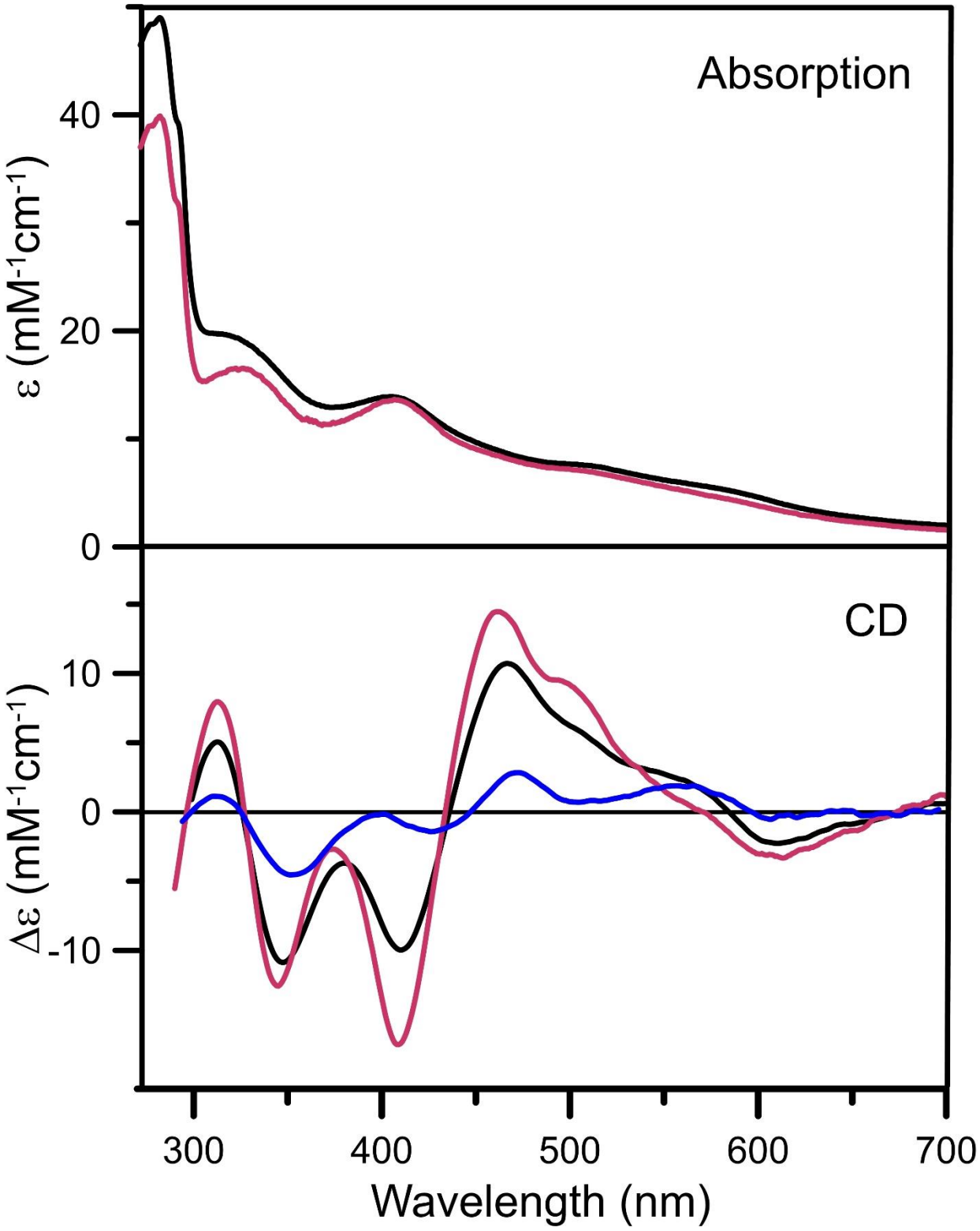
Absorption
40
20
0
ε (mM-1cm-1)
CD
10
0
-10
Δε (mM-1cm-1)
300
400
500
600
700
Wavelength (nm)

Figure 2.8. Comparison of the UV-visible absorption and CD spectra of holo $[4Fe\text{-}4S]^{2+}$ cluster-bound *Pf* Fdx (red lines) and repurified thioferrate-reconstituted apo *Pf* Fdx (black lines). Subtraction of 50% of the CD spectrum of holo *Pf* Fdx from that of thioferrate-reconstituted apo *Pf* Fdx, reveals the contribution of linear $[3Fe\text{-}4S]^{1+}$ clusters to the CD spectrum of thioferrate-reconstituted *Pf* Fdx (blue line). Samples were in in 100 mM Tris-HCl buffer, pH 7.5, with 250 mM NaCl. Spectra were recorded under anaerobic conditions in sealed 1 cm cuvettes. ε and $\Delta\varepsilon$ values are based on protein monomer concentration.

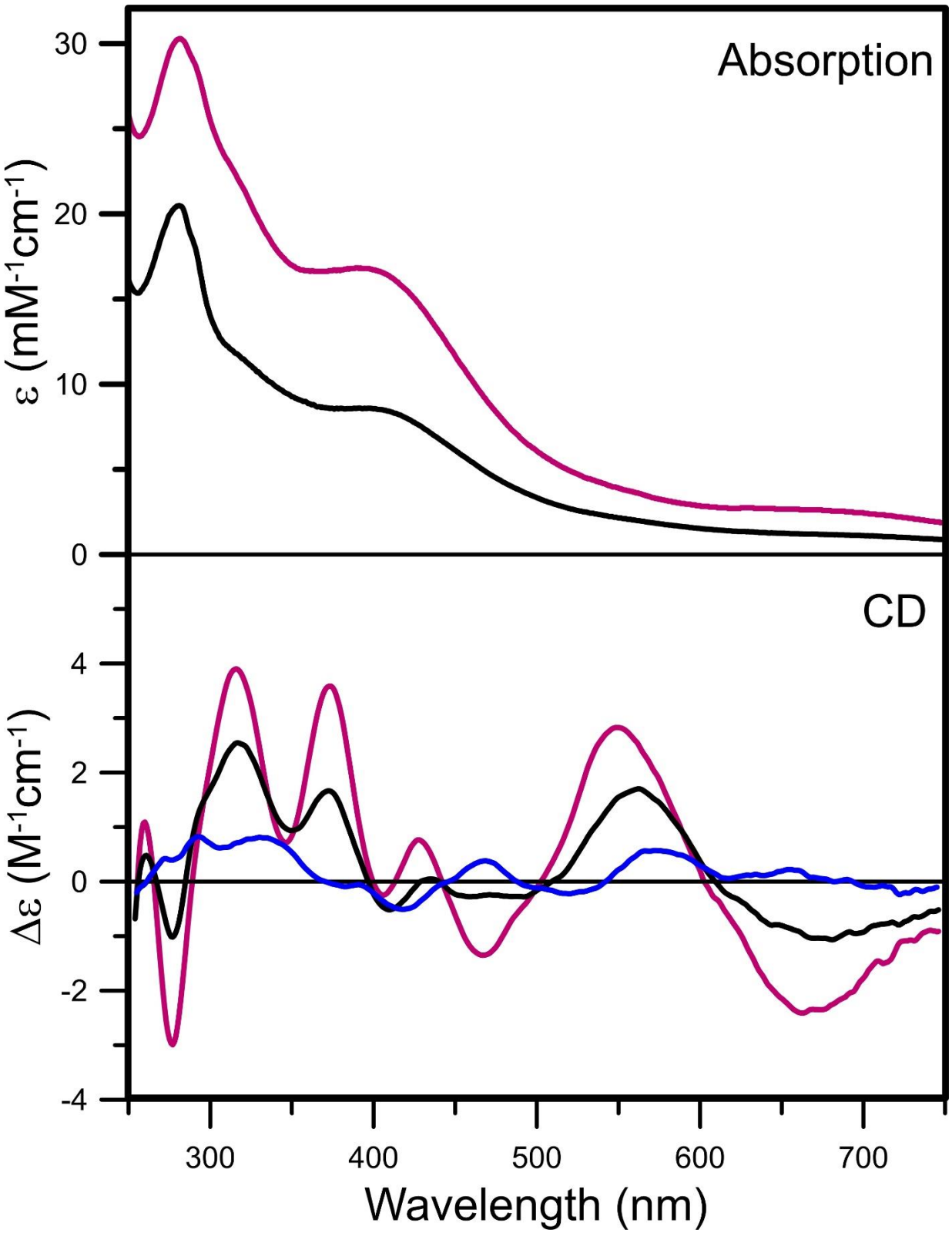
Absorption
ε (mM-1cm-1)
30
20
10
0
CD
Δε (M-1cm-1)
4
2
0
-2
-4
300
400
500
600
700
Wavelength (nm)

Figure 2.9. Comparison of the UV-visible absorption and CD spectra of holo $[2Fe\text{-}2S]^{2+}$ cluster-bound *Av* Fdx (red lines) and repurified thioferrate-reconstituted apo *Av* Fdx (black lines). Spectra were recorded under anaerobic conditions in sealed 1 cm cuvettes in 100 mM Tris-HCl buffer, pH 7.5, with 250 mM NaCl. ε and $\Delta\varepsilon$ values are based on protein monomer concentration.

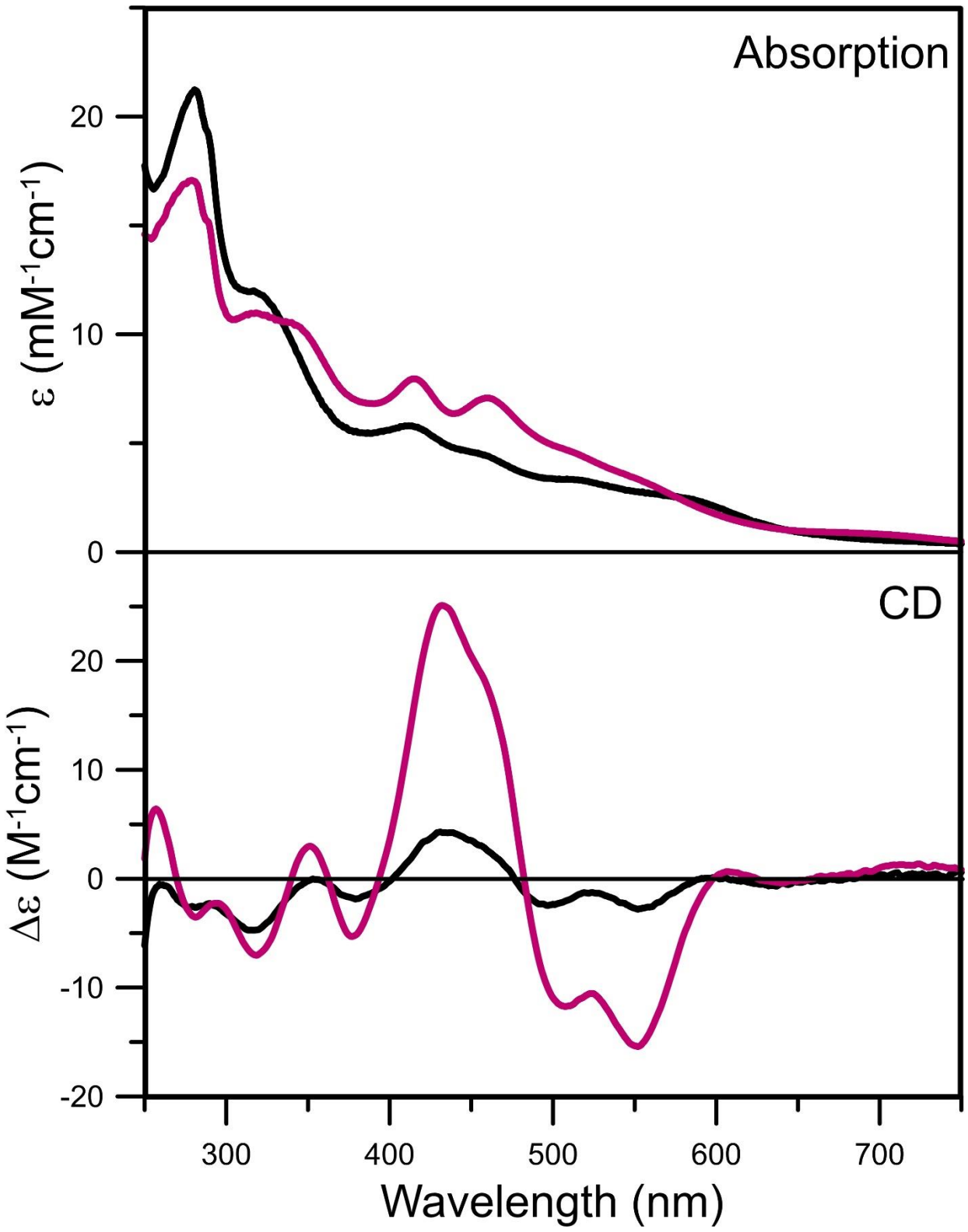
Absorption
ε (mM-1cm-1)
20
10
0
CD
Δε (M-1cm-1)
20
10
0
-10
-20
300
400
500
600
700
Wavelength (nm)

Figure 2.10. Comparison of the UV-visible absorption and CD spectra of holo *Av* Fdx (red lines) with chromatographically resolved fractions of thioferrate-reconstituted *Av* Fdx containing predominantly $[2Fe\text{-}2S]^{2+}$ clusters (A) or linear $[3Fe\text{-}4S]^{1+}$ clusters (B) (black lines). Spectra were recorded under anaerobic conditions in sealed 1 cm cuvettes in 100 mM Tris-HCl buffer, pH 7.5, with 250 mM NaCl. ε and Δε values are based on protein monomer concentration.

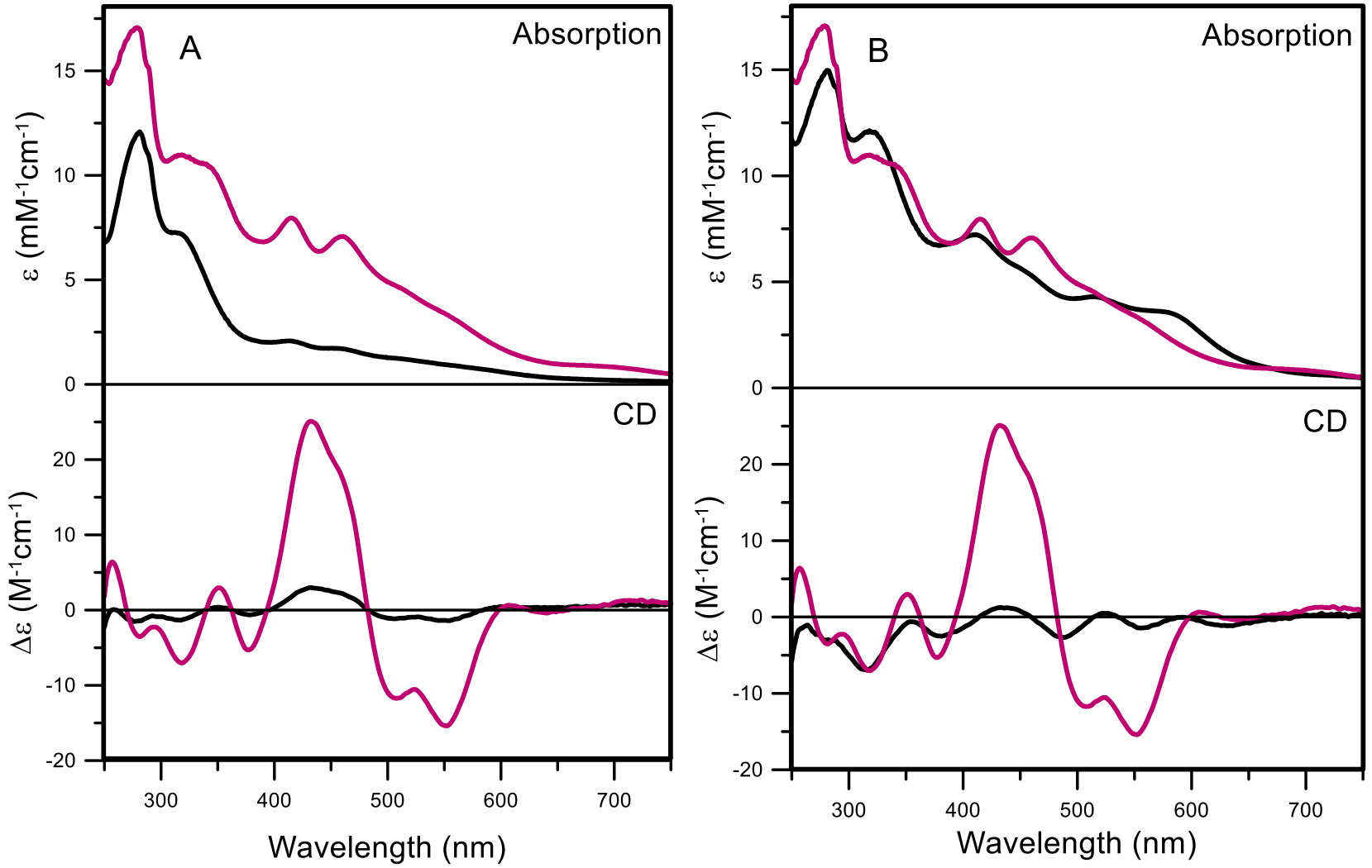
A
Absorption
ε (mM-1cm-1)
15
10
5
0
CD
Δε (M-1cm-1)
20
10
0
-10
-20
300
400
500
600
700
Wavelength (nm)
B
Absorption
ε (mM-1cm-1)
15
10
5
0
CD
Δε (M-1cm-1)
20
10
0
-10
-20
300
400
500
600
700
Wavelength (nm)

CHAPTER THREE

NEW INSIGHTS INTO THE MECHANISM AND INHIBITION OF $[2Fe\text{-}2S]^{2+}$ CLUSTER ASSEMBLY ON THE *AZOTOBACTER VINELANDII* ISCU SCAFFOLD PROTEIN

Sahel Mohebbi[1], Daniel P. Donnelly[2], Jeffrey N. Agar[2], and Michael K. Johnson[1]

To be submitted to J. Biol. Chem.

[1]Department of Chemistry Center for Metalloenzyme Studies, University of Georgia, Athens, Georgia 30602, USA. [2]Department of Chemistry and Chemical Biology, Northeastern University, 360 Huntington Avenue, Boston, Massachusetts 02115, USA

Abbreviations

Av, *Azotobacter vinelandii*; CD, circular dichroism; DT, dithionite; DTT, dithiothreitol; *Ec*, *E. coli*, *Escherichia coli*; EDTA, ethylenediaminetetraacetic acid; EPR, electron paramagnetic resonance; FAC, ferric ammonium citrate; FAS, ferrous ammonium sulfate; Fdx, ferredoxin; GSH, glutathione; ICP-MS, inductively coupled plasma mass spectrometry; IPTG, isopropyl β-D-thiogalactoside; LB, Lysogeny broth; L-Cys, L-cysteine; PLP, pyridoxal phosphate; PMSF, phenylmethylsulphonyl fluoride

Abstract

[Fe-S] clusters are one of the most ancient, ubiquitous, and structurally diverse classes of prosthetic groups in Nature. Proteins containing [Fe-S] clusters play essential roles in diverse biological processes including electron transfer, gene regulation, and substrate binding and activation. Thus, the process of Fe-S biosynthesis is essential to almost all forms of life and is remarkedly conserved in prokaryotic and eukaryotic organisms. Three distinct types of [Fe-S] cluster assembly machinery have been identified in prokaryotes, namely the NIF, ISC, and SUF systems. In each system the overall mechanism involves cysteine desulfurase-mediated assembly of transient [Fe-S] clusters on a scaffold proteins and intact cluster transfer clusters to apo proteins. However, the mechanism of $[2Fe\text{-}2S]^{2+}$ cluster assembly on the ubiquitous IscU scaffold protein has remained elusive. In this study, UV-visible CD spectroscopy and analytical studies are used to show that *Av* IscX binds a single Fe^{2+} ion that can be transferred to *Av* IscU, indicating that IscX is a specific Fe^{2+} donor for $[2Fe\text{-}2S]^{2+}$ cluster assembly on IscU in the bacterial ISC system. The role of *Av* Isc Fdx in IscS-mediated $[2Fe\text{-}2S]^{2+}$ cluster assembly on *Av* IscU was investigated by parallel UV-visible absorption and EPR studies. However, no evidence was forthcoming in support of the published proposal that reduced Fdx transfers an electron to form a transient IscS cysteine persulfide radical anion, which is subsequently transferred to a cysteine on IscU. We have also demonstrated that 5-, 6-, and 7-membered cyclic thiosulfinates cross-link cysteines on *Av* IscU and thereby inhibit Fe^{2+} binding and $[2Fe\text{-}2S]^{2+}$ cluster formation on IscU. The results show the potential of cyclic thiosulfinates for investigating the mechanism of $[2Fe\text{-}2S]^{2+}$ cluster assembly on IscU. Moreover, as the need for [Fe-S] cluster biogenesis is much greater in fast-growing cancer cells, potent inhibitors of the IscU scaffold protein such as cyclic thiosulfinates have the potential to be potent anticancer drugs.

Introduction

Iron-sulfur [Fe-S] clusters are one of the most ancient and versatile types of protein cofactors, that are found in all kingdoms of life and required for numerous biological activities (1). The most common types of [Fe-S] clusters are [2Fe-2S], [3Fe-4S], and [4Fe-4S] clusters that are ligated to proteins primarily or exclusively through cysteine residues, with histidine, aspartate, serine, and arginine residues also known to be cluster ligands (1). Because of their unique structural, chemical, and redox properties, [Fe-S] clusters play diverse roles in biology including electron transfer, coupled electron-proton transfer, substrate binding and activation, iron or cluster storage, regulation of gene expression, regulation of enzyme activity, disulfide reduction, and sulfur donation (1).

Under reducing and anaerobic conditions, [Fe-S] clusters can be assembled spontaneously from iron and sulfide ions *in vitro* (2). However, *in vivo* under partial oxidizing condition, this process is unlikely due to the cellular toxicity associated with free iron and sulfide ions in the concentrations needed for spontaneous Fe-S protein maturation (3-6). In addition, [Fe-S] clusters are often degraded rapidly by molecular oxygen and free iron ions produce reactive oxygen species by Fenton chemistry that can cause irreversible molecular damage, ultimately leading to cell death (3,6,7). Consequently, despite the relative structural and chemical simplicity of [Fe-S] clusters, their biosynthesis in living cells is a highly complex and coordinated process (8). Cells maintain tightly regulated machineries for [Fe-S] cluster biosynthesis (9). Three distinct systems for [Fe-S] cluster biosynthesis have been identified in prokaryotes: the nitrogen-fixation (NIF), the iron-sulfur cluster (ISC), and the sulfur-utilization factor (SUF) machineries (1,10-12). The NIF system is a specialized system for maturation of Fe-S proteins involved with nitrogen fixation, while ISC system is responsible for housekeeping [Fe-S] cluster biosynthesis . In contrast, the SUF system

acts as a backup system that functions under oxidative stress or Fe limitation conditions in many bacteria (11). In cyanobacteria and in many archaea, SUF is the only system for [Fe-S] cluster biogenesis (13). In eukaryotes, the biosynthesis of [Fe-S] clusters are performed by three main multi-protein machineries, the ISC machinery which is localized in mitochondria, the SUF machinery which is found in plant plastids, and the cytosolic iron-sulfur cluster assembly (CIA) machinery which is localized in the cytosol (8).

The biogenesis systems appear to have a general scheme for [Fe-S] cluster assembly comprising of two main steps. Assembly of an [Fe-S] cluster on a scaffold protein and subsequent transfer of the assembled cluster to either a carrier protein or an apo acceptor protein (9,14-22). Each of these steps involves participation of several proteins and cofactors and coordinated reactions. The prokaryotic ISC system has served as a useful model for understanding [Fe-S] cluster assembly and delivery (23). The proteins encoded by bacterial *isc* operon are IscR, IscS, IscU, IscA, HscB, HscA, Fdx, and IscX (1)(24). The first gene of *isc* operon encodes for the regulatory protein IscR which in its cluster-bound form is responsible for blocking the transcription of all the downstream *isc* genes (25). The homodimeric PLP-dependent cysteine desulfurase, IscS, serves as the sulfur source for cluster assembly (1). IscS forms a heterotetrameric complex with IscU in which one IscU molecule is bound to each subunit of the IscS homodimer. IscS converts L-cysteine to L-alanine with formation of a cysteine persulfide on a flexible side chain, which can be transferred to a cysteine on IscU (3,26). IscU serves as the scaffold on which clusters are formed and transferred intact to various carrier cluster proteins or apo-Fe-S proteins (15,27). The physiological role of A-type carrier (ATC) protein, IscA, has been the subject of much debate, since *in vitro* studies have shown IscA can bind Fe^{2+}, Fe^{3+}, $[2Fe\text{-}2S]^{2+}$ or $[4Fe\text{-}4S]^{2+}$ clusters in its dimeric form (28-30). However, gene-knockout studies have suggested a specific role for ATC

proteins in the maturation of $[4Fe\text{-}4S]^{2+}$ cluster-containing proteins in prokaryotic and eukaryotic organisms (31,32). Furthermore, *in vitro* studies have shown that ATC proteins can reversibly interconvert between $[2Fe\text{-}2S]^{2+}$ and $[4Fe\text{-}4S]^{2+}$ cluster-bound forms, suggesting a role in facilitating 2-electron reductive coupling of two $[2Fe\text{-}2S]^{2+}$ to from $[4Fe\text{-}4S]^{2+}$ clusters that can be used for maturation of apo $[4Fe\text{-}4S]^{2+}$-proteins (30,33). The DnaK- and DnaJ-like co-chaperones, HscA and HscB, respectively, have been shown to facilitate the $[2Fe\text{-}2S]^{2+}$ cluster transfer from holo-IscU to acceptor apo-proteins in an ATP-dependent process (15,34,35). Fdx in its reduced form acts as electron donor for sulfur reduction in the initial $[2Fe\text{-}2S]^{2+}$ cluster assembly on IscU (36). Fdx may also be the reductant for the reductive coupling process in which two $[2Fe\text{-}2S]^{2+}$ clusters dimerize at the interface of a IscU homodimer to form a $[4Fe\text{-}4S]^{2+}$ cluster (37). IscX is a small acidic protein encoded by the last gene in the *isc* operon. NMR studies indicate that IscX interacts with IscS and IscU to form a IscX-IscU-IscS ternary complex (7). IscX binds Fe^{2+} more avidly than Fe^{3+} and Fe^{2+}-binding strengthens the interaction between IscX and IscU (7). The exact functional properties of IscX is currently unclear, but it has been suggested that IscX can serve as both an iron donor to IscU and a regulator of IscS cysteine desulfurase activity (24).

The detailed mechanism IscS-mediated $[2Fe\text{-}2S]^{2+}$ cluster assembly on IscU is still unknown. To assemble a $[2Fe\text{-}2S]^{2+}$ cluster, a total of 4 electrons are required to reduce the sulfane sulfur, S^0, present in two cysteine persulfides to form the two bridging sulfides, μ_2- S^{2-}, present in a $[2Fe\text{-}2S]^{2+}$ cluster. Two of the electrons are believed to be provided by the oxidation of two substrate Fe^{2+} ions to form the all ferric $[2Fe\text{-}2S]^{2+}$ cluster and the remaining two electrons are provided by reduced Fdx. According to NMR studies using proteins from *Ec*, Fdx (in either oxidation state) interacts directly with IscS and competes with IscU for overlapping binding site on IscS (36). Previous studies have also shown that electron transfer from reduced Fdx to IscS

only occurs in the presence of L-Cys when a cysteine persulfide is generated on C328 by the enzymatic conversion of Cys to Ala, but does not occur with the IscS C328S variant (36). Therefore, it was suggested that one of the electrons required for reduction of S^0 is transferred from Fdx bound to IscS prior to the transfer of S to IscU. This raises the possibility of formation of a cysteine persulfide radical anion on IscS, which would generate a trisulfide radical anion intermediate on IscU in each S transfer step (7,36). However, there is currently no direct spectroscopic evidence for the existence of such radical species.

The objectives of this work were threefold. First, to use UV-visible CD spectroscopy to investigate Fe^{2+} binding to *Av* IscX and the ability of Fe^{2+}-bound IscX to transfer Fe^{2+} to *Av* IscU. Second, to use parallel UV-visible absorption and EPR studies to investigate the proposal that reduced *Av* Fdx generates a cysteine persulfide radical anion intermediate on IscS, that would be a precursor of a trisulfide radical anion intermediate on IscU. Third, to use UV-visible CD spectroscopy to investigate the potential of a new class of thiol cross-linking reagents, cyclic thiosulfinates with 5-, 6-, and 7-membered rings (38), to inhibit Fe^{2+} binding and $[2Fe\text{-}2S]^{2+}$ cluster assembly on *Av* IscU. These cyclic thiosulfinates were found to cross-link thiols up to 100-fold faster than their cyclic disulfide precursors (38). Moreover, they are well tolerated, potent, and cell-permeable, intracellular cross-linkers that function in the presence of biological concentrations of glutathione. The proposed thiol cross-linking mechanism for cyclic thiosulfinates is shown in Figure 3.1 (38). The mechanism shows that toxic binding to monothiols is fully reversible via thiolate-disulfide interchange, whereas thiol pair crosslinking is not. Furthermore, the reaction occurs in water and high yields of cross-linking are obtained because of the high enthalpies of formation of water and S-S bonds. Developing methods for inhibition of cluster assembly on the IscU scaffold protein is important for determining the mechanism of the first concerted step in Fe-

S assembly. In addition, non-toxic, potent inhibitors of the IscU scaffold protein have the potential to be anticancer drugs, as the need for [Fe-S] cluster biogenesis is much greater in fast-growing cancer cells.

Experimental procedures

Protein expression and purification. *Av* IscU, *Av* IscX, *Av* IscS, and *Av* Fdx plasmids were amplified and verified by amino acid sequencing. Amplified plasmids were separately transformed into the *Ec* expression strain BL21(DE3) and incubated on LB-agar plates with 100 mg/L ampicillin at 37°C. Colonies containing IscU or Fdx plasmids were grown at 37 °C, shaking at 250 rpm in LB media supplemented with 100 mg/L ampicillin and 50mg/L FAC. The bacterial culture was induced by adding 100 mg/L isopropyl β-D-1-thiogalactopyranoside (IPTG) supplemented with 50 mg/L FAC at exponential phase and further cultivated at 34 °C and shaking at 225 rpm for 4 hours. Cells were harvested by centrifugation at 5,000 g for 10 minutes at 4 °C. The cell pellets were stored at −80 °C until further use. Colonies containing IscS and IscX plasmids were grown as described above, except that in place of FAC, 1mM pyridoxin was added to the media growing IscS, no supplement was added to the media growing IscX. For aerobic purification, cells expressing recombinant *Av* IscU were thawed and resuspended in 100 mM Tris-HCl buffer, pH 7.4 (buffer A) with 15 μg/ml DNase, 5×10^{-3} μg/ml RNase, and 10 μg/mL phenylmethylsulphonyl fluoride (PMSF). The cell suspension was lysed on ice by intermittent sonication , and centrifuged to remove cell debris from the suspension at 12,000 rpm and 4 °C for 1 hour. The cell-free extract was then loaded onto HiTrap^{TM} Q-HP anion-exchange column (GE Healthcare) previously equilibrated with buffer A. The column was washed with buffer A until the absorbance at 280 nm reached the baseline absorbance while collecting the flow through due to weak interaction of IscU with the Q-sepharose column. *Av* IscU was then eluted using an

increasing linear gradient of 0-20% NaCl. Fractions containing IscU, as judged by SDS-PAGE analysis, were combined, and concentrated by Amicon ultrafiltration using a YM5 membrane. After addition of ammonium sulfate to the final concentration of 1 M, the protein sample was applied to a HiTrap^{TM} Phenyl-HP column (GE Healthcare), previously equilibrated with 100 mM Tris-HCl buffer, pH 7.4 containing 1M ammonium sulfate (buffer B). The column was washed with at least 5 column volumes of buffer B before IscU was eluted using a decreasing linear gradient of 100-0% ammonium sulfate. The purest fractions containing *Av* IscU were pooled and concentrated by Amicon ultrafiltration using a YM5 membrane and stored in liquid nitrogen. The integrity of the purified protein was assessed and confirmed by mass spectrometry.

The same procedure was used for aerobic purification of *Av* IscX except cells were thawed and resuspended in 20 mM Tris-HCl buffer, pH 8 and 0-100% NaCl gradient was used for the initial purification step using HiTrap^{TM} Q-HP anion-exchange column (GE Healthcare) column. The second step of purification with HiTrap^{TM} Phenyl-HP column (GE Healthcare) was performed as described above. The fractions containing *Av* IscX were then passed through Amicon ultrafiltration using a YM50 membrane and the flow through containing only *Av* IscX was concentrated via Amicon ultrafiltration using a YM3 membrane. The integrity of the purified protein was assessed and confirmed by mass spectrometry.

For aerobic purification, cells expressing recombinant *Av* Fdx were thawed and resuspended in 100 mM Tris-HCl buffer, pH 7.8 then lysed and centrifuged as described above. Brown fractions containing $[2Fe\text{-}2S]^{2+}$ cluster-bound *Av* Fdx were eluted by increasing NaCl concentration with linear gradient of 0-1 M NaCl using Q-sepharose column (GE healthcare). These fractions were further purified using phenol-sepharose column by decreasing ammonium sulfate concentration. The purity and integrity of the purified protein were assessed by SDS-PAGE

analysis and mass spectrometry. For anaerobic purification, same procedure was used except all steps were performed under strict anaerobic conditions using rigorously degassed buffers.

For anaerobic purifications, cells expressing recombinant *Av* IscS were thawed and resuspended in degassed 30 mM Tris-HCl buffer, pH 8 supplemented with 10% glycerol, 15 µg/ml DNase, 5×10^{-3} µg/ml RNase, and 10 µg/mL PMSF, lysed on ice by sonication under strict anaerobic conditions, then transferred into centrifuged tubes, sealed tightly and centrifuged at 12,000 rpm and 4 °C for 1 hour. The cell-free extract was taken under anaerobic condition and streptomycin sulfate was added to 1% w/v and centrifuged at 12,000 rpm for 20 minutes. Yellow fractions containing *Av* IscS were eluted by increasing NaCl concentration with linear gradient of 0-1 M NaCl using Q-sepharose column (GE healthcare). These fractions were further purified using phenol-sepharose column by decreasing ammonium sulfate concentration. The purest fractions containing *Av* IscS were pooled and concentrated by Amicon ultrafiltration using a YM30 membrane under anaerobic conditions and stored in liquid nitrogen. The integrity of the purified protein was assessed and confirmed by mass spectrometry.

Preparation of reduced *Av* Fdx. Reduced *Av* Fdx was prepared under strict anaerobic conditions by gradual addition of sodium dithionite and was monitored by UV-visible absorption spectroscopy. Sodium dithionite was added until the absorbance in the visible region decreased and the characteristic peak at 545 nm accompanied with rose color appeared. Reduced *Av* Fdx was buffer washed into rigorously degassed buffer (100 mM Tris-HCl, pH 7.8) using Amicon ultra centrifugal filtration with a YM3 membrane to remove excess sodium dithionite judge by disappearance of the band at 316 nm in the absorption spectrum.

Preparation of Fe^{2+}-bound *Av* IscX. *Av* IscX was incubated with 10-fold excess of FAS for 15 minutes under anaerobic conditions followed by multiple buffer exchanges with rigorously

degassed buffer (20 mM Tris-HCl, pH 8) using Amicon filtration with YM3 membrane. The Fe content was determined before and after FAS treatment by ICP-MS.

Preparation of Zn^{2+}-depleted *Av* IscU and Fe^{2+}-bound *Av* IscU. To remove Zn from *Av* IscU, the protein was incubated with 200-fold excess of EDTA on ice under anaerobic conditions for 1 hour. DTT was added to the final concentration of 1 mM and was incubated with the sample for another hour. The protein sample was then buffer exchanged into rigorously degassed buffer (100 mM Tris-HCl, pH 7.4) using a 20 ml HiTrap^{TM} Desalting column (GE Healthcare) to remove chelator and excess reducing agent. Fractions containing protein were pooled and concentrated via Amicon ultra centrifugal filtration with a YM3 membrane followed by 3 more buffer exchanges to effect removal of any remaining EDTA or DTT. Zn-depleted and reduced *Av* IscU was titrated with FAS under strict anaerobic conditions in 100 mM Tris-HCl buffer, pH 7.4 and was monitored via CD spectroscopy. Furthermore, Fe^{2+} transfer from *Av* IscX to *Av* IscU by stoichiometric addition of *Av* IscU to Fe^{2+} bound *Av* IscX was monitored by CD spectroscopy.

Parallel UV-visible absorption and EPR studies of the interaction of reduced Fdx with IscS. Equimolar reduced *Av* Fdx and *Av* IscS were mixed with 5-fold excess of L-Cys and the reaction was monitored via UV-visible absorption spectroscopy. Control experiments were conducted under the same conditions by monitoring the UV-visible absorption spectra of reduced Fdx and IscS without addition of L-Cys and reduced Fdx and L-Cys without addition of IscS over the same period of time. For EPR studies, the reaction was quenched 30 and 45 min after L-Cys addition by freezing the samples in liquid nitrogen.

In addition, a single turnover of IscS in the presence of IscU, reduced Fdx, and Fe^{2+}-bound IscX, and L-Cys was attempted. Equimolar Zn^{2+}-depleted, pre-reduced *Av* IscU, reduced *Av* Fdx, and *Av* IscS were mixed with Fe^{2+} bound *Av* IscX under strict anaerobic conditions. The reaction

was monitored via UV-visible absorption spectroscopy upon addition of an equimolar L-Cys. For EPR studies, the reaction was quenched immediately or 90 s, 180 s, and 300 s after L-Cys addition by freezing the samples in liquid nitrogen. A control sample was prepared with the same procedure described above except no L-Cys was added.

Preparation of cyclic thiosulfinate cross-linked *Av* IscUs and investigation of their ability to bind Fe^{2+} ions and assemble $[2Fe\text{-}2S]^{2+}$ clusters. Preparation of cross-linked *Av* IscU involved incubating Zn-depleted, DTT-pretreated and buffer exchanged *Av* IscU with a 5-fold excess of 5-, 6-, or 7- membered cyclic thiosulfinates (per monomer) for 2 hours at room temperature under strict anaerobic conditions. To assess Fe^{2+} binding to cyclic thiosulfinate cross-linked IscUs, equimolar FAS was added to apo *Av* IscU (control) or cross-linked *Av* IscUs under anaerobic conditions and Fe^{2+} binding to IscU was monitored by UV-visible CD spectroscopy. To assess the ability of cyclic thiosulfinate cross-linked IscUs to assemble a $[2Fe\text{-}2S]^{2+}$ cluster, apo *Av* IscU and cyclic thiosulfinate cross-linked IscUs were reconstituted by addition of 6-fold excess of FAC and 6-fold excess of sodium sulfide and the reaction was monitored via CD spectroscopy for 30 minutes. The ability of cyclic thiosulfinate cross-linked IscUs to assemble a $[2Fe\text{-}2S]^{2+}$ cluster was also assessed by adding a 6-fold excess of FAS and L-Cys, together with a catalytic amount of IscS, and 6-fold excess of L-Cys to apo *Av* IscU and cyclic thiosulfinate cross-linked IscUs and monitoring the reaction with CD spectroscopy for one hour. To investigate if excess cyclic thiosulfinate cross-linkers perturb cysteine desulfurase-mediated $[2Fe\text{-}2S]^{2+}$ cluster on cross-linked *Av* IscUs, these experiments were repeated with 5-, 6-, and 7-membered cyclic thiosulfinates with removal of excess cross-linker prior to cysteine desulfurase reconstitution. After 2 hours of incubation with the cross-linker, samples were buffer exchanged into degassed

100mM Tris-HCl buffer, pH 7.4 using Amicon ultra centrifugal filtration with a YM3 membrane to remove excess cross-linkers.

Analytical and spectroscopic characterization methods. Mass spectrometry experiments were carried out by University of Georgia Proteomic and Mass Spectrometry Facility. Protein concentrations were determined using the *DC*™ Protein Assay (Bio-Rad) with bovine serum albumin as the standard. Zinc concentrations were determined by ICP-MS and iron concentrations were determined by ICP-MS or colorimetrically using bathophenanthroline under reducing conditions after digestion of proteins in 0.8% potassium permanganate and 0.2 M HCl (39). Anaerobic samples for spectroscopic studies were prepared in a Vacuum Atmosphere glove box under argon atmosphere (O_2 < 2 ppm). UV-visible and CD spectra were recorded in septa-sealed 0.1 or 1 cm quartz cuvettes at room temperature using a Shimadzu UV-3101 PC scanning spectrophotometer and a Jasco J-715 spectropolarimeter, respectively. X-band (~ 9.6 GHz) EPR spectra were recorded using a ESP-300D spectrometer (Bruker, Billerica, MA) equipped with a dual-mode ER-4116 cavity and an ESR 900 helium flow cryostat (Oxford Instruments, Concord, MA).

Results and Discussion

Fe^{2+} binding to *Av* IscX and *Av* IscU and transfer of Fe^{2+} from *Av* IscX to *Av* IscU. As-purified samples of IscU have been shown to contain Zn^{2+} which is bound to the three conserved cysteine residues and inhibits Fe^{2+} binding (7,40,41). The samples of *Av* IscU used in this work are no exception, as ICP-MS revealed 0.77 ± 0.08 Zn^{2+} per IscU. Indeed, the higher binding ability of IscU for Zn^{2+} compared to Fe^{2+} (7), provides rationalization of the low levels of Fe^{2+} binding to *Av* IscU and the IscU domain of *Av* NifU that were reported in earlier studies (42). Consequently, it is necessary to remove Zn^{2+} before investigating Fe^{2+} binding to *Av* IscU and ICP-MS showed

that the Zn^{2+} content decreased to 0.05 ± 0.01 Zn^{2+} per IscU monomer on incubating with a 200-fold excess of EDTA followed by purification. Zn^{2+}-depleted and DTT pre-treated *Av* IscU was titrated with FAS using the intensity of the CD bands associated with $CysS^{-}$-to-Fe^{2+} charge transfer bands in the 290-370 nm region to assess Fe^{2+} binding, see Figure 3.2. Fe^{2+} binding by IscU occurs in three phases. The binding curve, shown as an inset in Figure 3.2, has an initial lag phase, followed by an exponential phase and finally a stationary phase with an asymptotic limit of 1.1 ± 0.1 Fe^{2+} per IscU indicating binding one Fe^{2+} per IscU monomer.

NMR studies have shown that IscU is a metamorphic protein that can adopt two conformational states in solution (7,43) . A largely structured S-state and a more dynamic and partially unfolded D-state conformation. These conformational states interconvert on the order of 1 s^{-1} under physiological conditions (44), and NMR studies indicate that the conformational transition involves cis/trans isomerization of two peptidyl–prolyl peptide bonds, both of which are trans in the S-state of IscU, and both are in the higher energy cis configuration in the D-state (45). The conformational equilibrium can be altered by various conditions. For instance, binding metal ions such as Zn^{2+} or Fe^{2+} stabilizes the more structured S-state conformation (23,40,43,46), whereas the absence of bound metal ions favors the D-state. Consequently, the lag phase in Fe^{2+} uptake by IscU is interpreted in terms of the conformational change from D-state to S-state.

ICP-MS analysis of *Av* IscX before and after incubation with excess FAS, followed by three buffer exchanges under anaerobic conditions, showed an increase of Fe content from 0.004 ± 0.001 to 0.91 ± 0.10 Fe atom per monomer. This is fully consistent with NMR studies of *Ec* IscX, which also indicate one Fe^{2+} per IscX monomer (24). *Av* IscX is a small acidic protein (68 amino acids) with one conserved histidine and no cysteine residues. This explains the absence of any significant CD bands for Fe^{2+}-bound *Av* IscX in the 290-370 nm region and facilitates the use

of CD spectroscopy to monitor Fe^{2+} transfer from *Av* IscX to *Av* IscU. Figure 3.3 shows the CD spectrum of Fe^{2+}-bound IscX (blue line), Fe^{2+}-IscU (black line), and equimolar Fe^{2+}-bound IscX and apo IscU after mixing for 2 min (red line). Moreover, no additional changes were evident on incubating at room temperature for 20 min. The near quantitative agreement between the black and red spectra indicates that transfer of Fe^{2+} from IscX to IscU is complete within 4 min. Based on the initial concentrations of Fe^{2+}-bound IscX and apo IscU monomer (both 0.5 mM) kinetic simulations indicate that the second order rate constant for Fe^{2+} transfer is > 50,000 $M^{-1}min^{-1}$. Hence, Fe^{2+}-bound IscX is shown to be a competent and rapid Fe^{2+} donor for bacterial $[2Fe\text{-}2S]^{2+}$ cluster assembly on the bacterial IscU scaffold protein.

Parallel UV-visible absorption and EPR studies show Fdx reduction of IscS in the presence of L-Cys. The role of Isc Fdx in IscS-mediated assembly of $[2Fe\text{-}2S]^{2+}$ clusters on the IscU scaffold protein has been investigated using *E. coli* proteins using NMR and UV-visible absorption spectroscopy (36). The results showed that Fdx binds to IscS and can transfer electrons to IscS in the presence of L-Cys. This led to the proposal that reduced Fdx transfers an electron to IscS to form a cysteine persulfide radical anion on the active-site cysteine, that would be a precursor of the formation a transient trisulfide radical anion intermediate on IscU in each S transfer step (7,36). To investigate this proposal, the time course of the reaction of equimolar reduced *Av* Isc Fdx and *Av* IscS, in the absence and presence of a 5-fold excess of L-Cys, was monitored using parallel UV-visible absorption and EPR studies, with the objective of detecting sulfur radical species, see Fig 3.4. No reaction was observed after 45 min when reduced Fdx was mixed with IscS in the absence of L-Cys or when reduced Fdx was mixed with L-Cys in the absence of IscS. However, in the presence of both IscS and L-Cys, reduced Fdx was fully oxidized to a $S = 0$ $[2Fe\text{-}2S]^{2+}$ center after 45 min, as judged by the characteristic changes in the UV-visible

absorption spectrum (the increased absorption in the 415 nm region results from the PLP chromophore in IscS) and the complete loss of the axial resonance ($g_{||}$ = 2.025 and $g_{\perp}$ = 1.945) from the S = 1/2 $[2Fe\text{-}2S]^{1+}$ center in the EPR spectrum. This result is fully consistent with the absorption data obtained for the equivalent experiment with *E. coli* Isc Fdx and IscS (36), and shows that reduced Fdx is slowly oxidized by IscS in the presence of excess L-Cys. However, no EPR signals indicative of a sulfur-based radical (see ref (47) and references therein) were observed at temperatures from 10-100 K, for the samples shown in Fig. 3.4 or for samples rapidly frozen immediately after addition of L-Cys. There do not appear to any well documented examples of cysteine persulfide radical anion EPR spectra in the literature. However, the EPR spectrum would be expected to be similar to those of cysteine disulfide radical anions (g_1 = 2.017-2.024, g_2 = 2.014-2.020, g_3 = 2.002) (47), which is distinct from that of the reduced Isc Fdx.

Parallel UV-visible absorption and EPR studies were also used to investigate the time course of the reaction between equimolar *Av* IscU, *Av* IscS, reduced *Av* Fdx and Fe^{2+} bound *Av* IscX and L-Cys, see Figure 3.5. The experiment was designed to involve a single turnover of S transfer from IscS to IscU concomitant with the addition of one Fe^{2+} to IscU. The results indicate complete oxidation of reduced Fdx within 5 minutes of adding L-Cys to initiate the IscS reaction, as judged by the changes in the absorption spectrum and the complete loss of the reduced Fdx EPR signal. Once again, EPR studies at temperatures from 10-100 K and samples frozen rapidly after L-Cys addition revealed no evidence in support of a sulfur-based radical species. However, a weak isotropic resonance at g = 4.3, indicative high-spin (S = 5/2) Fe^{3+} species was observed towards the end of the reaction. This could be adventitiously bound Fe^{3+} or a monomeric Fe^{3+} intermediate on the path to $[2Fe\text{-}2S]^{2+}$ cluster assembly.

Our inability to identify a sulfur-based radical species in the reaction of reduced Fdx with IscS in the presence of L-Cys argues against the formation of a cysteine persulfide radical anion prior to IscS-mediate sulfur transfer to IscU. Moreover, there is abundant MS evidence for S^0 transfer from IscS to IscU mediated by cysteine persulfide formation on a flexible loop of IscS (26,48). This begs the question of what is being reduced by Fdx when IscS interacts with its substrate L-Cys in the absence IscU and Fe^{2+}-bound IscX. The obvious answer is the cysteine persulfide which can undergo two-electron reduction to form cysteinate and sulfide. This reaction is rapid with two-electron reducing agents such as DTT and much slower with one-electron reducing agents such as dithionite. Consequently, it seems reasonable to propose reduced *Av* Fdx, which has a midpoint potential of –344 mV versus SHE is capable of two-electron reduction of the cysteine persulfide. This interpretation also accounts for the observation that oxidation of *Av* Fdx in the presence of IscS and excess L-Cys is much slower than in the reaction between equimolar *Av* IscU, *Av* IscS, reduced *Av* Fdx and Fe^{2+} bound *Av* IscX and L-Cys. The latter reaction would require one electron from Fdx and one from Fe^{2+} to form the putative ferric CysS-Fe-S intermediate of the first S transfer, if S^0 is transferred from IscS to IscU.

Thiol cross-linking cyclic thiosulfinates inhibit Fe^{2+} binding and $[2Fe\text{-}2S]^{2+}$cluster assembly on IscU. The critical role of IscU as the scaffold protein on which $[2Fe\text{-}2S]^{2+}$ clusters, the building block for the assembly of all higher nuclearity clusters, are assembled in the bacterial and mitochondrial ISC system, makes this protein an obvious target for inhibiting [Fe-S] cluster assembly in higher eukaryotes. Moreover, the ability of IscU to switch from a structured S-state, when the assembled $[2Fe\text{-}2S]^{2+}$ cluster is bound to the three conserved cysteines, to a folded but more dynamic D-state in the apo form, suggested that the new class of cyclic thiosulfinate thiol cross-linking reagents with variable sized cyclic rings have the potential to be effective inhibitors

(38). As shown in Figure 3.6, the CD spectrum of apo *Av* IscU in the 280-360 nm is quite different from those observed for apo IscU incubated with a 5-fold excess of 5-, 6-, or 7-membered cyclic thiosulfinates for 2 h under anaerobic conditions at room temperature. Hence, CD spectroscopy indicates that all three cross-linkers bind to apo IscU and the close similarity of the CD spectra indicates analogous structures for all three crosslinkers, see Figure 3.6. Moreover, unlike apo IscU in the absence of cross-linkers, the CD-spectra of all three cross-linked IscUs were not perturbed on incubating with stoichiometric FAS under anaerobic conditions for 10 min and do not show the characteristic positive bands at 345 and 313 nm that are indicative of Fe^{2+}-bound IscU. Analogous results were observed when stoichiometric Fe^{2+}-bound IscX was used as the Fe donor in place of FAS. Hence, the CD results demonstrate binding of all three cross-linkers and show that the cross-linkers inhibit Fe^{2+} binding by IscU.

The intense UV-visible CD spectrum of $[2Fe\text{-}2S]^{2+}$-cluster-bound *Av* IscU (15,34) makes CD spectroscopy the method of choice for monitoring the time course of $[2Fe\text{-}2S]^{2+}$ cluster reconstitution on IscU using a 6-fold excess of FAC and sulfide, as shown in Figure 3.7A. In the absence of a cross-linker, the reaction is completed after 30 min. In addition, incubation of holo $[2Fe\text{-}2S]^{2+}$ cluster-bound IscU with a 5-fold excess of the 5-, 6-, or 7-member cyclic thiosulfinate cross-linkers for 30 min did not perturb the CD spectrum. Consequently, the cross-linkers do not displace an assembled $[2Fe\text{-}2S]^{2+}$ cluster on IscU. The samples of apo IscU in the presence of a 5-fold excess of the 5-, 6-, or 7-member cyclic thiosulfinate cross-linker all had the same IscU monomer concentration as apo IscU control and were reconstituted in the same way. The results of the reconstitution reactions show that the 7-membered cross-linker completely inhibits $[2Fe\text{-}2S]^{2+}$ cluster reconstitution, whereas the 6-member and 5-member cross linkers show only 3% and 9% $[2Fe\text{-}2S]^{2+}$ cluster reconstitution after 30 min, respectively, see Figure 3.7. To assess the effect

of DTT on cyclic thiosulfinate cross-linked IscUs, a 10-fold excess DTT was added to a sample that was fully inhibited with 7-membered cyclic thiosulfinate and reconstitution of $[2Fe\text{-}2S]^{2+}$ cluster on *Av* IscU was monitored via CD spectroscopy for one more hour, see Figure 3.8. The addition of DTT initiates $[2Fe\text{-}2S]^{2+}$ cluster reconstitution that reaches completion after ~ 50 min. Hence, DTT is effective in alleviating the inhibition $[2Fe\text{-}2S]^{2+}$ cluster reconstitution on IscU by cleaving the disulfide cross-links. Analogous experiments using physiologically relevant levels of GSH (3 mM), rather than a 10-fold excess of DTT, failed to alleviate the inhibition $[2Fe\text{-}2S]^{2+}$ cluster reconstitution. While more experiments with physiologically relevant disulfide cleaving reagents are required, these results suggest that cyclic thiosulfinates have the potential to be inhibitors of IscU *in vivo*.

The effect of cross-linkers on the more physiologically relevant cysteine desulfurase-mediated assembly of $[2Fe\text{-}2S]^{2+}$ clusters on IscU was also investigated. Cysteine desulfurase-mediated reconstitution of cross-linked *Av* IscU with a 5-fold excess of the 5-membered cyclic thiosulfinate monitored by CD spectroscopy revealed no significant evidence for formation of $[2Fe\text{-}2S]^{2+}$ cluster on IscU after 60 min, see Figure 3.9. However, cysteine desulfurase-mediated reconstitution of cross-linked IscU with a 5-fold excess of 6- and 7-membered cyclic thiosulfinates resulted in precipitation after L-Cys addition to the reaction mixture, possibly due to aggregation of IscS by excess cross-linker. This interpretation was supported by the observation that precipitation did not occur when the cysteine desulfurase reconstitution reactions were repeated with IscU samples that had been incubated with excess cross-linker for 2 h and buffer washed to remove excess cross-linker. Cysteine desulfurase-mediated reconstitution of cross-linked *Av* IscU with no excess cross-linker show much slower formation of $[2Fe\text{-}2S]^{2+}$ cluster on IscU. Compared to cysteine desulfurase-mediated reconstitution of *Av* IscU in the absence of cross-linkers, *Av* IscU

cross-linked with stoichiometric 5-, 6-, and 7- membered cyclic thiosulfinates exhibit ~ 30%, 10%, and 7% $[2Fe\text{-}2S]^{2+}$ cluster assembly after 1 h, see Figure 3.10. Overall, for spontaneous and cysteine desulfurase mediated assembly of $[2Fe\text{-}2S]^{2+}$ clusters on IscU, 7-membered cyclic thiosulfinate is the most potent inhibitor, followed by 6-membered cyclic thiosulfinate, with 5-membered cyclic thiosulfinate as the weakest inhibitor.

The first step in $[2Fe\text{-}2S]^{2+}$ cluster assembly on bacterial IscU, i.e. S transfer from IscS or Fe^{2+} transfer from IscX, remains to be determined. Hence, it is interesting to note that IscU, cross-linked with 5-membered cyclic thiosulfinate in the absence of excess cross-linker, does not bind Fe^{2+}, indicating IscU cysteine residues were cross-linked. However, in the presence of IscS, L-Cys and FAS, $[2Fe\text{-}2S]^{2+}$ clusters bound by the three conserved cysteines are slowly formed on IscU, in a process that is likely to be initiated the IscS cysteine persulfide displacing a cross-linker via persulfide-disulfide interchange. This provides additional information regarding the mechanism of $[2Fe\text{-}2S]^{2+}$ cluster assembly suggesting that Fe^{2+} binding prior sulfur transfer is not essential for $[2Fe\text{-}2S]^{2+}$ cluster assembly on IscU.

The results presented herein demonstrate that inhibition of [Fe-S] cluster assembly on IscU by cyclic thiosulfinates is not permanent, since DTT, but not GSH, is able to cleave the disulfide bonds between cysteine residues of protein and thiols of cross-linker and thereby restore the ability of IscU to assemble $[2Fe\text{-}2S]^{2+}$ clusters IscU. Furthermore, addition of cyclic thiosulfinate to holo IscU does not replace $[2Fe\text{-}2S]^{2+}$ clusters from scaffold protein. However, in the cell, the $[2Fe\text{-}2S]^{2+}$ clusters on IscU are constantly being assembled and delivered to target proteins and the extent of this process will be greatly enhanced in fast-growing cancer cells. Hence inhibiting IscU $[2Fe\text{-}2S]^{2+}$ cluster assembly by cyclic thiosulfinate cross-linking of apo IscU will be far more deleterious to cancer cells.

Conclusions

In this work, we have investigated the mechanism of $[2Fe\text{-}2S]^{2+}$ cluster assembly on a bacterial IscU, identified the Fe^{2+} donor, evaluated the possibility of a cysteine persulfide radical anion intermediate on IscS, and established the utility of cyclic thiosulfinates as potent inhibitors of IscU Fe^{2+} binding and $[2Fe\text{-}2S]^{2+}$ cluster assembly. UV-visible CD spectroscopy and/or ICP-MS has demonstrated stoichiometric Fe^{2+} binding to IscU and IscX, and provided direct evidence that IscX rapidly transfers a Fe^{2+} ion to IscU. Parallel UV-visible absorption and EPR studies of IscS in the presence of reduced Fdx and L-Cys have confirmed stoichiometric Fdx oxidation, but have failed to identify any sulfur-based radical species. Consequently, the slow oxidation of reduced Fdx by IscS in the presence of L-Cys is attributed to non-physiological, sequential one-electron transfers from reduced Fdx to the cysteine persulfide formed on IscS to form cysteinate and sulfide. Hence, our results favor a mechanism involving IscS-mediated S^0 rather than a S^- radical transfer to IscU. Our efforts to find inhibitors of $[2Fe\text{-}2S]^{2+}$ cluster assembly on IscU have focused on 5-, 6-, and 7-membered cyclic thiosulfinate thiol cross-linkers which are shown to be potent inhibitors of IscU Fe^{2+} binding as well as spontaneous and cysteine desulfurase-mediated $[2Fe\text{-}2S]^{2+}$ cluster assembly on IscU. Moreover, the results show that this class of cross-linker can be useful in determining the mechanism of IscS-mediated assembly of $[2Fe\text{-}2S]^{2+}$ clusters on IscU and may have potential for use as a new class of anticancer therapeutic treatment that functions by inhibiting the growth of fast-growing cancer cells.

Acknowledgment

We thank Dr. Dennis Dean for providing plasmids for the recombinant expression of *Av* IscU, *Av* IscX, *Av* IscS, *Av* Fdx and Dr. Michael Adams for access to the ICP-MS facility.

References

1. Johnson, D. C., Dean, D. R., Smith, A. D., and Johnson, M. K. (2005) Structure, function, and formation of biological iron-sulfur clusters. *Annu. Rev. Biochem.* **74**, 247-281

2. Malkin, R., and Rabinowitz, J. C. (1966) The reconstitution of *clostridial* ferredoxin. *Biochem. Biophys. Res. Commun.* **23**, 822-827

3. Fridovich, I. (1998) Oxygen toxicity: a radical explanation. *J. Exp. Biol.* **201**, 1203-1209

4. Sawyer, D. T., and Valentine, J. S. (1981) How super is superoxide? *Acc. Chem. Res.* **14**, 393-400

5. Stohs, S. J., and Bagchi, D. (1995) Oxidative mechanisms in the toxicity of metal ions. *Free Radic. Biol. Med.* **18**, 321-336

6. Fridovich, I. (1997) Superoxide anion radical ($O_2^{-\cdot}$), superoxide dismutases, and related matters. *J. Biol. Chem.* **272**, 18515-18517

7. Kim, J. H., Bothe, J. R., Alderson, T. R., and Markley, J. L. (2015) Tangled web of interactions among proteins involved in iron-sulfur cluster assembly as unraveled by NMR, SAXS, chemical crosslinking, and functional studies. *Biochim. Biophys. Acta* **1853**, 1416-1428

8. Lill, R. (2009) Function and biogenesis of iron–sulphur proteins. *Nature* **460**, 831-838

9. Py, B., and Barras, F. (2010) Building Fe–S proteins: bacterial strategies. *Nat. Rev. Microbiol.* **8**, 436-446

10. Fontecave, M. (2006) Iron-sulfur clusters: ever-expanding roles. *Nat. Chem. Biol.* **2**, 171-174

11. Outten, F. W. (2015) Recent advances in the Suf Fe-S cluster biogenesis pathway: beyond the *Proteobacteria*. *Biochim. Biophys. Acta* **1853**, 1464-1469

12. Blanc, B., Gerez, C., and Ollagnier de Choudens, S. (2015) Assembly of Fe/S proteins in bacterial systems: biochemistry of the bacterial ISC system. *Biochim. Biophys. Acta* **1853**, 1436-1447

13. Ayala-Castro, C., Saini, A., and Outten, F. W. (2008) Fe-S cluster assembly pathways in bacteria. *Microbiol. Mol. Biol. Rev.* **72**, 110-125

14. Roche, B., Aussel, L., Ezraty, B., Mandin, P., Py, B., and Barras, F. (2013) Iron/sulfur proteins biogenesis in prokaryotes: Formation, regulation and diversity. *Biochim. Biophys. Acta* **1827**, 455-469

15. Shakamuri, P., Zhang, B., and Johnson, M. K. (2012) Monothiol glutaredoxins function in storing and transporting [Fe_2S_2] clusters assembled on IscU scaffold proteins. *J. Am. Chem. Soc.* **134**, 15213-15216

16. Balk, J., and Pilon, M. (2011) Ancient and essential: the assembly of iron–sulfur clusters in plants. *Trends Plant Sci.* **16**, 218-226

17. Fontecave, M., and Ollagnier-de-Choudens, S. (2008) Iron–sulfur cluster biosynthesis in bacteria: mechanisms of cluster assembly and transfer. *Arch. Biochem. Biophys.* **474**, 226-237

18. Bandyopadhyay, S., Chandramouli, K., and Johnson, Michael K. (2008) Iron–sulfur cluster biosynthesis. *Biochem. Soc. Trans.* **36**, 1112-1119

19. Takahashi, Y., and Nakamura, M. (1999) Functional assignment of the ORF2-iscS-iscU-iscA-hscB-hscA-fdx-0RF3 gene cluster involved in the assembly of Fe-S clusters in *Escherichia coli*. *J. Biochem* **126**, 917-926

20. Takahashi, Y., and Tokumoto, U. (2002) A third bacterial system for the assembly of iron-sulfur clusters with homologs in archaea and plastids. *J. Biol. Chem.* **277**, 28380-28383

21. Outten, F. W., Djaman, O., and Storz, G. (2004) A suf operon requirement for Fe–S cluster assembly during iron starvation in *Escherichia coli*. *Mol. Microbiol.* **52**, 861-872

22. Fontecave, M., Choudens, S. O. d., Py, B., and Barras, F. (2005) Mechanisms of iron–sulfur cluster assembly: the SUF machinery. *J. Biol. Inorg. Chem.* **10**, 713-721

23. Kim, J. H., Tonelli, M., and Markley, J. L. (2012) Disordered form of the scaffold protein IscU is the substrate for iron-sulfur cluster assembly on cysteine desulfurase. *Proc. Natl. Acad. Sci. USA* **109**, 454-459

24. Kim, J. H., Bothe, J. R., Frederick, R. O., Holder, J. C., and Markley, J. L. (2014) Role of IscX in iron-sulfur cluster biogenesis in *Escherichia coli*. *J. Am. Chem. Soc.* **136**, 7933-7942

25. Schwartz, C. J., Giel, J. L., Patschkowski, T., Luther, C., Ruzicka, F. J., Beinert, H., and Kiley, P. J. (2001) IscR, an Fe-S cluster-containing transcription factor, represses expression of *Escherichia coli* genes encoding Fe-S cluster assembly proteins. *Proc. Natl Acad. Sci. USA* **98**, 14895-14900

26. Smith, A. D., Agar, J. N., Johnson, K. A., Frazzon, J., Amster, I. J., Dean, D. R., and Johnson, M. K. (2001) Sulfur transfer from IscS to IscU: the first step in iron−sulfur cluster biosynthesis. *J. Am. Chem. Soc.* **123**, 11103-11104

27. Agar, J. N., Krebs, C., Frazzon, J., Huynh, B. H., Dean, D. R., and Johnson, M. K. (2000) IscU as a scaffold for iron−sulfur cluster biosynthesis: sequential assembly of [2Fe-2S] and [4Fe-4S] clusters in IscU. *Biochemistry* **39**, 7856-7862

28. Krebs, C., Agar, J. N., Smith, A. D., Frazzon, J., Dean, D. R., Huynh, B. H., and Johnson, M. K. (2001) IscA, an alternate scaffold for Fe−S cluster biosynthesis. *Biochemistry* **40**, 14069-14080

29. Ding, H., and Clark, R. J. (2004) Characterization of iron binding in IscA, an ancient iron-sulphur cluster assembly protein. *Biochem. J.* **379**, 433-440

30. Mapolelo, D. T., Zhang, B., Naik, S. G., Huynh, B. H., and Johnson, M. K. (2012) Spectroscopic and functional characterization of iron–sulfur cluster-bound forms of *Azotobacter vinelandii* ^{Nif}IscA. *Biochemistry* **51**, 8071-8084

31. Tan, G., Lu, J., Bitoun, J. P., Huang, H., and Ding, H. (2009) IscA/SufA paralogues are required for the [4Fe-4S] cluster assembly in enzymes of multiple physiological pathways in *Escherichia coli* under aerobic growth conditions. *Biochem. J.* **420**, 463-472

32. Mühlenhoff, U., Richter, N., Pines, O., Pierik, A. J., and Lill, R. (2017) Specialized function of yeast Isa1 and Isa2 proteins in the maturation of mitochondrial [4Fe-4S] proteins. *J. Biol. Chem.* **292**, 17979

33. Brancaccio, D., Gallo, A., Mikolajczyk, M., Zovo, K., Palumaa, P., Novellino, E., Piccioli, M., Ciofi-Baffoni, S., and Banci, L. (2014) Formation of [4Fe-4S] clusters in the mitochondrial iron–sulfur cluster assembly machinery. *J. Am. Chem. Soc.* **136**, 16240-16250

34. Chandramouli, K., and Johnson, M. K. (2006) HscA and HscB stimulate [2Fe-2S] cluster transfer from IscU to apoferredoxin in an ATP-dependent reaction. *Biochemistry* **45**, 11087-11095

35. Kim, J. H., Tonelli, M., Frederick, R. O., Chow, D. C.-F., and Markley, J. L. (2012) Specialized Hsp70 chaperone (HscA) binds preferentially to the disordered form, whereas J-protein (HscB) binds preferentially to the structured form of the iron-sulfur cluster scaffold protein (IscU). *J. Biol. Chem.* **287**, 31406-31413

36. Kim, J. H., Frederick, R. O., Reinen, N. M., Troupis, A. T., and Markley, J. L. (2013) [2Fe-2S]-ferredoxin binds directly to cysteine desulfurase and supplies an electron for iron-sulfur cluster assembly but is displaced by the scaffold protein or bacterial frataxin. *J. Am. Chem. Soc.* **135**, 8117-8120

37. Chandramouli, K., Unciuleac, M.-C., Naik, S., Dean, D. R., Huynh, B. H., and Johnson, M. K. (2007) Formation and properties of [4Fe-4S] clusters on the IscU scaffold protein. *Biochemistry* **46**, 6804-6811

38. Donnelly, D., Dowgiallo, M., Salisbury, J., Aluri, K., Iyengar, S., Chaudhari, M., Mathew, M., Miele, I., Auclair, J., Lopez, S., Manetsch, R., and Agar, J. (2018) Cyclic thiosulfinates and cyclic disulfides selectively cross-link thiols while avoiding modification of lone thiols. *J. Am. Chem. Soc.* **140**

39. Fish, W. W. (1988) Rapid colorimetric micromethod for the quantitation of complexed iron in biological samples. *Methods Enzymol.* **158**, 357-364

40. Ramelot, T. A., Cort, J. R., Goldsmith-Fischman, S., Kornhaber, G. J., Xiao, R., Shastry, R., Acton, T. B., Honig, B., Montelione, G. T., and Kennedy, M. A. (2004) Solution NMR structure of the iron–sulfur cluster assembly protein U (IscU) with zinc bound at the active site. *J. Mol. Biol.* **344**, 567-583

41. Liu, J., Oganesyan, N., Shin, D. H., Jancarik, J., Yokota, H., Kim, R., and Kim, S. H. (2005) Structural characterization of an iron-sulfur cluster assembly protein IscU in a zinc-bound form. *Proteins* **59**, 875-881

42. Agar, J. N., Yuvaniyama, P., Jack, R. F., Cash, V. L., Smith, A. D., Dean, D. R., and Johnson, M. K. (2000) Modular organization and identification of a mononuclear iron-binding site within the NifU protein. *J. Biol. Inorg. Chem.* **5**, 167-177

43. Markley, J. L., Kim, J. H., Dai, Z., Bothe, J. R., Cai, K., Frederick, R. O., and Tonelli, M. (2013) Metamorphic protein IscU alternates conformations in the course of its role as the scaffold protein for iron–sulfur cluster biosynthesis and delivery. *FEBS Lett.* **587**, 1172-1179

44. Kim, J. H., Füzéry, A. K., Tonelli, M., Ta, D. T., Westler, W. M., Vickery, L. E., and Markley, J. L. (2009) Structure and dynamics of the iron−sulfur cluster assembly scaffold protein IscU and its interaction with the cochaperone HscB. *Biochemistry* **48**, 6062-6071

45. Dai, Z., Tonelli, M., and Markley, J. L. (2012) Metamorphic protein IscU changes conformation by cis–trans isomerizations of two peptidyl–prolyl peptide bonds. *Biochemistry* **51**, 9595-9602

46. Shimomura, Y., Wada, K., Fukuyama, K., and Takahashi, Y. (2008) The asymmetric trimeric architecture of [2Fe–2S] IscU: implications for its scaffolding during iron–sulfur cluster biosynthesis. *J. Mol. Biol.* **383**, 133-143

47. Lawrence, C. C., Bennati, M., Obias, H. V., Bar, G., Griffin, R. G., and Stubbe, J. (1999) High-field EPR detection of a disulfide radical anion in the reduction of cytidine 5'-diphosphate by the E441Q R1 mutant of *Escherichia coli* ribonucleotide reductase. *Proc. Natl Acad. Sci. USA* **96**, 8979-8984

48. Smith, A. D., Frazzon, J., Dean, D. R., and Johnson, M. K. (2005) Role of conserved cysteines in mediating sulfur transfer from IscS to IscU. *FEBS Lett.* **579**, 5236-5240

Figure 3.1. Proposed mechanism of thiol crosslinking using a 6-membered cyclic thiosulfinate. Modified from Ref (38).

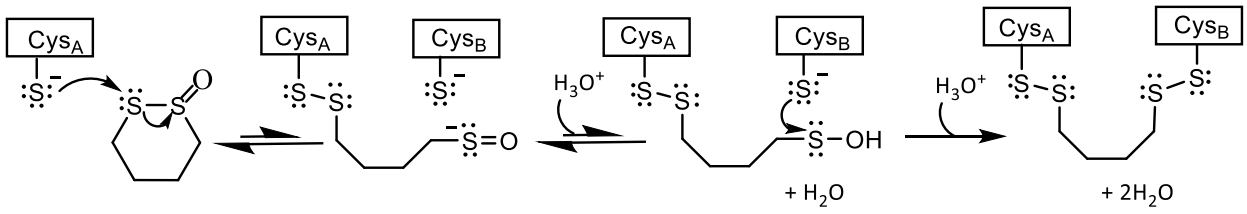
Cys$_A$
Cys$_B$
H$_3$O$^+$
+ H$_2$O
+ 2H$_2$O

Figure 3.2. Fe^{2+} binding to *Av* IscU monitored by CD spectroscopy. *Av* IscU (0.8 mM) was titrated with FAS under anaerobic conditions in 100 mM Tris-HCl buffer at pH 7.4. The inset shows a plot of the extinction coefficient at 314 nm as a function of the Fe^{2+}/IscU monomer ratio. Spectra were recorded under anaerobic conditions in sealed 1 cm cuvette. All ε values are based on the concentration of *Av* IscU monomer.

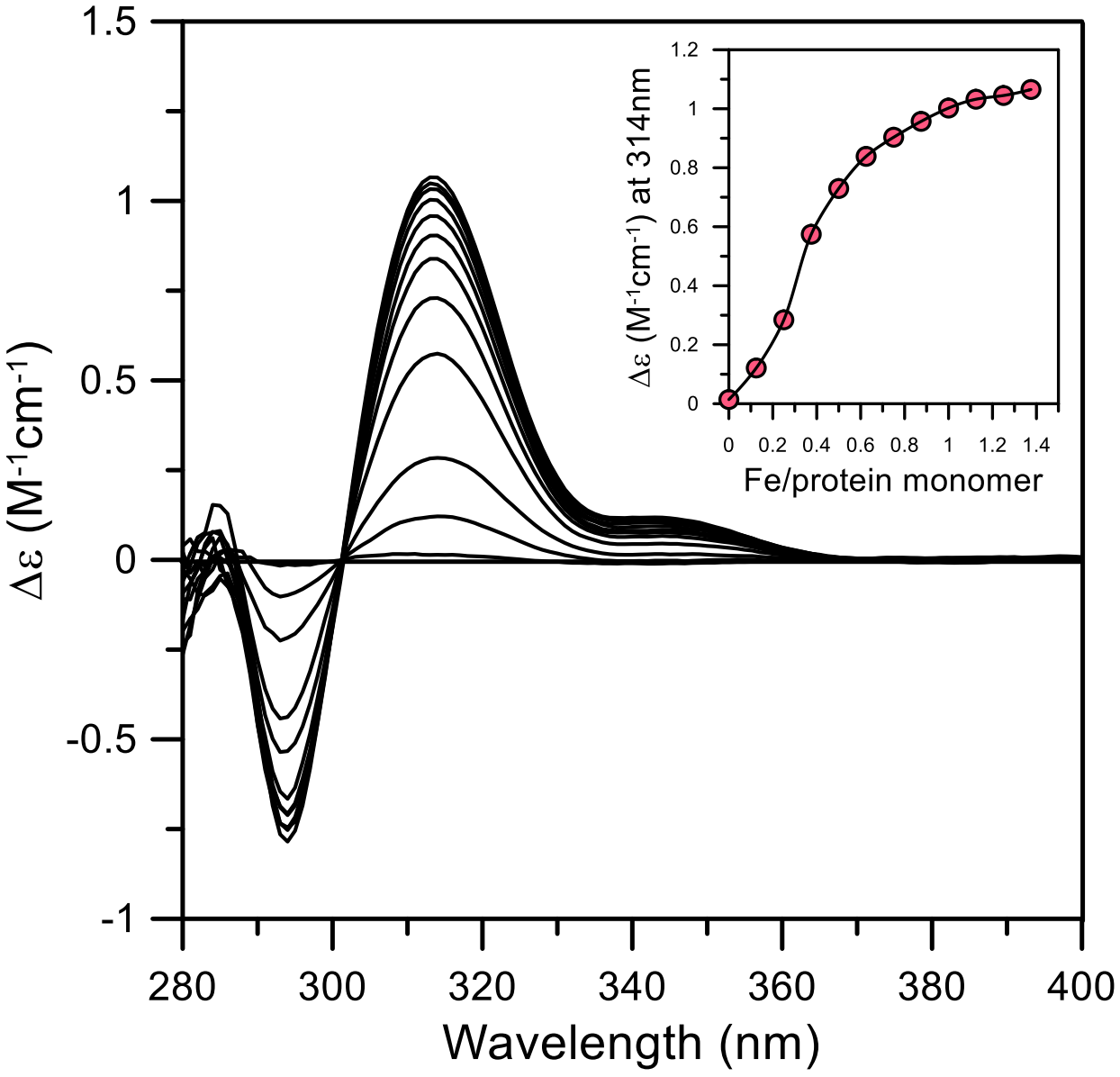
1.5
1
0.5
0
-0.5
-1
Δε (M-1cm-1)
280
300
320
340
360
380
400
Wavelength (nm)
1.2
1
0.8
0.6
0.4
0.2
0
Δε (M-1cm-1) at 314nm
0
0.2
0.4
0.6
0.8
1
1.2
1.4
Fe/protein monomer

Figure 3.3. Transfer of Fe^{2+} from *Av* IscX to *Av* IscU monitored by CD spectroscopy. CD spectra of Fe^{2+}-bound IscX and IscU are shown in blue and black lines, respectively. Δε values are based on the concentration of IscU and IscX monomers, respectively. Red line shows the CD spectrum of the product of mixing equimolar Fe^{2+}-bound IscX with apo IscU. Δε value is based on the concentration of *Av* IscU monomer (0.5 mM). Samples were in 100 mM Tris-HCl buffer at pH 7.4, and spectra were recorded under anaerobic conditions in sealed 1 cm cuvette.

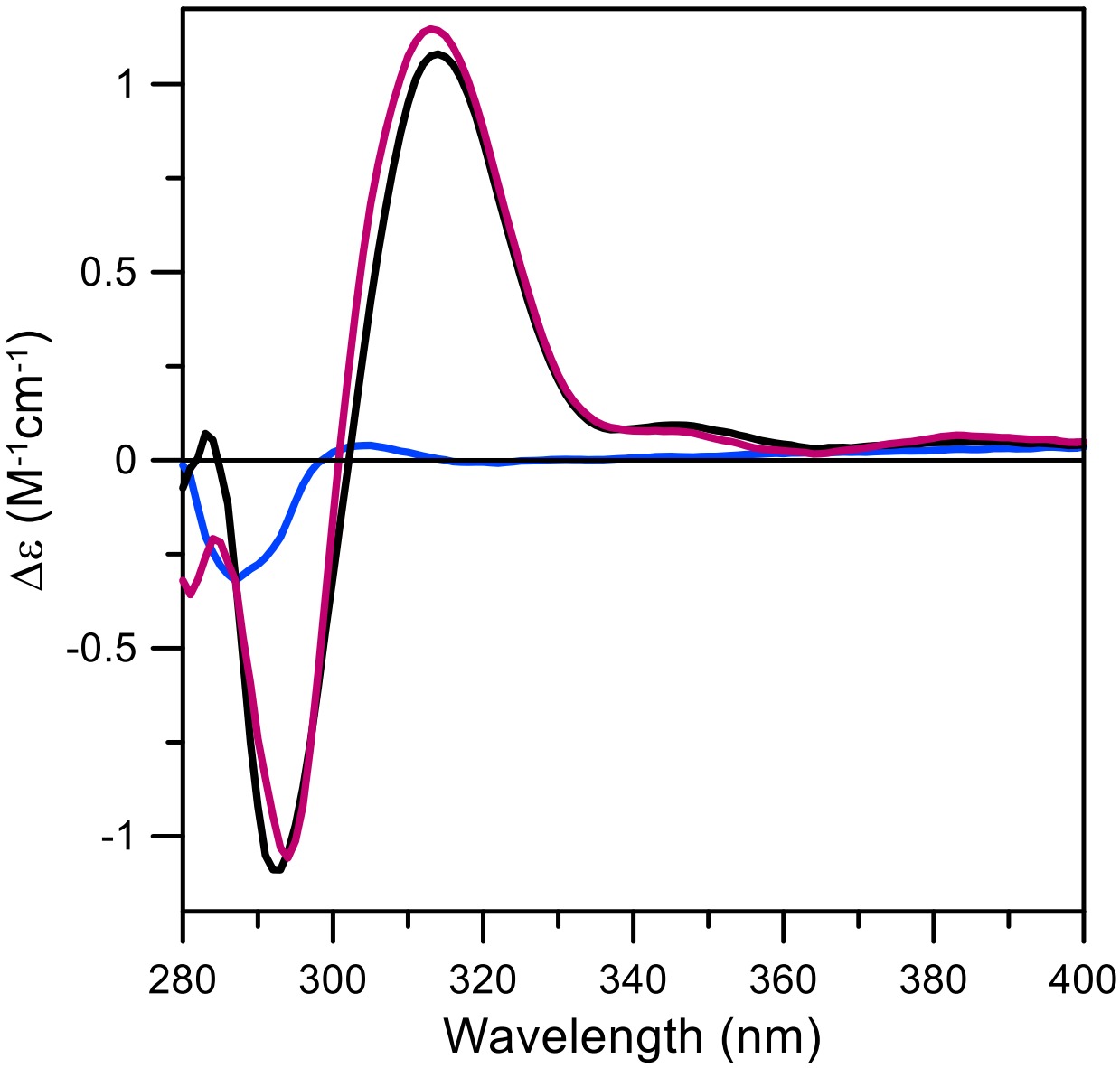
1
0.5
0
-0.5
-1
Δε (M-1cm-1)
280
300
320
340
360
380
400
Wavelength (nm)

Figure 3.4. Parallel (A) UV visible absorption and (B) EPR spectroscopy of the reaction between equimolar reduced *Av* Fdx and *Av* IscS with a 5-fold excess of L-Cys. Absorption and EPR spectra of reduced Fdx and IscS before addition of L-Cys are shown as black lines. Absorption and EPR spectra of reduced-Fdx and IscS 30 and 45 min after L-Cys addition are shown as blue and purple lines, respectively. UV visible absorption spectra were recorded under anaerobic conditions in sealed 1 cm cuvette in 100 mM Tris-HCl buffer at pH 7.8. EPR spectra were recorded at 30 K with the same spectrometer gain under non-power saturating conditions at a microwave frequency of 9.59 GHz, with a modulation amplitude of 0.64 mT and a microwave power of 10 mW.

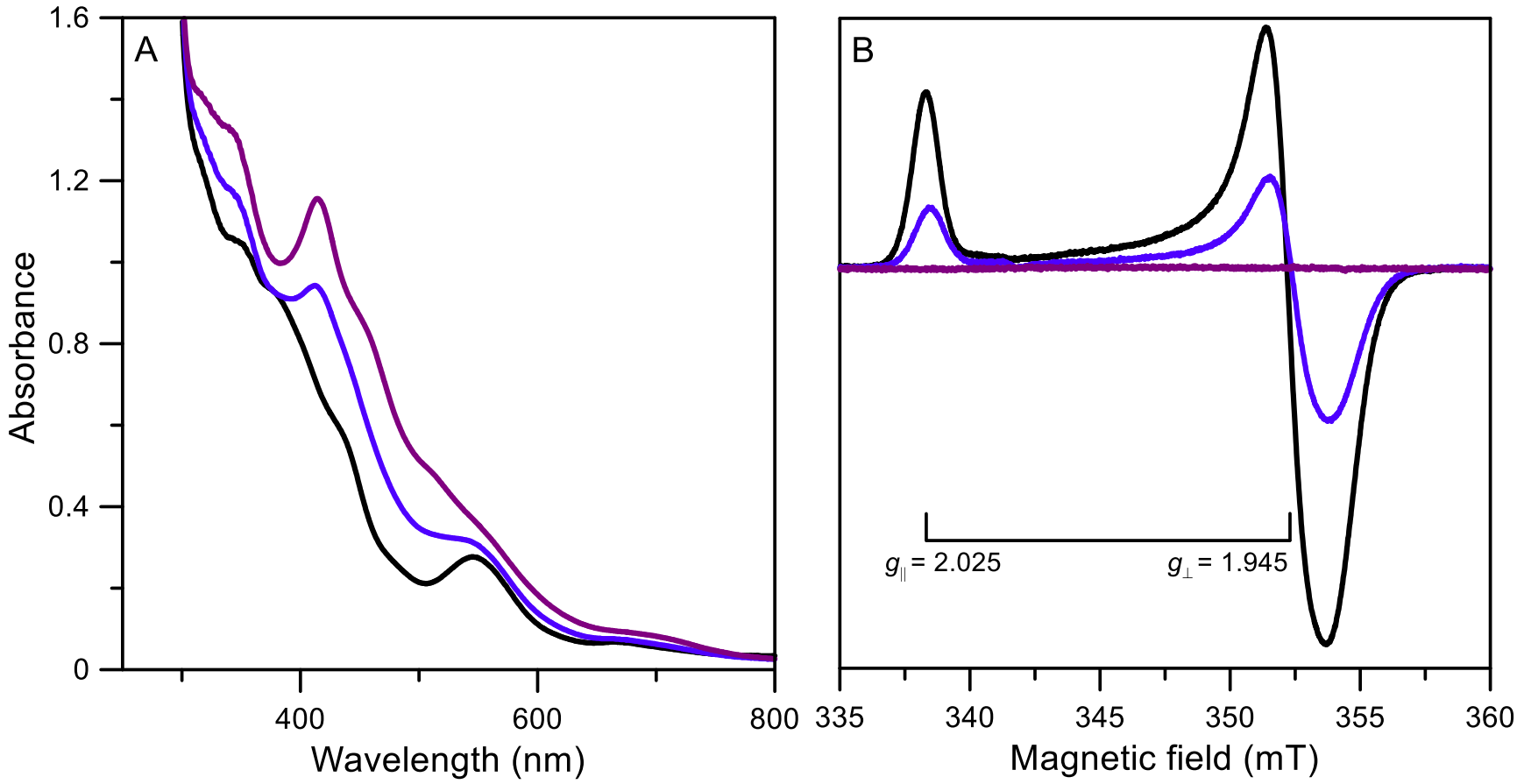
A
B
Absorbance
Wavelength (nm)
Magnetic field (mT)
1.6
1.2
0.8
0.4
0
400
600
800
335
340
345
350
355
360
$g_{\parallel}$ = 2.025
$g_{\perp}$ = 1.945

Figure 3.5. Parallel (A) UV visible absorption and (B) EPR spectra of the reaction between equimolar reduced *Av* Fdx, *Av* IscS, *Av* IscU, Fe^{2+} bound *Av* IscX, and L-Cys. Absorption and EPR spectra of the reaction mixture with all components except L-Cys are shown as black lines. UV-visible absorption spectra of the product 40 s, 110 s, 180 s, and 300 s min after L-Cys addition are shown in blue, purple, green, and magenta, respectively. EPR spectra of the reaction mixture after addition L-Cys and freezing in liquid nitrogen, and after 90 s, 180 s, and 300 s are shown in blue, purple, green, and magenta, respectively. Samples were in 100 mM Tris-HCl buffer at pH 7.8. UV-visible absorption spectra were recorded under anaerobic conditions in sealed 1 cm cuvettes. EPR spectra were recorded at 10 K with the same spectrometer gain under non-power saturating conditions at a microwave frequency of 9.59 GHz, with a modulation amplitude of 0.64 mT and a microwave power of 10 mW.

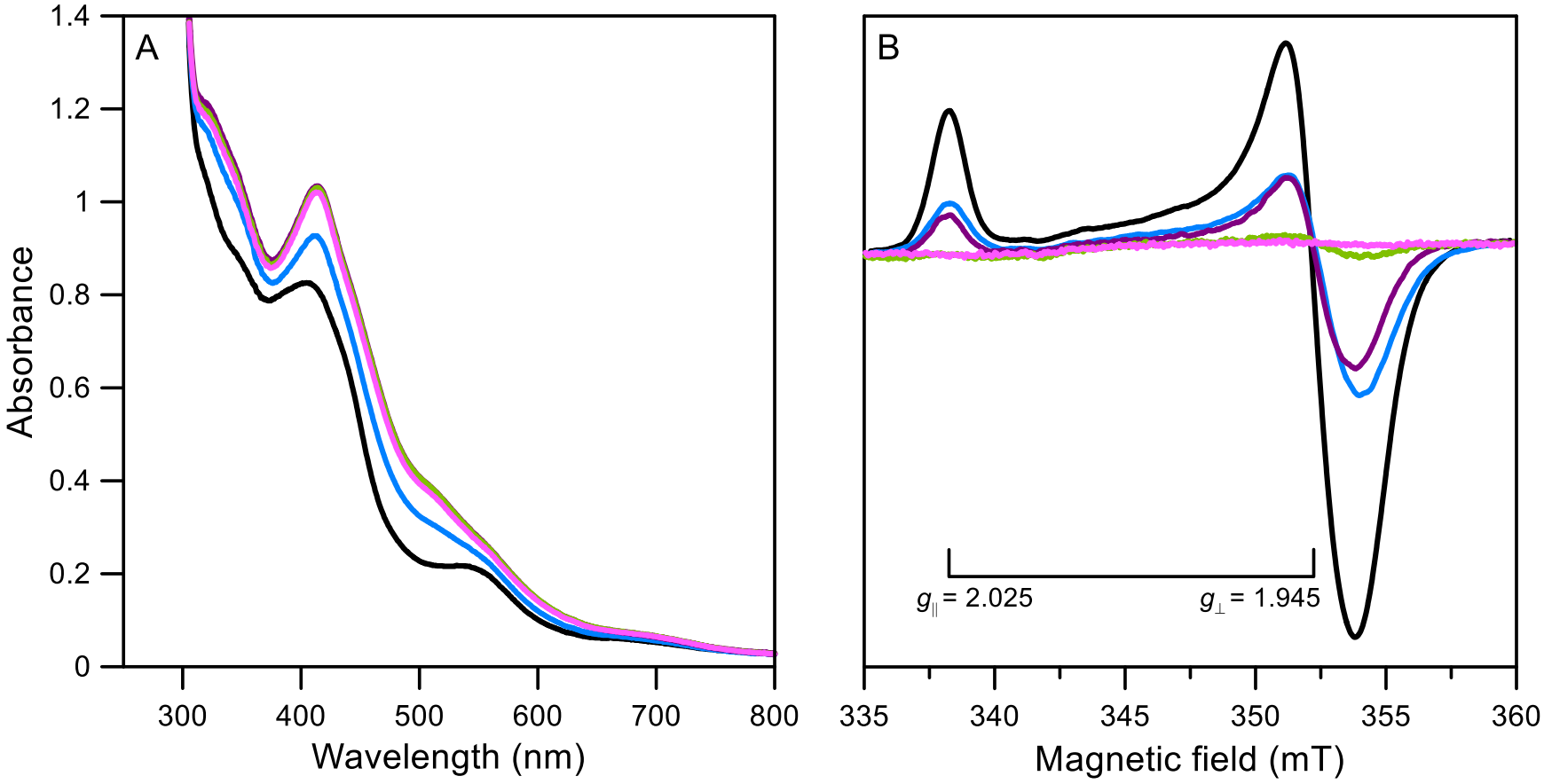
A
Absorbance
1.4
1.2
1
0.8
0.6
0.4
0.2
0
300
400
500
600
700
800
Wavelength (nm)
B
$g_{\parallel}$ = 2.025
$g_{\perp}$ = 1.945
335
340
345
350
355
360
Magnetic field (mT)

Figure 3.6. Thiol cross-linking using 5-, 6-, and 7- membered cyclic thiosulfinates inhibit Fe^{2+} binding to *Av* IscU. CD spectra of apo *Av* IscU and Fe^{2+}-bound *Av* IscU are shown as gray and black lines, respectively. CD spectra of *Av* IscU cross-linked with 5-, 6-, and 7-membered cyclic thiosulfinates are shown in blue, red, and purple lines, respectively, and were not perturbed by stoichiometric addition of Fe^{2+}, indicating cross-linked *Av* IscU can no longer bind Fe^{2+}. Spectra were recorded under anaerobic conditions in sealed 1 cm cuvette in 100 mM Tris-HCl buffer at pH 7.4. $\Delta\varepsilon$ values are based on concentration of *Av* IscU monomer.

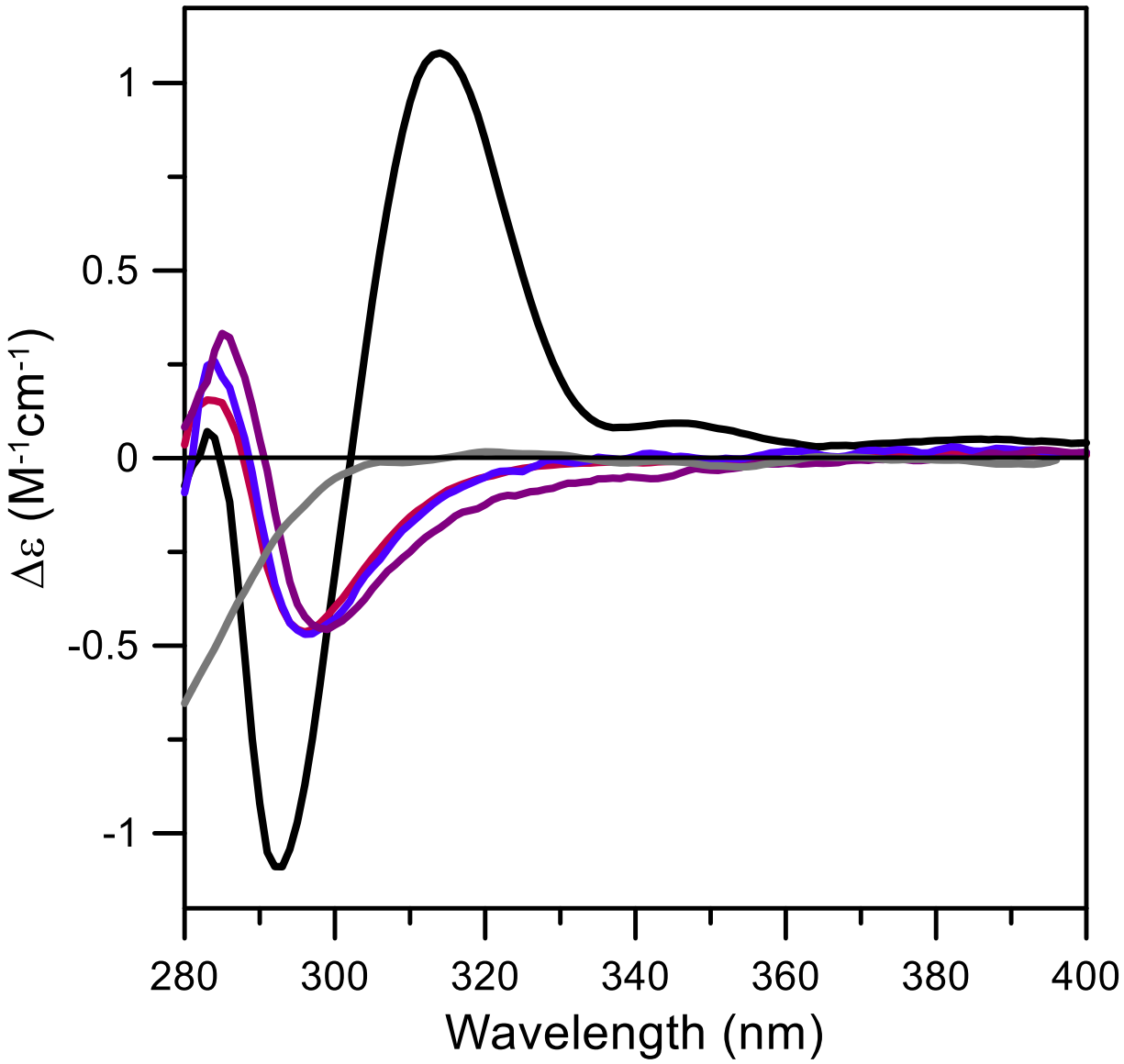
1
0.5
0
-0.5
-1
Δε (M-1cm-1)
280
300
320
340
360
380
400
Wavelength (nm)

Figure 3.7. 5-, 6- or 7- membered cyclic thiosulfinates inhibit $[2Fe\text{-}2S]^{2+}$ cluster assembly on *Av* IscU. (A) Time course of $[2Fe\text{-}2S]^{2+}$ cluster assembly on apo *Av* IscU monitored by CD spectroscopy in the absence of cyclic thiosulfinates. The CD spectrum of the reaction mixture 2 min after adding a 6-fold excess of FAC and sodium sulfide to apo IscU is shown as a black line. CD spectra taken at additional 3-min intervals are shown as gray lines. CD spectrum of $[2Fe\text{-}2S]^{2+}$ cluster-bound *Av* IscU after 30 min is shown as a purple line. The time course of $[2Fe\text{-}2S]^{2+}$ cluster assembly on cross-linked *Av* IscUs with a 5-fold excess of 5-, 6-, and 7- membered cyclic thiosulfinates monitored by CD spectroscopy are shown in (B), (C), and (D) respectively. The CD spectra of the reaction mixture 2 min after adding a 6-fold excess of FAC and sodium sulfide to each cross-linked IscU are shown as black lines. CD spectra taken at additional 3-min intervals are shown as gray lines. CD spectra of the products after 30 min are shown in blue lines and are compared to that of IscU without cross-linkers at 30 min, shown as a purple line. Spectra were recorded under anaerobic conditions in sealed 0.1 cm cuvettes. All samples were 0.3 mM in IscU monomer in 100 mM Tris-HCl buffer at pH 7.4. $\Delta\varepsilon$ values are based on concentration of *Av* IscU monomer.

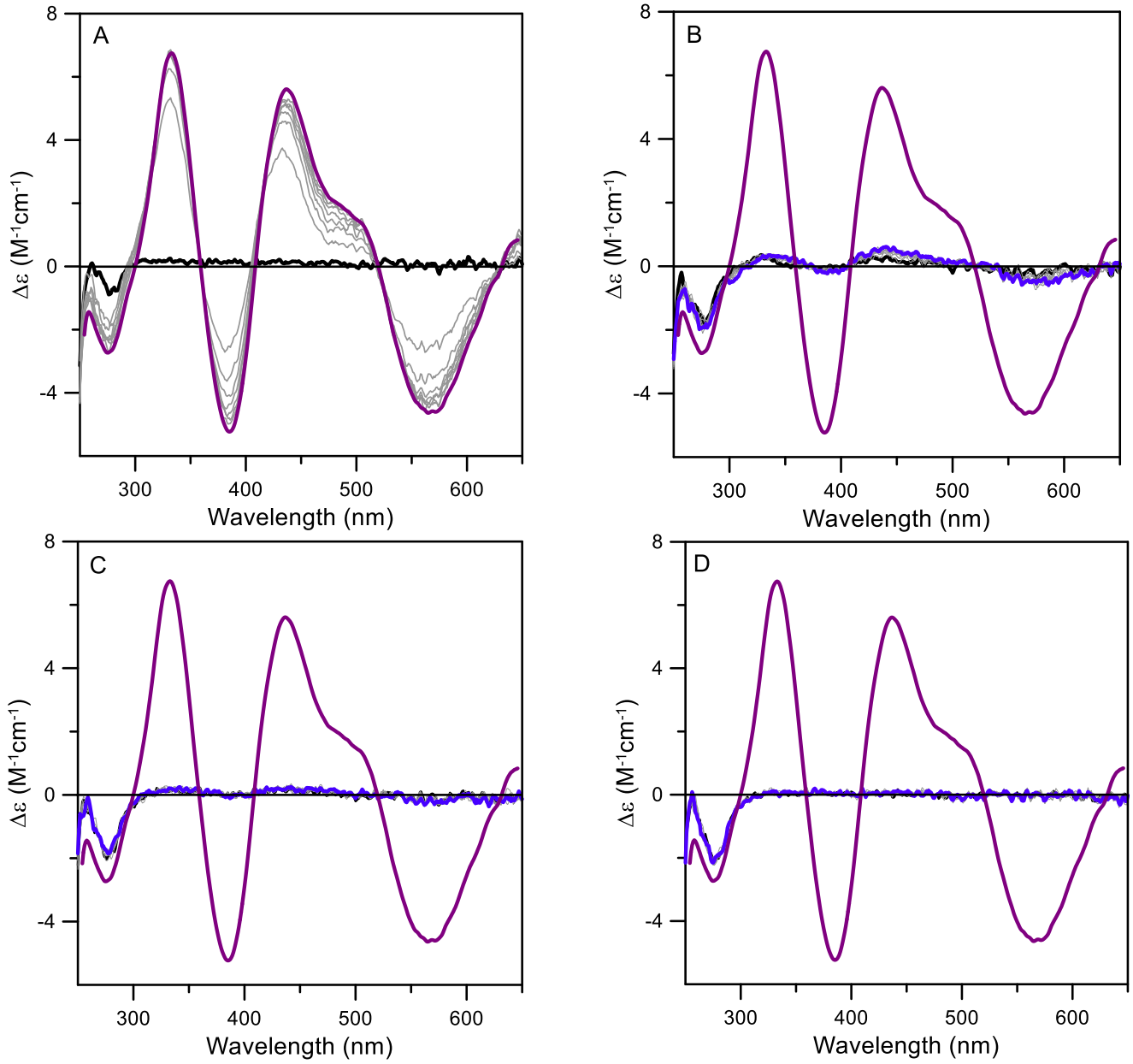
A
B
C
D
8
4
0
-4
300
400
500
600
Wavelength (nm)
Δε (M-1cm-1)

Figure 3.8. Time-course of $[2Fe\text{-}2S]^{2+}$ cluster assembly on *Av* IscU cross-linked with 7-membered cyclic thiosulfinate in the absence and presence of a 10-fold excess of DTT. The CD spectrum of cross-linked *Av* IscU 30 minutes after addition of 6-fold excess of FAC and sodium sulfide is shown in blue line. Scans at 3-minute intervals after adding a10-fold excess of DTT are shown in gray lines. CD spectrum corresponding to $[2Fe\text{-}2S]^{2+}$ cluster-bound *Av* IscU 50 minutes after DTT addition is shown in magenta line. Spectra were recorded under anaerobic conditions in sealed 0.1 cm cuvette in 100 mM Tris-HCl buffer at pH 7.4. $\Delta\varepsilon$ value is based on concentration of *Av* IscU monomer.

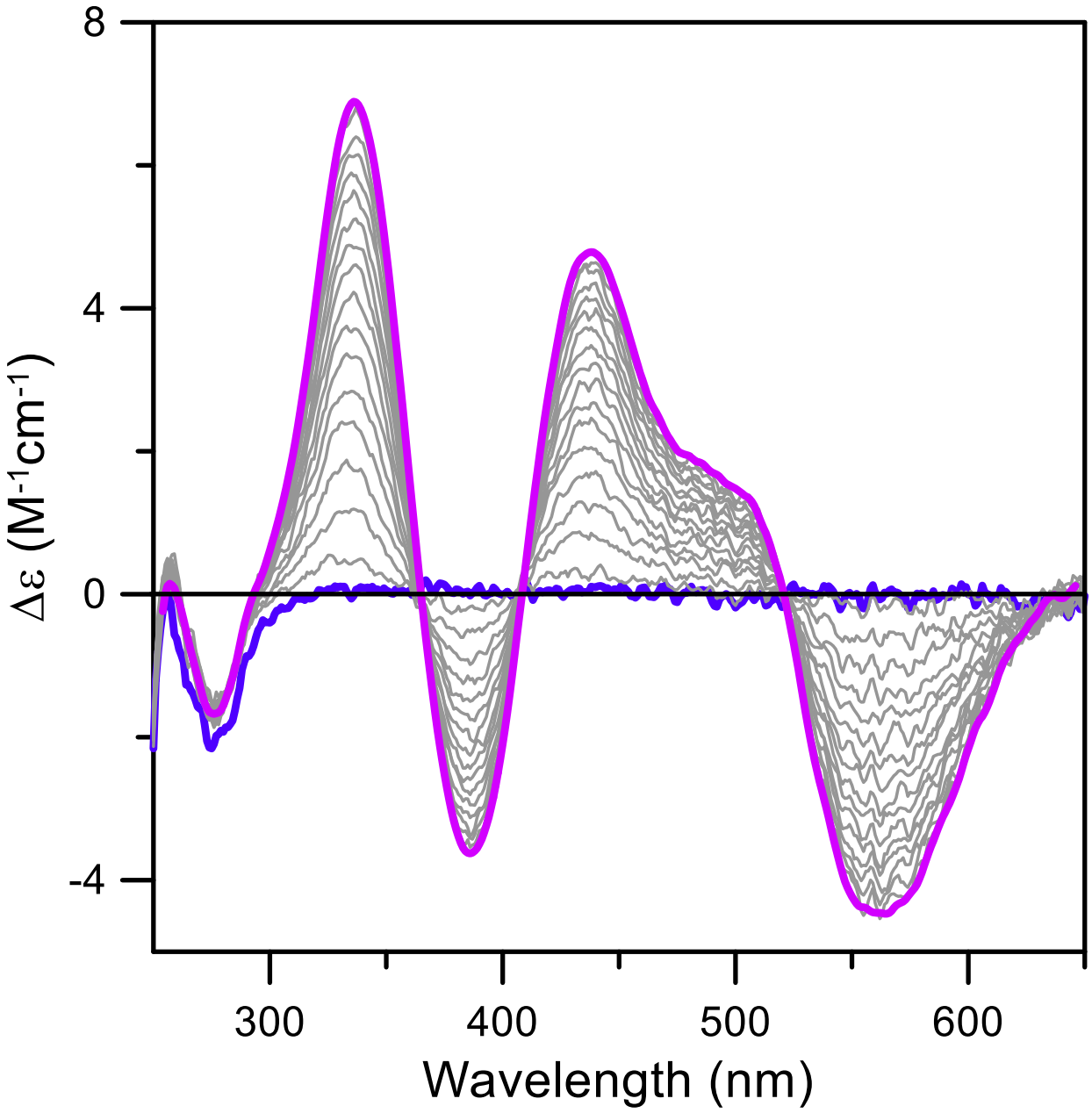
8
4
0
-4
Δε (M-1cm-1)
300
400
500
600
Wavelength (nm)

Figure 3.9. Excess 5-membered cyclic thiosulfinate inhibits cysteine desulfurase-mediated [2Fe-2S]$^{2+}$ cluster assembly on *Av* IscU. The CD spectrum of the product of cysteine desulfurase-mediated reconstitution of [2Fe-2S]$^{2+}$ clusters on apo *Av* IscU for 60 min is shown by a purple line. The CD spectra of cysteine desulfurase-mediated [2Fe-2S]$^{2+}$ cluster assembly on apo *Av* IscU in the presence of a 5-fold excess of 5-membered cyclic thiosulfinate after 2 min (thick black line), at 3 min intervals (thin gray lines), and after 60 min (thick blue line). Both samples had the same concentration of apo IscU (0.3 mM) and reconstitution involved adding a 6-fold excess of FAS and L-Cys and a catalytic amount of IscS. Spectra were recorded under anaerobic conditions in sealed 0.1 cm cuvette in 100 mM Tris-HCl buffer at pH 7.4. $\Delta\varepsilon$ values are based on concentration of *Av* IscU monomer.

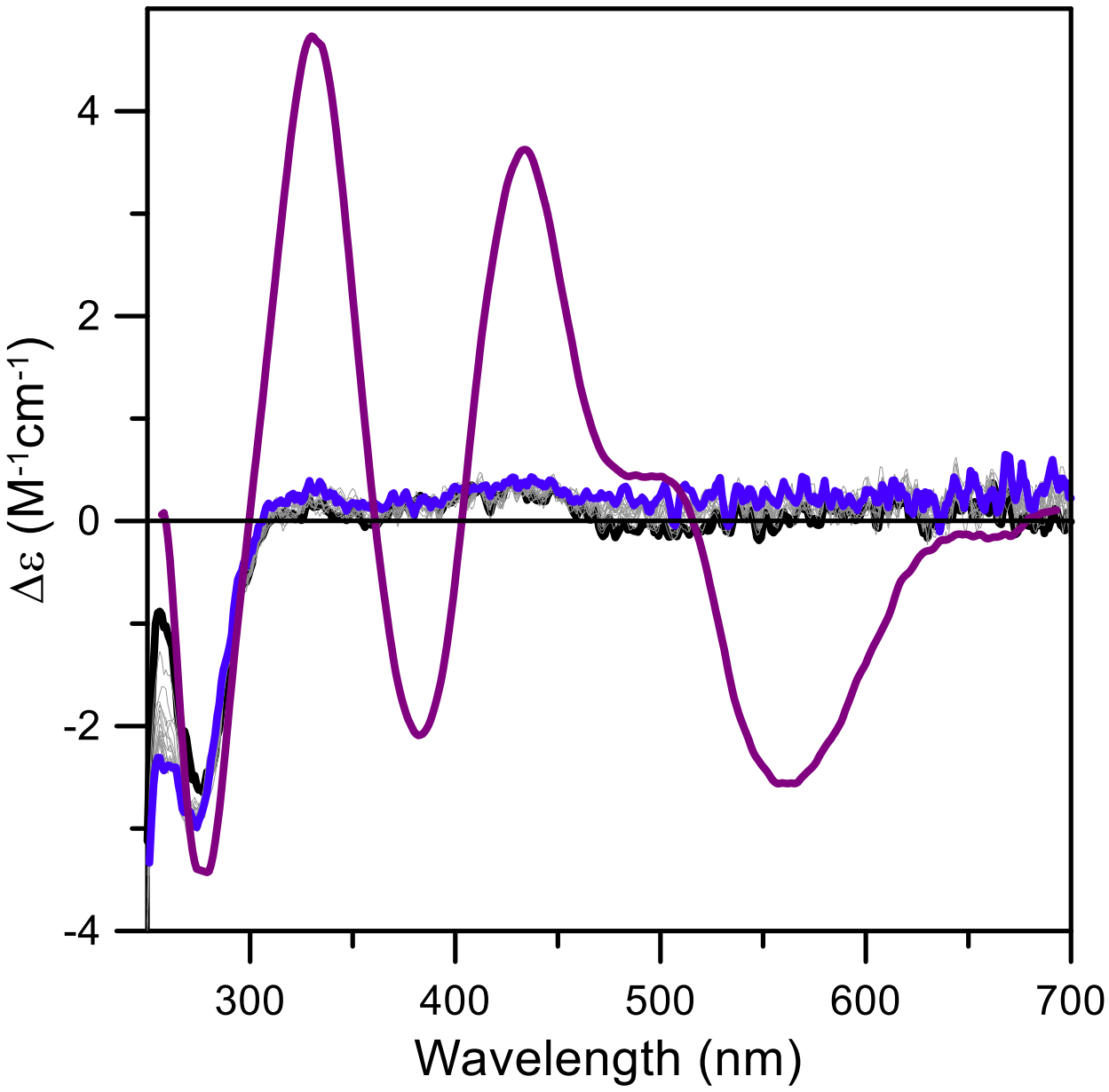
4
2
0
-2
-4
Δε (M-1cm-1)
300
400
500
600
700
Wavelength (nm)

Figure 3.10. Stoichiometric 5-, 6-, and 7- membered cyclic thiosulfinates inhibit cysteine desulfurase $[2Fe\text{-}2S]^{2+}$ cluster assembly on *Av* IscU. (A) Time course of cysteine desulfurase-mediated reconstitution of $[2Fe\text{-}2S]^{2+}$ cluster assembly on *Av* IscU monitored by CD spectroscopy in the absence of cyclic thiosulfinates. CD spectrum of the reaction mixture 2 min after adding a 6-fold excess of FAS and L-Cys and a catalytic amount of IscS to apo IscU is shown as a black line. CD spectra at additional 3-min intervals are shown as gray lines. The CD spectrum of $[2Fe\text{-}2S]^{2+}$ cluster-bound *Av* IscU after 5 h at reaction completion is shown as a purple line. The time course of cysteine desulfurase-mediated reconstitution of $[2Fe\text{-}2S]^{2+}$ cluster assembly on *Av* IscU cross-linked with 5-, 6-, and 7-membered cyclic thiosulfinates (in the absence of excess cross-linkers) monitored by CD spectroscopy are shown in (B), (C), and (D) respectively. CD spectra of the reaction mixture 2 min after starting reconstitution are shown as black lines. CD spectra at 3-min intervals are shown in gray lines. CD spectra of the product after 1 h are shown as blue lines and are compared to that of IscU without cross-linkers after 1 h, shown as a purple line. Spectra were recorded under anaerobic conditions in sealed 0.1 cm cuvette. All samples were 0.3 mM in IscU monomer in 100 mM Tris-HCl buffer at pH 7.4. $\Delta\varepsilon$ values are based on concentration of *Av* IscU monomer.

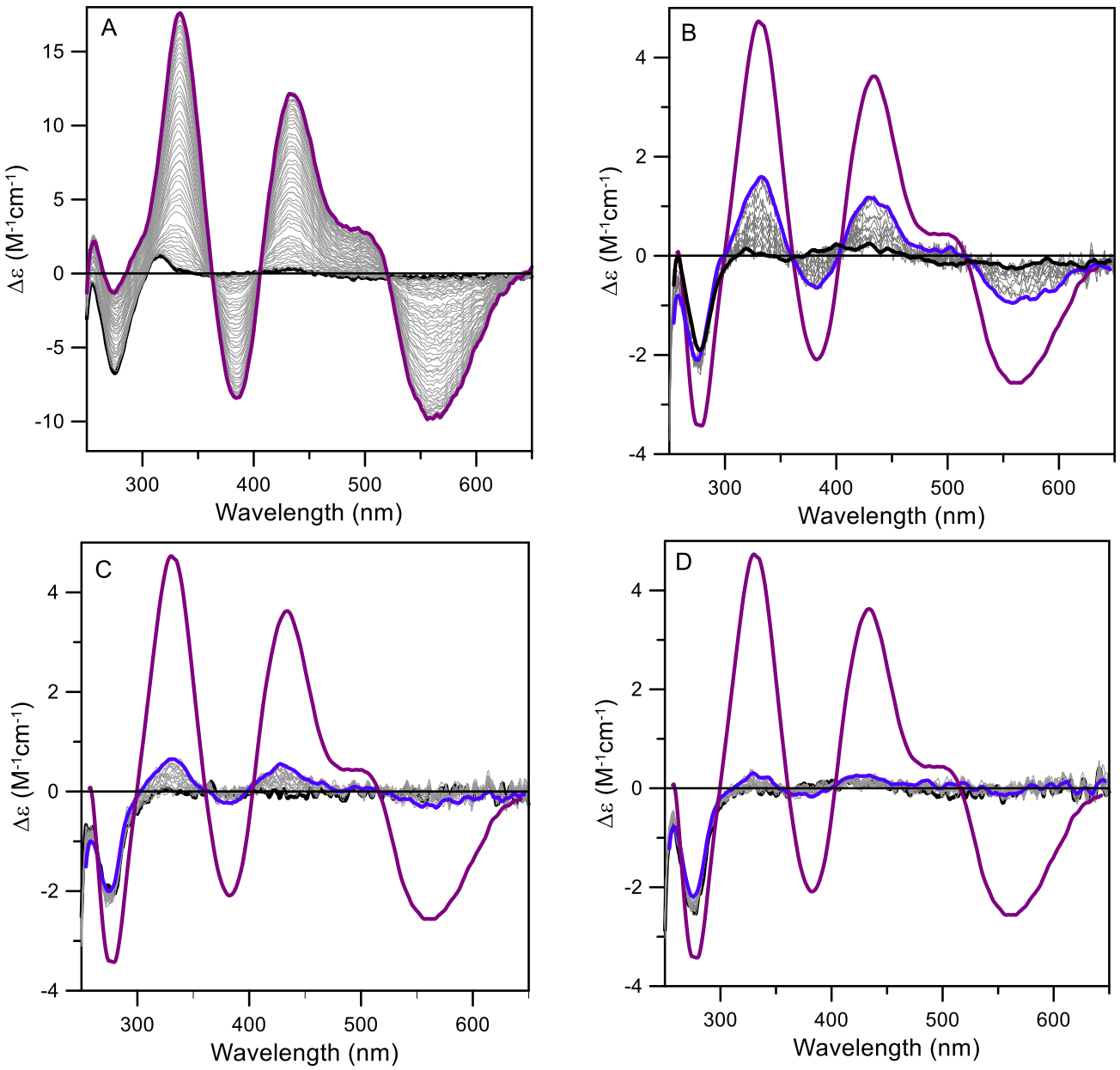
A
B
C
D
Δε (M-1cm-1)
Wavelength (nm)
300
400
500
600

CHAPTER FOUR

CONCLUSIONS AND FUTURE WORK

The overall objectives of this work were to elucidate the mechanism of [Fe-S] cluster assembly on Fe-S proteins using thioferrate as the source of iron and sulfide, and to investigate the mechanism and inhibition of $[2Fe\text{-}2S]^{2+}$ cluster assembly on the *Azotobacter vinelandii* IscU scaffold protein using *in vitro* spectroscopic, analytical, and biochemical techniques.

Spectroscopic characterization of synthesized colloidal thioferrate using UV-visible absorption/CD and X-ray absorption spectroscopy (XAS) confirmed that thioferrate nanoparticles are associated with the archaeal iron-sulfur storage protein, IssA (1). In addition, spectroscopic and biochemical characterization of the products of thioferrate-mediated reconstitution of $[2Fe\text{-}2S]^{2+}$ cluster and linear $[3Fe\text{-}4S]^{1+}$ cluster in monothiol glutaredoxins and ferredoxins, and $[4Fe\text{-}4S]^{2+}$ clusters in ferredoxins demonstrate the ability of apo iron-sulfur proteins to obtain fragments of thioferrate via ligand exchange and to use these fragments to generate the native [Fe-S] clusters under anaerobic conditions.

The *in vitro* thioferrate reconstitution results obtained in this study demonstrate presence of linear $[3Fe\text{-}4S]^{1+}$ clusters as a major or minor component in the reconstitution products, even in proteins that are known to have exclusive preference for binding and reconstituting $[2Fe\text{-}2S]^{2+}$ and $[4Fe\text{-}4S]^{2+}$ clusters, i.e. *Av* Fdx and *Pf* Fdx respectively (2,3). This strongly suggests that the mechanism of thioferrate-mediated reconstitution of [Fe-S] cluster involves thioferrate binding to two cysteine residues on the apo protein, followed by cleavage of the polymer chain to form a

bound linear $[3Fe\text{-}4S]^{1+}$ fragment that can be used *in situ* to form bound $[2Fe\text{-}2S]^{2+}$ and $[4Fe\text{-}4S]^{2+}$ clusters in process that is likely to be the rate determining step as a result of protein conformation changes. $[2Fe\text{-}2S]^{2+}$ cluster formation from a linear $[3Fe\text{-}4S]^{1+}$ cluster would involve loss of one Fe^{3+} and two S^{2-} ions and $[4Fe\text{-}4S]^{2+}$ cluster formation would involve addition of one Fe^{2+} ion and one electron to a linear $[3Fe\text{-}4S]^{1+}$ cluster under reducing conditions.

Additional informative and interesting future experiments such as thioferrate-mediated reconstitution of *Sc* Grx5 in the absence of GSH, but in the presence of DTT, can provide valuable information regarding involvement of linear $[3Fe\text{-}4S]^{1+}$ clusters in the formation of $[4Fe\text{-}4S]^{2+}$ clusters , as cysteine desulfurase-mediated reconstitution of *Sc* Grx5 in the presence of DTT results in formation of $[4Fe\text{-}4S]^{2+}$ cluster (4). Another interesting experiment would be thioferrate-mediated reconstitution of mitochondrial aconitase which can accommodate a variety of different [Fe-S] clusters (5). In its active form, aconitase contains a $[4Fe\text{-}4S]^{2+,+}$ cluster (6). Air exposure results in conversion of the active form of the enzyme to an inactive form by conversion of the $[4Fe\text{-}4S]^{2+,+}$ cluster to cuboidal $[3Fe\text{-}4S]^{1+}$ cluster (7). Moreover, the cuboidal $[3Fe\text{-}4S]^{1+}$ cluster undergoes conversion to a linear $[3Fe\text{-}4S]^{1+}$ cluster when aconitase is partially denatured with urea or exposure to pH > 9 (5). Characterization and comparison of the products of thioferrate-mediated reconstitution of aconitase at alkaline pH and physiological relevant pH values can provide further insight into proposed mechanism of thioferrate-mediated reconstitutions.

In vitro biophysical techniques and analytical studies have provided a wealth of information concerning the role of IscX and Fdx in the bacterial ISC assembly system. The results of UV-visible CD spectroscopy and ICP-MS studies demonstrated stoichiometric Fe^{2+} binding to IscX, and provided direct evidence that IscX rapidly transfers a Fe^{2+} ion to IscU, indicating the role of IscX as a specific Fe^{2+} donor for $[2Fe\text{-}2S]^{2+}$ cluster assembly on IscU in the bacterial ISC

biosynthesis. The role of *Av* Isc Fdx in IscS-mediated $[2Fe\text{-}2S]^{2+}$ cluster assembly on *Av* IscU was investigated by parallel UV-visible absorption and EPR studies to evaluate the possibility of a cysteine persulfide radical anion intermediate generation on IscS that would be a precursor of a trisulfide radical anion intermediate on IscU. Parallel UV-visible absorption and EPR studies of IscS in the presence of reduced Fdx and L-Cys, and a single turnover of IscS in the presence of stoichiometric IscU, reduced Fdx, Fe^{2+}-bound IscX, and L-Cys have confirmed stoichiometric Fdx oxidation, but have failed to identify any sulfur-based radical species. Consequently, the results presented in this work favor a mechanism involving IscS-mediated S^0 rather than a S^- radical transfer to IscU.

UV-visible CD spectroscopy was also effective in demonstrating that a new class of variable-length thiol cross-linking reagents, 5-, 6-, and 7-membered cyclic thiosulfinates (8) are potent inhibitors of Fe^{2+} binding and $[2Fe\text{-}2S]^{2+}$ cluster assembly on *Av* IscU. UV-visible CD spectroscopy demonstrated 5-, 6-, and 7-membered cyclic thiosulfinates as potent inhibitors that cross-link cysteines on *Av* IscU and thereby inhibit Fe^{2+} binding, spontaneous as well as cysteine desulfurase-mediated $[2Fe\text{-}2S]^{2+}$ cluster assembly on IscU. The inhibition of [Fe-S] cluster assembly on IscU by cyclic thiosulfinates, however, was shown not to be permanent, since DTT was able to cleave the disulfide bonds between cysteine residues of protein and thiols of cross-linker and thereby restore the ability of IscU to assemble $[2Fe\text{-}2S]^{2+}$ clusters. Inhibiting $[2Fe\text{-}2S]^{2+}$ cluster assembly on the homologous mitochondrial ISU1 scaffold protein using cyclic thiosulfinates would effectively shut down [Fe-S] cluster assembly, which would be particularly deleterious to fast-growing cancer cells. Therefore, potent inhibitors of the [Fe-S] cluster assembly on IscU scaffold proteins such as cyclic thiosulfinates have the potential constitute a new class of targeted anticancer drugs. The first step in exploring this possibility is to assess the ability of cyclic

thiosulfinates to inhibit $[2Fe\text{-}2S]^{2+}$ cluster assembly on the homologous human mitochondrial ISU1 scaffold protein.

The detailed mechanism of IscS-mediated $[2Fe\text{-}2S]^{2+}$ cluster assembly on IscU remains to be determined. Therefore developing methods for inhibiting cluster assembly on the scaffold protein, IscU, is important for determining the mechanism of the first concerted step of IscS-mediated assembly of $[2Fe\text{-}2S]^{2+}$ clusters on IscU, i.e. S transfer from IscS or Fe^{2+} transfer from IscX. For example, IscU cross-linked with a 5-membered cyclic thiosulfinate in the absence of excess cross-linker, does not bind Fe^{2+} ions. However, in the presence of IscS, L-Cys and FAS, $[2Fe\text{-}2S]^{2+}$ clusters bound by the three conserved cysteines are slowly assembled on IscU suggesting that Fe^{2+} binding prior to sulfur transfer is not essential for $[2Fe\text{-}2S]^{2+}$ cluster assembly on IscU. In light of the results presented in this work, demonstrating the effect of 5-, 6-, and 7-membered cyclic thiosulfinate cross-linkers for fully or partially inhibiting and slowing $[2Fe\text{-}2S]^{2+}$ cluster assembly on IscU, future studies can benefit from slower reconstitution reactions in order to trap and characterize intermediates by parallel rapid freeze quench EPR/Mössbauer studies. In addition to rapid freeze quench Mössbauer studies that can characterize the status of Fe during $[2Fe\text{-}2S]^{2+}$ cluster assembly, future studies can also benefit from cryo-Electron Microscopy (cryo-EM) technique. Interaction of proteins involved in $[2Fe\text{-}2S]^{2+}$ cluster assembly can be determined and the ones competing for the same docking site can be detected. The $[2Fe\text{-}2S]^{2+}$ cluster assembly steps can be traced by freezing the reaction at different time points owing to recent advances in single-particle cryo-EM, enabling generation of numerous near-atomic resolution structures for protein complexes with sizes $\geq \sim$200 kDa (9).

In summary, the research projects undertaken in this work are linked together through the insights provided towards the understanding of [Fe-S] cluster biogenesis. Understanding both the physiological functions of Fe-S proteins and the mechanism of [Fe-S] clusters assembly can undoubtedly enhance our ability to identify and ultimately treat disorders associated with defects in [Fe-S] cluster biogenesis.

References

1. Vaccaro, B. J., Clarkson, S. M., Holden, J. F., Lee, D.-W., Wu, C.-H., Poole Ii, F. L., Cotelesage, J. J. H., Hackett, M. J., Mohebbi, S., Sun, J., Li, H., Johnson, M. K., George, G. N., and Adams, M. W. W. (2017) Biological iron-sulfur storage in a thioferrate-protein nanoparticle. *Nat. Commun.* **8**, 16110

2. Aono, S., Bryant, F. O., and Adams, M. W. (1989) A novel and remarkably thermostable ferredoxin from the hyperthermophilic archaebacterium *Pyrococcus furiosus*. *J. Bacteriol.* **171**, 3433-3439

3. Jung, Y. S., Gao-Sheridan, H. S., Christiansen, J., Dean, D. R., and Burgess, B. K. (1999) Purification and biophysical characterization of a new [2Fe-2S] ferredoxin from *Azotobacter vinelandii*, a putative [Fe-S] cluster assembly/repair protein. *J. Biol. Chem.* **274**, 32402-32410

4. Zhang, B., Bandyopadhyay, S., Shakamuri, P., Naik, S. G., Huynh, B. H., Couturier, J., Rouhier, N., and Johnson, M. K. (2013) Monothiol glutaredoxins can bind linear $[Fe_3S_4]^+$ and $[Fe_4S_4]^{2+}$ clusters in addition to $[Fe_2S_2]^{2+}$ clusters: spectroscopic characterization and functional implications. *J. Am. Chem. Soc.* **135**, 15153-15164

5. Kennedy, M. C., Kent, T. A., Emptage, M., Merkle, H., Beinert, H., and Münck, E. (1984) Evidence for the formation of a linear [3Fe-4S] cluster in partially unfolded aconitase. *J. Biol. Chem.* **259**, 14463-14471

6. Beinert, H., Kennedy, M. C., and Stout, C. D. (1996) Aconitase as iron−sulfur protein, enzyme, and iron-regulatory protein. *Chem. Rev.* **96**, 2335-2374

7. Kent, T. A., Dreyer, J. L., Kennedy, M. C., Huynh, B. H., Emptage, M. H., Beinert, H., and Münck, E. (1982) Mössbauer studies of beef heart aconitase: evidence for facile interconversions of iron-sulfur clusters. *Proc. Natl Acad. Sci. USA* **79**, 1096-1100

8. Donnelly, D., Dowgiallo, M., Salisbury, J., Aluri, K., Iyengar, S., Chaudhari, M., Mathew, M., Miele, I., Auclair, J., Lopez, S., Manetsch, R., and Agar, J. (2018) Cyclic thiosulfinates and cyclic disulfides selectively cross-link thiols while avoiding modification of lone thiols. *J. Am. Chem. Soc.* **140**

9. Merk, A., Bartesaghi, A., Banerjee, S., Falconieri, V., Rao, P., Davis, M. I., Pragani, R., Boxer, M. B., Earl, L. A., Milne, J. L. S., and Subramaniam, S. (2016) Breaking cryo-EM resolution barriers to facilitate drug discovery. *Cell* **165**, 1698-1707

APPENDIX A

BIOLOGICAL IRON-SULFUR STORAGE IN A THIOFERRATE-PROTEIN NANOPARTICLE

Brian J. Vaccaro[1,2], Sonya M. Clarkson[2,3], James F. Holden[2,4], Dong-Woo Lee[2,5], Chang-Hao Wu[2], Farris L. Poole[2], Julien J. H. Cotelesage[6], Mark J. Hackett[6,7], Sahel Mohebbi[1], Jingchuan Sun[8], Huilin Li[8], Michael K. Johnson[1], Graham N. George[6] and Michael W.W. Adams[2]

Nat. Commun. **2017**, 8, 16110.

[1] Dept. of Chemistry, Univ. of Georgia, Athens, GA 30602, USA; [2] Dept. of Biochemistry and Molecular Biology, Univ. of Georgia, Athens, GA 30602, USA; [3] Current address: Conagen Inc., Bedford, MA 01730, USA; [4] Current address: Dept. of Microbiology, Univ. of Massachusetts, Amherst, MA 01003, USA; [5] Current address: School of Applied Biosciences, Kyungpook National University, Daegu 41566, Korea; [6] Depts. of Geological Sciences and Chemistry, Univ. of Saskatchewan, Saskatoon, Saskatchewan, Canada; [7] Current address: Dept. of Chemistry, Curtin University, Perth, Western Australia 6102, Australia; [8] Cryo-EM Structural Biology Laboratory, Van Andel Research Institute, Grand Rapids, MI 49503, USA

Abstract

Iron-sulfur clusters are ubiquitous in biology and function in electron transfer and catalysis. They are assembled from iron and cysteine sulfur on protein scaffolds. Iron is typically stored as iron oxyhydroxide, ferrihydrite, encapsulated in 12 nm shells of ferritin, which buffers cellular iron availability. Here we have characterized IssA, a protein that stores iron and sulfur as thioferrate, an inorganic anionic polymer previously unknown in biology. IssA forms nanoparticles reaching 300 nm in diameter and is the largest natural metalloprotein complex known. It is a member of a widely-distributed protein family that includes nitrogenase maturation factors, NifB and NifX. IssA nanoparticles are visible by electron microscopy as electron-dense bodies in the cytoplasm. Purified nanoparticles appear to be generated from 20 nm units containing ~6,400 Fe atoms and ~170 IssA monomers. In support of roles in both iron-sulfur storage and cluster biosynthesis, IssA reconstitutes the [4Fe-4S] cluster in ferredoxin *in vitro*.

Introduction

Iron is an essential nutrient for almost all known organisms. It functions as a protein cofactor in fundamental pathways including respiration, photosynthesis and the biogeochemical cycling of sulfur and nitrogen. There are two major types of iron-containing protein cofactors, hemes and iron-sulfur clusters. The most common iron-sulfur cluster is the cubane-type [4Fe-4S] cluster, which is involved in electron transfer, catalysis, DNA repair and small molecule sensing[1]. In spite of their high sensitivity to degradation by oxygen and reactive oxygen species, [4Fe-4S] clusters are ubiquitous in biology. More complex iron-sulfur-containing cofactors containing modified [4Fe-4S] clusters catalyze more chemically challenging reactions in nitrogenase, carbon monoxide dehydrogenase, acetyl-coA synthase and hydrogenase[1].

Iron-sulfur cluster biosynthesis is carried out by two main systems in microorganisms. Due to the insolubility of free ferric iron at neutral pH and the toxicity of free ferrous iron in the presence of O_2, iron trafficking and storage is tightly controlled[1]. The ISC (Iron-Sulfur Cluster) system is found throughout bacteria (and in mitochondria) while the SUF (Sulfur-Utilization Factors) system is used in archaea and bacteria (and in some plastids). They have similar mechanisms[2] wherein an iron donor and a cysteine desulfurase provide Fe and S to a scaffold protein, and the metastable scaffold-bound cluster is rapidly delivered to a carrier protein[3]. Due to the complex chemistry and energetic cost involved (ATP is used in initiating cluster release or recruiting Fe and cysteine must be regenerated), it is efficient for a cell to repair iron-sulfur clusters that become damaged by reactive oxygen or nitrogen species, and several repair systems have been proposed[4,5]. In particular, many $[4Fe\text{-}4S]^{2+}$ clusters will lose Fe reversibly upon oxidation, to form cubane-type $[3Fe\text{-}4S]^{+}$ clusters or cysteine persulfide-ligated $[2Fe\text{-}2S]^{2+}$ clusters. Repair of such

degraded forms is efficient because they can be restored simply by reduction and the addition of ferrous iron without the need for the full biosynthetic machinery.

While the identity or need for a specific Fe donor for iron-sulfur cluster biosynthesis is still under debate[6], Fe import and storage systems that are able to accommodate the cellular Fe demands in a wide range of extracellular Fe concentrations have been well characterized[7,8]. In many organisms, Fe is stored in ferritin, which assembles into a 24-mer hollow sphere. Ferritin catalyzes the assembly (and release) of a ferrihydrite-type ferric oxy-hydroxide (FeOOH) from Fe^{2+} and O_2 in the interior of the sphere using catalytic iron sites, but the mechanism of Fe release from the mineral core is still largely unresolved. Although ferritin homologs exist throughout the three domains of life, including anaerobes, an anaerobic oxidant that facilitates oxidation of Fe^{2+} has yet to be identified, and the physiological role of ferritin in many organisms is not clear[8]. The exact composition of the iron oxide component of ferritin also varies among different species, as does its crystallinity[8]. Abiotic ferrihydrite is disordered or nanocrystalline and porous[9]. Thus this material lends itself to a highly dense form of iron storage that maintains accessibility of the iron due to the high specific area (~300 m^2 g^{-1}) and metastability (relative to other minerals)[9].

To investigate the process of iron and sulfur storage and their incorporation into iron-sulfur clusters in an anaerobic microorganism that cannot use oxygen to oxidize ferrous iron, we examined the archaeon *Pyrococcus furiosus*, which grows optimally near 100°C in hydrothermal marine vents [10]. This strict anaerobe grows in the presence of elemental sulfur (S^0) and uses it as an (insoluble) electron acceptor to generate (soluble) hydrogen sulfide [10]. It has been shown that at least some Archaea use extracellular sulfide directly, rather than cysteine, for iron-sulfur cluster biosynthesis[11]. *P. furiosus* does contain a homolog of the SufS cysteine desulfurase[1,2], but its natural hydrothermal vent environment is typically rich in sulfide and this could be directly

incorporated into Fe-S clusters, which would be much more efficient than cysteine degradation to produce sulfide. In support of this idea, transcriptional analysis comparing *P. furiosus* grown with and without S^0 revealed up-regulation in the expression of numerous genes during hydrogen sulfide production, including those involved in iron and iron-sulfur cluster metabolism [12]. However, the most highly up-regulated of these genes (PF2025) encodes a conserved hypothetical protein that at the time was termed sulfur-induced protein A, or SipA[13]. Since expression of *sipA* is only up-regulated by sulfide in the presence of sufficient iron[14], this prompted us to investigate whether this protein acts in iron-sulfur cluster metabolism with direct sulfide incorporation. Based on the results presented herein, we rename SipA to the more specific iron-sulfur storage protein A, or IssA.

In this study, we present characterization of IssA. Transmission electron microscopy (TEM) of *P. furiosus* cells expressing IssA shows naturally electron dense particles that co-locate with IssA immunolabeling. TEM of purified IssA reveals particles up to 300 nm, which appear to be comprised of ~20 nm spheres. X-ray absorption spectroscopy (XAS) strongly supports a thioferrate-type linear $(FeS_2^-)_n$ structure of iron and sulfur, and the EPR of IssA is in accord with this assignment. Finally, we show that IssA is capable of assembling a [4Fe-4S] cluster on *P. furiosus* ferredoxin (Fd), an abundant electron carrier in this organism, in the presence of the small molecule thiol, dithiothreitol (DTT). These properties of IssA together with the conditions under which it is expressed[13,14] lead us to conclude that *P. furiosus* stores excess Fe and S, when they are both highly abundant, in IssA-bound thioferrate, an iron-sulfur structure not previously known in biology. The stored thioferrate can subsequently be mobilized for assembly of [4Fe-4S] clusters, which are widely used in *P. furiosus*. Phylogenetic analyses suggest that homologs of IssA in many archaea, and possibly bacteria as well, may also store iron as thioferrate.

Experimental procedures

Thin section electron microscopy. *P. furiosus* was grown as described[12]. Cells were fixed with 2% paraformaldehyde and 1% glutaraldehyde, dehydrated with ethanol, infiltrated with LR White and polymerized at 50°C. Final samples were sectioned with a diamond ultratome and placed on nickel grids. Grids were blocked with 50 mM TrisHCl (pH 7.4), 0.5 M NaCl, 0.05% v/v Tween 20 with 3% w/v bovine serum albumin, then incubated with primary antibody[14] (1:10,000) followed by 10 nm gold-conjugated anti-rabbit IgG (1:50). Samples were stained with 2% uranyl acetate; imaging and energy dispersive X-ray analysis was performed using a FEI Technai 20 transmission electron microscope (Center for Advanced Ultrastructural Research, University of Georgia).

IssA aggregate protein analysis. The IssA nanoparticle aggregate was immunoprecipitated from *P. furiosus* cells grown continuously with elemental iron-sulfur[12]. Cells were lysed[15], DNA was sheared using a 21 gauge needle, and protein concentration was brought to 2.5 mg/mL. Cell lysates were pre-cleared with rabbit IgG and then immunoprecipitated with purified IssA antibody cross-linked to Protein A magnetic beads according to the manufacturer's protocol. The immunoprecipitated sample was digested with 10 ng/µL trypsin at 37°C overnight and spotted onto a MALDI Anchor plate according to the manufacturer's protocol using NuTip C-18 tips with α-cyano-4-hydroxycinnamic acid matrix. The resulting peptide masses were analyzed using MASCOT software searching a *Pyrococcus furiosus*-specific database and allowing for 2 missed cleavages and a mass difference of ±0.4 Da.

Native protein purification. IssA was purified from *Pyrococcus furiosus* cells grown continuously with S^0 [12]. Cells were lysed[15] and centrifuged at 100,000 x *g* for 1 h. The pellet was washed first in 50 mM Tris-HCl (pH 8.0), 2 mM dithionite, and 2 mM dithiothreitol (DTT) (buffer

A) containing 1% w/v sodium dodecyl sulfate, then twice in buffer A and applied to a cesium chloride gradient (density = 1.4 g/mL, 260,000 x *g*, 9.5 h) to remove precipitated material from the media. Fractions containing IssA were pooled and dialyzed against 4 L buffer A and concentrated using a Centricon centrifugal concentrator with a 10 kDa cut-off (Millipore). Protein concentration was estimated using the bicinchoninic acid method at 60°C[16], following precipitation with 20% w/v trichloroacetic acid. Gel electrophoresis and Western blot analyses were performed as described[14].

Metal, sulfide and sulfane sulfur analysis. An Agilent 7500c ICP-MS was used to quantify iron and other metals. Sample processing, instrument settings and analysis of mass spectrometry data have been previously described[17]. Colorimetric assays were used to measure iron[18], sulfide[12], and sulfane sulfur[19] in purified protein.

Negative stain electron microscopy. Purified IssA exists as a suspension that settles in ~1 hr. TEM was conducted on purified IssA as well as on solubilized samples. Solubilization was achieved by adding 20 µL denaturing buffer (6 M guanidinium chloride, 50 mM Tris, 1 mM EDTA, 50 mM DTT) to 20 µL IssA sample. This mixture was shaken at room temperature for 4 hours after which the sample was fully dissolved. We diluted the solution six fold with deionized water (dH_2O) and applied 3 µL to a glow discharged carbon-coated TEM grid. The grid was washed with 3 µL dH_2O and stained with 3 µL of 2% uranyl acetate. Microscopy was conducted on a JEOL 2010F TEM operated at 200 kV high tension and 50 kX magnification. 100 electron micrographs were recorded in a Gatan Ultrascan 4K by 4K CCD camera. We automatically selected 30,000 raw particles and performed 2D image classification in EMAN 2[20]. Composition of the complexes observed in solubilized IssA was estimated using the volume of a 20 nm sphere,

protein density of 1.37 g/mL, FeS density of 4.28 g/mL, a ratio of 38 Fe : 76 S : 1 Zn : 1 protein, and the assumption that all volume is occupied by FeS or protein.

XAS data acquisition and analysis. Details of iron and sulfur K-edge data collection are described in Supplementary Methods, and the effects of radiation exposure on the sulfur K-edge signal from IssA are shown in Supplementary Figure A.8. The EXAFS oscillations $\chi(k)$ were quantitatively analysed as previously described[21] by curve-fitting using the EXAFSPAK suite of computer programs[22] using *ab initio* theoretical phase and amplitude functions calculated using the program FEFF version 8.25[23]. No smoothing, filtering or related operations were performed on the data.

EPR analysis. 100 mg purified IssA was loaded into a quartz EPR tube and centrifuged for 30 min. at 1000 x *g*. The supernatant was removed and the X-band (~9.6 GHz) EPR spectrum was obtained using a Bruker ESP-300E EPR spectrometer equipped with an ER-4116 dual-mode cavity and an Oxford Instruments ESR-9 flow cryostat.

***In vitro* IssA-mediated reconstitution of apo-Fd from *P. furiosus*.** Apo-Fd from *P. furiosus* was prepared using the method of Moulis and Meyer[24], except that a 2-hour incubation with 8% (w/v) TCA at room temperature was required to fully bleach and precipitate the protein. After centrifugation, the apo-protein pellet was dissolved in 200 mM PIPES buffer, pH 6.8, with 1 M NaCl and 1 M KCl, under anaerobic conditions. Apo-Fd (0.25 mM) was incubated with IssA (0.052 mM in monomer, i.e. ~8:1 ratio of Fe:Fd) in the same buffer for 24 hours at room temperature in the presence of 10 mM DTT, 10 mM sodium dithionite or 10 mM TCEP. The experiment was repeated using the same protocol except that apo-Fd (0.58 mM) was incubated with IssA (0.067 mM in monomer, i.e. ~4.4:1 ratio of Fe:Fd) at 80 °C for 1 hour. In all cases the resultant Fd was repurified by centrifugation to remove unreacted IssA, buffer exchanged into 50

mM Tris-HCl buffer, pH 7.8, loaded onto a HiTrap Q column and removed as a single band with a 0-1 M NaCl gradient. After desalting and concentrating by Amicon ultrafiltration with a 3 kDa membrane, purity was assessed to be > 95% based on gel electrophoresis and the protein concentration was determined using the Bradford assay. [4Fe-4S] cluster content and integrity were assessed compared to the holo-Fd using UV-visible absorption and CD spectra with ε and Δε values based on protein concentrations.

Expression and purification of apo-IssA using *E. coli.* Details of design, expression and purification of the apo-IssA construct are described in Supplementary Methods.

Apo-IssA reconstitution. IssA reconstitution was carried out by adding ferrous ammonium sulfate (10 mM) and sodium sulfide (10 mM) in buffer A to apo-IssA (0.25 mM) and incubating with shaking for 1 hour at 80°C. Excess iron and sulfide were removed by buffer exchange using a Centricon concentrator (Millipore) with a 10 kDa cut-off.

Phylogenetic analysis and structural model. Details of IPR003731 sequence selection and alignment, phylogenetic tree generation and refinement, construction of the structural model of IssA, and related analyses are described in Supplementary Methods.

Results

Expression of IssA nanoparticles is sulfur-responsive. When S^0 was added to a growing *P. furiosus* culture, IssA could be detected in cells by TEM and immuno-gold labeling after 20 min (Figure A.1a). IssA concentration increased over subsequent hours (Supplementary Figure A.1) as well as the area of the cytoplasm occupied by IssA (Figure A.1a), eventually reaching 10-30% of the sectioned cellular area (Figure A.1). IssA is visible not only by immunolabeling but also as electron dense blotches that co-locate with immunolabeling of IssA both spatially and temporally (Figure A.1). These observations indicate that this protein forms large (≥ 50 nm)

aggregates *in vivo* after 1 hr of IssA expression. Energy dispersive X-ray analysis of the TEM-visualized electron dense blotches indicated that IssA is associated with iron and sulfur *in vivo* (Supplementary Figure A.2). In addition, proteomic analysis of IssA immunoprecipitated from *P. furiosus* cell extract showed that no other protein is associated with the purified IssA nanoparticle *in vitro* (Supplementary Table A.1), suggesting homomeric IssA nanoparticles exist *in vivo*.

IssA binds iron and sulfur. IssA was purified from cell extracts of S^0-grown *P. furiosus* based on its massive size and high density relative to other cellular components. Even though the amino acid sequence showed no indication of membrane-association, when cytoplasmic and membrane-associated proteins were separated by ultracentrifugation, IssA was the major protein in the sedimented pellet, as determined by SDS-gel electrophoresis (Supplementary Figure A.3). The membrane-bound proteins in the pellet were dissolved by treatment with detergent (sodium dodecyl sulfate, 1%), however, IssA was not solubilized by this treatment. Density equilibrium centrifugation of the detergent-insoluble material resulted in a black band in which IssA is the only protein present (Supplementary Figure A.3). Metal analysis by inductively-coupled plasma mass spectrometry (53 elements) of purified IssA showed that it contains approximately 38 iron atoms and 1 zinc atom per 19 kDa IssA monomer (Supplementary Table A.2). Colorimetric assays indicated that IssA contains 38 acid-labile sulfide ions and 17 sulfane sulfur atoms per protein monomer. The interpretation of the sulfur measurements is discussed further below.

Characterization of IssA nanoparticles. Sedimentation of IssA after ultracentrifugation was consistent with the observation of large particles via TEM. This was investigated further using size exclusion chromatography. Most (~90%) of the protein was too large to enter the chromatography column and was retained on the pre-column filter (diameter 1 μm). IssA that entered and eluted from the chromatography column did so in a peak at the exclusion limit (40

MDa) or just after the exclusion limit (100 MDa dextran or 400 nm spheres) from Superose 6 and Sephacryl S-1000 SF columns, respectively (Supplementary Figure A.4). Dynamic light scattering (DLS) analysis was attempted to obtain more precise sizing information. However, reproducible results could not be obtained from IssA. Centrifugation to minimize DLS interference by small air bubbles led to sedimentation of IssA, overall signal was low due to the high extinction coefficient of IssA samples (Gregory L. Hura, personal communication), which appear black, and IssA particles are not uniform in size, as was observed on electron micrographs.

Negative stain TEM of the purified protein showed IssA assemblages with dimensions ranging from 20 to 300 nm (Figure A2a). Incubation of IssA with 3 M guanidinium chloride, 0.5 mM EDTA and 25 mM DTT, however, yields a more monodisperse sample comprised of roughly spherical particles 16-22 nm in diameter (Figure A.2b). Thus it appears that the 19 kDa IssA monomer forms modular nanostructures based on a ~20 nm packing unit, containing ~6,400 Fe atoms and ~170 IssA monomers. A protein complex of this size of average density would have a mass of ~3.5 MDa.

XAS and EPR spectroscopy of IssA-bound iron and sulfide. XAS was conducted at both Fe K-edge and S K-edge absorption energies to characterize the iron and sulfur bound by IssA. Figure A.3a compares the X-ray absorption near-edge spectra of IssA with a number of different iron-sulfur proteins. For both the S and Fe K-edges, the spectra strongly resemble those of the linear $[3Fe\text{-}4S]^{+}$ cluster in the high pH form of the enzyme aconitase[17]. The sulfur K-edge data of IssA show two pronounced peaks, one at low energy at 2467.1 eV, and a broader less-well defined feature at 2470.2 eV. The former, lower energy absorption, is characteristic of sulfide coordinated to ferric ions, arising from dipole-allowed transitions of the 1s electron to unfilled molecular orbitals involving both sulfur 3p and metal 3d orbitals, with vacancies due to covalency

of the Fe—S bond [25,26]. The second, higher energy transition is attributable to other types of sulfur in the system, such those in the one cysteine and four methionine residues in the IssA monomer (see below). In both S and Fe K-edge cases, the IssA spectra are highly characteristic of a Fe(III) oxidation state[25,27].

The S and Fe K-edge EXAFS oscillations, together with the corresponding EXAFS Fourier transforms, are shown in Figure A.3b, with the best fits. The Fe EXAFS data is dominated by intense backscattering from four Fe—S interactions at 2.24 Å, plus backscattering attributable to two Fe···Fe interactions at 2.70 Å. The sulfur K-edge EXAFS, on the other hand, fits to two S—Fe interactions, with no substantial outer shell contributions (Figure A.3b). Experiments at the low X-ray energies of the sulfur K-edge are more challenging than at the iron K-edge, and for this reason the latter data is of substantially better signal to noise ratio. The iron EXAFS also shows a second less intense outer shell Fourier transform peak at 5.4 Å, twice that of the shorter Fe···Fe interaction. This fits well to a long range Fe···Fe interaction once multiple scattering interactions for a linear arrangement of iron atoms are included. This 5.4 Å interaction is close to the limit of the noise, being about three times the transform peak height of the noise as estimated from higher *R* values, using data to 18 $Å^{-1}$. However, it shows behavior characteristic of real EXAFS, rather than a noise peak in the Fourier transform, so that the feature persists irrespective of the *k*-ranges, and moreover fits to a very similar Fe···Fe distance with different *k*-ranges. The use of multiple scattering EXAFS reproduces many weaker features in the EXAFS (Figure A.3b) that also appear to be above the noise level (Supplementary Figure A.5). Other weak interactions in the EXAFS data, such as the 3.3 Å feature in the S K-edge EXAFS, do not behave in this manner and these are likely due to noise. Similar long-range Fe···Fe interactions have previously been observed in the Fe K-edge EXAFS of aconitase containing a linear $[3Fe\text{-}4S]^{+}$ cluster[28].

Taken together these XAS data indicate that IssA contains a linear $(FeS_2^-)_n$ polymer with two sulfur atoms bridging each pair of Fe(III) ions. Compounds with such a structure are known as thioferrates[29,30]. They have been synthesized intentionally[31] and unintentionally[32] and occur naturally as the mineral erdite[33], however, this is the first time they have been found in a biological system. Thioferrates contain Fe^{3+} and S^{2-} in anionic chains of edge-sharing FeS_4 tetrahedra separated by charge-balancing cations (Figure A.4), and the oxidation states and atomic structure are in agreement with our conclusions for IssA based on XAS. In agreement with this hypothesis, the sulfur K near-edge spectrum of $CsFeS_2$ has been reported[26], and shows a distinctive low-energy peak at 2467.0 eV (allowing for the different energy calibration used by Rose *et al.*[26]). Other mineral forms of iron sulfide are inconsistent with the EXAFS because they would show more than two short-range Fe⋯Fe interactions and would lack the observed long-range 5.4 Å Fe⋯Fe interactions. Moreover, discrete clusters such as the aconitase linear [3Fe-4S] cluster would require protein-based external thiolate donors that are not present in IssA (it contains only one Cys residue/monomer, see below). We therefore conclude that IssA contains polymeric ferric sulfide with a thioferrate-type $(FeS_2^-)_n$ structure. This is also supported by the measured acid-labile iron, sulfide and sulfane sulfur content of IssA (38 Fe, 38 S^{2-} and 17 S^0 atoms/monomer). Degradation of synthetic thioferrates in acid (the conditions used for the assays) has been shown to produce Fe^{2+}, S^{2-} and S^0 in a 2:3:1 ratio[32], which explains the detection of "S^0" in a 1:2 ratio with iron. Since S^0 will also be produced under the acidic conditions of the S^{2-} assay, formation of polysulfides further reduces the amount of sulfur available for detection as H_2S[34].

IssA exhibits a very broad, isotropic-type EPR signal spanning ~3000 Gauss and centered around g ~ 2.2. It is only observable above ~60 K and increases in intensity with increasing temperature (Supplementary Figure A.6). At 60 K, the spectra show weak resonances centered

around *g* values of 4.3 and 2.0, which increase in intensity with decreasing temperature. The *g* = 4.3 signal is indicative of trace amounts of adventitiously-bound high-spin (*S* = 5/2) Fe^{3+} or magnetically isolated linear $[3Fe\text{-}4S]^{+}$ clusters (*S* = 5/2)[4]. The origin of the weak signal in the *g* = 2 region (< 0.01 spin/IssA monomer) is unknown. The anomalous temperature dependence of the very broad isotropic signal is unique among protein-derived EPR signals, but is in agreement with the EPR signal observed for synthetic thioferrates[30,35]. Generally, EPR signals increase in intensity with decreasing temperature, however, the antiferromagnetic coupling between high-spin Fe^{3+} ions in thioferrate polymers results in decreased intensity at temperatures below the Néel temperature[36]. At elevated temperature, thermal disordering of the orientation of electron spins results in increased net magnetization and synthetic thioferrates yield a broad, isotropic EPR signal centered near *g* = 2.[30,35]

***In vitro* IssA-mediated reconstitution of apo-Fd.** To test the hypothesis that IssA functions as a storage protein for Fe and S that can be used for the assembly of iron-sulfur clusters, the ability of IssA to reconstitute the [4Fe-4S] cluster in the apo-form of *P. furiosus* ferredoxin (Fd) was investigated. *P. furiosus* almost exclusively contains [4Fe-4S] cluster-containing Fe-S proteins, and *P. furiosus* Fd is an abundant protein that is used as electron donor for numerous enzymes. Reconstitution experiments were carried out anaerobically under a variety of conditions. IssA with stoichiometric or a two-fold excess of bound Fe and S (as thioferrate) was mixed with apo-Fd at pH 6.8 (the physiological pH for *P. furiosus* growth) and incubated at room temperature for 24 hr or at 80 °C for 1 hr. Since a $[4Fe\text{-}4S]^{2+}$ cluster is more reduced than the all-Fe^{3+} thioferrate iron and sulfide donor, sodium dithionite (E_m~ -420 mV vs NHE) , DTT (E_m ~ -330 mV vs NHE), or tris(2-carboxyethyl) phosphine (TCEP; E_m~ -280 mV vs NHE) were included in the reaction mixture as a reductant, a disulfide-cleaving reagent (DTT and TCEP) and a dithiol-metal chelating

agent (DTT). After centrifugation to remove unreacted IssA, the Fd was purified and the cluster content and integrity were assessed compared with native holo-Fd based on UV-visible absorption and CD spectra quantified based on protein determinations. No reconstitution occurred in the presence of dithionite or TCEP. However, reconstitution of the $[4Fe\text{-}4S]^{2+}$ cluster was observed in the presence of DTT (Figure A.5). Reconstitutions with a two-fold excess of IssA-bound Fe and S resulted in 50±5 % cluster incorporation after incubation with IssA for 24 hr at room temperature. Cluster incorporation was greatly accelerated at more physiologically relevant temperatures, with 45±5 % cluster incorporation after incubation with near stoichiometric IssA Fe and S at 80 °C for 1 hr**.** These results provide *in vitro* evidence that the IssA thioferrate core can provide iron and sulfide for [4Fe-4S] cluster assembly in *P. furiosus.* They also suggest that *in vivo* an as yet unknown thiol(s), that is replaced *in vitro* by DTT, plays a role in disassembling the thioferrate polymer into transferrable pieces by chelating Fe, $[2Fe\text{-}2S]^{2+}$, or linear $[3Fe\text{-}4S]^{1+}$ fragments under reducing conditions that are then assembled into $[4Fe\text{-}4S]^{2+}$ clusters in acceptor proteins such as Fd.

Phylogeny of IssA is distinct from Nif-related families. IssA from *P. furiosus* is composed of 179 amino acids and has a predicted molecular weight of 19 kDa from its gene sequence (PF2025). The N-terminal 109 residues comprise an IPR003731 InterPro globular domain[37] while the C-terminal residues form a tail region that contains the one cysteine residue in the protein. The globular domain has been identified in over 5,000 proteins widely distributed throughout Archaea and Bacteria. These include many hypothetical proteins as well as members of the NifB, NifX and NafY protein families that function in the maturation of the iron-molybdenum-sulfur (Fe-Mo-S) cluster used by nitrogenase. A cladogram of all proteins containing the IPR003731 domain (Figure A.6a) clearly differentiates a NifX clade (84% bootstrap

confidence) and a closely-related NafY clade (100% confidence). NifB proteins, which also contain a radical-SAM domain, form a distinct clade (92% confidence) that is the most distantly related of the Nif proteins to the IssA clade (78% confidence), which is based on the *P. furiosus* protein.

NifB, NifX and NafY all bind complex iron-sulfur clusters and transfer them to other proteins. NifB and NifX bind a precursor (NifB-co)[38] in the biosynthesis of the nitrogenase Fe-Mo-S cluster ($MoFe_7S_9C$)[39], which is bound by NafY. NifB-co is assembled on the IPR003731 domain of NifB with a proposed composition of Fe_8S_9C[40]. NifB proteins contain many highly conserved cysteine residues that bind the Fe-S cluster precursors to NifB-co. However, most IPR003731 domain-containing proteins (2948) contain fewer than the four cysteines required to fully ligate an iron-sulfur cluster (Supplementary Figure A.7). Due to sequence diversity in this large InterPro family, there is little broad amino acid conservation. However, members of the IssA clade contain conserved acidic residues suited to binding the ferric iron necessary for thioferrate synthesis. Thus, we propose that the IPR003731 domain in *P.furiosus* IssA functions as a scaffold for thioferrate assembly and binding, analogous to the role of the homologous NifB domain in NifB-co assembly. Unlike thioferrate, NifB-co likely contains ferrous iron[40,41]. However according to the proposed Fe_6S_9C composition[40], it is likely an anionic iron-sulfur species like thioferrate (overall charge of -2 or -4[40,41]) and may require electrostatic interactions with the protein for stable binding.

The IssA IPR003731 domain binds iron and sulfur. A gene encoding the polyhistidine-tagged globular IPR003731 domain of IssA (residues 1-109) was constructed, expressed in *E. coli,* and purified by affinity chromatography (apo-IssA) to investigate whether the is able to bind iron and sulfide and how this affects oligomerization. When colorless monomeric apo-IssA was

incubated with a 40-fold excess of iron (ferrous ammonium sulfate) and sulfur (sodium sulfide), the black product eluted from a Superose 6 SEC column with molecular weights ranging from ~200 kDa to ~900 kDa with up to 25 Fe per IssA monomer. Hence, the IPR003731 globular domain of IssA clearly binds Fe and S, stimulating oligomerization *in vitro*, although the product is very heterogeneous and it was not characterized further.

Chemical character and conservation of the IssA C-terminus. The C-terminal tail (70 of 179 residues) of *P. furiosus* IssA contains a proline-rich region (9 prolines in 23 amino acids; or 11 in 70) followed by a flexible region comprised predominantly of cationic (7 of 70), aromatic (14 of 70) and glycine (15 of 70) residues. Secondary structure prediction[42] indicates that this tail is unstructured. We propose that this cationic region (the predicted tail pI is 10.7) is involved in binding thioferrate formed by the N-terminal domain. Many members of the IssA clade (Figure A.6a) also have a positively-charged tail region with a high aromatic and glycine content (Supplementary Figure A.7) although the sequence of the tail in the *P. furiosus* protein is highly conserved only in IssA proteins in species within the Thermococcales. Indeed, some members of the IssA clade have a shortened tail (< 70 residues) and some have little or no tail region, which includes the IssA-type protein from *Methanothermobacter thermautotrophicus* that was used to model the structure of the IPR003731 domain of *P. furiosus* IssA (Figure A.6b). In spite of a lack of high sequence conservation in long-tailed IssA members the prevalence of key residues (tryptophan, glycine and arginine) is conserved and a similar repeating pattern is present thereby conserving the chemical character of the C-terminal region of these IssA-like proteins. This is consistent with their proposed role in binding electrostatically to thioferrate, which is negatively charged along its length and does not require ligands with precise positioning. Interestingly, the cladogram reveals another clade of non-themrophilic IssA homologs (termed IssX, Supplementary

Figure A.7) that share key features with IssA including a high pI and a glycine rich tail, although none have yet been characterized.

Discussion

The results presented herein show that IssA is a novel type of protein with a unique role in iron-sulfur metabolism. As indicated by TEM analysis of natively purified protein, it assembles into massive polymeric nanostructures reaching 300 nm in size. XAS analyses indicate that Fe and S are bound to the protein in thioferrate-type linear chains of ferric sulfide (Figure A.3 and A.4). While other large monomeric metalloprotein complexes are known (~12 nm diameter ferritin[43] and a 30-35 nm diameter calcium-binding piscine betanodavirus capsid[44]), IssA forms much larger particles and by far the most iron of any complex known (96,000 in a 300 nm string of 20 nm spheres), though less iron per kDa of protein than ferritin (1.8 Fe/kDa vs 9.6 Fe/kDa respectively)[8]. Treatment of purified IssA with guanidinium, EDTA and DTT in an aerobic environment leads to homogeneous, spherical particles of ~20 nm diameter (Figure A.2b), which may comprise a basic unit of assembly for larger structures observed *in vivo* (Figure A.1a and A.1b) and *in vitro* (Figure A.2a). These treatment conditions are capable of destabilizing protein structure as well as likely degrading thioferrate through chelation of ferric iron by EDTA and removal of sulfide to form DTT persulfide from DTT disulfide. Thus it seems likely that thioferrate is involved in holding these 20 nm units together in the larger nanostructures. A 20 nm sphere would be expected to contain approximately 6,400 Fe atoms and 170 copies of the 19 kDa polypeptide. Ferrihydrite iron, found in ferritin, is accessible to iron removal due to its low crystallinity and high specific area [9]. Similarly, thioferrate iron may be relatively accessible due to its one-dimensional structure, requiring fewer bond scissions for iron removal than three-dimensional minerals.

We have also demonstrated that IssA can provide Fe and S for assembly of $[4Fe\text{-}4S]^{2+}$ clusters in apo-Fd from *P. furiosus* under anaerobic conditions in the presence of DTT (Figure A.5). The mechanism of this process has yet to be determined, but likely involves the ability of DTT (*in vitro*) or a cellular thiol (*in vivo*) to bind Fe^{3+} and/or $[2Fe\text{-}2S]^{2+}$/$[3Fe\text{-}4S]^{1+}$ thioferrate fragments (Figure A.4). For example, DTT is known to ligate Fe^{3+} and Fe^{2+} [45] and the non-cysteinyl-ligated sites of protein-bound $[4Fe\text{-}4S]^{2+}$ clusters[46]. Moreover, a $[2Fe\text{-}2S]^{2+}$ or $[3Fe\text{-}4S]^{+}$ fragment of thioferrate could theoretically be obtained from IssA by simple ligand exchange if appropriately activated (e.g. by reduction), and both clusters can be readily converted to $[4Fe\text{-}4S]^{2+}$ clusters in biological and in synthetic chemistry[47,48]. The conversion of two $[2Fe\text{-}2S]^{2+}$ clusters to generate a $[4Fe\text{-}4S]^{2+}$ cluster occurs via two-electron reductive coupling[47,48], and this reaction is believed to be involved in *de novo* cluster assembly in the ISC system[48,49]. In aconitase and in synthetic chemistry, linear $[3Fe\text{-}4S]^{1+}$ clusters can be converted to a $[4Fe\text{-}4S]^{2+}$ cluster by the addition of Fe^{2+} and one electron[47]. While we have yet to determine the physiological mechanism for Fe-S cluster assembly in *P. furiosus*, the *in vitro* cluster assembly results presented here, coupled with the high Fe and S content of IssA and its iron- and sulfide- dependent expression, strongly support a role for IssA in storing Fe and S that can be used for the biosynthesis of Fe-S clusters. Moreover, the *in vitro* results raise the possibility of spontaneous [4Fe-4S] cluster assembly from $Fe^{3+,2+}$ and S^{2-} on acceptor proteins under Fe and sulfide replete conditions in some strictly anaerobic hyperthermophilic archaea such as *P. furiosus*. Except for SufCBD and two putative SufS cysteine desulfurases, *P. furiosus* does not encode any other known Fe-S cluster assembly protein. Moreover, SufC and SufD contain no cysteine residues and the putative SufB scaffold protein has only two cysteines (compared to 13 in *E. coli* SufB), which are both rigorously

conserved in other SufB proteins. Hence, the scaffolding hypothesis that constitutes the current paradigm for Fe-S cluster assembly[49], may not apply in *P. furiosus* and related organisms.

Because IssA is only produced in *P. furiosus* when the organism is grown in the presence of abundant iron and sulfide, we propose that the thioferrate structure is synthesized directly from these inorganic precursors. The fact that apo-IssA binds Fe and S from inorganic salts also supports this idea. Interestingly, expression of the genes encoding the two cysteine desulfurase homologs in *P. furiosus* (PF0164 and PF1066) are strongly down-regulated (5.1- and 3.2-fold) in response to S^0, while the *sufBD* homologs, which are likely to be involved with some aspect of Fe-S cluster trafficking, are strongly up-regulated along with *issA* when S^0 is present[12]. Thus, sulfide itself rather than cysteine is likely to provide sulfur for Fe-S cluster assembly under conditions of intracellular sulfide production in *P. furiosus*. Consequently, Fe-S clusters synthesized from thioferrate may require less energy than canonical ATP-driven scaffold-assembled Fe-S clusters.

Binding of inorganic Fe and S to IPR003731 domain of apo-IssA suggests that native IssA binds anionic thioferrate $(FeS_2^-)_n$ and that the tail region stabilizes the structure through electrostatic interactions. The 70 amino-acid C-terminal region of IssA contains 7 cationic residues (mostly arginine) that are sufficiently close to each other to preclude a folded structure without a negatively charged counterpart such as thioferrate. In addition, the abundance of glycine residues further indicates a lack of secondary structure in the absence of thioferrate. Hence, we propose a model in which the cationic tail may bind the anionic thioferrate chain by wrapping around thioferrate in perhaps a helical arrangement, which is further stabilized by interactions between the tail's aromatic residues. This interaction would confer a defined structure on the otherwise disordered IssA tail. Since apo-IssA is purified as a monomer, but oligomerizes in the Fe-S bound state, we suggest that formation of the observed ~20 nm spherical IssA particles is

also dependent on association with thioferrate. According to the estimated Fe-protein ratio, additional cations are needed to completely balance the negative charge on thioferrate, and we expect these are provided by loosely bound cations as well as the single zinc ion per protein (Supplementary Table A.1), which may also play a structural role in nanoparticle formation.

Acknowledgements

This research was supported by a grant from the Division of Chemical Sciences, Geosciences and Biosciences, Office of Basic Energy Sciences of the U.S. Department of Energy (DOE; DE-FG05-95ER20175 to M.W.W.A.) We thank Robert M. Glaeser for providing negative stain electron micrographs and John P. Shields for assistance with whole cell electron microscopy. Bioinformatic analysis was conducted using the Georgia Advanced Computing Resource Center, a partnership between the University of Georgia's Office of the Vice President for Research and Office of the Vice President for Information Technology. Work at the University of Saskatchewan was supported by the CRC (G.N.G.), NSERC Canada and CIHR (J.J.H.C is a CIHR-THRUST Associate, M.J.H. held a CIHR PDF award, and is a CIHR-THRUST fellow). SSRL is supported by the U.S. DOE and NIH. EPR and IssA-mediated apo-Fd reconstitution studies were supported by a grant from the National Institutes of Health (GM62524 to M.K.J)

References

1 Johnson, D. C., Dean, D. R., Smith, A. D. & Johnson, M. K. Structure, function, and formation of biological iron-sulfur clusters. *Annu. Rev. Biochem.* **74**, 247-281, (2005).

2 Py, B. & Barras, F. Building Fe–S proteins: bacterial strategies. *Nat. Rev. Microbiol.* **8**, 436-446, (2010).

3 Shakamuri, P., Zhang, B. & Johnson, M. K. Monothiol glutaredoxins function in storing and transporting [Fe_2S_2] clusters assembled on IscU scaffold proteins. *J. Am. Chem. Soc.* **134**, 15213-15216, (2012).

4 Johnson, M. K., Duderstadt, R. E. & Duin, E. C. Biological and synthetic [Fe_3S_4] clusters. *Adv. Inorg. Chem.* **47**, 1-82, (1999).

5 Zhang, B. *et al.* Reversible cycling between cysteine persulfide-ligated [2Fe-2S] and cysteine-ligated [4Fe-4S] clusters in the FNR regulatory protein. *Proc. Natl. Acad. Sci. USA* **109**, 15734-15739, (2012).

6 Lill, R. *et al.* The role of mitochondria in cellular iron–sulfur protein biogenesis and iron metabolism. *BBA-Mol Cell Res* **1823**, 1491-1508, (2012).

7 Raymond, K. N., Allred, B. E. & Sia, A. K. Coordination chemistry of microbial iron transport. *Acc. Chem. Res.* **48**, 2496-2505, (2015).

8 Bradley, J. M., Le Brun, N. E. & Moore, G. R. Ferritins: furnishing proteins with iron. *J. Biol. Inorg. Chem.*, 1-16, (2016).

9 Hiemstra, T. & Van Riemsdijk, W. H. A surface structural model for ferrihydrite I: sites related to primary charge, molar mass, and mass density. *Geochim. Cosmochim. Acta* **73**, 4423-4436, (2009).

10 Fiala, G. & Stetter, K. *Pyrococcus furiosus* sp. nov. represents a novel genus of marine heterotrophic archaebacteria growing optimally at 100°C. *Arch. Microbiol.* **145**, 56-61, (1986).

11 Liu, Y., Sieprawska-Lupa, M., Whitman, W. B. & White, R. H. Cysteine is not the sulfur source for iron-sulfur cluster and methionine biosynthesis in the methanogenic archaeon *Methanococcus maripaludis*. *J. Biol. Chem.* **285**, 31923-31929, (2010).

12 Schut, G. J., Bridger, S. L. & Adams, M. W. W. Insights into the metabolism of elemental sulfur by the hyperthermophilic archaeon *Pyrococcus furiosus*: characterization of a coenzyme A-dependent NAD(P)H sulfur oxidoreductase. *J. Bacteriol.* **189**, 4431-4441, (2007).

13 Schut, G. J., Zhou, J. & Adams, M. W. W. DNA microarray analysis of the hyperthermophilic archaeon *Pyrococcus furiosus*: evidence for a new type of sulfur-reducing enzyme complex. *J. Bacteriol.* **183**, 7027-7036, (2001).

14 Clarkson, S. M., Newcomer, E. C., Young, E. G. & Adams, M. W. W. The elemental sulfur-responsive protein (SipA) from the hyperthermophilic archaeon *Pyrococcus furiosus* is regulated by sulfide in an iron-dependent manner. *J. Bacteriol.* **192**, 5841-5843, (2010).

15 Adams, M. W. W. *et al.* Key role for sulfur in peptide metabolism and in regulation of three hydrogenases in the hyperthermophilic archaeon *Pyrococcus furiosus*. *J. Bacteriol.* **183**, 716-724, (2001).

16 Smith, P. K. *et al.* Measurement of protein using bicinchoninic acid. *Anal. Biochem.* **150**, 76-85, (1985).

17 Cvetkovic, A. *et al.* Microbial metalloproteomes are largely uncharacterized. *Nature* **466**, 779-782, (2010).

18 Lovenberg, W., Buchanan, B. B. & Rabinowitz, J. C. Studies on the chemical nature of clostridial ferredoxin. *J. Biol. Chem.* **238**, 3899-3913, (1963).

19 Schauder, R. & Müller, E. Polysulfide as a possible substrate for sulfur-reducing bacteria. *Arch. Microbiol.* **160**, 377-382, (1993).

20 Tang, G. *et al.* EMAN2: an extensible image processing suite for electron microscopy. *J. Struct. Biol.* **157**, 38-46, (2007).

21 George, G. N., Garrett, R. M., Prince, R. C. & Rajagopalan, K. V. The molybdenum site of sulfite oxidase: A comparison of wild-type and the cysteine 207 to serine mutant using X-ray absorption spectroscopy. *J. Am. Chem. Soc.* **118**, 8588-8592, (1996).

22 George, G. N. *EXAFSPAK*, <http://ssrl.slac.stanford.edu/exafspak.html> (2001).

23 Rehr, J. J. & Albers, R. C. Theoretical approaches to X-ray absorption fine structure. *Rev. Mod. Phys.* **72**, 621-654, (2000).

24 Moulis, J. M. & Meyer, J. Characterization of the selenium-substituted 2[4Fe-4Se] ferredoxin from *Clostridium pasteurianum*. *Biochemistry* **21**, 4762-4771, (1982).

25 Anxolabéhère-Mallart, E. *et al.* Sulfur K-edge X-ray absorption spectroscopy of 2Fe−2S ferredoxin: covalency of the oxidized and reduced 2Fe forms and comparison to model complexes. *J. Am. Chem. Soc.* **123**, 5444-5452, (2001).

26 Rose, K. *et al.* Investigation of the electronic structure of 2Fe−2S model complexes and the Rieske protein using ligand K-edge X-ray absorption spectroscopy. *J. Am. Chem. Soc.* **121**, 2353-2363, (1999).

27 Dey, A. *et al.* Ligand K-edge X-ray absorption spectroscopy and DFT calculations on $[Fe_3S_4]^{0,+}$ clusters: delocalization, redox, and effect of the protein environment. *J. Am. Chem. Soc.* **126**, 16868-16878, (2004).

28 Gailer, J. *et al.* Human cytosolic iron regulatory protein 1 contains a linear iron−sulfur cluster. *J. Am. Chem. Soc.* **123**, 10121-10122, (2001).

29 Bronger, W., Kyas, A. & Müller, P. The antiferromagnetic structures of $KFeS_2$, $RbFeS_2$, $KFeSe_2$, and $RbFeSe_2$ and the correlation between magnetic moments and crystal field calculations. *J. Solid State Chem.* **70**, 262-270, (1987).

30 Seidov, Z. *et al.* Magnetic susceptibility and ESR study of the covalent-chain antiferromagnets $TlFeS_2$ and $TlFeSe_2$. *Phys. Rev. B* **65**, 014433, (2001).

31 Al-Ahmad, S. A., Kampf, J. W., Dunham, R. W. & Coucouvanis, D. Oxidation by elemental sulfur and coupling of iron/sulfur complexes. Synthesis and structural characterization of $(Et_4N)_4[Fe_4S_6(SEt)_4]$, a new Fe/S cluster with a linear Fe_4 backbone. *Inorg. Chem.* **30**, 1163-1164, (1991).

32 Taylor, P. & Shoesmith, D. W. The nature of green alkaline iron sulfide solutions and the preparation of sodium iron (III) sulfide, $NaFeS_2$. *Can. J. Chem.* **56**, 2797-2802, (1978).

33 Konnert, J. & Evans, H. The crystal structure of erdite, $NaFeS_2 \cdot 2H_2O$. *Am. Mineral.* **65**, 516-521, (1980).

34 Steudel, R. in *Elemental Sulfur und Sulfur-Rich Compounds II* (ed Ralf Steudel) 127-152 (Springer Berlin Heidelberg, 2003).

35 Sweeney, W. V. & Coffman, R. E. Magnetic properties of potassium dithioferrate: a linear chain antiferromagnet and model compound for the exchange interactions in two-iron ferredoxins. *Biochim. Biophys. Acta* **286**, 26-35, (1972).

36 Souza, A. M. C., Oliveira Neto, S. R. & Macedo, C. A. Magnetic behavior of the $KFeS_2$. *J. Magn. Magn. Mater.* **272–276, Part 1**, 521-522, (2004).

37 Mitchell, A. *et al.* The InterPro protein families database: the classification resource after 15 years. *Nucleic Acids Res.* **43**, D213-221, (2015).

38 Hernandez, J. A. *et al.* NifX and NifEN exchange NifB cofactor and the VK-cluster, a newly isolated intermediate of the iron-molybdenum cofactor biosynthetic pathway. *Mol. Microbiol.* **63**, 177-192, (2007).

39 Lancaster, K. M. *et al.* X-ray emission spectroscopy evidences a central carbon in the nitrogenase iron-molybdenum cofactor. *Science* **334**, 974-977, (2011).

40 Guo, Y. *et al.* The nitrogenase FeMo-cofactor precursor formed by NifB protein: a diamagnetic cluster containing eight iron atoms. *Angew. Chem. Int. Ed.* **55**, 12764-12767, (2016).

41 Kowalska, J. & DeBeer, S. The role of X-ray spectroscopy in understanding the geometric and electronic structure of nitrogenase. *BBA-Mol Cell Res* **1853**, 1406-1415, (2015).

42 Drozdetskiy, A., Cole, C., Procter, J. & Barton, G. J. JPred4: a protein secondary structure prediction server. *Nucleic Acids Res.*, (2015).

43 Khare, G. *et al.* Ferritin structure from *Mycobacterium tuberculosis*: Comparative study with homologues identifies extended C-terminus involved in ferroxidase activity. *PLoS One* **6**, e18570, (2011).

44 Chen, N.-C. *et al.* Crystal structures of a piscine betanodavirus: mechanisms of capsid assembly and viral infection. *PLoS Pathog.* **11**, e1005203, (2015).

45 Mapolelo, D. T., Zhang, B., Naik, S. G., Huynh, B. H. & Johnson, M. K. Spectroscopic and functional characterization of iron-bound forms of *Azotobacter vinelandii* ^{Nif}IscA. *Biochemistry* **51**, 8056-8070, (2012).

46 Hanzelmann, P. & Schindelin, H. Crystal structure of the S-adenosylmethionine-dependent enzyme MoaA and its implications for molybdenum cofactor deficiency in humans. *Proc. Natl. Acad. Sci. USA* **101**, 12870-12875, (2004).

47 Beinert, H., Holm, R. H. & Münck, E. Iron-sulfur clusters: nature's modular, multipurpose structures. *Science* **277**, 653-659, (1997).

48 Chandramouli, K. *et al.* Formation and properties of [4Fe-4S] clusters on the IscU scaffold protein. *Biochemistry* **46**, 6804-6811, (2007).

49 Agar, J. N. *et al.* IscU as a scaffold for iron−sulfur cluster biosynthesis: sequential assembly of [2Fe-2S] and [4Fe-4S] clusters in IscU. *Biochemistry* **39**, 7856-7862, (2000).

Figure A.1. Electron micrographs showing IssA assemblies *in vivo*. (a) The area of IssA localization (immunolabelled with gold nanoparticles) increases over time after addition of S^0 to a growing culture of *P. furiosus* (scale bars are 200 nm). (b) Cells grown using a S^0 electron acceptor exhibit native electron-dense regions that overlap with immunolabelled IssA (scale bar is 200 nm).

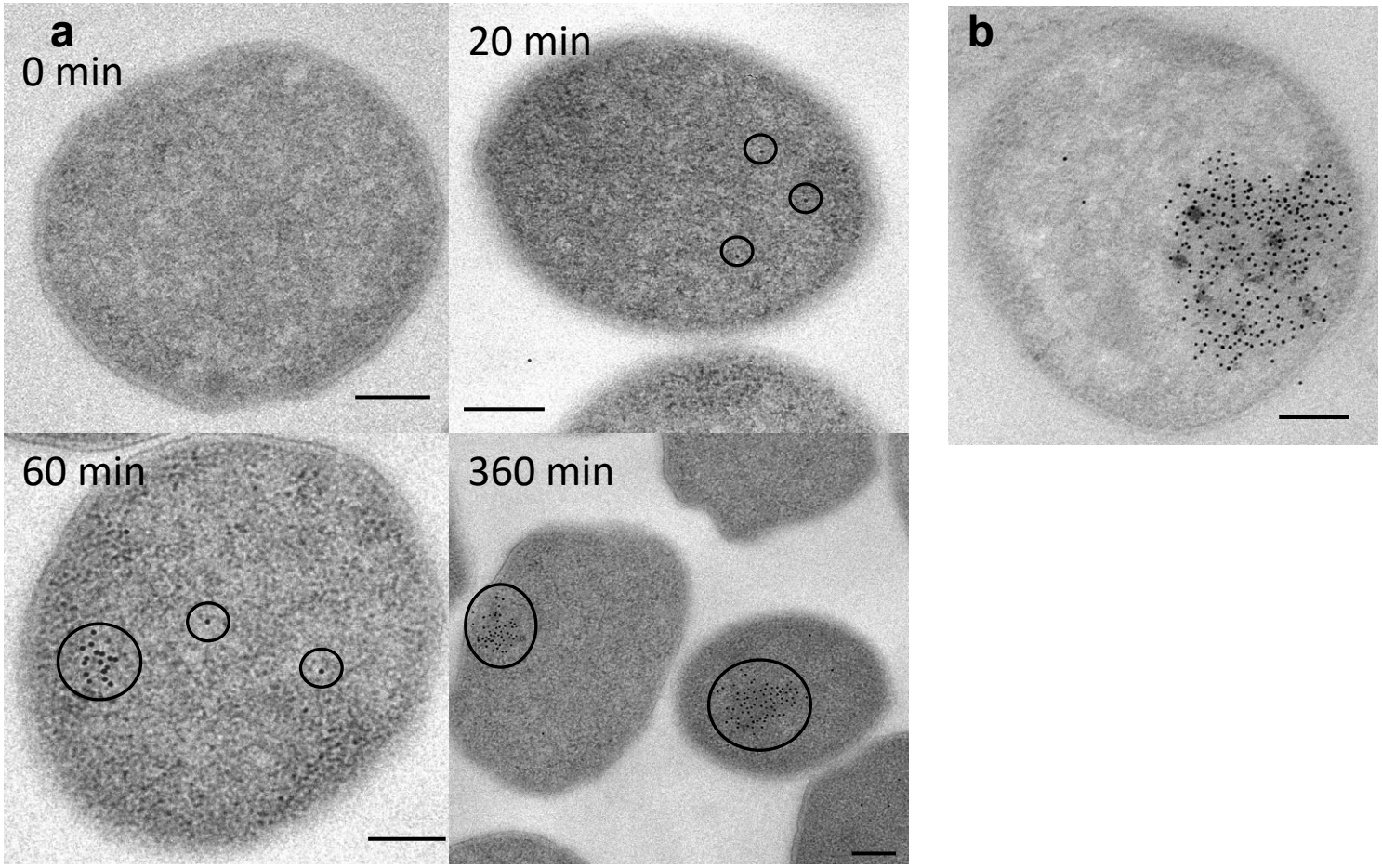
a
0 min
20 min
60 min
360 min
b

Figure A.2. Electron micrographs showing IssA assemblies *in vitro*. (a) IssA is purified as nanoparticles of 20–300 nm as shown by negative stain TEM (scale bar is 50 nm). (b) Magnified region of a to match scale of c. (c) Treatment of IssA with guanidinium, EDTA and DTT yields a more uniform size distribution of 16–22 nm (scale bar is 50 nm). (d) Individual particles from **c** at higher magnification (scale bar is 25 nm).

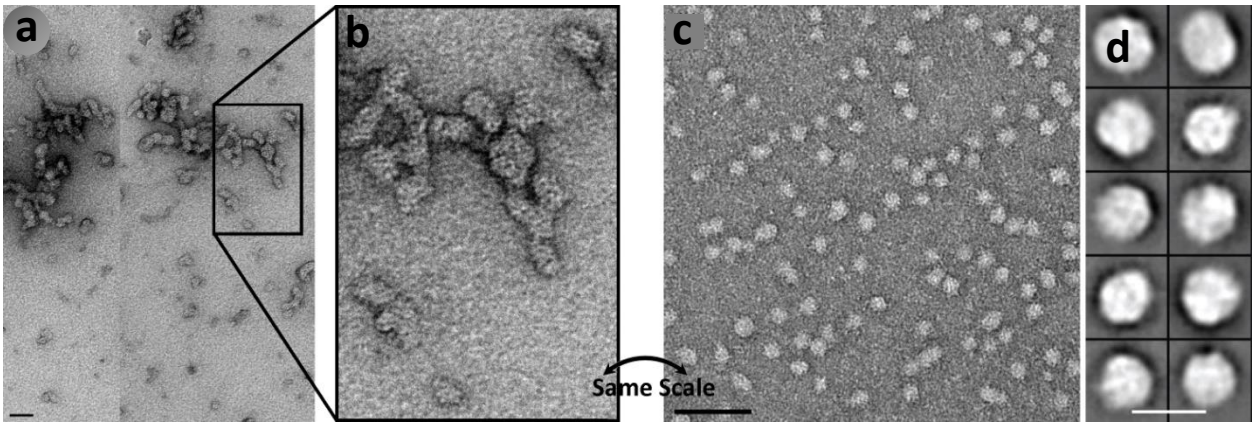
a
b
c
d
Same Scale

Figure A.3. IssA X-ray absorption spectra. (a) X-ray absorption near-edge spectra of IssA compared with a number of Fe–S proteins; a: IssA, b: linear 3Fe-4S cluster in human aconitase, c: P. furiosus 3Fe-4S ferredoxin and d: P. furiosus rubredoxin. The feature marked (*) in the IssA spectrum is due to a trace amount of sulfonate buffer. For both the S and Fe K-edge data, the IssA spectrum most resembles that of the linear 3Fe-4S cluster. (b) S and Fe K-edge EXAFS spectra, together with EXAFS Fourier transforms (S–Fe and Fe–S phase-corrected, respectively) showing experimental data (blue lines) together with best fits (red lines), the inset in the Fourier transform figure shows the structure used to compute the multiple scattering EXAFS. Best fits were computed with two S–Fe at 2.239(3) Å, σ2=0.0049(3) Å2 and four Fe–S at 2.243(1) Å, σ2=0.0044(1) Å2, two Fe···Fe at 2.704(1) Å, σ2=0.0032(1) Å2 and two Fe···Fe at 5.408 Å and σ2=0.0064 Å2.

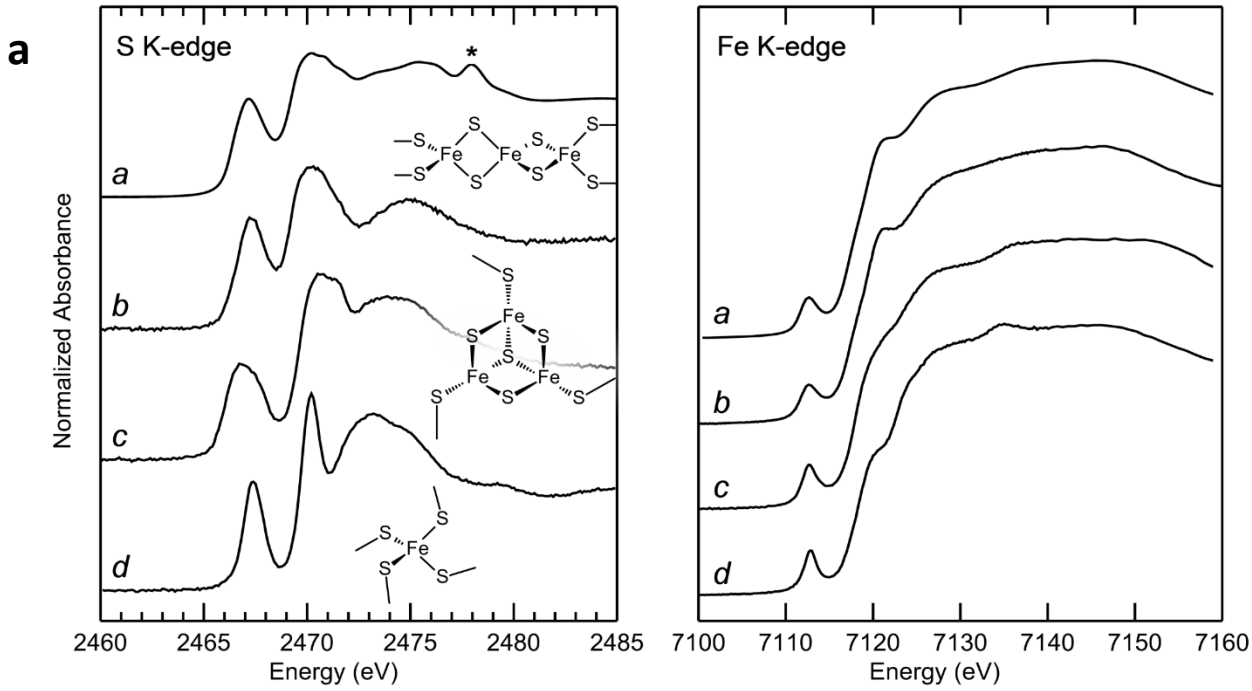
a
S K-edge
*
a
b
c
d
Normalized Absorbance
2460
2465
2470
2475
2480
2485
Energy (eV)
Fe K-edge
a
b
c
d
7100
7110
7120
7130
7140
7150
7160
Energy (eV)

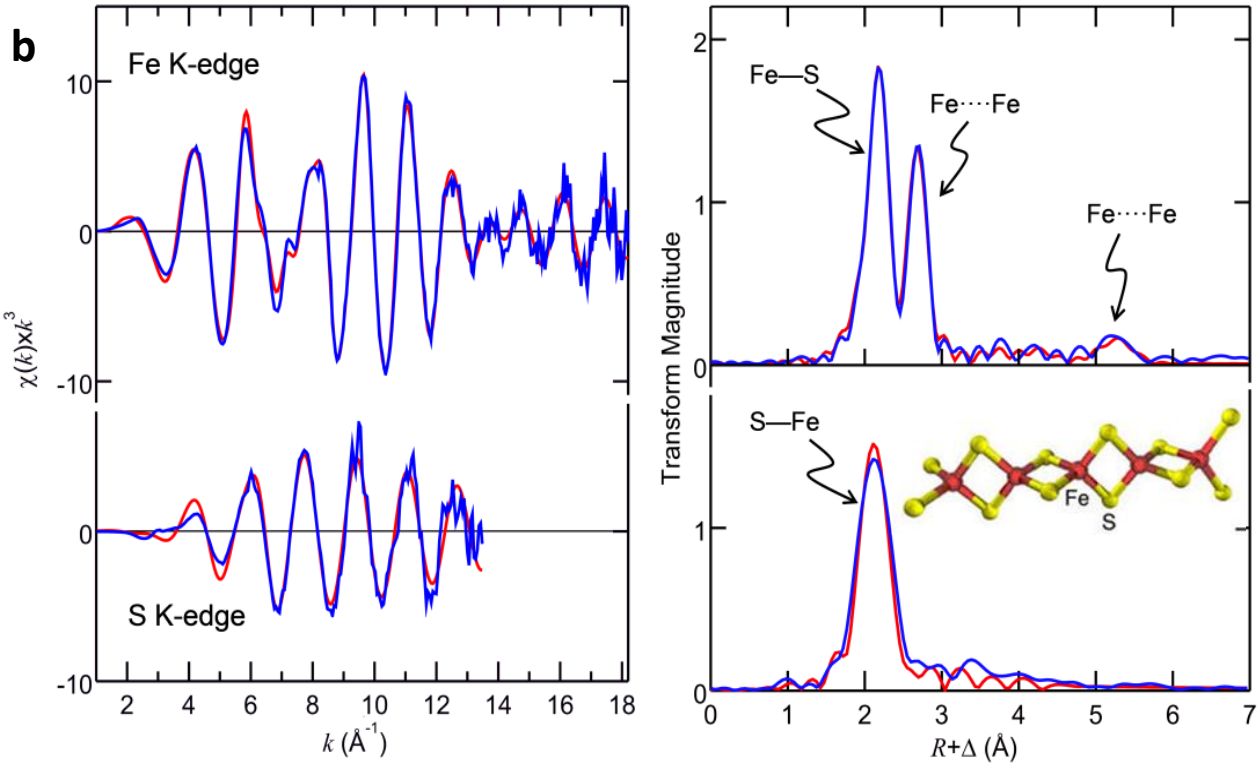
b
Fe K-edge
S K-edge
10
0
-10
0
-10
2
4
6
8
10
12
14
16
18
k (Å-1)
χ(k)×k3
Fe—S
Fe····Fe
Fe····Fe
S—Fe
Fe
S
2
1
0
1
0
0
1
2
3
4
5
6
7
R+Δ (Å)
Transform Magnitude

Figure A.4. Thioferrate structure. (a) Inorganic potassium thioferrate ($KFeS_2$) supercell of the crystal structure using three times the crystallographic *c* axis. Potassium is shown as purple spheres, iron as red spheres and sulfur as yellow spheres. Sections of five linear FeS_2 chains are visible. (b) A five Fe section of a single thioferrate chain, the proposed Fe–S component of IssA.

a

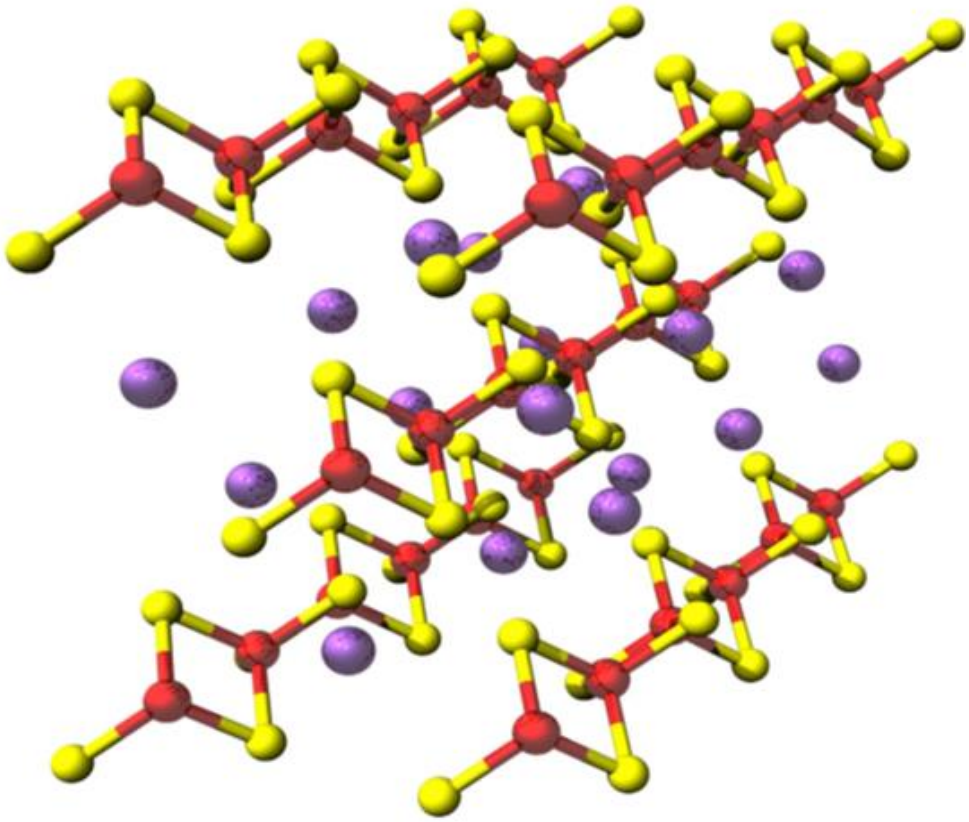

b

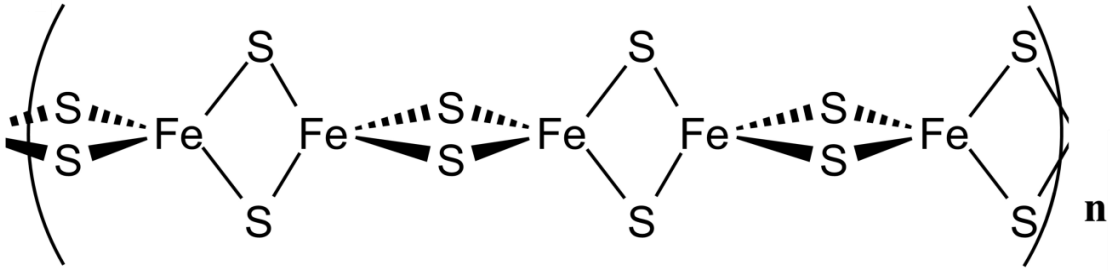

Figure A.5. IssA-mediated reconstitution of a $[4Fe\text{-}4S]^{2+}$ cluster. Reference UV-visible and CD spectra for holo- and apo- forms of *P. furiosis* Fd are shown by black and magenta lines, respectively. Repurified Fd products of IssA-mediated reconstitution of apo-Fd in the presence of DTT are shown in red (room temperature for 24 hours) and blue (80 °C for 1 hour).

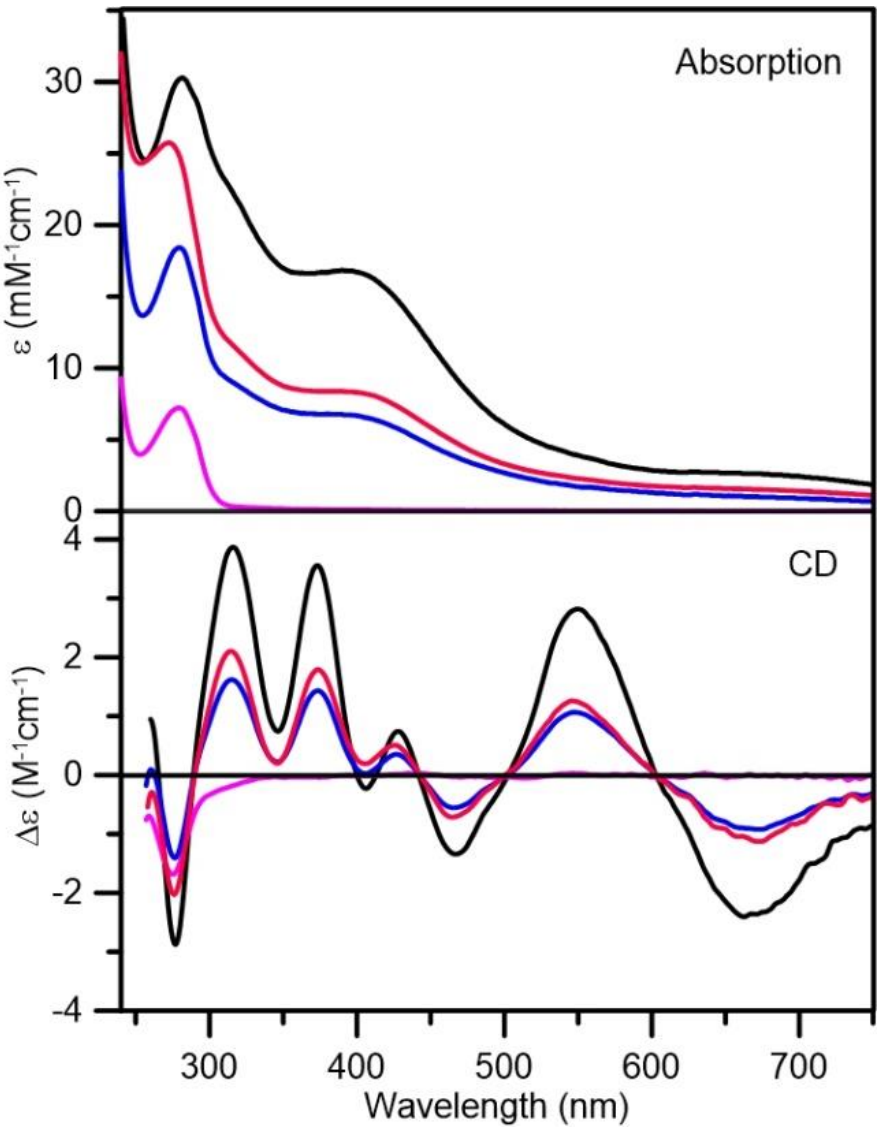
Absorption
CD
ε (mM-1cm-1)
Δε (M-1cm-1)
Wavelength (nm)
30
20
10
0
4
2
0
-2
-4
300
400
500
600
700

Figure A.6. IssA bioinformatic analysis. (a) Cladograms of proteins containing the IPR003731 domain. Coloured clades contain members of the NifB (IPR005980, blue), NifX (IPR013480, turquoise) and NafY (IPR031763, purple) InterPro protein families. The proposed IssA clade (red) is based on predicted protein isoelectric point (pI) and occurrence of proteins with a glycine rich region at the C-terminus. *P. furiosus* IssA and the homologue from *Methanothermobacter thermautotrophicus* (MTH1175) are shown by red and yellow arrowheads respectively. (b) Modelled structure of the IssA IPR003731 domain based on the NMR structure of MTH1175 (red). The C-terminal region is shown unstructured, as predicted for the apo-form.

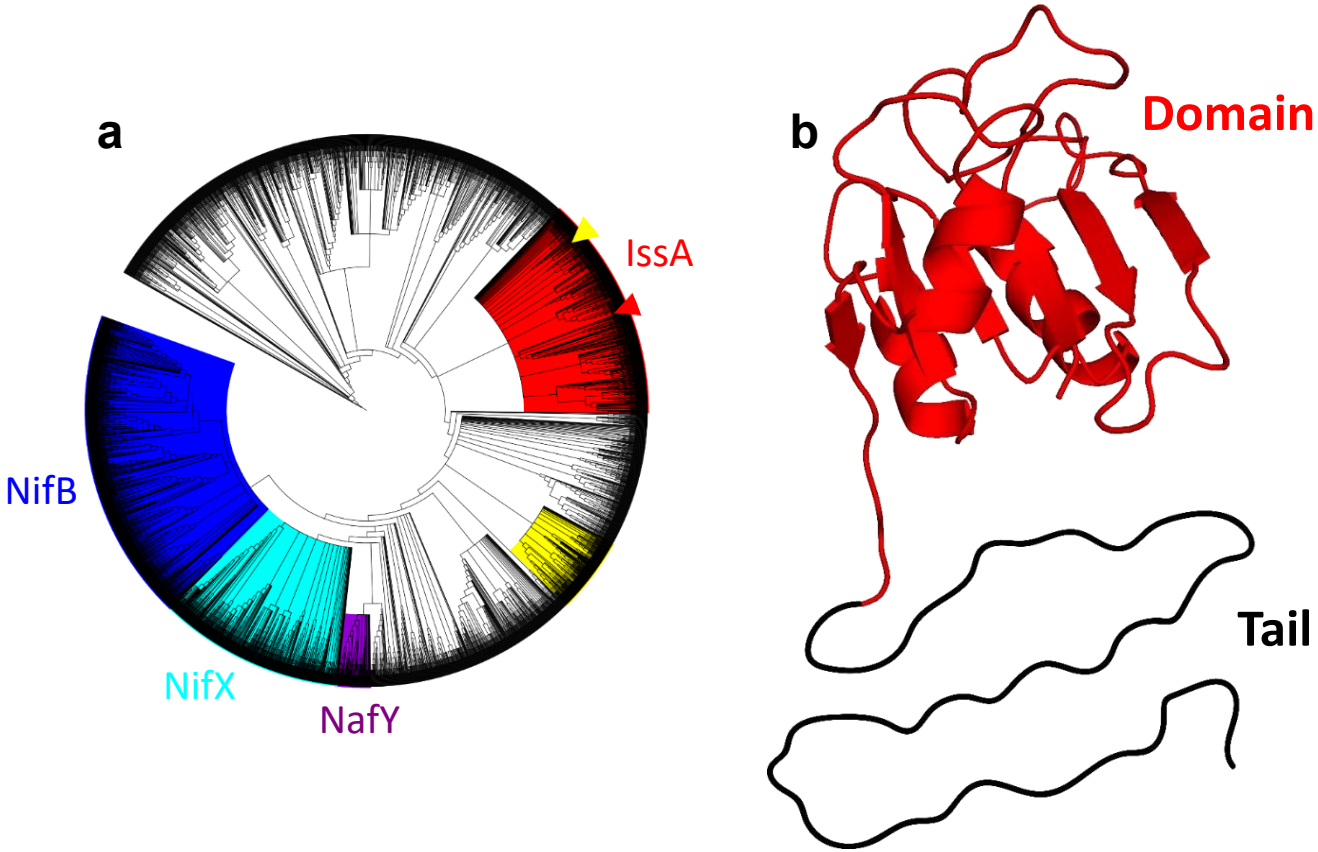
a
IssA
NifB
NifX
NafY
b
Domain
Tail

Supplementary Methods

XAS data acquisition and analysis. Iron K-edge XAS data were collected on solutions of IssA in 50 mM Tris buffer in the presence of 30% glycerol, frozen in 1 mm × 3 mm × 23 mm acrylic sample cuvettes closed with metal free kapton adhesive tape. Data were collected using the Stanford Synchrotron Radiation Lightsource (SSRL) structural molecular biology XAS beamline 7-3, employing a Si(220) double-crystal monochromator with harmonic rejection by setting the collimating mirror cut-off to 9 keV. Incident and transmitted X-ray intensities were monitored using N_2-filled gas ionization chambers with a sweeping voltage of 1.8 kV, and X-ray absorption was measured as the iron $K_{\alpha 12}$ fluorescence excitation spectrum using an array of 30 germanium detectors equipped with a manganese filter and a Soller slit assembly. During data collection, samples were maintained at a temperature of approximately 10 K using an Oxford instruments liquid helium flow cryostat. For each iron K-edge data set, eight scans each of 40 min. duration were accumulated, and the energy was calibrated by reference to the absorption of a metallic iron foil measured simultaneously with each scan, assuming a lowest energy K- edge inflection point of 7,111.3 eV. The energy threshold of the extended X-ray absorption fine structure (EXAFS) oscillations (k = 0 Å^{-1}) was assumed to be 7130.0 eV. Data were collected over the extended k-range to a maximum k of 18.2 Å^{-1}, in order to obtain the best resolution.

Sulfur K-edge XAS data were collected on frozen solutions using an Oxford Instruments helium cryostream apparatus at 20 K, yielding an estimated sample temperature of 20-50 K. The presence of the chlorine K-edge at 2,833 eV meant that the sample needed to be prepared in the absence of added chloride and sulfonate based buffers, and samples were contained in acrylic cuvettes closed with 6 μm thick polypropylene windows to minimize attenuation of the X-ray beam. Sulfur K-edge XAS data were collected on SSRL beamline 4-3, using a Si(111)

monochromator and rejection of Si(333) and higher harmonics was achieved by setting the angle of the upstream vertically collimating mirror to give a high energy cutoff of ~5 keV. The incident X-ray intensity was measured with a helium filled gas ionization chamber with a sweeping voltage of 1 kV, and total fluorescence was measured by using a nitrogen-filled Stern-Heald-Lytle fluorescence ion chamber detector (The EXAFS Co., Pioche NV, USA). The incident X-ray energy was calibrated by reference to the lowest K-edge energy peak of a sodium thiosulfate ($Na_2S_2O_3$) standard, assuming a peak energy of 2,469.2 eV as previously described[1]. The energy threshold of the extended X-ray absorption fine structure (EXAFS) oscillations (k = 0 $Å^{-1}$) was assumed to be 2,475.0 eV. The high X-ray cross sections at the low X-ray energies of the sulfur K-edge mean that samples in such experiments are particularly prone to radiation damage[2]. The near-edge portion of the spectrum was monitored for changes indicative of radiation damage and only small changes were observed (Supplementary Figure 8). Sixteen scans each of 30 minutes duration from three different samples were averaged to obtain a final data set, with careful screening of data to remove scans with irreproducible features with a maximum number of 8 scans per sample. Sulfur K-edge EXAFS data were collected to a maximum k of 13.5 $Å^{-1}$ because of truncation due to the presence of residual atmospheric argon which has a K-absorption edge at 3,205.9 eV. For both iron and sulfur K-edge data the program XAS collect was used to collect data[3].

Expression and purification of the apo-IssA construct using *E. coli.* The gene encoding IssA (PF2025) was amplified by PCR using *Pyrococcus furiosus* DSM 3638 genomic DNA isolated by ZymoBead Genomic DNA Kit (Zymo Research) and a set of primers, sense (5'-GGGCATATGAAGATAGCGATCCCAACTAATGGAGGAGG-3') and anti-sense (5-GGGCTCGAGAGTTGCTACTTTAATTGCCTCTTCAACTGGAG-3'). Nde I and Xho I restriction enzyme sites were designed on the sense and anti-sense primers, respectively. The N-

terminal 107 residues of PF2025 were amplified in order to remove the IssA tail in the recombinant form. The amplified DNA fragment and pET-24a(+) vector (Novagen) were digested by Nde I and Xho I and ligated by T4 DNA ligase (New England Biolabs). The assembled plasmid was transformed into XL1-blue E. coli competent cells for sequence confirmation. The plasmid was then transformed into the BL21-CodonPlus (DE3)-RIPL strain (Agilent Technologies) for protein expression. The *E. coli* transformant was grown at 37°C in 2xYT medium with 20 μg/ml chloramphenicol and 50 μg/ml kanamycin to an OD_{600} of 0.6-0.8. The protein expression was induced with 300 μM IPTG and switched to 25°C for 16 to 18 hours. Cells were harvested by centrifugation at 10,000 x *g* for 10 minutes and resuspended in 50 mM Tris, 300 mM NaCl, 2 mM DTT, pH 8.0 (buffer A) and complete protease inhibitor (Roche) at a ratio of 1 g wet cell wt. to 3 ml buffer. All the purification steps were carried out under anaerobic condition. Cells were lysed by 0.5 mg/ml lysozyme with stirring for 1 hour at room temperature. The mixture was frozen at -20°C overnight and thawed at room temperature for 2 hours. DNase I (0.002%, Sigma) was then added and stirred for 1 hour. After centrifugation at 7,500 rpm for 10 minutes to remove cell debris and insoluble material, the supernatant was collected and applied to a column containing Ni Sepharose 6 Fast Flow (GE Healthcare Life Sciences), which was equilibrated with buffer A. The column was washed with buffer A and the adsorbed protein was eluted with 500 mM imidazole in buffer A. Protein purity was examined by SDS-PAGE.

Phylogenetic analysis and structural model. Metagenomic sequences and identical (duplicate) sequences were removed from the 5041 sequences containing the IPR003731 domain, and the resulting 4630 sequences were aligned using Clustal Omega, version 1.2.1, with the default parameters[4]. TrimAl[5] was used to remove multiple alignment positions with greater than 99.78% gaps (i.e. 10 or fewer sequences had sequence content at that position), and the resulting alignment

was used to construct a maximum likelihood phylogenetic tree using IQ-Tree[6] (version 1.5.3). The IQ-Tree standard model selection test was used to automatically determine the best-fit model (WAG+G4: general amino acid matrix with a discrete Gamma model). This model tree was refined using ultrafast bootstrap approximation (UFBoot) and Shimodaira–Hasegawa-like approximate likelihood ratio tests with 1000 bootstrap replicates for each. iTol[7] was used for analysis and display of the phylogenetic tree. For visualization and clade selection, branch lengths were not used (e.g. cladogram) and branches with bootstrap confidence values less than 70% were removed. The COPid[8,9] server was used for amino acid analysis and pI was calculated with a custom program based on the ExPASy Compute pI/Mw algorithm[8,9]. The Phyre 2.0[10] server was used to thread model the IssA sequence on the homologous *M. thermautotrophicus* structure (PDB ID 1EO1).

Supplementary References

1 Pickering, I. J., Prince, R. C., Divers, T. & George, G. N. Sulfur K-edge X-ray absorption spectroscopy for determining the chemical speciation of sulfur in biological systems. *FEBS Lett.* **441**, 11-14, (1998).

2 George, G. N. *et al.* X-ray-induced photo-chemistry and X-ray absorption spectroscopy of biological samples. *J. Synchrotron Radiat.* **19**, 875-886, (2012).

3 George, M. XAS-Collect: a computer program for X-ray absorption spectroscopic data acquisition. *J. Synchrotron Radiat.* **7**, 283-286, (2000).

4 Sievers, F. *et al.* Fast, scalable generation of high-quality protein multiple sequence alignments using Clustal Omega. *Mol. Syst. Biol.* **7**, (2011).

5 Capella-Gutiérrez, S., Silla-Martínez, J. M. & Gabaldón, T. trimAl: A tool for automated alignment trimming in large-scale phylogenetic analyses. *Bioinformatics* **25**, 1972-1973, (2009).

6 Minh, B. Q., Nguyen, M. A. T. & von Haeseler, A. Ultrafast Approximation for Phylogenetic Bootstrap. *Mol. Biol. Evol.* **30**, 1188-1195, (2013).

7 Letunic, I. & Bork, P. Interactive Tree Of Life v2: Online annotation and display of phylogenetic trees made easy. *Nucleic Acids Res.* **39**, W475-478, (2011).

8 Gasteiger, E. *et al.* in *The Proteomics Protocols Handbook* (ed John M. Walker) 571-607 (Humana Press, 2005).

9 Bjellqvist, B. *et al.* The focusing positions of polypeptides in immobilized pH gradients can be predicted from their amino acid sequences. *Electrophoresis* **14**, 1023-1031, (1993).

10 Kelley, L. A., Mezulis, S., Yates, C. M., Wass, M. N. & Sternberg, M. J. E. The Phyre2 web portal for protein modeling, prediction and analysis. *Nat. Protocols* **10**, 845-858, (2015).

Supplementary Table A.1. Analysis of IssA immunoprecipitate for additional binding proteins. The top twenty protein hits are shown from the resulting peptide masses after analysis using MASCOT software, searching a *Pyrococcus furiosus*-specific database, and allowing for 2 missed cleavages and a mass difference of ± 0.4 Da. An expectation value of 0.05 or less is significant; significant expectation values are highlighted in bold.

All peptides queried (19)

PF number	ORF number	InterPro name	MW (Da)	Expect value	Peptide matches	Percent coverage
PF2025	18978397	**IssA**	18990	**0.0047**	5	27.9
PF1027	18977399	putative RNA methylase	43494	3.9	6	16.1
PF0938	18977310	aconitase/3-isopropylmalate dehydratase large subunit	46181	4.6	4	15.3
PF0193	18976565	ABC transporter-like	35846	5.4	3	21.6
PF0738	18977110	methyltransferase type 11	21023	7.7	4	18.2
PF1604	18977976	cystathionine beta-synthase, core	17979	7.9	3	25.2
PF0920	18977292	metal-dependent phosphohydrolase, HD region	25773	9.7	3	15.7
PF1095	18977467	NULL	11453	12	2	37.9
PF1612	18977984	NULL	9806	12	2	39.5
PF1459	18977831	L-fucose isomerase-like	54272	14	4	8.5
PF1335	18977707	hydroxyethylthiazole kinase	28309	15	3	15.1
PF1379	18977751	probable translation factor pelota	40482	15	4	16.6
PF0209	18976581	lysine biosynthesis enzyme LysX	30991	15	3	12.1
PF0236	18976608	phosphoribosyl pyrophosphokinase	30928	16	3	14.7
PF1807	18978179	ribosomal protein L32e	15525	19	2	28.5
PF1128	18977500	CRISPR-associated protein, TM1793	36293	22	3	18
PF2015	18978387	DNA/RNA helicase, C-terminal	86885	24	6	11
PF0475	18976847	initiation factor 2B related	31078	31	3	13
PF1896	18978268	NULL	28483	31	3	9.5
PF1345	18977717	ribonuclease Z	35105	35	3	16

Supplementary Table A.2. Elemental composition of IssA purified from *Pyrococcus furiosus*. Values are from ICP-MS data and are expressed as mole atom/mole IssA monomer, assuming pure IssA. Shown are the metals out of fifty-five measured by ICP-MS that gave values ≥ 0.1. Error bars indicate standard deviation of two independent ICP-MS runs.

Element	**Atoms per IssA monomer**
Fe	38.73 ± 3.60
Zn	1.33 ± 0.13
Cu	0.68 ± 0.06
Mg	0.24 ± 0.08
Co	0.14 ± 0.01

Supplementary Figure A.1. Western blot analysis of whole cell extract from *P. furiosus* grown on maltose medium after S^0 addition at mid-log phase. Lanes are 0, 10, 20, 30, 60, 120, 180, 240, 300, and 360 minutes after S^0 addition. (a) IssA antibody, (b) SOR antibody as a loading control. M: protein standard marker.

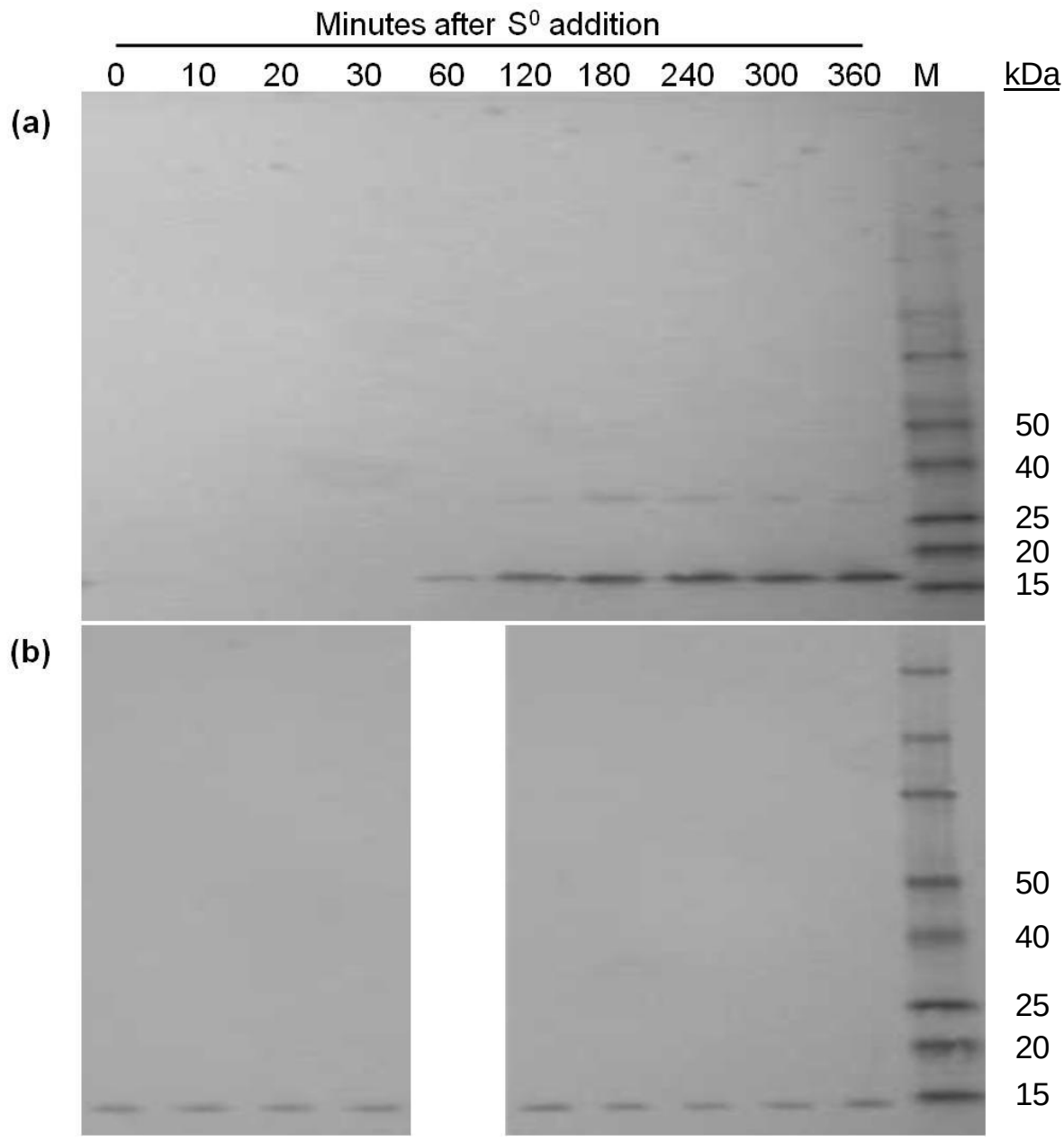
Minutes after S0 addition
0
10
20
30
60
120
180
240
300
360
M
kDa
(a)
50
40
25
20
15
(b)
50
40
25
20
15

Supplementary Figure A.2. Energy dispersive X-ray analysis of an electron dense particle associated with IssA. Element names are noted; nickel and copper are from the support grid and uranium was used to stain the cells. Arrows indicate the Kα energies of S at 2.47 keV and Fe at 7.11 keV.

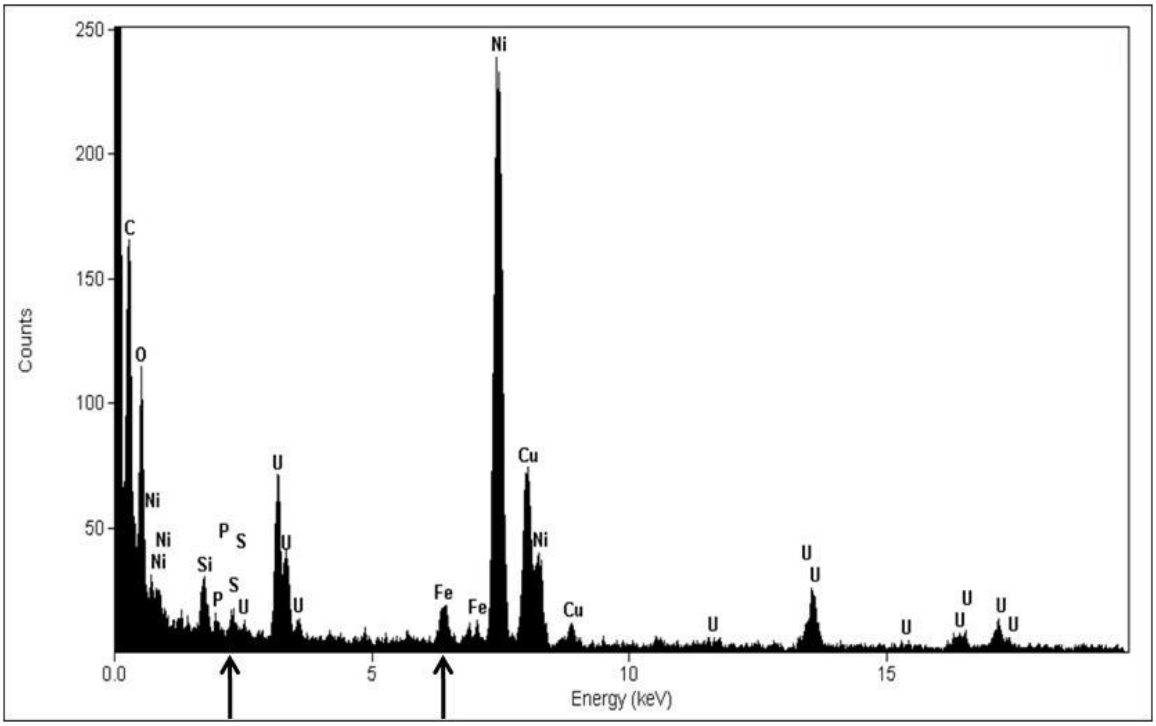
Counts
250
200
150
100
50
0.0
5
10
15
Energy (keV)
C
O
Ni
Ni
Ni
Si
P
S
P
S
U
U
U
Fe
Fe
Ni
Cu
Ni
Cu
U
U
U
U
U
U
U
U

Supplementary Figure A.3. IssA purification from *Pyrococcus furiosus*. (a) SDS-PAGE gel showing IssA purification from cells grown on maltose with 2 g/L S^0; IssA runs at approximately 17 kDa and was confirmed by MALDI-TOF mass spectrometry. M: protein size markers (Invitrogen); lane 1: whole cell extract; lane 2-3: 100,000x*g* supernatant, pellet; lane 4-5: 1% SDS-treated supernatant, pellet; lane 6-7: first wash supernatant, pellet; lane 8-9: second wash supernatant, pellet; lane 10: final IssA sample after CsCl gradient and concentration. (b) Purified IssA is black in color.

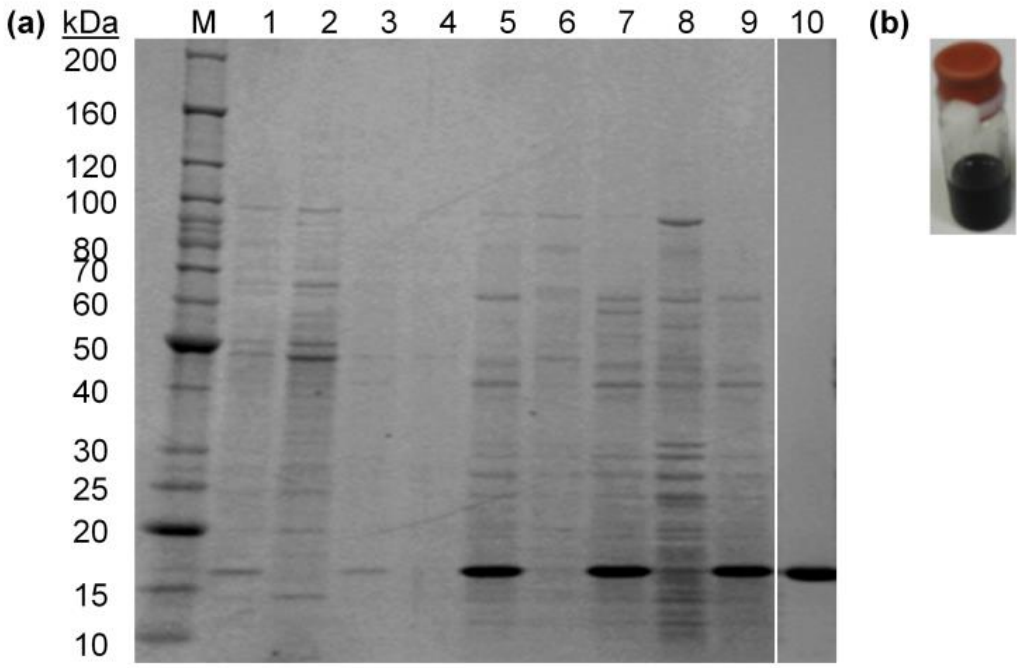
(a)
kDa
M
1
2
3
4
5
6
7
8
9
10
200
160
120
100
80
70
60
50
40
30
25
20
15
10
(b)

Supplementary Figure A.4. IssA molecular weight determination by size exclusion chromatography. The molecular weight of IssA was estimated using analytical column chromatography (Sephacryl S-1000 SF) pre-equilibrated with 50 mM TrisHCl (pH 8.0), 300 mM NaCl, 1 mM DTT. Native IssA from *P. furiosus* eluted near the exclusion limit (100 MDa dextran).

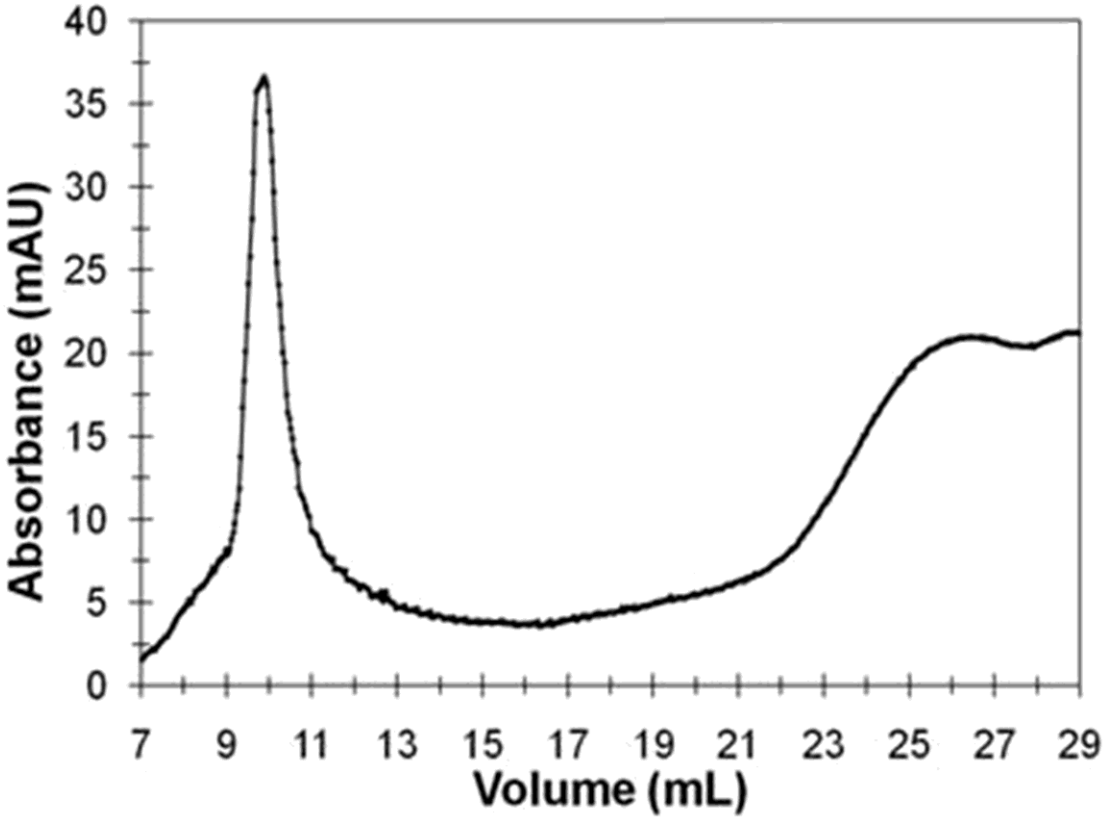
Absorbance (mAU)
40
35
30
25
20
15
10
5
0
7
9
11
13
15
17
19
21
23
25
27
29
Volume (mL)

Supplementary Figure A.5. Detailed analysis of 5.4 Å iron EXAFS peak. (a) Shows EXAFS Fourier transforms (Fe—S phase-corrected) for different *k*-ranges showing persistence of the 5.4 Å transform peak. (b) Shows the EXAFS Fourier transform of the high-*k* data (18 $Å^{-1}$) (blue line) modeled using multiple scattering (red line) or single scattering (green line) plus the estimated noise level in the data at this *k*-range (broken line). We note that the EXAFS noise level is expected to be "white" with equal amplitudes at all frequencies but that the noise at very low frequency will be effectively removed by the EXAFS spline function, which is why the apparent Fourier transform noise level falls below the broken line at low *R* values.

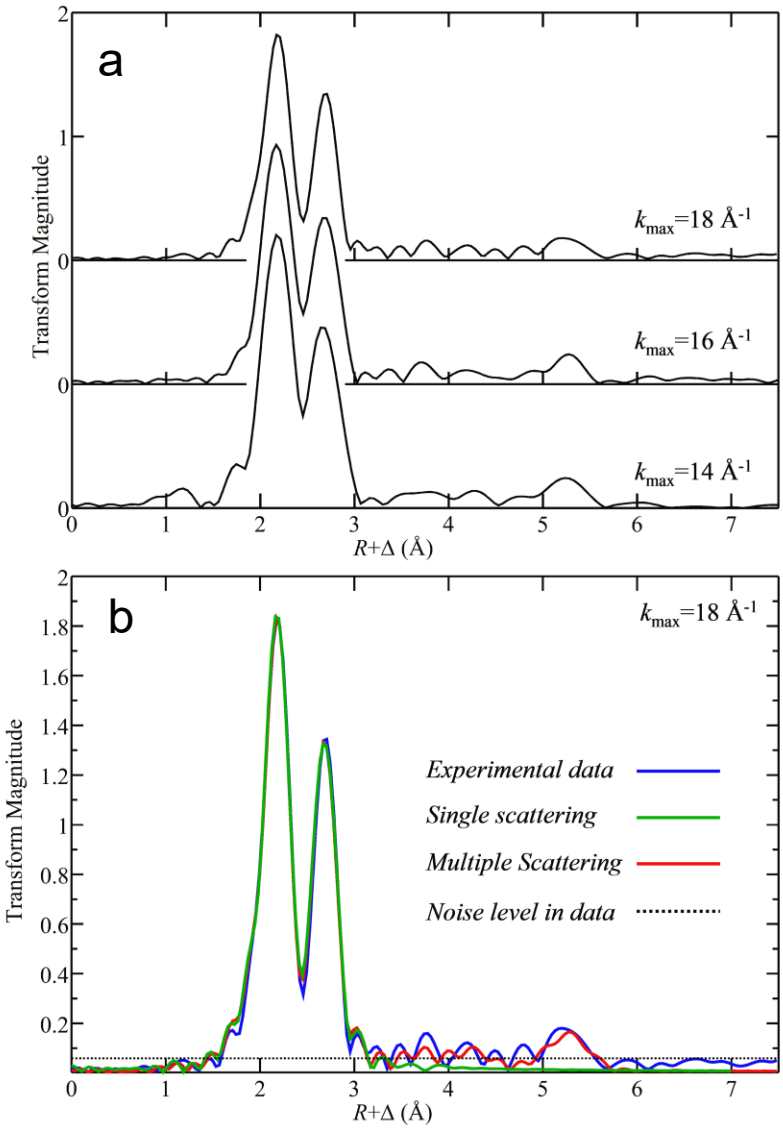
a
Transform Magnitude
k_{max}=18 Å^{-1}
k_{max}=16 Å^{-1}
k_{max}=14 Å^{-1}
R+Δ (Å)
b
Transform Magnitude
k_{max}=18 Å^{-1}
Experimental data
Single scattering
Multiple Scattering
Noise level in data
R+Δ (Å)

Supplementary Figure A.6. Temperature-dependence of the EPR spectra of IssA. The spectra were recorded under non-power-saturating conditions at a microwave frequency of 9.60 GHz, with a modulation amplitude of 6.4 G and a microwave power of 20 mW. Broad scans at various temperatures show a very broad signal centered around $g = 2.2$ (marked by the long vertical line) that increases in intensity with increasing temperature due to antiferromagnetic coupling in the thioferrate chains. The positions at $g = 4.3$ and $g = 2.0$ are marked. The former is indicative of trace adventitiously-bound high-spin ($S = 5/2$) Fe^{3+} or magnetically isolated linear $[3Fe\text{-}4S]^{+}$ clusters ($S = 5/2$). The origin of the weak signal in the $g = 2$ region is unknown.

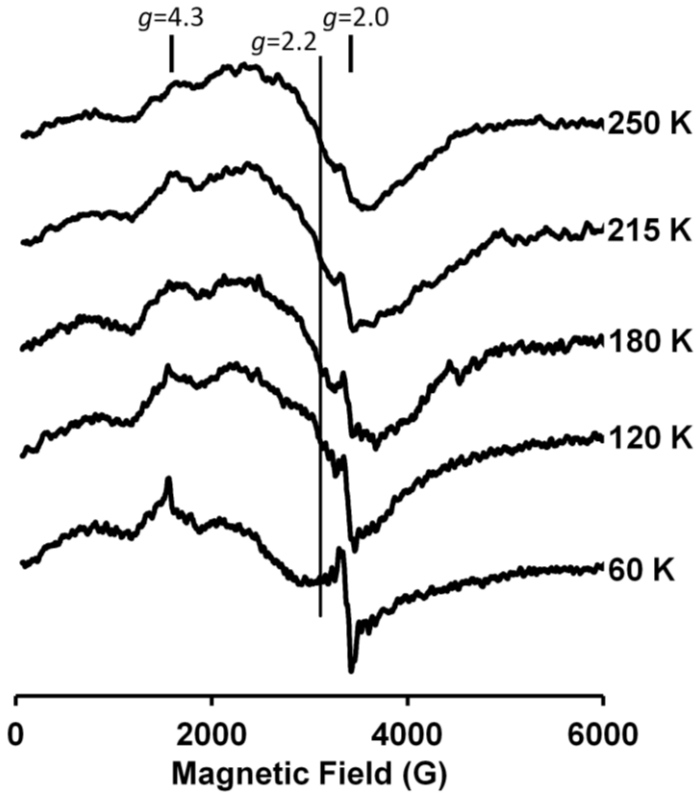
g=4.3
g=2.2
g=2.0
250 K
215 K
180 K
120 K
60 K
0
2000
4000
6000
Magnetic Field (G)

Supplementary Figure A.7. Cladogram of proteins containing the IPR003731 domain. Colored clades contain members of the NifB (IPR005980, blue), NifX (IPR013480, turquoise), and NafY (IPR031763, yellow) InterPro protein families. The proposed IssA clade based on *P. furiosus* IssA (red) contains member proteins (red lines on innermost ring) with pI ≥ 9, fewer than 5 cysteines and at least 20% glycine in the C-terminal 40 residues, similar to IssA including the C-terminal tail. The IssX clade (78% confidence; yellow) shares some of these features, but is more distantly related to *P. furiosus* IssA and contains member proteins (yellow lines on innermost ring) with pI ≥ 8, fewer than 10 cysteines and at least 10% glycine residues in the last 40 amino acids. Many members of this clade appear to contain a shortened version of the *P. furiosus* IssA C-terminal tail. Blue, green and purple lines on the innermost ring mark individual members of IPR005980, IPR013480 and IPR031763, respectively. The second ring (green) plots the percentage of glycine in the last 40 residues. The third ring (blue) plots the number of cysteines in the protein where the red scale line shows 4 cysteines. The outer ring (black) plots predicted protein pI centered at pH 7.0. *P. furiosus* IssA and the *Methanothermobacter thermautotrophicus* homolog (MTH1175) used to predict the structure of the *P. furiosus* N-terminal domain (Figure A.6a), are shown by red and yellow arrowheads, respectively.

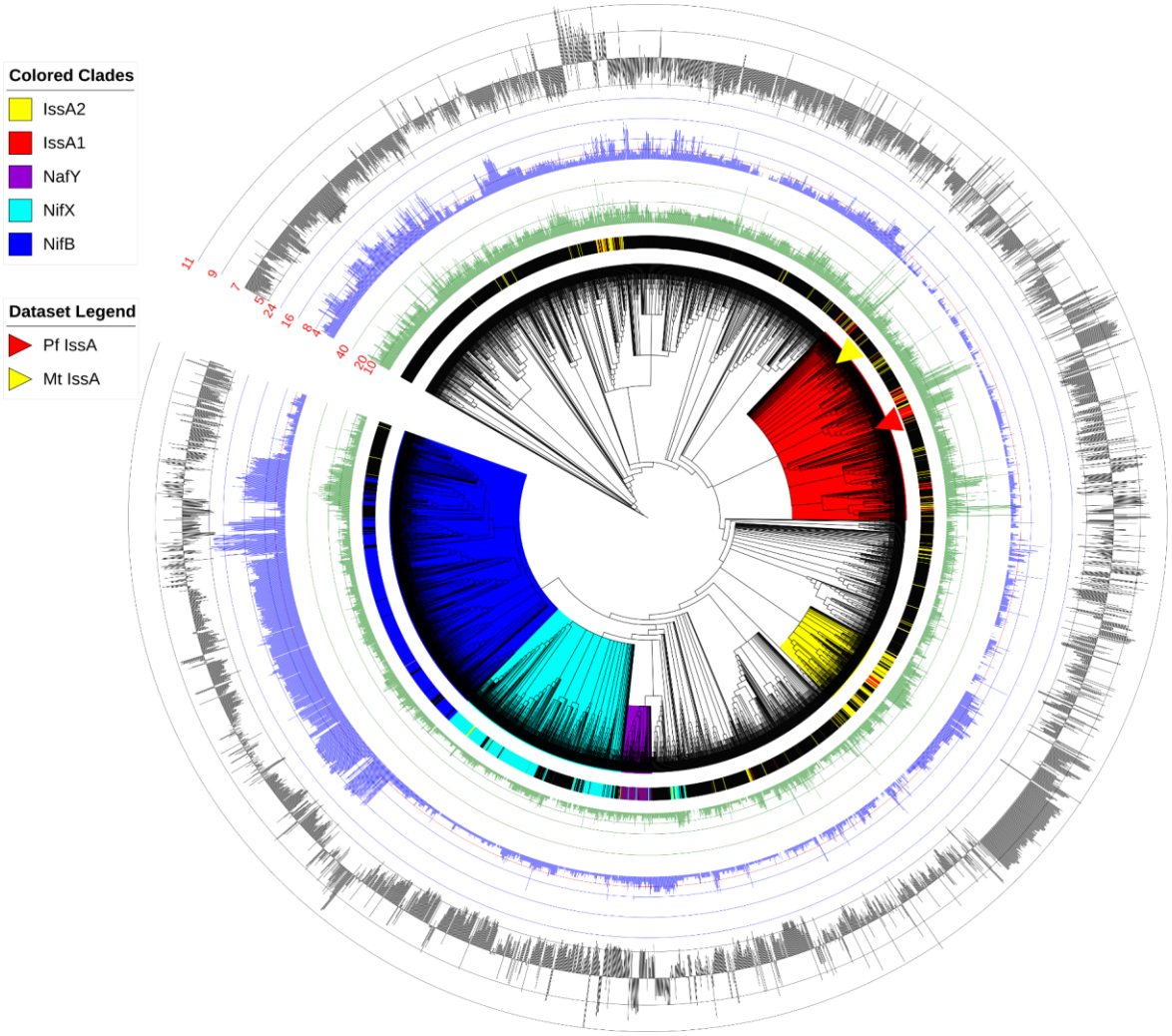
Colored Clades
IssA2
IssA1
NafY
NifX
NifB
Dataset Legend
Pf IssA
Mt IssA
11
9
7
5
24
16
8
4
40
20
10

Supplementary Figure A.8. Effects of extended X-ray beam exposure on the sulfur K-edge XAS spectrum of a single IssA sample. Spectra are shown for the first scan, the fourth scan and the eighth scan with each scan taking approximately 30 min. Only subtle changes in the near-edge spectrum are observed in this sample and these are most pronounced at around 2475 eV (indicated by the arrow), suggesting that photo-oxidation of a small fraction of the sample has occurred.

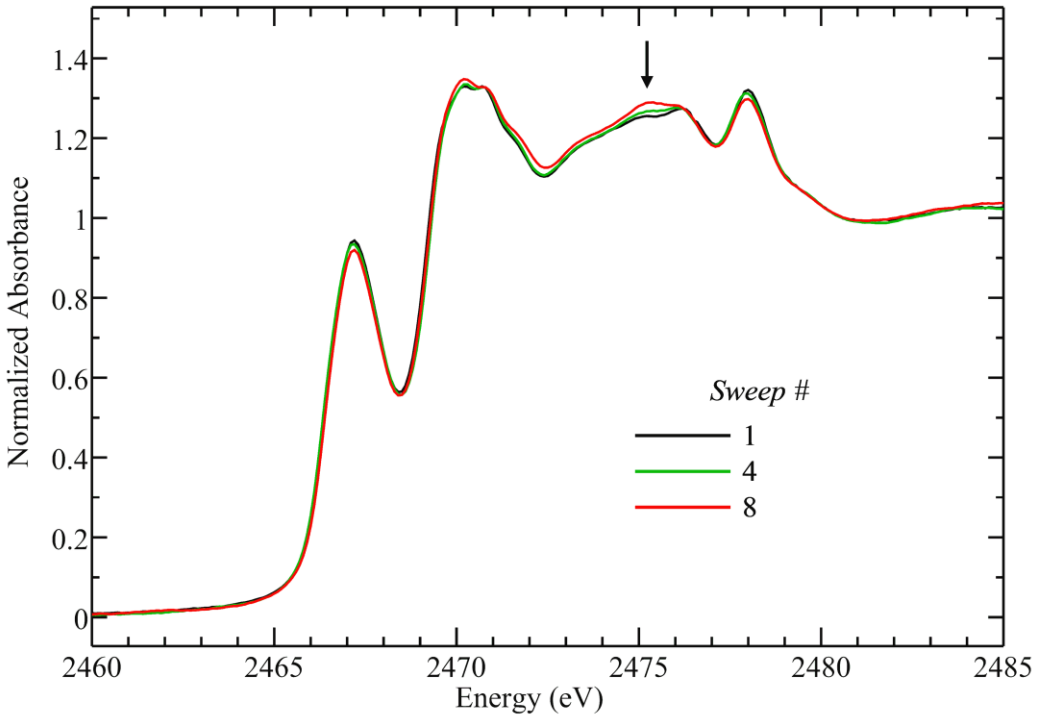
Normalized Absorbance
Energy (eV)
Sweep #
1
4
8